UNIVERSIDAD NACIONAL AUTÓNOMA DE MÉXICO

PROGRAMA DE MAESTRÍA Y DOCTORADO EN CIENCIAS QUÍMICAS

FLUID DYNAMICS IN OSCILLATING NANOTUBES A CONTINUUM MECHANICS APPROACH

TESIS

PARA OPTAR POR EL GRADO DE

DOCTOR EN CIENCIAS

PRESENTA

ING. ULISES TORRES HERRERA

TUTORA: DRA. EUGENIA CORVERA POIRÉ
FACULTAD DE QUÍMICA, UNAM

CIUDAD UNIVERSITARIA, CIUDAD DE MÉXICO, FEBRERO DE 2020.

UNIVERSIDAD NACIONAL AUTÓNOMA DE MÉXICO

PROGRAMA DE MAESTRÍA Y DOCTORADO EN CIENCIAS QUÍMICAS

FLUID DYNAMICS IN OSCILLATING NANOTUBES A CONTINUUM MECHANICS APPROACH

T E S I S

PARA OPTAR POR EL GRADO DE

DOCTOR EN CIENCIAS

P R E S E N T A

ING. ULISES TORRES HERRERA

TUTORA: DRA. EUGENIA CORVERA POIRÉ
FACULTAD DE QUÍMICA, UNAM

CIUDAD DE MÉXICO, FEBRERO DE 2020.

JURADO ASIGNADO

Presidente:	Dr. Miguel Antonio Costas Basín
Secretario:	Dr. José Esteban López Aguilar
Vocal:	Dr. Wolf Luis Mochán Backal
Vocal:	Dr. José Alejandre Ramírez
Vocal:	Dra. Elena Golovataya Dzhymbeeva

TUTOR DE TESIS:

Dra. Eugenia Corvera Poiré

El presente trabajo de investigación se desarrolló en el cubículo 317 del Edificio F de la Facultad de Química de la Universidad Nacional Autónoma de México, bajo la dirección de la Dra. Eugenia Corvera Poiré. Also, a 6-month research stay was carried out at Rutherford Building, in the Department of Physics of McGill University under the supervision of Prof. Hong Guo.

Los resultados de este trabajo de investigación fueron presentados en los siguientes congresos:

- Cuarta Reunión Anual de la Red Temática de Materia Condensada Blanda. Zacatecas, Zacatecas, México, 2015. *Flujo de agua confinada en nanoestructuras.*
- XLV Winter Meeting on Statistical Physics. Taxco, Guerrero, México, 2016. *Water flow confined within nanostructures.*
- 28^{th} International Conference on Science and Technology of Complex Fluids. San Luis Potosí, San Luis Potosí, México, 2016. *Oscillations of nanotubes induced by viscous flow: A theoretical study.*
- Self Assembly: From atoms to life. Tuxtla Gutiérrez, Chiapas, México, 2016. *Effect of boundary conditions in the vibration frequencies of nanotubes conveying flow.*
- Jornada de la Investigación en la Facultad de Química. Ciudad de México, México, 2016. *Flujo pulsado y sus aplicaciones biológicas de macro a nanoescalas.*
- XLVI Winter Meeting on Statistical Physics. Taxco, Guerrero, México, 2017. *Determination of flow within nanostructures by measurement of tube oscillations: A theoretical study.*
- 29^{th} International Conference on Science and Technology of Complex Fluids. San Luis Potosí, San Luis Potosí, México, 2017. *Strategy to measure flow within elastic nanostructures: A theoretical proposal.*
- Quinta Reunión Anual de la Red Temática de Materia Condensada Blanda. León, Guanajuato, México, 2017. *Estrategia para medir flujo al interior de nanoestructuras elásticas por medio de su frecuencia de oscilación.*
- XLVII Winter Meeting on Statistical Physics. Puebla, Puebla, México, 2018. *Determination of flow within nanostructures by measurement of tube oscillations: A theoretical study.*

- International School of Nanomedicine, 3^{rd} Course: Nanofluidics, Nanoimaging and Nanomanipulation. Erice, Sicilia, Italia, 2018. *Accurate determination of flow within elastic nanostructures by the measurement of their characteristic frequencies.*

- Jornada de la Investigación en la Facultad de Química. Ciudad de México, México, 2018. *Control de flujos pulsados de la macro a la nanofluídica.*

- Encuentro Académico QuimiUNAM. Ciudad de México, México, 2018. *Induction of water flow within elastic nanotubes by an asymmetric deformation on the tubes: A theoretical study.*

- 30^{th} International Conference on Science and Technology of Complex Fluids. San Luis Potosí, San Luis Potosí, México, 2018. *Induction of Water flow within elastic nanostructures by oscillatory tube deflections: A theoretical study.*

Asimismo, se expusieron los resultados en el siguiente seminario:

- *Fluid flow inside an oscillating nanotube: Insights into non-linear dynamics.* McGill University, Montreal, Quebec, Canadá, 2018.

Como producto de esta investigación, fue publicado el siguiente artículo:

- U. Torres-Herrera and E. Corvera Poiré. An analytical framework to determine flow velocities within nanotubes from their vibration frequencies. *Physics of Fluids*, *30*(12): 122001, 2018.

AGRADECIMIENTOS

A la Dra. Eugenia Corvera Poiré, por su labor incansable en transmitirme su pasión por la ciencia y su valentía al abordar un proyecto que habría resultado imposible sin su guía, su tiempo y su dedicación. Sus esfuerzos, enseñanzas y apoyo han hecho posible la culminación de este trabajo; su ejemplo como investigadora ha sido una inspiración.

I would like to acknowledge Professor Hong Guo, for supervising my work during my Research Stay at McGill University. Thank you for providing me with new insights and a wide panorama of science.

A los doctores Wolf Luis Mochán Backal y Eduardo Vivaldo Lima, integrantes de mi comité tutor, por sus valiosas aportaciones a lo largo de la realización de este trabajo, que han contribuido a dar una mayor profundidad a mi trabajo y a ahondar en los fundamentos conceptuales y prácticos del mismo.

A los miembros del jurado de mi examen de grado, doctores Wolf Luis Mochán Backal, José Esteban López Aguilar, José Alejandre Ramírez, Elena Golovataya Dzymbheeva y Miguel Antonio Costas Basín, por su dedicación a la lectura de esta tesis, así como por sus comentarios, observaciones y correcciones, que mejoraron mucho la presentación del trabajo.

Al Programa de Maestría y Doctorado en Ciencias Químicas de la UNAM, por otorgarme la oportunidad y los recursos para realizar mis estudios de doctorado.

Al profesor Jesús Gumaro Viacobo Flores, Gestor de becas CONACyT en el Programa de Maestría y Doctorado en Ciencias Químicas por su labor constante y eficiente y por su trato siempre respetuoso, que coadyuvó a la consecución de las diferentes metas alcanzadas durante mis estudios de doctorado.

Al Consejo Nacional de Ciencia y Tecnología, CONACyT, por la beca con folio 589015 otorgada para la realización de mis estudios de doctorado.

Al CONACyT, por la beca de movilidad al extranjero, (convocatoria número 291250) para participar en una estancia de investigación en McGill University, Canadá, del 1 de septiembre de 2018 al 28 de febrero de 2019.

Al Programa de Apoyo a los Estudios de Posgrado (PAEP) de la UNAM, por el apoyo proporcionado para asistir al congreso:

- International School of Nanomedicine, 3^{rd} Course: Nanofluidics, Nanoimaging and Nanomanipulation. Erice, Sicilia, Italia, 2018.

Al proyecto CONACyT 219584 por el apoyo proporcionado para asistir a las reuniones:

- XLV Winter Meeting on Statistical Physics. Taxco, Guerrero, México, 2016.
- 28^{th} International Conference on Science and Technology of Complex Fluids. San Luis Potosí, San Luis Potosí, México, 2016.
- 29^{th} International Conference on Science and Technology of Complex Fluids. San Luis Potosí, San Luis Potosí, México, 2017.
- 30^{th} International Conference on Science and Technology of Complex Fluids. San Luis Potosí, San Luis Potosí, México, 2018.

A la Facultad de Química de la UNAM, por el apoyo proporcionado para asistir a las reuniones:

- XLVI Winter Meeting on Statistical Physics. Taxco, Guerrero, México, 2017.
- XLVII Winter Meeting on Statistical Physics. Puebla, Puebla, México, 2018.

A la Red Temática de Materia Condensada Blanda del CONACyT por el apoyo proporcionado para asistir a las reuniones:

- Cuarta Reunión Anual de la Red Temática de Materia Condensada Blanda. Zacatecas, Zacatecas, México, 2015.
- Quinta Reunión Anual de la Red Temática de Materia Condensada Blanda. León, Guanajuato, México, 2017.

I would like to acknowledge financial support from Department of Chemistry and Biochemistry of University of California Los Angeles (UCLA), for attendance to the conference:

- Self Assembly: From atoms to life. Tuxtla Gutiérrez, Chiapas, México, 2016.

Al Dr. Martin-Daniel Lacasse, por el formato LaTeX de esta tesis.

For Marisol and Geraldine

Statement of originality

Original results of this Thesis are:

- Incorporation of the non-conservative viscous stress tensor in the variation of external forces in the Minimal Action's Principle in Eqs. (3.1) and (3.22).
- Obtention of the coupled dynamic equations of motion, for the fluid and the oscillating tube, in Eqs. (3.36) and (3.37). These ones constitute the departing point of our proposed Continum Mechanics approach to the problem.
- Obtention of relevant equations of motion in three special regimes: the fully decoupled limit, the limit where tube dynamics is influenced by the fluid and the limit in which fluid dynamics is influenced by the tube. Considerations are explained in Chapter 4, and the physical conditions of validity, and the equations pertaining the different regimes, are summed up in Fig. 4.1.
- Analytical exact expression for the flow velocity in the limit of fluid dynamics influenced by tube vibration, for a general form of tube vibration and no-slip boundary condition (Eq. 4.24).
- Proposal to determine the fluid velocity from the tube vibration spectrum. Presented in Chapter 5 and published in *Physics of Fluids* 2018. This has established a theoretical framework to determine flow velocities within elastic nanotubes, and potentially other fluid properties, from their vibration frequencies.
- Analytical approximated expressions for the flow/frequency relation in the limit of tube dynamics influenced by fluid flow, for each set of boundary conditions. These ones are presented in Appendix A.7.
- Analytical approximated expression of flow velocity for a single-mode tube vibration, in the limit of fluid dynamics influenced by tube vibration (Eqs. 6.6-6.9 or 6.19-6.22, with parameters for the different boundary conditions given in Appendix A.9). This is presented in Chapter 6 and constitutes the core of a paper to be submitted to a high impact Fluid Mechanics journal. Our results establish, theoretically, a way to generate high frequency fluid flow oscillations, with a non-negligible finite amplitude, via the external control of single-mode vibrations on the tube.

Table of contents

Figures

Tables

FLUID DYNAMICS IN OSCILLATING NANOTUBES
A CONTINUUM MECHANICS APPROACH

Ulises Torres Herrera

Advisor: Prof. Eugenia Corvera Poiré

1

General introduction

Fluid dynamics under nanometric confinement is an area of great importance for the development of basic and applied sciences. The nanoscale world offers insights into chemical and physical concepts that could not have been experimentally proven for centuries. Ideas such as the slippage and friction at a solid/liquid interface, the role of intermolecular interactions in the rheological response of fluids, the relation between tube rugosity and fluid arrangement in the formation of a hydrodynamic boundary layer, have been corroborated and observed in recent years, thanks to novel methodologies to design micro and nanofluidic systems, along with the development of techniques and strategies to control and measure flow velocity at those scales.

Physical and chemical behavior of several nanofluidic systems have challenged the classical picture of the tube/fluid interaction, requiring a revision of the assumptions and considerations that support our understanding of liquids and solids at non-equilibrium situations.

In some cases, nanoscale systems demand a more complicated description than macroscopic systems, and require a physicochemical picture accounting for the formation of complex molecular aggregates and structures, never found in bulk and macroscopical flow systems. Most of the theoretical efforts to improve the existing physicochemical models to describe nanoscale flow systems have followed this approach.

In some other cases, the characteristics of the nanoscopic world allows for assump-

tions that have not been suitable in the theoretical modelling of macroscopic systems. Surprisingly, some of these considerations lead to rather simplified equations that govern the nanofluidic systems, in comparison with their macroscopic equivalents. This is possible because the nanoscopic scale is a unique one, where two physical peculiarities convey:

- The amount of molecules is large enough to make a mechanical description of the flow system in terms of continuum properties and descriptors.
- The confinement size is small enough, so features that arise when fluids at macroscales are subject to complex stresses -such as secondary flows and 3-D flow patterns- are not possible at nanoscales, because these phenomena require a minimal space to develop.

In the rest of the Introduction, we present the phenomenology of nanoscale flow systems.

1.1 Importance of micro and nanometric flow systems

The physics of flow across nanometric channels plays an important role in the design of chemical and biomedical technological devices. Several technological developments have arisen to assist the chemical processes in aspects where the conventional techniques are limited. Most of these limitations are related to waste generation and process efficiency [14, 15].

In such aspects, micro and nanofluidic devices constitute promising substrates. Miniaturization of processes implies a considerable reduction of the amount of reactants and chemical residues. Besides, diffusion control is enhanced in micro and nanoscale channels, since convective effects such as flow instabilities, and vortex formation are almost completely inexistent at such confinement scales. It is therefore possible to generate flow systems where conditions for fluid mixing and stable fluid-fluid interfaces, are perfectly controlled. Under such conditions, the efficiency of

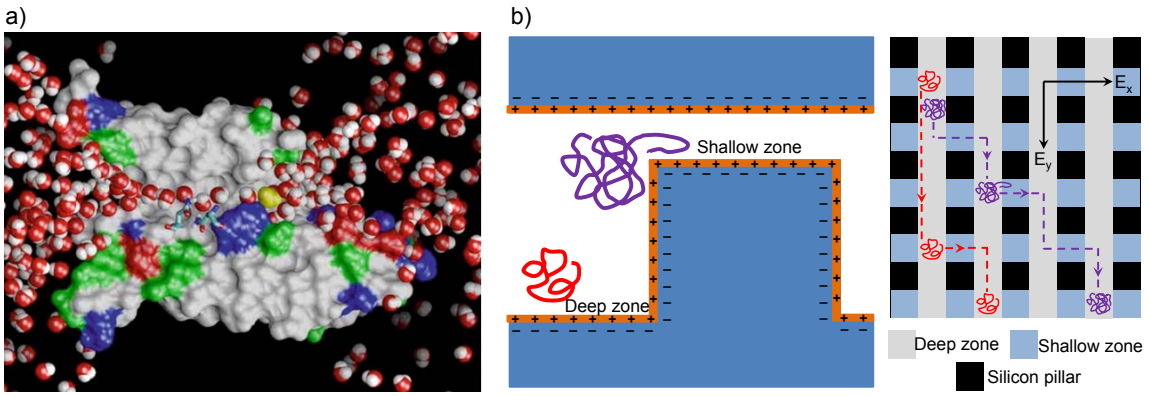

Figure 1.1: The capability to control and manipulate chemical species at the nanoscale is illustrated in: a) where water molecules are flowing across an aquaporin (Image is a still from the movie published at www.ks.uiuc.edu); b) where a nanofluidic device for separation of DNA fragments, via their controlled stretching and unfolding, is shown. Taken from [1].

chemical processes increases considerably [16]. Moreover, it is possible to manipulate chemical species at a level of precision that was never expected within the conventional methods (see Fig. 1.1).

Nanofluidic devices have allowed for the creation of novel instruments that span through a wide range of applications, from nanometric biosensors for cancer detection [17, 18, 19] to ultrafast filtration membranes [20, 21, 22, 2, 10, 23, 24].

Most of the current applications of nanofluidic devices are inspired in the mimetization of biological channels [25] by synthesizing nanostructures of similar size and geometry [26, 27, 28]. As a consequence, considerable efforts have been made to expand the spectrum of nanostructures capable to convey fluid flow. Nowadays, nanofluidic systems are composed of a diversity of materials and arrangements of channels [29, 30, 31], whose size ranges from a few nanometers to tenths of micrometers, both in radius and length [32, 33, 34]. However, understanding the physics underlying water flow across nanostructures is still a challenge for flow magnitude prediction and control. Such a gap has limited, to some extent, the implementation of nanofluidic devices into chemical technology and manufacturing processes [35, 36, 37, 38].

1.2 Experimental evidence of anomalous behavior

The first approaches towards the design of nanofluidic flow devices consisted of an extrapolation of the models used to describe macroscopic systems to explore the consequences of a change in scale in the classical picture of flow systems [39, 40]. However, the experimental evidence soon demonstrated the limitations of such a strategy. For the case of nanotubes conveying fluid, the most interesting and surprising phenomena can be separated in two groups:

- The enhancement of flow velocity inside non-polar nanotubes.
- The rheological properties developed by simple fluids at nanoscales confined in polar substrates.

A description of the effects of flow in non-polar and in polar substrates at nanoscales is presented in the following two subsections.

1.2.1 Flow enhancement in carbon nanotube membranes

Most of the experimental work regarding water flow in nanostructures is focused on flow across carbon nanotube membranes. Such devices are built departing from carbon nanotubes synthesized in a bundle-like array [41, 15]. In such an arrangement, the carbon nanotubes are aligned to each other as illustrated in Fig. 1.2, so it is possible to apply polystyrene on both edges. Afterwards, the nanotube pores are recovered by chemical etching on both surfaces. This procedure is validated to ensure that the polymer has completely covered the interspace between tubes. By surface measurement techniques, it is possible to detect cracking and leakage in the polymer coating, allowing one to ensure that the pores of such a membrane are given by the cylindrical hollows of the carbon nanotubes [10]. Afterwards, the performance of the membrane is tested and its potential use in ultrafiltration technology is evaluated.

This strategy has allowed for the preparation of CNT membranes in a wide range of tube sizes and surface areas [42, 38, 43, 44, 45, 46, 47]. However, the reproducibility

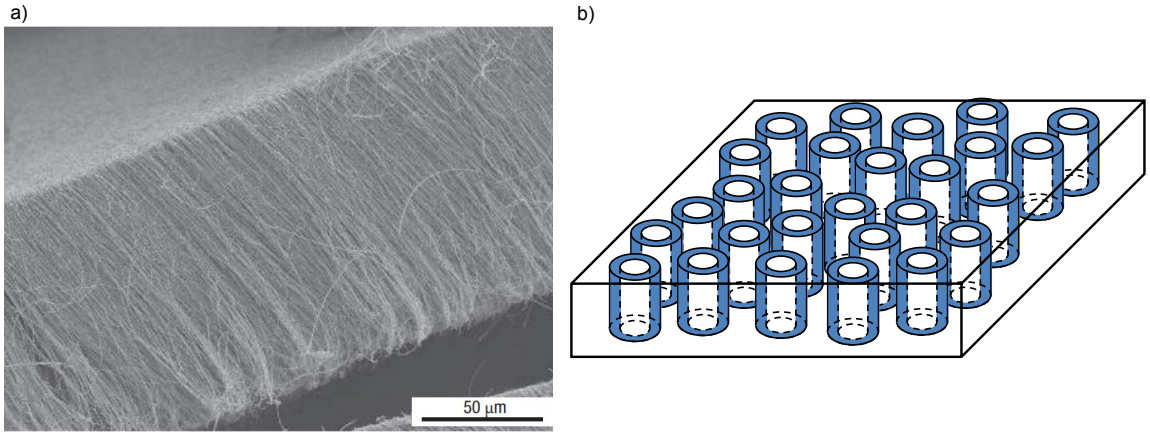

Figure 1.2: Carbon nanotube membranes as a tool for ultrafiltration technology. a) SEM image of the synthethized nanotube bundles. Taken from [2]. b) After polystyrene coating, the nanotube bundles behave like a membrane where flow only occurs across the cylindrical hollows of carbon nanotubes, without leakage.

and transferability of the observed flow rates are aspects of their performance that still demand considerable efforts. The most impressive result concerning such a system arises when the experimental results are compared with theoretical data for the classical theory of porous media, where each tube is considered independent. Inside each tube, a Hagen Poiseuille profile is assumed to be completely developed, with the condition of no slip at the fluid/wall interface [10]. It turns out that the permeability of the membrane is three or four orders of magnitude larger than the one predicted by theoretical means (see Table 1.1).

From a technological point of view, the high performance of CNT membranes conveys an enormous reduction of the energetic cost required to exploit them for water filtration. From a physical point of view, the flow enhancement implies that the classical description is no longer valid to understand flow across channels of such scales. Both perspectives have inspired considerable efforts to improve even further the efficiency of CNT membranes. Particularly, the weak interaction and low rugosity between water and carbon-based nanotubes has shown to be responsible for the low-friction flow observed in experiments with membranes [2, 10, 23, 48, 49, 50]. As a consequence, chemical functionalization of the tube has shown to allow for tuning of the magnitude

Liquid	Experimental flow velocity (cm/s)	Predicted flow velocity (cm/s)	Fitted slip length (μm)
Water	9.5	0.00015	39
Ethanol	4.5	0.00014	28
Iso-Propanol	1.12	0.00077	13
Hexane	5.6	0.00052	9.5
Decane	0.67	0.00017	3.4

Table 1.1: Comparison of observed flow velocities with theoretical Poiseuille-like flow predictions for flow across the CNT membranes schematized in Fig. 1.2. Average tube diameter is 7 nm, tube density is 5×10^{10} pores per cm^2, pressure difference across membrane is 0.8 bar and tube length is 126 micron. Taken from [10]

.

of friction at the tube/fluid interface [42, 43, 44, 45, 46, 51, 47]. Besides, the sensitivity of flow permeability to changes in tube rugosity has been verified from observations in several types of nanopipes and nanochannels [2, 52, 53, 54, 36, 55, 56, 57]. Understanding these phenomena has also allowed for the incorporation of electrochemical and electrosmotic flow-control parts [52, 58]; however, the capability to functionalize the tube surface and modify its rugosity is limited [59, 60, 61]. Novel strategies to push such limits are continuously being developed. The progress expected due to the implementation of CNT membranes in fields of chemical technology, such as purification and separation techniques, will rely on the better understanding of the nanotube/fluid interactions.

1.2.2 Rheological properties of nano-confined water

While it has been observed that nanoscale flow is enhanced when fluids are confined within non-polar smooth surfaces, a different approach has been employed for the study of fluid dynamics confined in between polar rough surfaces.

Particularly, the response of water has been tested in a nano-rheometer, composed

of a fluid droplet confined between mica surfaces. One surface remains static, while the other one is an AFM tip, that exerts an oscillatory shear stress on the droplet [3, 62, 63, 64, 65]. Such experiment is of great importance, because it allows both, to measure the time-changing stress exerted on the droplet, and to have an instantaneous measurement of the fluid velocity, since this one is given by the time derivative of the tip displacement.

Since both the exerted stress and the fluid motion are oscillatory in the experimental arrangement - illustrated in Fig. 1.3a-, the analysis of the flow velocity oscillation amplitude and its phase difference with stress, conveys the information of the rheological fluid response. Moreover, such an experimental setting allows for changing the wall-to-wall distance, enabling the control of the confinement size from 0.1 nm to 20 nm.

This apparatus is used to measure the drag force per unit area at the tip -caused by the confined fluid- and the one exerted along the whole immersed probe -caused by the bulk water-. They define F as the bulk drag force per unit area and δF as the difference between the confined and bulk drag forces per unit area. The ratio between the force at the tip and the one along the probe, is plotted in Fig. 1.3b. A change in such ratio can be related with a reduction or increase of the viscosity, as follows. When the confined water presents the same behavior than the bulk, $\delta F = 0$. Positive values are associated with an increase of the apparent confined viscosity, i.e., shear thickening, whereas negative values are associated with shear thinning.

Under such conditions, water exhibits a size-dependent viscosity. This result is summarized in Fig. 1.3. At relatively large confinement -which is still nanometric-, water behaves as a typical viscous fluid; when the confinement goes lower than 7 nm, the viscosity increases slightly. In such a regime, the tube/fluid interaction causes the arrangement of water molecules, decreasing their mobility and increasing their apparent viscosity. When the confinement size goes below 2 nm, $\delta F/F$ diminishes to negative values, showing a shear-thinning behavior. This regime is associated with the

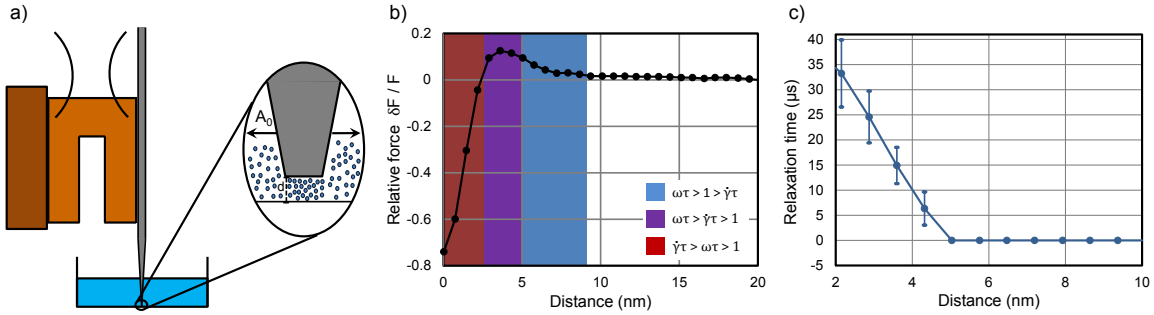

Figure 1.3: Arising of viscoelastic and shear-thinning behavior in confined water. a) Experimental setting, consisting of an AFM probe immersed in a fluid, whose tip is located very close to the flask's bottom, creating a nanoconfinement space between the tip and the mica flask surface. b) Relative difference between the drag force exerted by confined water and the bulk water. c) Relaxation time of water as a function of confinement size. Taken from [3].

remotion of water layers and the reduction of water density. In a molecular picture, these regimes are understood because the solid/fluid interface has two effects, namely, the interaction arranges the water molecules in ordered layers, at the same time that repels them from the immediate viccinity of the wall, causing a small empty space.

Besides, when the confinement decreases up to a threshold of approximately 5 nm, confined water presents another abnormality: an elastic behavior (see Fig. 1.3c), that is typically associated with structured fluids. In this case, related with the formation of ordered water-molecule layers, enhancing the global strength of the hydrogen bonds network [66, 67, 68]. Moreover, the relaxation time, that is characteristic of such an elastic response, tends to increase when the experiment is performed at lower confinement sizes.

The size-dependent rheological behavior described above, has been understood in terms of the structural response of water at small confinement scales, where the effect of wall/fluid interaction is dominant.

1.3 Effect of nanometric confinement in tube/fluid systems

The role of wall/fluid interaction in flow systems was first studied in microfluidics. Since then, it has been clear that the reduction of the confinement size is key to study the fluid-substrate interaction.

The previous works have demonstrated that such a statement is valid for the nanoscale fluids. The fluid-substrate interaction is not only relevant but dominant in the physical description of fluid dynamics at such confinement sizes. However, there is one fundamental difference between micro and nanoscale confinement: the static picture of the confining media. In most cases, a microfluidic substrate is rigid; in some other cases, the walls exhibit an elastic behavior, allowing for small radial tube deformations in response to relatively large forces. In contrast, typical nanoscale substrates offer a wide spectrum of phenomena related to their elastic response.

In this section, an overview of the current physical picture of the tube dynamics is presented to establish a departing point for the study of the system that concerns us.

1.3.1 Temperature, energy and elastic vibrations

There are some aspects of the physics of nanofluidic systems that have not been addressed in complete detail in the literature. Numerous techniques and materials have been developed for the preparation of nanostructures for fluid transport, such as solid-state pores [69, 70, 71, 72, 73] nanochannels,[27, 26, 74, 75, 76, 77], nanotubes [10, 23, 78], nanopipes [2, 52, 53, 54, 36, 55, 56] and protein-based nanopores [79, 80, 81]. Most of this nanostructures share one property: they have an elastic response to small mechanical deformations [11, 82, 83, 84, 85, 86].

The different types of deformations exerted on a tube, allow for different strategies of mechanical manipulation. The role of radial expansion and compression, which

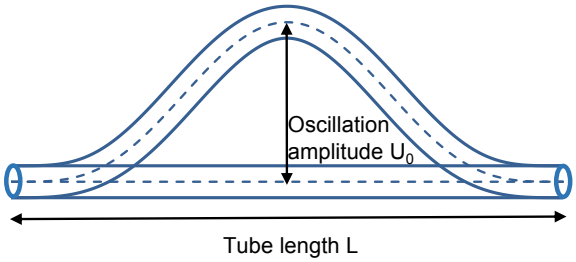

Figure 1.4: Flexural deflections in elastic tubes. The maximum tube displacement and tube length are exemplified.

is very small in nanotubes, has been studied and compared with previously-known results in micro and macrofluidic devices [87, 88, 89]. Moreover, the role of size in the dynamics of elastic nanotubes is particularly important in a very specific type of elastic deformation: flexural bending (see Fig. 1.4). This is because the aspect ratio length/radius is generally very large in nanotubes. At nanoscales, axial deflection provides two interesting and useful qualities, namely, they require very small external forces, from several pN to nN, -which are considerably smaller than the ones involved in radial expansion/compression [90]-, and are so low that are of the order of thermal fluctuations (see Fig. 1.5). Also, they have a high frequency response, from several kHz up to few GHz [91, 92, 93, 94] (see Table 1.3.1 and Fig. 1.6).

The capability to generate high frequency vibrations by mechanical manipulation at a small energetic cost opens a landscape of possibilities that deserve further exploration, and could be of potential use to improve the understanding and control of fluid dynamics at nanoscales. Elastic vibrations offer new possibilities for the development of nanofluidic devices and technology to measure, control and manipulate flow at such scales.

Tube material	Diameter nm	Length μm	Thickness nm	Fundamental frequency (MHz)
Graphene	1-200	0.1-10	1-40	10-1000
Boron nitride	5-50	0.1-10	3-50	10-1000
Titania	30-80	0.2-1	10-20	100-10000
Silicon	10-100	0.1-10	5-30	100-1000
Gallium nitride	30-200	2-5	5-50	10-100
Steel	5-500 $\times 10^7$	1-10 $\times 10^6$	2-25 $\times 10^6$	1-100 $\times 10^{-6}$
PVC	5-200 $\times 10^7$	0.1-10 $\times 10^6$	2-10 $\times 10^6$	1-10 $\times 10^{-6}$

Table 1.2: Elastic behavior of different types of tubes. Typical values of physical properties are taken from [11, 12, 13].

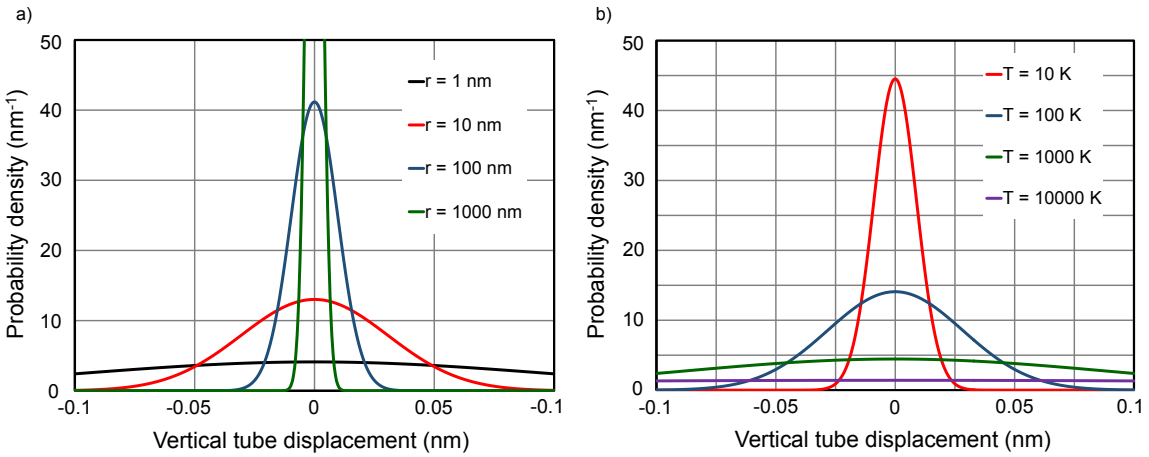

Figure 1.5: Role of thermal energy in the excitation of the fundamental vibration mode of an elastic bended tube. The probability of spontaneous deflection is plotted for different temperatures and tube diameter. a) Effect of tube radius in the probability of tube vertical displacement. b) Effect of temperature in the probability of tube vertical displacement. Details of the obtention of these curves are given in Appendix A.1.

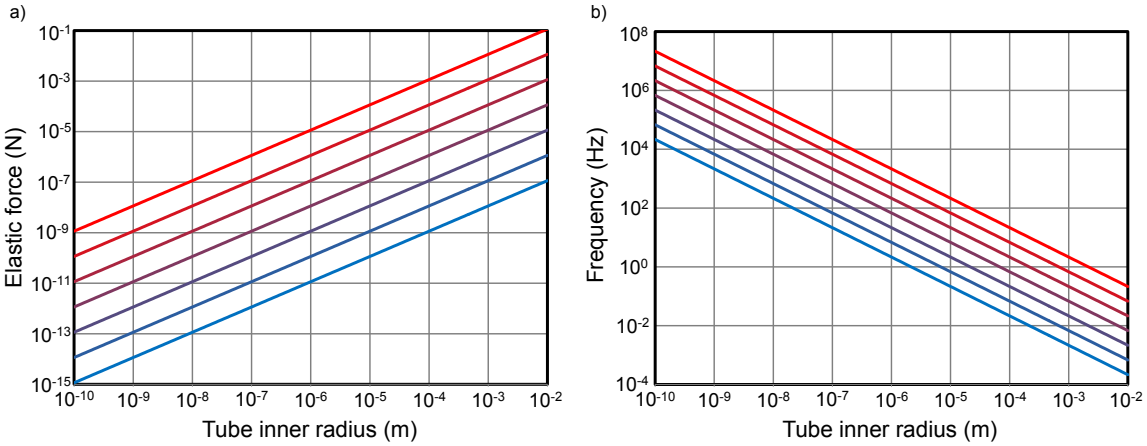

Figure 1.6: Elastic tube deflections from nano to macroscales. Color spectrum corresponds to Young moduli ranging from 1 MPa (red) to 1 TPa (blue). a) Effect of tube size on the force required to deflect the tube center by 1% of the tube's length, as illustrated in Fig 1.4. b) Effect of tube size on the vibration frequency of a tube filled with a stagnant fluid.

2

Background

Theoretical approaches to study nanotube/fluid systems can be classified in three categories:

- Molecular Dynamics (MD)
- Continuum Mechanics (CM)
- Hybrid Models

The most important difference consists of the use of a discrete or a continuum description of the system. Both, MD and CM approaches have been proved to be useful under different approximations and physical situations.

2.1 Discrete model: Molecular Dynamics

MD simulations are specially useful to account for tubes of small radii, where strong density gradients are present and a discrete description of matter is needed, due to regimes such as single-file ballistic flow, where molecules are in a one-dimensional arrangement, moving one behind the other as in a queue, or the so called Knudsen-flow regime, dominated by collisions and the interaction of particles of the fluid with particles of the wall [95, 35].

MD simulations have also been fundamental to understand density fluctuations of water in the proximity of tube walls (see Fig. 2.1a); also, they have demonstrated

that water molecules arrange in complex equilibrium structures never found in bulk systems, when confined within very small carbon nanotubes (see Fig. 2.1b). Such results have served to establish a theoretical framework of the tube/fluid interaction and its influence on the deviation of continuum properties at nanoscales [96, 66, 97].

However, simulation of long tubes and long sampling times are not attainable within such calculations due to the computational expense they demand. Moreover, the force field parameters used in MD simulations are different depending on the experimental arrangement they intend to reproduce [98, 99, 100]. In general, force field parameters are specially adapted to simulate electro-osmotic flow [58], formation of anomalous radius-dependent water aggregates and structures [5, 101, 102, 103, 104], diffusion-driven flow [105] and proton transport [106], among others. Such limitations have been an obstacle to establish general qualitative and quantitative trends in the behavior of nanoconfined flows.

In other words, the comprehension of the underlying physical principles is a challenge in MD frameworks, because there is no simple procedure to reduce the complexity of the fluid/fluid and fluid/tube dynamic interactions into global simplified expressions that generalize the behavior of nanotubes conveying flow. Every achievement reached to understand the tube/fluid systems at nanoscales in a MD framework is dependent on the force field parameters used, the chemical composition of tube and fluid and on practical details of the simulation such as the arrangement and artificial constraints over the atoms. The establishment of generalizations concerning the behavior of fluid/tube systems at nanoscales, is lacking in such theoretical frameworks.

2.2 Continuum Mechanics

In contrast to atomistic simulations, CM has been useful to simulate relatively large tubes at any time scale [2, 107, 108, 109, 110, 111]. The CM approach allows for an

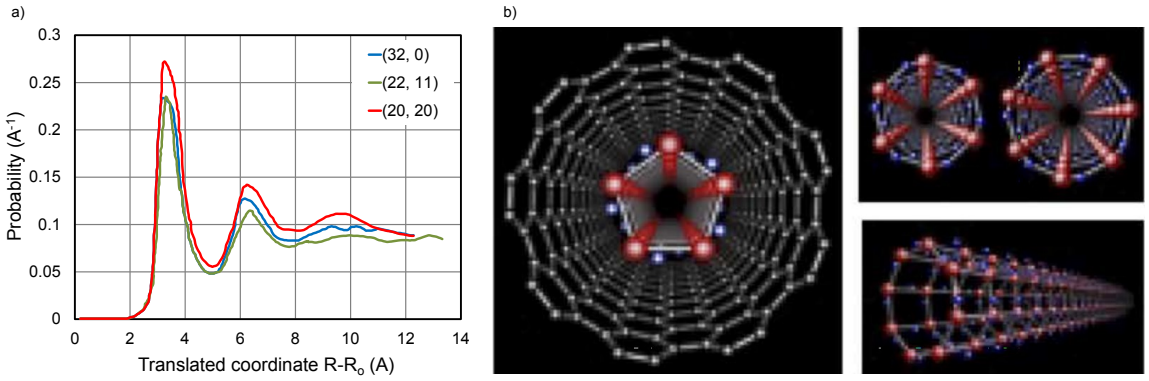

Figure 2.1: a) Anomalous density of water in the proximity of a CNT wall, computed by MD simulations, taken from [4]. b) Helicoidal structure of water molecules inside a single-walled carbon nanotube, taken from [5]

understanding of the complex tube/fluid interaction, via a mean description of the interaction.

In the literature, CM studies of nanostructures conveying fluids started by considering static rigid tubes. In such simulations, the tube/fluid interaction was incorporated by the slippage of the fluid at the tube/fluid interface [2, 10]. Also, studies on fluid dynamics across static deflected tubes gave analytical solutions that exhibited a complex flow, consisting of a primary flow, parallel to the tube, and a secondary ellyptical flow, forming a helical 3D flow pattern that does not exhibit turbulent instabilities [6, 112]. Such a result appears only for tubes deflected with a large local curvature, which is related to a large value of the Dean dimensionless number (see Fig. 2.2).

The incorporation of tube vibrations in the description of nanoscale flows has only been addressed for plug-like flows regardless of the causes, profile or dynamics of flow velocity across the tube, *i.e.*, in these models, flow velocity is a constant parameter of the model [107, 108, 109, 113, 114]. A CM model incorporating both, the effect of fluid motion on tube dynamics, along with a description of fluid dynamics when the confining tube is oscillating is missing in the literature.

As a first approximation, the interaction between an oscillating elastic confining

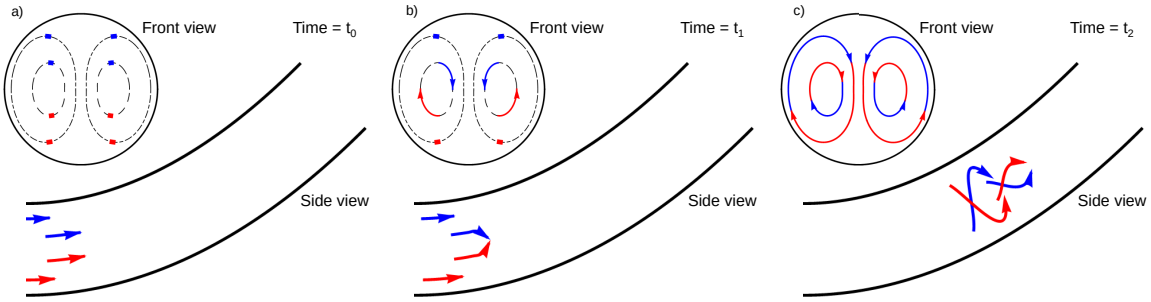

Figure 2.2: Schematic representation of the stream lines of a fluid moving inside a bent static tube, according to the macroscopic stable helicoidal solution developed by Talbot. Left figure indicates that far from the elbow, flow is parallel to the tube; middle figure indicates that as flow approaches an elbow, an helical pattern is developed in the center of the tube; figure at the right indicates that as flow advances further, the helical flow pattern extends outwards. The development of such a helicoidal 3D pattern depends on local bending curvature and tube radius. Taken from [6].

tube and a confined fluid subject to external driving forces could be approximated by simple physical and geometrical constraints, via a formulation based on the Minimal Action's Principle [115, 116, 117, 118, 119, 120, 121], as has been done for others systems to study flow in complex geometries [122, 117, 123, 120]. Such an approach has been useful, for example, to study flow inside compressible nanobubbles [124] and to study systems subject to very complicated physical interactions, like magnetorrheological fluids [125].

2.3 Hybrid models

The desire to account for both levels of physical description has inspired the development of hydrid approaches [7, 126, 127, 128]. The first attempts to conceal the atomistic and the continuum pictures of nanoscale flow phenomena, were developed with the purpose of simulating NEMS and MEMS, that incorporate large fluidic systems where macro, micro and nanometric channels are embedded in intrincated networks and patterns.

Such arrays incorporate bifurcations, elbows and curved channels where multi-scale flow transitions occur. This multi-scale phenomena could also be observed in tubes whose radius lies in the nanoscale, and whose lengths are close to the micro

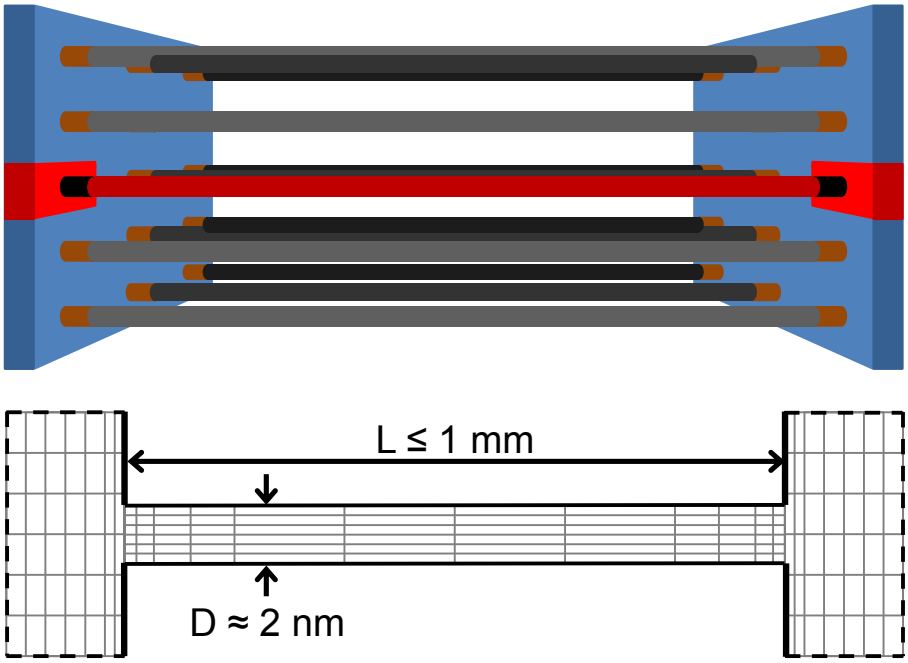

Figure 2.3: Capabilities of simulations performed with hybrid models. Simulation of flow across an array of parallel tubes [7]. Tubes' length is close to the one of typical tubes in carbon nanotube membranes fabricated experimentally [2].

or macroscales (see Fig. 2.3). Under such conditions, these theoretical approaches combine the advantages of a nano and a macroscopic understanding of flow, without the computational expenses required to perform a full MD simulation. Despite of the computational and conceptual conveniences of such strategy, the construction of a hybrid model has to deal with a challenge, namely, the consistent and accurate description of the continuum-to-subcontinuum transition region. Such consistency is related to the continuity of the flow velocity and spatial density profiles, along with other thermodynamic and transport properties. This is achieved by spliting the simulation into three different regions:

- An atomistic region, governed by Newton's second law for the whole set of interacting particles.
- A continuum region, governed by Navier Stokes equations.
- A transition region, where both theoretical treatments should converge.

In general, each hybrid model provides a particular strategy to describe the transition region (see Fig. 2.4a).

The first strategy of hybrid approaches considered the transition region as a portion of the simulation where both the CM and the MD stress tensor computations have the same value [8]. This is possible by computing the CM stress tensor and then, performing a MD dynamics where an additional damping force is exerted on fluid particles in order to relax their momentum to the one obtained within the continuum computation. Afterwards, such treatment was improved by allowing different time scales in the computation of the continuum and discrete regions, enhancing the computational efficiency [129]. Later on, work has been done in order to improve the computation of the thermodynamic properties obtained from MD, along with better representations of the damping force that couples MD and CM computations [130, 131].

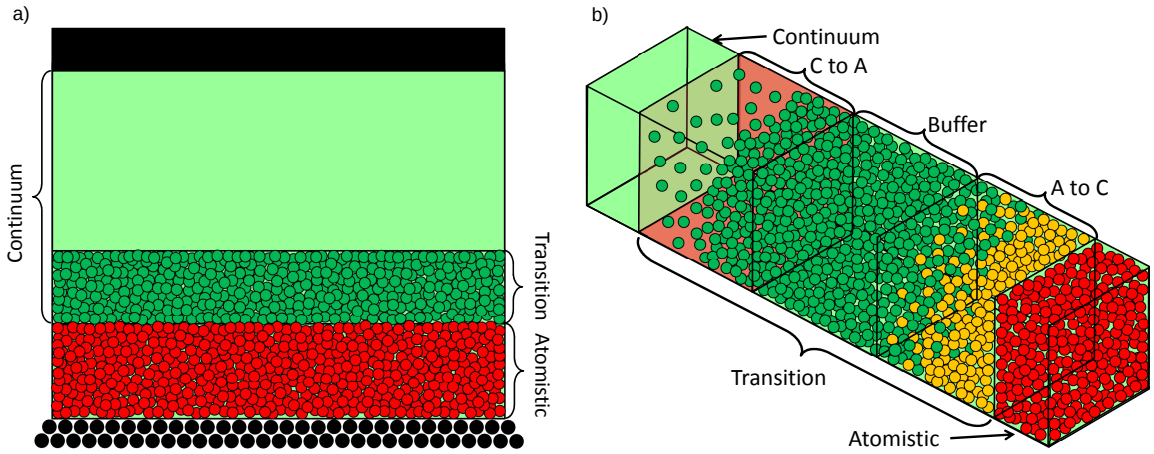

Figure 2.4: Hybrid models. a) Thompson model, with a single transition zone, taken from [8]. b) Flekkoy model, where the transition region has been split into three subregions, taken from [9].

Besides the previous approaches, another strategy was proposed, where the coupling could be obtained with MD simulations, without imposing artificial constrains on the particles, but where a definition of consecutive subregions within the transition zone, called cells [9], was necessary. In this strategy, the cells of the transition zone are given by:

- An atomistic-to-continuum cell (in contact with the atomistic region) where the momentum flux exerted on fluid particles is computed purely by MD means.
- A continuum-to-atomistic cell (in contact with the continuum region) where the momentum flux exerted of fluid particles is computed purely by CM means.
- An intermediate, buffer cell, located between the two previous cells, where particles are subject to a damping force that allows for a smooth transition between the velocity computed in the adjacent cells, to avoid particle stacking.

The coupling between cells takes into account mass conservation, so, any particle leaving one cell, flows into the next one. Such a model is represented in Fig. 2.4b.

More sophisticated hybrid methodologies are developed continuously. They have been useful to profit from the advantages of two complimentary descriptions in the

same system. They have pushed the boundaries of the results obtained merely by MD means, by expanding the system size by several orders of magnitude, and by enhancing the complexity of the systems geometries. Also, in other areas of Soft Matter and Materials Science, such as modelling of heterogeneous porous media and liquid crystals with impurities, there is an alternative hybrid approach that involves MD simulation of coarse-grain particles that take advantage of simplified models of single atoms, molecules, protein fragments, clusters and nanoparticles, spreading different physical, chemical and biological scales.

Despite the advances achieved when atomic and molecular details are fully accounted in the description of nanoscale flow systems, the comprehension of the underlying physical principles presents the same challenge in hybrid frameworks as in MD approaches. That is, there is no simple procedure to reduce the complexity of the fluid/fluid and fluid/tube interactions into global simplified expressions. Moreover, studies of fluid/confining media systems using hybrid methods are dependent on the particular values of the parameters used.

2.4 Remarks on theoretical approaches

It is convenient to remark that the problems associated to MD and hybrid approaches that were previously mentioned, lead to the impossibility to summarize and condensate the existing results in literature, in order to obtain general trends. Advances in MD simulation of nanotubes conveying flow are always restricted to particular fluids, tube dimensions, and fluid-wall interactions; such limitations are not present in CM approaches. In CM frameworks, modelling the complex fluid/tube interactions can be at once done for many fluids, many tube dimensions, and many confining media, via a mean description of the interactions.

In this work, a CM theoretical framework is therefore proposed to study fluids confined within oscillating deflected nanotubes. Given the physical assumptions made,

this scheme allows us to study the system dynamics by means of an analytical treatment, both, for the establishment of the equations of motion, as well as for their solution.

3

Modelling the tube/fluid interaction

In this work, a continuum mechanics theoretical framework is proposed for the study of fluids confined within oscillating deflecting nanotubes. One fundamental physical consideration is assumed, namely, that the fluid can only move parallel to the tube. This assumption is justified because of the impossibility of fluids to develop secondary flows at nano-confinement scales. It turned out to be very convenient mathematically, since it allowed us to study analytically the system dynamics, both in the establishment of the equations of motion, as well as in their solution.

3.1 The principle of minimal action

Our approach is based on the Minimal Action's Principle, which has successfully been used to establish the Navier Stokes dynamics when a fluid is subject to a wide range of forces and restrictions [115, 122, 116, 117, 118, 119, 123, 120]. Such methodology is particularly useful when constrains are imposed on a physical system, since it is capable to account for the restrictions in the resulting equation of motion in a straightforward and consistent manner [124, 121, 115].

The principle of minimal action for an open system, at constant temperature, is given by

$$\delta S + \delta W + \delta C = 0 \tag{3.1}$$

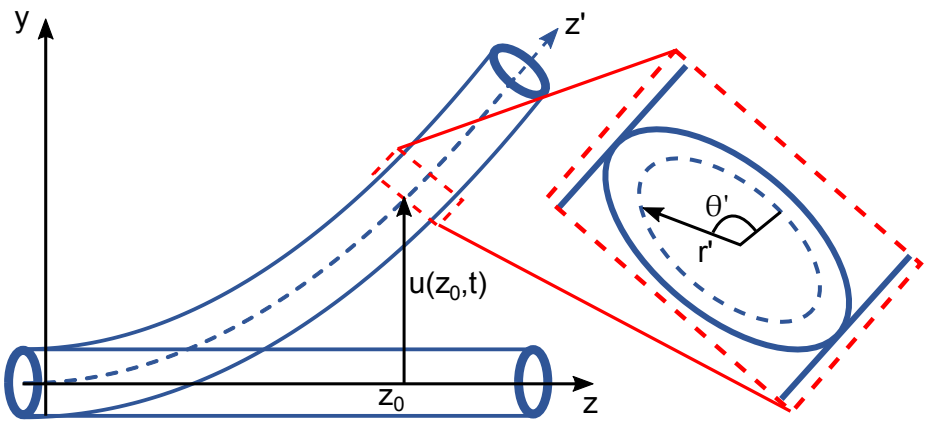

Figure 3.1: Illustration of the system that consists of an elastic tube, described by its vertical displacement, $u(z,t)$, conveying a fluid described by an axial flow, $v(r',\theta',z',t)$, according to a cylindrical coordinate framework located in the tube center as it moves. The z axis coincides with the center of the tube when this one is undeformed.

where S, is the action of the system given in terms of the Lagrangian, $L = T - V$, as

$$S = \int_t L\, dt\,, \tag{3.2}$$

where T is the kinetic energy of the system, and V its potential energy; W accounts for the external and the non-conservative work, applied on the system; and C accounts for the constrains. δS, δW, and δC, denote the variation of those quantities. In what follows, we define the system of study and the physical assumptions considered.

3.2 Theoretical construction of the Minimal action's principle for the tube/fluid system

We model a tube/fluid system via two dynamic variables: the vertical tube position, u, and the flow velocity, v. The physical system is illustrated in Fig. 3.1.

Two natural frames of reference arise in the study of a fluid confined within an oscillating tube: a static inertial frame, for which rectangular coordinates (x, y, z) are used to describe the tube motion; and a moving frame, which is a non-inertial frame and is used to describe the fluid motion, for which primed cylindrical coordinates

(r', θ', z') or equivalently, primed rectangular coordinates (x', y', z') are used, in such a way that the z'-axis is located at the center of tube as it moves.

In Cartesian coordinates, the relation between the inertial and non-inertial frames of reference is given by

$$x = x' \ , \tag{3.3}$$

$$y = u(z', t) + \frac{y'}{\sqrt{1 + \left(\frac{\partial u}{\partial z}(z', t)\right)^2}} \ , \tag{3.4}$$

$$z = z' - \frac{y' \frac{\partial u}{\partial z}(z', t)}{\sqrt{1 + \left(\frac{\partial u}{\partial z}(z', t)\right)^2}} \ . \tag{3.5}$$

Geometrical details and limitations of the coordinates transformation in Eqs. (3.3)-(3.5) are presented in Fig. 3.2. The most important limitation is that the tube radius cannot be arbitrarily large, but it has to be smaller than the maximum local radius of curvature of $u(z, t)$. Typical nanotube dimensions and amplitude of bending motion are in agreement with this consideration.

Since the equation of fluid motion will be given in the non-inertial frame, the spatial derivatives of vector functions -typically, the fluid velocity- need to be incorporated in such a framework. These ones will be computed when required in the derivation. Along with it, the small-deformation limit will allow us to simplify their expressions.

In order to use the Minimal Action's Principle, the comparison field for tube and fluid displacement are denoted by u^{var} and v^{var}, respectively, and defined as follows:

$$u^{var}(z, t, \alpha) = u^{var}(z, t, 0) + \alpha\eta(z, t) \tag{3.6}$$

$$z^{var}_{fluid}(r', z', t, \beta) = v^{var}(r', z', t, 0) + \beta\epsilon(r', z', t) \tag{3.7}$$

and the variations δu and δv are defined as

$$\delta u = \alpha\eta(z, t) \ , \tag{3.8}$$

$$\delta z_{fluid} = \beta\epsilon(r', z', t) \ . \tag{3.9}$$

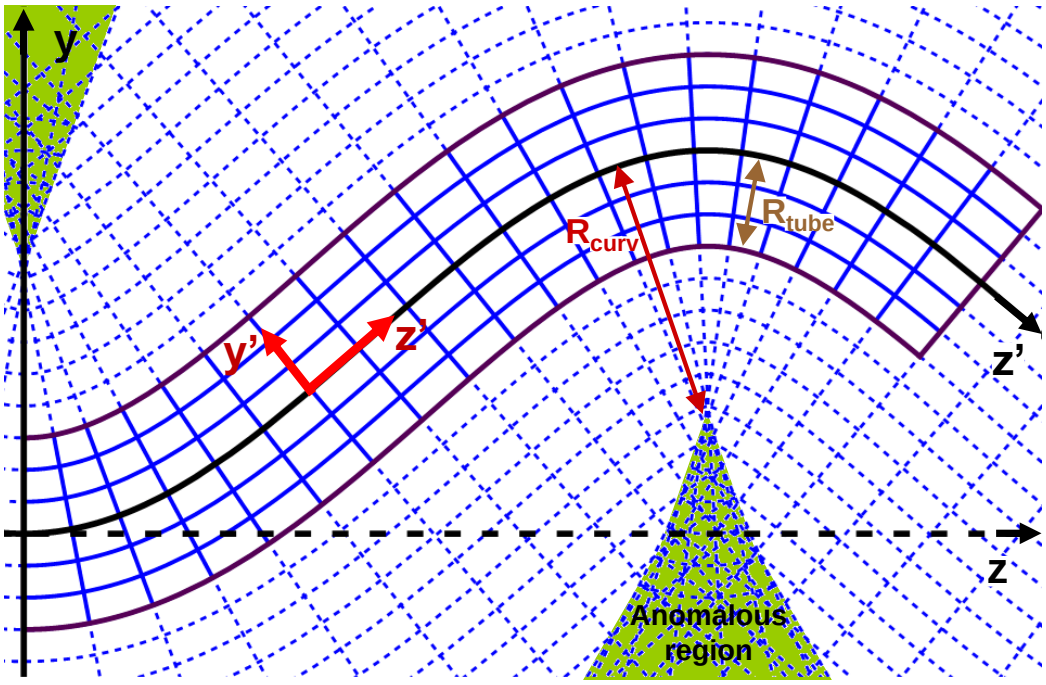

Figure 3.2: The non-inertial frame of reference, that moves with the tube as it vibrates. The defined transformation works fine for low values of y'; however, when the magnitude of y' is larger than the local radius of curvature, the transformation leads to an anomalous behavior and is no longer valid for the theoretical treatment desired.

Arbitrary path functions $\eta(z,t)$ and $\epsilon(r',z',t)$ are subject to the following restrictions:

$$\eta\Big|_{z=0} = 0, \quad \eta\Big|_{z=L} = 0, \quad \frac{\partial\eta}{\partial z}\Big|_{z=0} = 0, \quad \frac{\partial\eta}{\partial z}\Big|_{z=L} = 0 \tag{3.10}$$

$$\eta\Big|_{t=t_1} = 0, \quad \eta\Big|_{t=t_2} = 0, \tag{3.11}$$

$$r'\epsilon\Big|_{r'=0} = 0, \quad r'\epsilon\Big|_{r'=R} = 0, \tag{3.12}$$

$$\epsilon\Big|_{z'=0} = 0, \quad \epsilon\Big|_{z'=L} = 0, \quad \epsilon\Big|_{t=t_1} = 0, \quad \epsilon\Big|_{t=t_2} = 0. \tag{3.13}$$

In the rest of the treatment, we will consider spatial integrals over the tube and fluid subsystems. The tube volume is denoted by V_1, and defined as

$$V_1 = \left\{(r',\theta',z') \;\middle|\; R \le r' \le R_o,\ 0 \le \theta' \le 2\pi,\ 0 \le z' \le L\right\}, \tag{3.14}$$

the fluid volume is denoted by V_2, and defined as

$$V_2 = \left\{(r',\theta',z') \;\middle|\; 0 \le r' \le R,\ 0 \le \theta' \le 2\pi,\ 0 \le z' \le L\right\}, \tag{3.15}$$

whereas the surfaces that surround such volumes are denoted by S_1 and S_2, respectively.

We consider that the tube is an Euler-Bernoulli elastic cylindrical shell subject to small deformations and no axial tension. Also, the tube radius is much smaller than its length, and much smaller that the radius of curvature of the tube at its maximum deflection. The tube is filled with a Newtonian incompressible fluid, since this work is focused on the effect of tube motion in fluid dynamics that is independent on the anomalous rheological behavior of fluids encountered in some experiments, as explained in Section 1.2.2. The system is kept at constant temperature.

The action, S, is given in terms of the Lagrangian of the tube/fluid system, L, as

$$S = \int_t (T_t + T_f - V_t - V_f - V_{t/f})\, dt \ . \tag{3.16}$$

where T_t, T_f, V_t and V_f, denote the kinetic and potential energies of the tube and the fluid, given in terms of the vertical displacement of the tube, u, and the fluid velocity vector, $\vec{v}_{fluid}$; and $V_{t/f}$ is the interaction potential between tube and fluid. [1]

We consider that fluid motion occurs parallel to the tube at any time; this simplifies the treatment of the flow velocity vector in the dynamic framework; it also implies a geometrical restriction that appears as a force in the equations of motion, one that couples the tube and the fluid dynamics. As a consequence of the tube/fluid coupling, that prevents the formation of an angular-dependent helical flow, the angular dependence of fluid velocity is neglected. With these considerations, terms in Eq.(3.16) are given by:

$$T_t = \int_{V_1} \frac{1}{2}\rho_t \left|\vec{v}_{tube}\right|^2 dV \ , \tag{3.17}$$

$$T_f = \int_{V_2} \frac{1}{2}\rho \left|\vec{v}_{fluid}\right|^2 dV \ , \tag{3.18}$$

$$V_t = \int_{V_1} \frac{1}{2}\rho_t \, e_t \left(\frac{\partial u}{\partial z}, \frac{\partial^2 u}{\partial z^2}\right) dV \ \text{ and} \tag{3.19}$$

$$V_f = \int_{V_2} \rho \, e \left(\rho, \frac{\partial \vec{r}_{fluid}}{\partial x'}, \frac{\partial \vec{r}_{fluid}}{\partial y'}, \frac{\partial \vec{r}_{fluid}}{\partial z'}\right) dV \ . \tag{3.20}$$

Here e_t and e are local potential energies per unit mass, for the tube and the fluid, respectively.

The potential energy of the tube is given by the bending energy of an Euler-Bernoulli cylindrical shell, which is a widely used model to study the properties of a bent tube [132, 108, 94, 133]. Despite typical macroscopic tubes consider a mechanical axial load applied on the tube edges, most of experimental settings involving nanotubes does not exert an external axial tension. However, some tension could arise form changes in length during tube deflection; such a change in length is negligible for deformations of small amplitude. Thus, when there is no axial tension,

[1] The study can be applied to any elastic hollowed nanostructure, regardless of the specific geometry of its cross section.

Euler-Bernoulli potential energy leads to the following expression:

$$V_t = \int_{V_1} \frac{1}{2} y^2 E \left(\frac{\partial^2 u}{\partial z^2} \right)^2 dV \ . \tag{3.21}$$

The potential energy of the fluid arises from the interaction between its particles. In a CM approach, the interaction potential between particles responds to changes in the bulk density, ρ, and the strain, $\frac{\partial \vec{r}_{fluid}}{\partial x'_i}$. For this reason, the potential energy is given in terms of a local potential energy per unit mass, e, that depends on those quantities in Eq. (3.20). The potential energy of incompressible fluids with no elastic properties is considered as a constant [115]. Incompressibility is considered as a constrain in fluid dynamics in the theoretical treatment, as described later.

3.2.1 Modelling non-conservative forces: the role of external work

The pressure and the viscosity of the fluid are considered through the term W in Eq. (3.1). The viscous forces are excluded from the potential energy because they are dissipative. From a mathematical point of view, dissipative forces have a functional dependence on fluid velocity and its spatial derivatives, rather than on fluid position. For an incompressible fluid that moves along the z'-direction subject to a stress given by pressure p and the axial component of the viscous shear stress, $\underline{\underline{\tau}}$,

$$\begin{aligned} \delta W &= \int_t \int_{S_2} \vec{F}_{ext} \cdot \delta \vec{r}_{fluid} \, dS \, dt = \int_{S_2} \int_t (-p \underline{\underline{1}} + \underline{\underline{\tau}}) \cdot \hat{n} \cdot \delta \vec{r}_{fluid} \, dS \, dt \ . \\ &= \int_t \int_{r'=0}^{r'=R} \int_{\theta'=0}^{\theta'=2\pi} \int_t (-p + \tau_{r'z'}) \delta z_{fluid} \, d\theta' \, dr' \, dt \Big|_{z'=L} \\ &\quad - \int_t \int_{r'=0}^{r'=R} \int_{\theta'=0}^{\theta'=2\pi} \int_t (-p + \tau_{r'z'}) \delta z_{fluid} \, d\theta' \, dr' \, dt \Big|_{z'=0} \end{aligned} \tag{3.22}$$

where $\hat{n}$ denotes a vector normal to the surface at which the force is exerted.

3.2.2 Modelling the tube/fluid coupling: Restrictions

Finally, constraints should be incorporated.

As previously discussed, in MD simulations, the interaction between tube and fluid is not clearly established in the literature, because the nature of the interaction

forces between water molecules and graphene-like structures has shown to be strongly dependent on the value of the parameters used in the different force fields [23, 35, 37, 48, 49, 61, 46, 98]. The choice of an appropriate force field is always dependent on the type of property desired to simulate computationally [99, 100], rather than on the accurate description of the chemical interaction. In contrast, there are strategies to overcome such difficulty in CM frameworks. In particular, the analytical mechanics approach allows one to account for the interaction between tube and fluid by means of a constraint that couples their motion. In this work, we consider that the tube exerts a force on the fluid that restricts it to move parallel to it. This assumption is characteristic of tubes conveying flow at nanoscales, because the influence of the tube affects all of the confined fluid, not only the water molecules in the tube surface vicinity. For macroscopic tubes, in contrast, the wall only interacts with a thin, infinitesimal layer of fluid, and affects fluid equations as boundary conditions.

The first constraint in our system is therefore, very specific to the system of study: It allows us to incorporate the coupling between tube and fluid dynamics. As the tube oscillates, its direction is time dependent. Our assumption implies that the relative velocity between fluid and tube is always parallel to the tube direction. Mathematically, this is expressed as follows:

$$\vec{v}_{fluid} = \vec{v}_{tube} + v(r', t)\vec{q}_{tan} \ , \tag{3.23}$$

where the relative flow velocity $\vec{v}^{rel}_{fluid} = v(r', t)\vec{q}_{tan}$, whereas $\vec{q}_{tan}$ is a unitary vector that points in the direction of the tube, defined in agreement with the contour lines which are locally transversal to the tube, as were presented in Fig. 3.2b. In Cartesian coordinates, $\vec{v}_{tube}$ and $\vec{q}_{tan}$ are given by

$$\vec{v}_{tube} = \left(0, \frac{\partial u}{\partial t}, 0\right) \ , \tag{3.24}$$

$$\begin{aligned}\vec{q}_{tan}(z',t) &= \left(0, \frac{\frac{\partial u}{\partial z}(z',t)}{\sqrt{1+\left(\frac{\partial u}{\partial z}(z',t)\right)^2}}, \frac{1}{\sqrt{1+\left(\frac{\partial u}{\partial z}(z',t)\right)^2}}\right) \\ &\approx \left(0, \frac{\partial u}{\partial z}(z',t), 1\right) \end{aligned} \tag{3.25}$$

Since Eq. (3.23) is sufficient to account for the tube/fluid interaction, the interaction potential between the tube and the fluid is considered null, *i.e.*, $V_{tube/fluid} = 0$. [1]

The second constraint is the conservation of fluid mass for an incompressible fluid, given by

$$\int_{V_2} \nabla \cdot \vec{v}_{fluid} \; dV = 0 \; . \tag{3.26}$$

Eq. (3.26) is stated for the entire volume of fluid; also, it is important to remark that it holds for an arbitrary volume enclosing fluid, so mass conservation is also valid in its local differential form, as $\nabla \cdot \vec{v}_{fluid} = 0$. From Eq. (3.23) we have

$$\nabla \cdot \vec{v}_{fluid} = \frac{1+\left(\frac{\partial u}{\partial z}\right)^2}{\left(1+\left(\frac{\partial u}{\partial z}\right)^2\right)^{\frac{3}{2}} - r' \sin(\theta') \frac{\partial^2 u}{\partial z^2}} \frac{\partial v}{\partial z'} \; . \tag{3.27}$$

An approximated expression for the prefactor is given as follows. In the small deformation limit, the numerator can be approximated as the unit. Also, if the tube radius is much smaller than the radius of curvature of the tube at its maximum deflection (proportional to $1/\frac{\partial^2 u}{\partial z^2}$, then the denominator can also be approximated as the unit. Hence, the mass conservation of fluid is simplified as

$$\frac{\partial v}{\partial z'} = 0 \tag{3.28}$$

Without loss of generality, it is possible to rewrite Eq. (3.28) in terms of the fluid displacement, z_{fluid}, which is related to fluid velocity by $v = \frac{\partial z_{fluid}}{\partial t}$-. Thus, integration in time of the restriction in Eq. (3.28) leads to

$$\frac{\partial z_{fluid}}{\partial z'} = 0 \; , \tag{3.29}$$

[1] An alternative formulation could be proposed in order to account for this restriction through an interaction potential.

and the restriction C incorporated in the minimal action's principle is given by

$$C = \int_t \int_{V_2} \Lambda(z', t) \frac{\partial z_{fluid}}{\partial z'} dV \, dt \ , \tag{3.30}$$

where $\Lambda(z', t)$ is a Lagrange multiplier. Eq. (3.30) has been typically used in the context of deformable media rather than in the field of fluid mechanics, and it is useful since it simplifies the mathematical treatment [115, 134, 135].

3.3 Obtention of equations of motion

The variation of the restriction given by Eq. (3.30), leads to

$$\delta C = \int_{S_2} \Lambda \delta z_{fluid} \, dS - \int_{V_2} (\nabla \cdot \Lambda) \cdot \hat{n} \delta z_{fluid} \, dV \ . \tag{3.31}$$

When the surface integral in Eq. (3.31) is incorporated along with the term δW given in Eq. (3.22), into the minimal action's principle in Eq. (3.1), it becomes clear the physical meaning of the Lagrange multiplier, Λ, since it turns out to be a component the Cauchy's stress tensor, given by

$$\Lambda = (-p\underline{\underline{1}} + \underline{\underline{\tau}}) \cdot \hat{n} \tag{3.32}$$

However, another component of the stress tensor is not included in Λ, which accounts for the change in flow velocity direction as it goes through a bended oscillating tube. Such a term will be given by the other restriction.

Also, it is possible to see that the volume integral in δC in Eq. (3.31) incorporates a force in the equation of motion, given by the divergence of Λ, as follows:

$$(\nabla \cdot \Lambda) \cdot \hat{n} = -\frac{\partial p}{\partial z'} + \left(\nabla \cdot \underline{\underline{\tau}}\right) \cdot \hat{n} \ , \tag{3.33}$$

where the stress tensor of a Newtonian fluid and its divergence must be given in terms

of the dynamic coordinates (r', θ', z'), leading to the following expression:

$$\begin{aligned}\left(\nabla \cdot \underline{\underline{\tau}}\right) \cdot \hat{n} = \quad & \frac{\partial^2 v}{\partial r'^2} + \frac{1}{r'}\frac{\partial v}{\partial r'} + \frac{1}{r'^2}\frac{\partial^2 v}{\partial \theta'^2} - \frac{\frac{\partial^2 u}{\partial z'^2}\left(\sin(\theta')\frac{\partial v}{\partial r'} + \frac{\cos(\theta')}{r'}\frac{\partial v}{\partial \theta'}\right)}{\left(1 + \left(\frac{\partial u}{\partial z}\right)^2\right)^{3/2} - r'\sin(\theta')\frac{\partial^2 u}{\partial z^2}} \\ & - \frac{\left(\frac{\partial^2 u}{\partial z^2}\right)^2 v}{\left(\left(1 + \left(\frac{\partial u}{\partial z}\right)^2\right)^{3/2} - r'\sin(\theta')\frac{\partial^2 u}{\partial z^2}\right)^2}\end{aligned} \tag{3.34}$$

When the small deformation limit is considered in the divergence of stress tensor in Eq. (3.34), and the angular dependence of the flow velocity is neglected, the last three terms in Eq. (3.34) vanish, leading to the following approximated expression:

$$\left(\nabla \cdot \underline{\underline{\tau}}\right) \cdot \hat{n} = \frac{\partial^2 v}{\partial r'^2} + \frac{1}{r'}\frac{\partial v}{\partial r'} \tag{3.35}$$

The prime notation in (x', y', z') or (r', θ', z') will be omitted in the rest of the theoretical treatment, it is implicitly understood that the fluid velocity is studied in the dynamic coordinate framework, whereas the tube position is studied in the static framework. Including all the results from Eqs. (3.16-3.35) into Hamilton's Principle (Eq. (3.1)), two coupled equations of motion are obtained, for the dynamics of the tube displacement $u(z,t)$ and the fluid velocity $v(r,t)$. These are:

$$\left(\rho A_f + \rho_t A_t\right)\frac{\partial^2 u}{\partial t^2} + EI\frac{\partial^4 u}{\partial z^4} + \rho A_f \langle v^2 \rangle \frac{\partial^2 u}{\partial z^2} + 2\rho A_f \langle v \rangle \frac{\partial^2 u}{\partial z \partial t} + \rho A_f \frac{\partial u}{\partial z}\frac{\partial \langle v \rangle}{\partial t} = 0 \tag{3.36}$$

$$\rho\frac{\partial v}{\partial t} + \frac{\partial p}{\partial z} - \mu\left(\frac{\partial^2 v}{\partial r^2} + \frac{1}{r}\frac{\partial v}{\partial r}\right) + \rho g(t) v + \rho h(t) = 0 \ , \tag{3.37}$$

A_f and A_t are the cross sectional areas of fluid and tube, respectively, I is the second moment of inertia of a cylindrical hollowed tube, given by

$$I = \int_A y^2 dA = \frac{\pi}{4}\left(R_o^4 - R^4\right) \tag{3.38}$$

where R_o and R are the tube's outer an inner radii, respectively. $\langle v \rangle$, $\langle v^2 \rangle$, are averages of the velocity and the squared velocity over the cross sectional area, and are given by

$$\langle v \rangle = \frac{\int_0^R 2\pi r v(r,t)\, dr}{A_f} \ , \tag{3.39}$$

$$\langle v^2 \rangle = \frac{\int_0^R 2\pi r (v(r,t))^2 \, dr}{A_f} \ , \tag{3.40}$$

and $g(t)$ and $h(t)$ have been defined as

$$g(t) = \frac{2}{L} \int_0^L \frac{\partial u}{\partial z} \frac{\partial^2 u}{\partial z \partial t} dz \ , \tag{3.41}$$

$$h(t) = \frac{1}{L} \int_0^L \left(\frac{\partial u}{\partial t} \frac{\partial^2 u}{\partial z \partial t} + \frac{\partial u}{\partial z} \frac{\partial^2 u}{\partial t^2} \right) dz \ , \tag{3.42}$$

where L is the tube length.

It is useful to give a name to the terms involved in Eq. 3.37 The term $-\rho g(t) v$ in Eq. (3.37) is the Coriolis force. The term $-\rho h(t)$ —that we call effective pushing force— is the sum of two contributions: the centrifugal force, given by $-\rho \frac{\partial u}{\partial t} \frac{\partial^2 u}{\partial z \partial t}$ and the pushing force exerted on the fluid, given by $-\frac{\partial u}{\partial z} \frac{\partial^2 u}{\partial t^2}$. Their interpretation will be established later in this work. Accordingly, in Eq. (3.36), the term $-\rho A_f \langle v^2 \rangle \frac{\partial^2 u}{\partial z^2}$ is called the centrifugal force; the term $-2\rho A_f \langle v \rangle \frac{\partial^2 u}{\partial z \partial t}$ is the Coriolis force; and the term $-\rho A_f \frac{\partial u}{\partial z} \frac{\partial \langle v \rangle}{\partial t}$ is the fluid pushing force. More mathematical details on the derivation of Eqs. (3.36) and (3.37) are included in Appendix A.2.

Eqs. (3.36) and (3.37) are two coupled integro-differential equations for the dynamics of the tube displacement $u(z,t)$ and the fluid velocity $v(r,t)$. They constitute the theoretical framework that we will use to study fluid dynamics in oscillating nanotubes, which is the central topic of this Thesis. They will also be useful to study the tube dynamics when it is influenced by the fluid motion and to propose alternative experiments to determine flow in nanotubes that might eventually change the current paradigma of flow enhancement.

3.3.1 Boundary conditions

In order to get a complete theoretical framework to study the coupled tube/fluid dynamics, it is necessary to incorporate boundary conditions at the tube-fluid interface and at the tube extremes, to solve the equations of motion 3.36 and 3.37.

In the literature, boundary conditions for the flow velocity at the tube walls account for the polarity of the tube/fluid interaction via a slip length. From a mathematical point of view, the slip length is related to the flow velocity at the fluid/wall interface. From a physical perspective, it is related to the friction exerted by the tube wall on the fluid particles. However, there is no clear agreement on the realistic functional form that slip velocity should have as a function of the flow velocity spatial derivatives. In this work, we desire to establish the features that arise in the fluid dynamics, due to the tube vibrations, regardless of the fluid slippage. For this reason, we consider no slip at the tube/fluid interface.[1] This, is expressed as follows:

$$v(r = 0, t) = \text{finite and } v(r = R, t) = 0 \tag{3.43}$$

The boundary conditions on the tube extremes depend on the experimental arrangement employed in a particular nanofluidic system. They reflect the way in which tube edges are constrained. The most common boundary conditions exerted on the tube edges are:

- Pinned edge. It consists of an edge, whose position is fixed with no stress exerted to deflect the tube. Therefore, there is no bending at the tube extreme. Mathematically, a tube pinned at position $z = z_0$ is described by

$$u(z_0, t) = 0 \text{ and } \frac{\partial^2 u}{\partial z^2}(z_0, t) = 0\,. \tag{3.44}$$

- Clamped edge. It consists of an edge where the position is fixed and a stress is exerted on the tube to keep it aligned horizontally. Mathematically, a tube clamped at position $z = z_0$ is given by

$$u(z_0, t) = 0 \text{ and } \frac{\partial u}{\partial z}(z_0, t) = 0 \tag{3.45}$$

[1] This condition can be easily changed, for instance by a Navier hypothesis for the slip velocity.

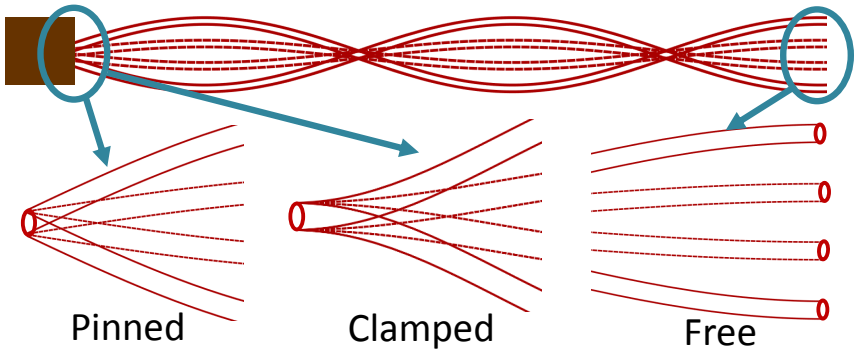

Figure 3.3: Illustration of the possible boundary conditions used for the tube edges. These ones reflect the way in which the tube edges are supported in experimental settings.

- Free edge. It consists of an edge where no restriction is imposed regarding its position or inclination. Therefore, the tube edge is relaxed with no deflection, so there is no bending moment nor shear force exerted on such edge. Bending moment is related to the local tube curvature, whereas shear force is related to the spatial derivative of tube curvature. Mathematically, this is expressed as

$$\frac{\partial^2 u}{\partial z^2}(z_0, t) = 0 \text{ and } \frac{\partial^3 u}{\partial z^3}(z_0, t) = 0 \tag{3.46}$$

These conditions are depicted in Fig. 3.3. Since a tube has two edges and each edge can be subject to any of the three conditions described above, there are six possible combinations of boundary conditions: pinned-pinned, pinned–clamped, pinned-free, etc, etc.).

Among these possibilities, one is rather atypical: a free-free tube. The other 5 conditions enclose a big spectrum of experimental arrangements and situations. In this work, our main focus is to establish general trends shared by all sets of boundary conditions for the tube extremes.

4

General notions on the tube/fluid interaction

The theoretical treatment described in Chapter 3 allowed us to construct a set of equations of motion that couple the tube and the fluid dynamics.

In order to obtain any relevant result from such equations, it is necessary to have a strategy for their solution. The typical procedure in the literature to deal with complex non-linear systems of integro-differential equations, consists of the numerical integration of the equations following several numerical methods. Such strategy leads to an exact description of the time evolution of tube and fluid motion when the value of every physical parameter is provided. The computational expense demanded for such calculations is high, and practical mathematical details of the solution depend on an analysis of the magnitude of the physical parameters involved in the system; otherwise, the computations may diverge or lead to spurious results. However, the most important limitation of the numerical solutions relies on the amount of simulations required to obtain a qualitative trend among the results, since this approach requires performing a large number of calculations spanning the whole spectrum of values of each physical parameter.

In contrast, the analytical solutions convey significant convenience for further analysis. First, an analytical treatment allows one to identify and understand the role of the different physical parameters and forces in the final solution for fluid and tube dynamics. Also, the computation of asymptotic limits is usually attainable, where the theoretical model developed can be tested when compared with previous results

from the literature.

The obtention of analytical solutions usually comes along with approximations and simplifications that lead to a deviation from the exact solution. Depending on the complexity of the equations and their solutions, the analytical approximated solutions may keep the qualitative features of the exact solution and differ only in quantitative aspects. However, in some other cases, the approximated results ignore qualitative characteristics of the physics underlying the theoretical model.

In general, the choice between approximated analytical results and exact numerical ones is specific to the area of study, and for the desired applications of the results. Sometimes the decision is limited by the difficulty to obtain approximations that allow for analytical solutions that still contain relevant information of the system.

In this work, a theoretical treatment is carried out to derive analytical expressions for the solution of the system of coupled equations. First, the system of coupled equations is expressed in terms of dimensionless parameters that allow us to compare systematically the influence of one of the dependent dynamic variables on the other one. In other words, it is possible to quantify the influence of fluid motion on the tube dynamics and vice versa.

Such analysis allows one to establish regimes in which one part of the system -for instance, the tube- can be considered independent of the other one -for instance, the fluid-, but with an equation for the fluid dynamics dependent on tube parameters. To this regime we refer to as the one in which the tube influences the fluid. The complementary case would be given when the fluid equation is independent on the tube vibrations, but the tube dynamics depends on the way that the fluid is flowing within the tube. To this regime we refer to as the one in which the fluid influences the tube. Clearly, there is also the fully decoupled case, in which non of the system parts influences the other one.

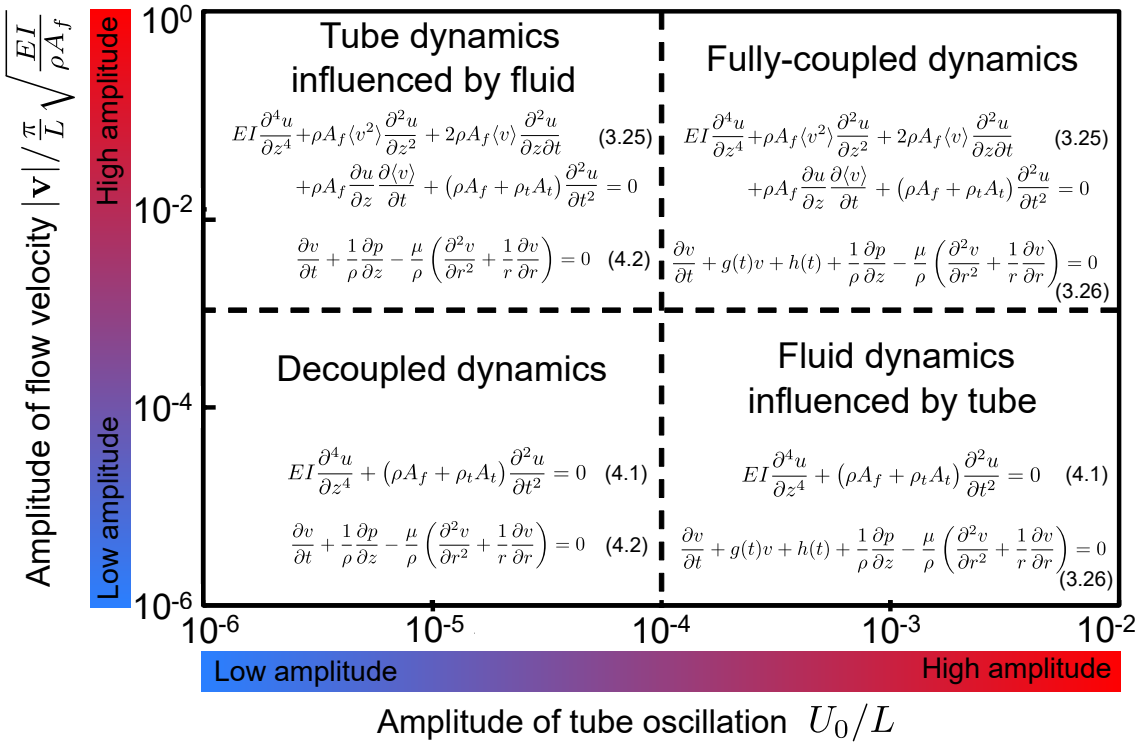

Figure 4.1: Effect of the amplitude of tube and fluid motion in the coupling predicted in this model.

4.1 Decoupling the tube and fluid motion

The fully decoupled set of equations is:

$$EI\frac{\partial^4 u}{\partial z^4} + \left(\rho A_f + \rho_t A_t\right)\frac{\partial^2 u}{\partial t^2} = 0\,, \tag{4.1}$$

$$\frac{\partial v}{\partial t} + \frac{1}{\rho}\frac{\partial p}{\partial z} - \frac{\mu}{\rho}\left(\frac{\partial^2 v}{\partial r^2} + \frac{1}{r}\frac{\partial v}{\partial r}\right) = 0\,. \tag{4.2}$$

Equation (4.1) is, the Euler-Bernoulli model for an elastic cylindrical shell filled with a stagnant fluid. Equation (4.2) is the Navier-Stokes equation of uniaxial flow moving inside a cylindrical static tube.

Comparing Eqs. (3.36) and (3.37) with Eqs. (4.1) and (4.2), we can realize that the decoupled equations are particular cases of the coupled ones. Equation (4.1) is a particular case of Eq. (3.36) when the flow velocity is null ($v(r,t) = 0$). In turn, equation (4.2) is a particular case of Eq. (3.37) when the amplitude of tube motion is null ($u(z,t) = 0$).

Because of this totally decoupled limit, we think of Eq. (3.36) as the equation that describes the tube dynamics, since it is basically a modified Euler-Bernoulli equation [133]; whereas we think of Eq. (3.37) as the one describing the fluid dynamics, as it is basically a modification of Navier-Stokes equation. In other words, the vertical oscillation of the tube is affected by fluid motion; and the dynamics of the fluid is affected by tube vibrations.

In general, the solution of Eqs. (3.36) and (3.37) is not possible by analytical means, because it is not possible to separate the tube displacement, $u(z,t)$, and the fluid flow, $v(r,t)$, variables. It is necessary to solve both integro-differential equations simultaneously. However, it is possible to establish additional physical considerations that make possible an analytical solution, and the clue is to look for conditions for which one of the dynamic variables is weakly dependent on the other one. These considerations lead to analytical solutions for tube and fluid dynamics in two regimes:

- When the amplitude of the tube vibration is very small, so the fluid dynamics is not affected by tube oscillation, but the tube equations keeps the parameters from fluid flow.

- When the flow magnitude is small, so the tube dynamics is not affected by fluid motion, but the flow equation contain terms from the tube dynamics.

Such regimes are discussed at length in the following two sections.

Fig. 4.1 summarizes four dynamic regimes. Equations in the upper-left quadrant in Fig. 4.1 (high flow magnitude and low tube oscillation amplitude) allow one to study the influence of fluid motion on tube dynamics. In contrast, the lower-right quadrant (low flow magnitude and high tube oscillation amplitude) establish a framework to explore the influence of tube vibration on the fluid dynamics. The upper-right quadrant corresponds to a case where both fluid and tube motion are of a high magnitude, so none of the terms in Eqs. (3.36) and (3.37) can be neglected. Finally, the lower-left

quadrant shows the equations of the case were tube and fluid dynamics that are fully decoupled and the dynamics of each element is "blind" to the motion of the other one, except at the fluid-tube boundary conditions.

4.2 Tube dynamics influenced by fluid motion

The limit that concerns this section corresponds to the regime of the upper left frame in Fig. 4.1 and is described by Eqs. (3.36) and (4.2).

To derive such a limit, it is necessary to explore the role of the amplitude of the tube deformation on the modified Navier Stokes equation. An inspection of Eq. (3.37) shows that the amplitude of tube deformation was incorporated in the Coriolis and effective pushing terms, via the functions $g(t)$ and $h(t)$, respectively, as defined in Eqs. (3.41) and (3.42).

Regardless of the specific details of the tube dynamics, we could say that the tube oscillates around its equilibrium position (which is $u(z,t) = 0$), with a maximum amplitude given by

$$Max\left(u(z,t)\right) = U_0\,. \tag{4.3}$$

For a tube of length L, its maximum deformation can be estimated as

$$\mathrm{Max}\left(\frac{\partial u}{\partial z}\right) \approx \frac{U_0}{L} \tag{4.4}$$

whereas the maximum tube vertical velocity can be estimated as

$$\mathrm{Max}\left(\frac{\partial u}{\partial t}\right) \approx \nu_0 U_0 \approx \left(\frac{1}{L^2}\sqrt{\frac{EI}{\rho A_f + \rho_t A_t}}\right) U_0 \tag{4.5}$$

where ν_0 is the characteristic frequency of motion of an elastic tube of length L.

Eq.(4.4) is necessary to estimate the order of magnitude of the Coriolis and effective pushing forces, namely, $\rho g(t) v$ and $\rho h(t)$. In order to compare these tube-induced forces with the pressure difference to which the fluid is subject to, we write forces times the tube length and incorporate typical values of the physical parameters, of different materials and tube geometries, from Table 1.3.1, to obtain:

$$|\rho g(t) v L| \approx \sqrt{E\,\rho v_{max}^2}\frac{R_o}{L}\frac{U_0^2}{L^2} \approx \frac{U_0^2}{L^2}\left[10^4 - 10^6\right] \text{Pa} \ , \tag{4.6}$$

$$|\rho h(t) L| \approx E\ \frac{R_0^2}{L^2}\frac{U_0^2}{L^2} \approx \frac{U_0^2}{L^2}\left[10^4 - 10^6\right] \text{Pa} \ , \tag{4.7}$$

The sum of the pressure gradient, Coriolis and effective pushing forces is rewritten in Eq. (3.37), as follows:

$$\rho\frac{\partial v}{\partial t} - \mu\left(\frac{\partial^2 v}{\partial r^2} + \frac{1}{r}\frac{\partial v}{\partial r}\right) + f_{global} = 0 \ , \tag{4.8}$$

where the global driving force f_{global} is given by

$$f_{global} = \frac{\partial p}{\partial z} + \rho g(t) v + \rho h(t) \ , \tag{4.9}$$

When Eqs. (4.6) and (4.7) are compared with typical pressure drops along a tube, which are in the range of $[10^5 - 10^7]$ Pa, the role of the maximum tube deformation becomes clear in the global driving force in Eq. (4.9). Roughly-speaking, U_0^2/L^2 quantifies the weight of pressure drop and the tube-induced forces (multiplied by tube length) in Eq. 3.37. For example, a relative amplitude of tube oscillation of 1% ($U_0/L = 0.01$) implies that a typical pressure drop is greater than the tube-induced forces (multiplied by tube length) by five orders of magnitude.

Therefore, the regime in which fluid dynamics does not depend on tube motion, corresponds to the one for which the amplitude of tube oscillations is small. In this work, we take a threshold of $U_0/L = 10^{-4}$ to consider the fluid motion independent of the tube dynamics. In other words, we neglect the tube-induced forces on the fluid (multiplied by tube length) when there are approximately nine orders of magnitude smaller than typical values of the pressure drop exerted on the fluid.

In this regime, Eq. (3.37) reduces to the classical Navier-Stokes equation given by Eq. (4.2). The solution of Eq. (4.2) is independent of the tube motion. Once flow velocity is determined for a specific driving force, it is incorporated into the tube dynamics, in Eq. 3.36, via the functions $\langle v \rangle$ and $\langle v^2 \rangle$.

Regardless of the specific driving force exerted on the fluid, one can establish general features of the influence of fluid motion on tube dynamics. For the subsequent discussion, the average flow velocity and the average squared flow velocity, are incorporated in the tube dynamics by defining two parameters to describe fluid flow velocity,

$$v_{rms} \equiv \sqrt{\langle v^2 \rangle}\,, \qquad\qquad \beta \equiv \frac{\langle v \rangle}{\sqrt{\langle v^2 \rangle}}\,. \tag{4.10}$$

The definitions of v_{rms} and β allow to write Eq. (3.36) as:

$$(\rho A_f + \rho_t A_t)\frac{\partial^2 u}{\partial t^2} + EI\frac{\partial^4 u}{\partial z^4} + \rho A_f v_{rms}^2 \frac{\partial^2 u}{\partial z^2} + 2\rho A_f \beta v_{rms}\frac{\partial^2 u}{\partial z \partial t} + \rho A_f \beta \frac{\partial u}{\partial z}\frac{\partial v_{rms}}{\partial t} = 0 \tag{4.11}$$

Equation (4.11) is a fourth-order linear partial differential equation for the tube vertical displacement $u(z,t)$. Its solution is the superposition of planar waves of complex frequency that depend on the flow velocity via v_{rms} and β and lead to unstable tube motion in some cases. The consequences of this result deserve further study, and could be of great importance for technological purposes, in order to design strategies for indirect measurement of flow velocity in nanotubes and nanostructures. This will be exploited and described in Chapter 5.

4.3 Fluid dynamics influenced by tube vibrations

The limit that concerns this section corresponds to the regime of the lower right frame in Fig. 4.1 and is described by Eqs. (3.37) and (4.1).

The key point to establish the equations governing this regime is to look at the relative value of the fluid-induced forces in Eq. (3.36) relative to the elastic force, which causes the propagation of elastic waves along the tube.

Eq. (3.36) states that in the absence of fluid motion, the tube dynamics is only given by the elastic bending force, leading to the Euler Bernoulli model given by Eq. (4.1). Solutions of Eq. (4.1) are plane waves of the form

$$u(z,t) = U_0 e^{i(kz-\omega t)}\,, \tag{4.12}$$

where U_0 is the amplitude, k the wavenumber and ω corresponds to the frequency; frequency and wavenumber are related by a dispersion relation, through

$$\omega = \pm k^2 \sqrt{\frac{EI}{\rho A_f + \rho_t A_t}}\,. \tag{4.13}$$

where sign of frequency indicates the direction of the travelling wave, since a plane wave can be rewritten as

$$u(z,t) = U_0 e^{i\,k(z - v_{prop}t)}\,, \tag{4.14}$$

where the phase velocity of propagation of the plane wave is given by

$$v_{prop} = \left|\frac{\omega}{k}\right| = k\sqrt{\frac{EI}{\rho A_f + \rho_t A_t}}\,. \tag{4.15}$$

For a tube of finite length L, the wavenumber is proportional to $1/L$, and we can estimate the velocity of propagation of the elastic waves along the tube as

$$v_{prop} \approx \frac{1}{L}\sqrt{\frac{EI}{\rho A_f + \rho_t A_t}}\,. \tag{4.16}$$

Then, Eq. (3.36) is rewritten in terms of the velocity of propagation, as follows:

$$\begin{aligned} &EI\frac{\partial^4 u}{\partial z^4} + \rho A_f \frac{1}{L^2}\left(\frac{EI}{\rho A_f + \rho_t A_t}\right)\frac{\langle v^2\rangle}{v_{prop}^2}\frac{\partial^2 u}{\partial z^2} + \frac{2\rho A_f}{L}\sqrt{\frac{EI}{\rho A_f + \rho_t A_t}}\frac{\langle v\rangle}{v_{prop}}\frac{\partial^2 u}{\partial z \partial t} \\ &+\frac{\rho A_f}{L}\sqrt{\frac{EI}{\rho A_f + \rho_t A_t}}\frac{\partial u}{\partial z}\frac{\partial}{\partial t}\left(\frac{\langle v\rangle}{v_{prop}}\right) + (\rho A_f + \rho_t A_t)\frac{\partial^2 u}{\partial t^2} = 0 \end{aligned} \tag{4.17}$$

In order to estimate the order of magnitude of each term in Eq. (4.17), it is necessary to estimate the derivatives of u and v. Spatial derivatives can be estimated in terms of the characteristic tube length L, shereas the derivatives in time are estimated as

$$\frac{\partial\langle v\rangle}{\partial t} \approx \nu_\mu v_{max} \approx \left(\frac{\mu}{\rho R^2}\right) v \tag{4.18}$$

where ν_μ is the characteristic frequency of a confined Newtonian fluid and μ is the fluid viscosity.

Incorporating Eqs. (4.5) and (4.18) into Eq. (4.17), it is possible to estimate the fluid-induced forces that affect the tube motion in Eq. (3.36) and compare them with the elastic term $F_{ela} = EI\frac{\partial^4 u}{\partial z^4}$. Using typical parameters from Table 1.3.1, each force in Eq. (reftube reescaled freq) divided by the amplitude of tube displacement, U_0, is given by

$$F_{Cent}/U_0 \approx \left(\frac{EI}{L^4}\right)\frac{\rho A_f}{\rho A_f + \rho_t A_t}\frac{v^2}{v_{prop}^2} \approx \left(10^0 - 10^2 \text{ Pa}\right)\frac{v^2}{v_{prop}^2} , \tag{4.19}$$

$$F_{Cor}/U_0 \approx \left(\frac{EI}{L^4}\right)\frac{2\rho A_f}{\rho A_f + \rho_t A_t}\frac{v}{v_{prop}} \approx \left(10^0 - 10^2 \text{ Pa}\right)\frac{v}{v_{prop}} , \tag{4.20}$$

$$F_{push}/U_0 \approx \left(\sqrt{\frac{EI}{L^4}}\sqrt{\nu_\mu(\rho A_f + \rho_t A_t)}\right)\frac{2\rho A_f}{\rho A_f + \rho_t A_t}\frac{v}{v_{prop}} \approx \left(10^{-2} - 10^0 \text{ Pa}\right)\frac{v}{v_{prop}} . \tag{4.21}$$

Then, magnitude of the fluid-induced forces is compared with the typical values of the elastic bending force, given by

$$F_{elastic}/U_0 \approx \frac{EI}{L^4} \approx 10^0 - 10^2 \text{ Pa} . \tag{4.22}$$

Such analysis allows one to consider that the velocity ratio v/v_{prop} quantifies the relative dominance of the Coriolis force and the pushing force respect to the elastic force, whereas the ratio v^2/v_{prop}^2 plays the same role for the Centrifugal force.

For nanotubes of typical lengths (between $10\mu m$ and $1mm$) and Young moduli (between $0.1TPa$ and $1TPa$) [107, 47], the velocity of propagation of elastic waves lies between 10 and 100 m/s.[1] In comparison, flow velocities measured across such nanotubes are about $0.1m/s$ and lower, when driving forces of low to medium magnitude are exerted on such confined fluids [35, 2, 38]. Thus, in the low pressure gradient regime, $v/v_{prop} < 0.01$ and it the fluid-induced forces turn out to be 2 or more orders of magnitude lower than the elastic force. Summarizing, if low pressure gradients are exerted on the fluid, it is possible to describe the tube dynamics independently of the fluid motion; however, the fluid dynamics will be modified by the tube oscillations.

[1] A bent tube is a dispersive media for elastic waves, their phase velocity is strongly dependent on their wavenumber.

In other words, Eq. (4.1) is solved for the tube displacement $u(z,t)$ considering initial and boundary conditions that account for the specific experimental setting intended to study; the solution is incorporated into Eq. (3.37) via the auxiliar functions $g(t)$ and $h(t)$. Finally, Eq. (3.37) should be solved for the flow velocity $v(r,t)$.

A solution for the flow velocity accounting for the no-slip boundary condition at the tube walls -as stated in Eq. (3.43)-, can be obtained without considering an explicit form of the functions $g(t)$ and $h(t)$. This solution is given by

$$\begin{aligned} v(r,t) &= \frac{e^{-\int_{t_0}^{t} g(t')dt'}}{2\pi} \\ &\times \int_{-\infty}^{\infty} \frac{1}{i\rho\lambda} \left(1 - \frac{J_0\sqrt{\frac{i\rho\lambda r^2}{\mu}}}{J_0\sqrt{\frac{i\rho\lambda R^2}{\mu}}} \right) \int_{-\infty}^{\infty} \left(\frac{\partial p}{\partial z} + \rho\, h(t') \right) e^{\int_{t_0}^{t'} g(t'')dt''} e^{-i\lambda t'} dt' e^{i\lambda t} d\lambda \end{aligned} \tag{4.23}$$

where J_0 is the zero-order Bessel function. An explicit solution of $v(r,t)$ is given when a specific form for the tube motion $u(z,t)$ is incorporated via the functions $g(t)$ and $h(t)$. Details of the derivation of the solution for $v(r,t)$ in Eq. (4.24) are presented in Appendix A.3.

In general terms, an inspection of the analytical solution in Eq. (4.24) allows one to explain the influence of tube vibrations on fluid dynamics, via the functions $g(t)$ and $h(t)$. Particularly, $h(t)$ plays a role similar to the pressure gradient, since both appear as quantities added up in the term $(\frac{\partial p}{\partial z} + \rho h(t))$. In other words, the tube motion induces a second driving force on the fluid that, in general, is oscillating -since the tube position is also oscillating-.

In contrast, $g(t)$ has a complex role in the solution, because it is incorporated as the argument of an exponential function, and then multiplied by other driving forces. This occurs because of the specific form of the term, $\rho g(t) v$, where the overall flow velocity (which will be time dependent due to the tube vibrations) is multiplied by the oscillatory function $g(t)$. In the absence of $g(t)$, the influence of tube on fluid motion could be explained in a simple statement: it adds a second oscillatory driving force, so the overall flow velocity is simply a sum of the contributions of each frequency

peak, as described in the classical theory of pulsatile flow [136]. However, the Coriolis force modifies qualitatively the response of the fluid to the driving forces, because the product of oscillatory functions usually has a more complex frequency spectrum than the one of the original factors.

The peculiar phenomena arising from Eq. (4.24) deserve a deeper and systematic study. This will be the subject of the last chapter in this Thesis where the fluid dynamics is studied, when it is influenced by representative cases of tube motion.

4.4 Understanding the dynamic tube/fluid coupling

The equations of motion that described the coupled tube/fluid dynamics can be seen as a variation of the Euler-Bernoulli equation for bending mechanics subject to the effect of fluid motion inside the tube [Eq. (3.36)] and a variation of the Navier-Stokes equation for a viscous fluid subject to the effect of tube motion inside the tube [Eq. (3.37)]. The modification done in tube dynamics has already been explored in literature [132]. However, in the case of the tube forces acting on the fluid, it is necessary to do the first steps towards the comprehension of the effect of the tube motion on fluid dynamics.

The theoretical treatment proposed in this work has incorporated the condition of parallelism between the tube and the fluid motion and, as a consequence, coupled forces have appeared in the fluid dynamics. When the fluid is restricted to move along the tube axis, it implies that a force will be exerted by the tube on the fluid, such that any force that tends to avoid such parallel motion, will be cancelled. In order to know which forces are present when a fluid is confined in an oscillating tube, it is easier to ask what happens to a free fluid particle which is initially moving in an static tube, when such tube starts developing an oscillatory motion.

For macroscopic tubes conveying flow, the answer is interesting: nothing happens to the fluid in the bulk located far from the walls; however, at the tube/wall bound-

aries, the fluid must exactly follow the tube motion. This leads to complicated free boundary conditions on the Navier Stokes three-dimensional equations. In turn, such boundaries induce a complicated helical pattern on the fluid stream lines, that have extensively been discussed in the literature to model fluid dynamics in macroscopic bent tubes [6].

However, from the point of view of the tube framework, fluid particles are affected by the tube motion, because a coordinate framework located at the tube is no longer inertial. In a non-inertial framework, three fictitious forces arise. Their expressions in the static framework (x, y, z) are shown below:

- A fictitious acceleration given if the entire tube is translating. Such force per unit volume of fluid is given by:

$$\begin{aligned} \vec{F}_{push} &= -\rho \vec{a}_{trans,tube} \\ &= \left(0,\ -\frac{\rho \frac{\partial^2 u}{\partial t^2}}{1+\left(\frac{\partial u}{\partial z}\right)^2},\ \frac{\rho \frac{\partial^2 u}{\partial t^2}\frac{\partial u}{\partial z}}{1+\left(\frac{\partial u}{\partial z}\right)^2} \right) \end{aligned} \tag{4.24}$$

- The Coriolis force, given by the effect of the local rotational motion of the tube, expressed as follows:

$$\begin{aligned} \vec{F}_{Cor} &= -2\rho\ \vec{\Omega} \times \vec{v}_{fluid} \\ &= \left(0,\ -\frac{2\rho v \frac{\partial^2 u}{\partial t \partial z}}{\sqrt{1+\left(\frac{\partial u}{\partial z}\right)^2}},\ \frac{2\rho v \frac{\partial^2 u}{\partial t \partial z}\frac{\partial u}{\partial z}}{\sqrt{1+\left(\frac{\partial u}{\partial z}\right)^2}} \right) \end{aligned} \tag{4.25}$$

- The centrifugal force, given by the effect of rotational motion, as

$$\begin{aligned} \vec{F}_{cent} &= -\rho \vec{\Omega} \times (\vec{\Omega} \times \vec{r}) \\ &= \left(0,\ \frac{\rho \frac{\partial^2 u}{\partial t \partial z}\frac{\partial u}{\partial t}\frac{\partial u}{\partial z}}{1+\left(\frac{\partial u}{\partial z}\right)^2},\ \frac{\rho \frac{\partial^2 u}{\partial t \partial z}\frac{\partial u}{\partial t}}{1+\left(\frac{\partial u}{\partial z}\right)^2} \right) \end{aligned} \tag{4.26}$$

In general, these forces lie all along the YZ plane as illustrated in Fig. 4.2. The fictitious forces arise as an effect of the observation of fluid motion within the tube framework. In the absence of tube forces, a free fluid particle, in the absence of

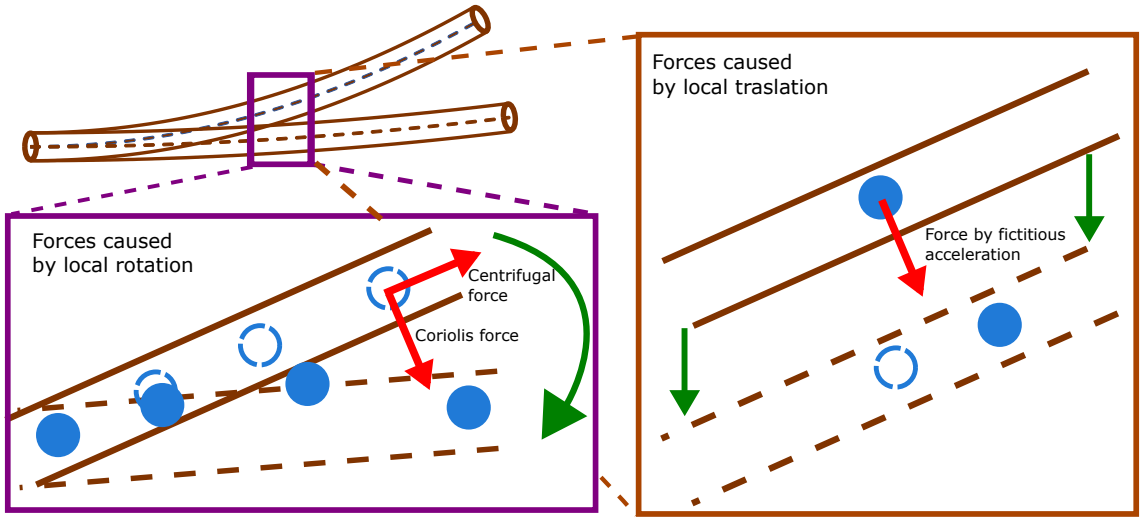

Figure 4.2: Effect of the tube motion on the fluid dynamics. As tube moves, it develops a motion that can be locally simplified in two components: a rotational and a translational motion. Both affect the fluid motion since the tube pushes the fluid normally to the local axial direction, leading to a net axial force that pushes the fluid.

external non-fictitious forces, tends to follow its original horizontal motion. However, within the tube framework, such horizontal motion is not so, fluid is observed moving in a very complicated fashion. Thus, the fictitious forces in Eqs. (4.24)-(4.26) cause the fluid motion to be non-parallel from the point of view of the tube.

When the constraint is imposed, tube and fluid are required to interact in such a way that these fictitious forces are no longer detected, and fluid moves parallel to the oscillating tube. This means that the tube should exert a force on the fluid such that it cancels the fictitious forces. As a result, from the point of view of an static external framework, the tube pushes the fluid with a force which is opposite to the ones defined in Eqs. (4.24)-(4.26). Particularly, the z-component of such tube/fluid forces turns out to be the only relevant to modify Navier Stokes equation.

The horizontal z-component of the tube forces are summarized below:

$$F_{acc}^{hor} = -\rho \frac{\partial^2 u}{\partial t^2} \frac{\frac{\partial u}{\partial z}}{1 + \left(\frac{\partial u}{\partial z}\right)^2} \tag{4.27}$$

$$F_{Cor}^{hor} = -2\rho\, v \frac{\partial^2 u}{\partial z \partial t} \frac{\frac{\partial u}{\partial z}}{\sqrt{1 + \left(\frac{\partial u}{\partial z}\right)^2}} \tag{4.28}$$

$$F_{cent}^{hor} = -\rho \frac{\partial u}{\partial t} \frac{\partial^2 u}{\partial z \partial t} \frac{1}{1 + \left(\frac{\partial u}{\partial z}\right)^2} \tag{4.29}$$

The axial components of such forces turn out to be identical to the coupled terms involved in our theoretical treatment, except for the factor $1/\sqrt{1 + (\partial u/\partial z)^2}$. The reason for that discrepancy is the small deformation approximation that we have considered. According to this analysis, we conclude that the tube-induced forces which are incorporated into the Navier-Stokes equations are exerted on the fluid to cancel the fictitious forces generated by the tube vibration. This explanation is summarized in Fig. 4.2.

5

Tube dynamics influenced by flow velocity

Despite all of the experimental advances and theoretical efforts towards the comprehension of enhanced water flow within nanostructures, there are current limitations, both, experimental and theoretical ones, regarding the precision with which flow is determined. Moreover, flow enhancement differs by orders of magnitude among the different experimental works in the literature [35, 36, 37, 38]. The main experimental difficulties in the determination of flow, are related to the uncertainty in the cross sectional area available for flow in carbon nanotube membranes. These ones lead to uncertainties of over 50% in flow measurements [23, 10, 48]. Techniques used to determine porosity in materials, such as the BET isotherm and impedance spectroscopy [137, 138], lead to huge errors in pore density and cross-sectional areas that in turn affect the precision in the determination of flow velocity. Moreover, at nanoscales, it is not clear that the pore surface, that is determined by nitrogen adsorption, is the same as the effective cross-sectional area available for water flow. This is because repulsion might lead to empty spaces between the tube and the fluid that diminish the effective area for flow. Alternative ways to measure flow velocities within nanotubes seem to be necessary.

In this chapter, we study the influence of fluid motion on tube dynamics that was developed in Chapter 4 and is summarized in Eqs. (3.36) and (4.2). Particularly, we found that the frequency of tube vibration is considerably modified by the flow velocity developed within. The consequences of such effect could be exploited to

determine flow velocities based on knowledge of the vibration frequency spectrum of a single nanotube. This methodology could be applied to different sets of boundary conditions at the nanotube edges. Our approach proposes to record the nanotube displacement as a function of time (for example by AFM measurements); to use this information to determine the relevant frequencies associated to the tube dynamics via Fourier Analysis; and finally, to determine the magnitude of flow velocity inside a nanostructure, through the analytical relations between frequency and flow velocity obtained in this work.

We obtain analytical expressions for the fluid velocity as a function of the natural frequencies of the nanotube deflection, that allow for an easy error propagation analysis of the uncertainties involved in each of the system parameters. Our expressions allow us to establish the framework for indirect determination of flow, via experimental measurements of the nanotube oscillatory bending motion. Our analysis indicates that the experimental uncertainties in the flow magnitude, could be dramatically reduced in wide ranges of tube sizes and flow velocities, by using the proposed methodology. These uncertainties allow one to know under which circumstances the proposed framework to measure flow velocities would lead to accurate results.

5.1 Characteristic scale for flow velocity and tube vibration frequency

A visual inspection of Eq. (4.11) allows one to find a characteristic frequency of the system, ω_c, in the absence of flow, when $v = 0$. That is, a frequency characteristic of a tube of length L with a stagnant fluid inside it:

$$\omega_c = \frac{1}{L^2}\sqrt{\frac{EI}{\rho_t A_t + \rho_f A_f}} \ . \tag{5.1}$$

It also allows us to find a characteristic flow velocity for a steady tube in the absence of vibrations, $\mathbf{v}_c$, when the partial derivatives in time of the tube displacement are

zero:

$$v_c = \frac{1}{L}\sqrt{\frac{EI}{\rho_f A_f}} \ . \tag{5.2}$$

These characteristic quantities allow us to rewrite Eq. (4.11) in terms of the dimensionless variables, $\tilde{z} = \frac{z}{L}$, $\tilde{t} = \omega_c t$, and $\tilde{v} = \frac{v_{rms}}{v_c}$ as

$$\frac{\partial^4 u}{\partial \tilde{z}^4} + \tilde{v}^2 \frac{\partial^2 u}{\partial \tilde{z}^2} + 2\alpha\beta\tilde{v}\frac{\partial^2 u}{\partial \tilde{z}\partial \tilde{t}} + \alpha\beta\frac{\partial \tilde{v}}{\partial \tilde{t}}\frac{\partial u}{\partial \tilde{z}} + \frac{\partial^2 u}{\partial \tilde{t}^2} = 0 \ , \tag{5.3}$$

where the quantity α, that we name *thickness ratio*, has been defined as

$$\alpha^2 \equiv \frac{1}{1 + \frac{\rho_t A_t}{\rho_f A_f}} \ . \tag{5.4}$$

Such thickness ratio, α, might take values between 0 and 1. It decreases when the tube thickness increases, because of the ratio of cross-sectional areas, of tube and fluid, in the denominator of Eq. (5.4). In order to have a simple notation, we will omit tildes from this point until the end of this Chapter, but, z, t, and v refer to non-dimensional variables.

The dimensionless equation for the tube displacement [Eq. (5.3)], is a differential equation in space and time, which depends explicitly on only three physical parameters, namely,

- The dimensionless flow velocity, v, that has been normalized with the flow in a steady tube.
- The thickness ratio, α, which depends only on the ratio of tube and fluid densities, and the ratio of tube and fluid cross-sectional areas.
- The structure factor, β, which depends only on the specific form of the radial profile.

The solution of [Eq. (5.3)] will allow for the establishment of a relation between flow magnitude and tube frequency.

5.2 Relation between flow magnitude and tube frequency

The solution of Eq. (5.3) incorporates the physical and geometrical characteristics of tube, along with the fluid motion given by the solution of Eq. (4.2). In order to focus on the role of flow velocity on the tube vibration described in Eq. (5.3), it will be considered that a constant flow velocity is developed within the tube, and the parameters α and β are fixed and known for the rest of the derivation carried out in this section. The role of β will be discussed afterwards.

The Fourier Transform in time of Eq. (5.3) when a steady flow velocity is considered, leads to

$$\frac{d^4\hat{u}}{dz^4} + v^2\frac{d^2\hat{u}}{dz^2} - 2i\omega\alpha\beta v\frac{d\hat{u}}{dz} - \omega^2\hat{u} = 0 \tag{5.5}$$

where $\hat{u}(z,\omega)$ denotes the displacement in frequency domain. As this is a linear fourth-order differential equation for $\hat{u}$ with constant coefficients, the solution of Eq. (5.5) is the superposition of four terms, resulting in a general form given by

$$\hat{u}(z,\omega) = C_1e^{ik_1z} + C_2e^{ik_2z} + C_3e^{ik_3z} + C_4e^{ik_4z}, \tag{5.6}$$

where k_1, k_2, k_3 and k_4 are wavenumbers, and are functions of v, ω and α. For a given tube and fluid, the latter one is a constant. The wavenumbers are given as follows:

$$\begin{aligned} k_1 &= -a - b; \quad k_2 = -a + b; \\ k_3 &= a - b; \qquad k_4 = a + b, \end{aligned} \tag{5.7}$$

where a and b are given by

$$a = \frac{1}{2}\sqrt{\frac{2v^2}{3} + \frac{2^{\frac{1}{3}}\left(v^4 - 12\omega^2\right)}{3q^{\frac{1}{3}}} + \frac{q^{\frac{1}{3}}}{3(2)^{\frac{1}{3}}}} \tag{5.8}$$

$$\begin{aligned} b^2 = \quad & \frac{v^2}{3} - \frac{2^{\frac{1}{3}}\left(v^4 - 12\omega^2\right)}{12q^{\frac{1}{3}}} - \frac{q^{\frac{1}{3}}}{12(2)^{\frac{1}{3}}} \\ & - \frac{v\alpha\beta\omega}{\sqrt{\frac{2v^2}{3} + \frac{2^{\frac{1}{3}}\left(v^4 - 12\omega^2\right)}{3q^{\frac{1}{3}}} + \frac{q^{\frac{1}{3}}}{3(2)^{\frac{1}{3}}}}} \end{aligned} \tag{5.9}$$

and q is given by

$$q = -2v^6 - 72v^2\omega^2 + 108v^2\alpha^2\beta^2\omega^2 + \sqrt{s} \tag{5.10}$$

where s is

$$\begin{aligned} s = \quad & \left(2v^6 + 72v^2\omega^2 - 108v^2\alpha^2\beta^2\omega^2\right)^2 \\ & -4\left(v^4 - 12\omega^2\right)^3 \end{aligned} \tag{5.11}$$

When a set of boundary conditions at the tube edges is chosen, one obtains a linear homogeneous 4×4 system of algebraic equations for the coefficients C_n. Such a system allows for a non-trivial solution, only if the determinant, D, vanishes. This discretizes the allowed values of the wavenumbers, and therefore the allowed values of the frequency, ω, giving rise to the different vibration frequency modes of the tube, ω_n. General details of the dispersion relation are included in Appendix A.4. Moreover, such determinant is different for each set of boundary conditions. As an example, for a pinned-pinned tube, the determinant, D_{PP}, is given by

$$D_{PP}(v,\omega) = \begin{vmatrix} 1 & 1 & 1 & 1 \\ -k_1^2 & -k_2^2 & -k_3^2 & -k_4^2 \\ e^{ik_1} & e^{ik_2} & e^{ik_3} & e^{ik_4} \\ -k_1^2 e^{ik_1} & -k_2^2 e^{ik_2} & -k_3^2 e^{ik_3} & -k_4^2 e^{ik_4} \end{vmatrix} \tag{5.12}$$

Explicit expressions for the determinants for the other sets of boundary conditions are given in Appendix A.5.

As stated above, the condition for non-trivial solutions of the tube dynamics is achieved when

$$D(v,\omega_n) = 0\ . \tag{5.13}$$

From Eq. (5.13), it is possible to know the relation between the frequency of a tube oscillating in any of its vibration modes, ω_n, and the flow velocity, v, inside it.

From this point, we use two different approaches in order to obtain the flow/frequency relations from Eq. (5.13). An analytical approach, which will be discussed in the following sections, and a numerical approach, that we implement in order to determine

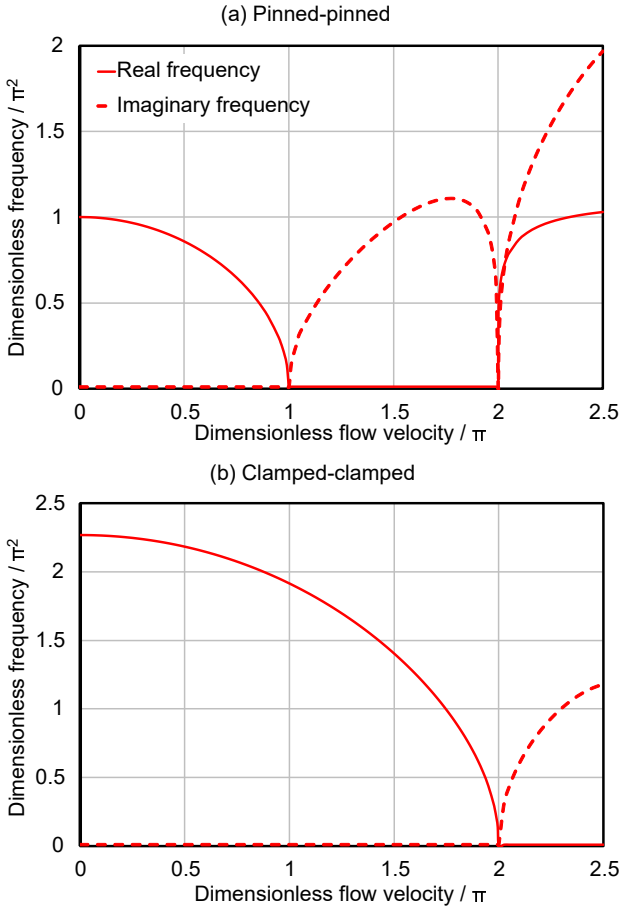

Figure 5.1: Effect of flow in the fundamental frequency mode of the tube oscillations, for two sets of boundary conditions. Solid lines correspond to the real part of the frequency and dashed lines to its imaginary part. A typical value of the thickness ratio times the fluid-structure factor $\alpha\beta = 0.6$ is used in the calculations.

the range of validity of our analytical solutions. The latter one consists of the numerical obtention of the frequency of every vibration mode, ω_n, given a known value of the flow velocity. This treatment is useful when the tube starts in an initial deformed condition with a known flow velocity induced inside it, and allows for a determination of the tube dynamics. The frequency of each mode is obtained with any degree of precision, so it can be considered as the exact solution of $\omega_n(v)$. We solved Eq. (5.13) by a Newton-Raphson method using Wolfram Mathematica 11. The effect of a specific set of boundary conditions in the fundamental frequency vs. flow diagram is illustrated in Fig. 5.1 for the pinned-pinned and clamped-clamped cases. The qualitative behavior of the curves in Fig. 5.1 has been studied in the literature [139, 140], by numerical solution of models similar to Eq. (5.3), with the purpose of identifying the flow conditions that induce unstable tube motion. For the lowest flow velocities, a purely real frequency is obtained, which leads to stable oscillatory motion of the tube. On the other hand, when the frequency is purely imaginary, the dynamics leads to buckling, or when it is complex, with non-zero real and imaginary parts, it leads to fluttering [141, 108, 142, 143].

In Fig. 5.1, a decrease of the fundamental mode, ω_1, with increasing flow velocity in the stable motion zone can be observed, this implies that the larger the flow velocity, the smaller the fundamental frequency is; when flow increases above a certain threshold that depends on the set of boundary conditions, an unstable behavior emerges -indicated by a non-zero imaginary part of the frequency-. For the other sets of boundary conditions, equivalent figures are included in Appendix A.6.

5.3 Role of flow structure: Disentangling the flow magnitude and the radial profile

The previous discussion has been centered on the role of the magnitude of flow velocity on the frequency of tube vibration. Our model recovers the flow/frequency

Type of fluid	β
Plug flow	1.0
Newtonian fluid	0.866
Pseudoplastic fluid	0.94
Dilatant fluid	0.84
Newtonian fluid with slip	0.99

Table 5.1: Radial structure factor, β, of fluids with different rheological behavior and boundary conditions.

relation developed previously in the literature, but it also accounts for the effect of the radial velocity profile in the tube dynamics via the structure factor, β. Particularly, Eq. (4.11) is reduced to the one developed by Paidoussis [132], and used by Wang to study fluid flow within nanotubes [108] for plug-like flows, for which $\beta = 1$.

For a fluid subject to a constant pressure gradient and no-slip boundary conditions, the steady flow velocity is given by the parabolic Poiseuille profile. When Poiseuille profile is incorporated into Eqs. (3.39) and (3.40), the following expressions are obtained:

$$\langle v \rangle = -\frac{R^2}{8\mu}\frac{\partial p}{\partial z}\,, \quad \langle v^2 \rangle = \frac{R^4}{48\mu^2}\left(\frac{\partial p}{\partial z}\right)^2 \tag{5.14}$$

which in turn, using Eq. 4.10, lead to $\beta = \sqrt{3}/2 \approx 0.867$, that can be incorporated into Eq. (4.11) or, equivalently, in Eq. (5.3).

Keeping the conditions established in this limit —*i.e.*, when the fluid motion is independent of the tube vibration—, it would be possible to explore the flow/frequency relation of different types of fluids subject to a constant driving force. To do so, the rheological behavior of the fluid in question would be incorporated in an equation of motion analogous to Eq. (4.2) and solved independently of the tube dynamics. Afterwards, the complex velocity profile for this fluid would be incorporated in the tube dynamics by computing its corresponding structure factor, β. The same procedure could be carried out for a simple fluid subject to complex boundary conditions, such

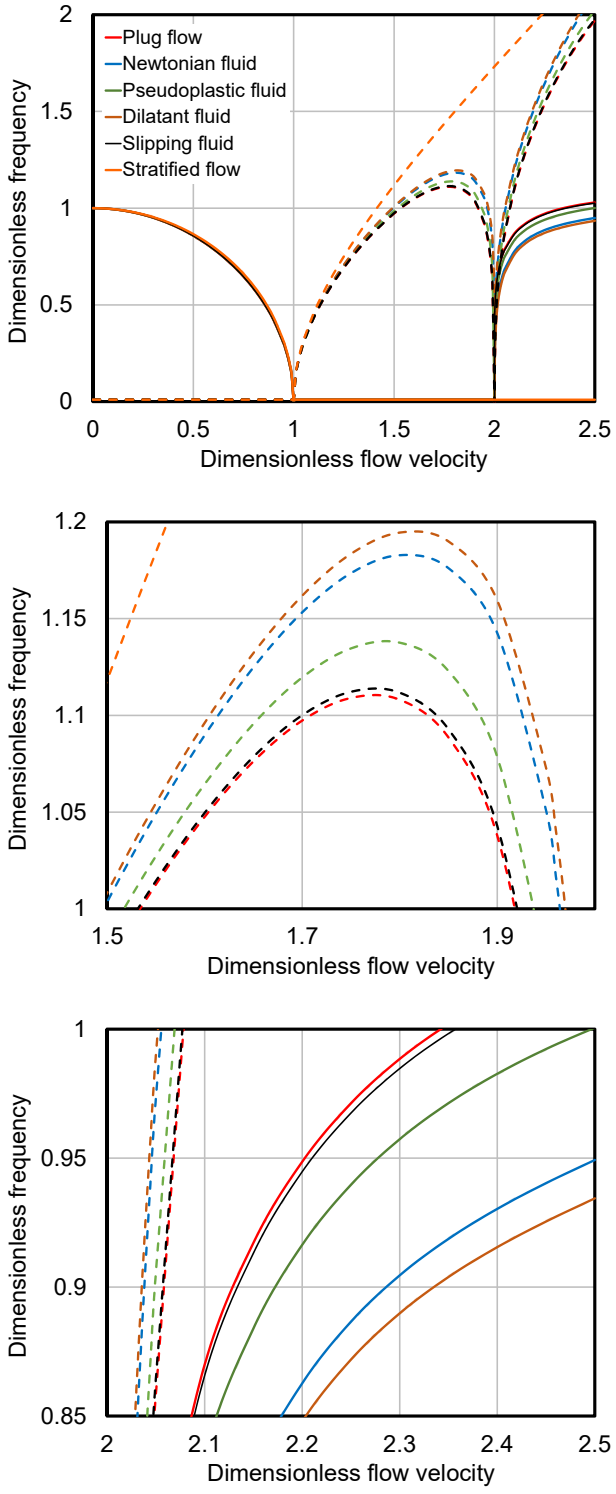

Figure 5.2: Effect of the radial flow profile in the flow/frequency relation for the fundamental mode of a tube that is pinned at both edges. Each color represents a value of the structure factor, β, that corresponds to a specific rheological behavior. The real component of frequency is shown with continuous lines, whereas the imaginary component is plotted with dashed lines. Top: Global view. Middle: Zoom-in at the buckling regime. Bottom: Zoom-in at the fluttering regime.

as an effective slippage at tube walls. Structure factors, β, for typical fluids and conditions encountered in the literature, that turn out to be independent of the applied pressure gradient, have been summarized in Table 5.1. A change in the value of β modifies quantitatively the flow/frequency relationship observed for the tube vibration, particularly in the buckling and fluttering regimes. This is observed in a global view of the flow/frequency relation for different fluid profiles, shown in Fig. 5.2a. In order to emphasize such effect, the plot has been zoomed-in at the buckling regime (see Fig. 5.2b) and at the fluttering regime (see Fig. 5.2c).

The effect of β on the flow-frequency relationship can be used as a tool to analyze velocity profiles within nanostructures.

5.4 Analytical approach

An alternative approach to solve Eq. (5.13) that is key to the proposed framework for flow determination, consists of obtaining analytical expressions for the flow velocity as a function of the tube oscillation modes, $v(\omega_n)$. The purpose of this is to determine the flow magnitude inside a tube when the frequency spectrum of tube bending motion is known. Such strategy is based on the assumption that experimentally-attainable flows are small in comparison to the critical flow velocity of the first mode, given by the characteristic flow velocity in Eq. (5.2). This assumption is supported by the typical flow velocities measured within carbon nanotubes [2]. With this consideration, it is possible to perform a Taylor expansion, around small flow velocities, of the determinant, D, in Eq. (5.13), as follows:

$$D(v,\omega) = D\Big|_{v=0} + \sum_{n=1}^{\infty} \frac{\partial^n D}{\partial v^n}\Big|_{v=0} \frac{v^n}{n!} \quad . \tag{5.15}$$

It turns out that, for several sets of boundary conditions (P-P, C-C, F-F, and P-C), the odd derivatives of the determinant vanish. For these cases, a truncation to order m in Eq. (5.15), leads to an algebraic equation of order $\frac{m}{2}$ for $v^2(\omega)$. Since analytic solutions of polynomial equations are known up to quartic order, we have obtained

analytic approximations of Eq. (5.15) for v^2, for truncation orders $m = 2, 4, 6$ and 8. As an example, a second-order truncation of the determinant in Eq. (5.15) for the pinned-pinned case is

$$v_{P-P}(\omega, \alpha) = \sqrt{\frac{A_{PP}}{B_{PP}}} \tag{5.16}$$

where A_{PP} and B_{PP} are given by

$$A_{PP} = 8\omega \sin(\sqrt{\omega}) \sinh(\sqrt{\omega}) \tag{5.17}$$

$$B_{PP} = 4\alpha^2\beta^2 - \cosh(\sqrt{\omega})G_{PP} - \sqrt{\omega}\sinh(\sqrt{\omega})H_{PP} \tag{5.18}$$

and G_{PP} and H_{PP} are given by

$$G_{PP} = 4\alpha^2\beta^2 \cos(\sqrt{\omega}) + (\alpha^2\beta^2 - 2)\sqrt{\omega}\sin(\sqrt{\omega}) \tag{5.19}$$

$$H_{PP} = (2 - \alpha^2\beta^2)\cos(\sqrt{\omega}) \ . \tag{5.20}$$

A comparison of the analytical expression in Eq. (5.16) (and equivalent expressions to higher truncation orders) with the exact numerical solutions, is shown in Fig. 5.3a, in order to exhibit the range of velocities in which each of the approximations is adequate. Fig. 5.3b shows the percentage error between the different analytical approximations and the exact numerical solution. We can observe that there is a wide range of flow velocities in which the analytical approximations differ no more than few percentage points from the exact solution. For excited modes (not shown in Fig. 5.3), the analytical approximations are valid for wider velocity ranges than the fundamental mode.

For the two sets of boundary conditions for which odd derivatives of the determinant do not vanish (P-F and C-F), algebraic equations for v (and not for v^2) can be obtained up to quartic order. Analytic expressions for higher truncation orders (needed for higher flow velocities) and for the other sets of boundary conditions, as well as figures comparing analytical expressions of the fundamental mode with numerical solutions are included in Appendix A.7.

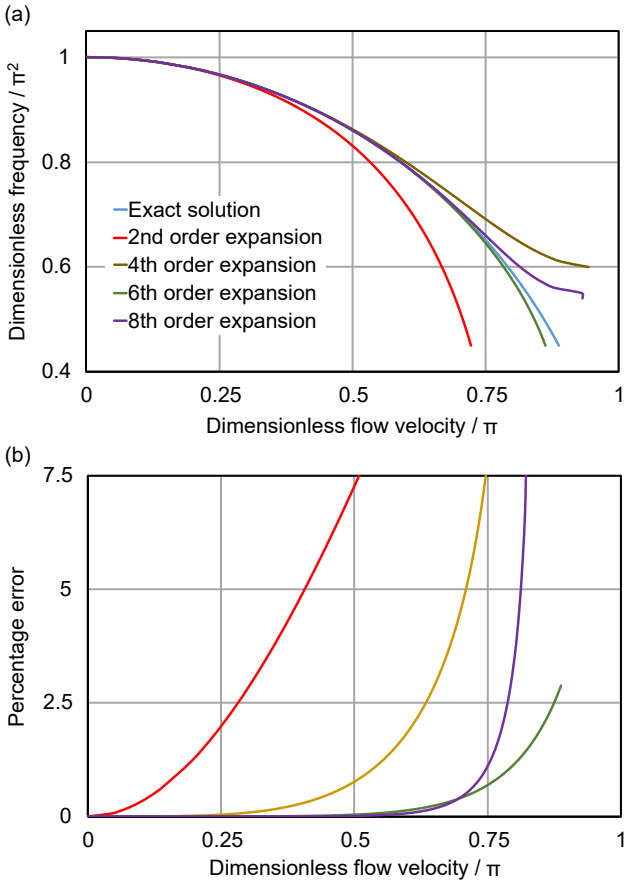

Figure 5.3: (a) Comparison between the approximated analytical expressions and the exact numerical solution for the flow velocity as a function of the fundamental frequency for the pinned-pinned case. As expected, incorporation of more terms in the Taylor expansion for v^2, leads to an increase in accuracy and the range of applicability of the analytical expressions for higher flows. (b) Percentage error in the velocity as a function of the flow velocity. A typical value of the thickness ratio $\alpha = 0.6$ is used in the calculations.

Contrary to exact solutions that are multivalued, our analytical solutions for the first degree of truncation, give expressions for $v(\omega_n)$ such that for each value of ω only one value of the velocity could be obtained Moreover, the expression for the velocity is exactly the same one for each of the tube vibration modes in the spectrum. Therefore, if the frequency spectrum of the tube dynamics were available, any of the frequencies composing it, could be in principle used in Eq. (5.16), and the same flow velocity would be obtained. This, together with the knowledge of the range of flow velocities in which the approximation is valid (for example, from Fig. 5.3) gives an important advantage of our analytical approach over numerical schemes [139, 140]. This fact could be useful in real experiments, where different sources of uncertainty may induce noise and spurious peaks in the frequency spectra, because every physical peak must be related to the same flow velocity. For higher truncation orders of the determinant in Eq. (5.15), the analytical solution will give several values for the flow velocity, however, careful analysis would allow to distinguish which is the physical solution, because this one should give a real value for the velocity (see for example, Table I in Appendix A.7). The physical solution will also comply with the fact that any of the frequencies in the spectrum will be associated to a single value of the fluid velocity (see for example Fig. 3 in Appendix A.7 for the fourth truncation order for v^2).

5.5 Simulation of the tube dynamics

An illustrative example of our proposal consists of the theoretical solution of a tube with an initial condition that imitates a possible deformation induced by AFM, this one is given by

$$\begin{aligned} u(z, t=0) &= 256\left(z^4 - 4z^5 + 6z^6 - 4z^7 + z^8\right) \\ \text{and} \qquad \dot{u}(z, t=0) &= 0\ . \end{aligned} \tag{5.21}$$

Geometrical details of the tube used in this example and its initial condition are illustrated in Fig. 5.4. A polynomial function was chosen in order to satisfy any of

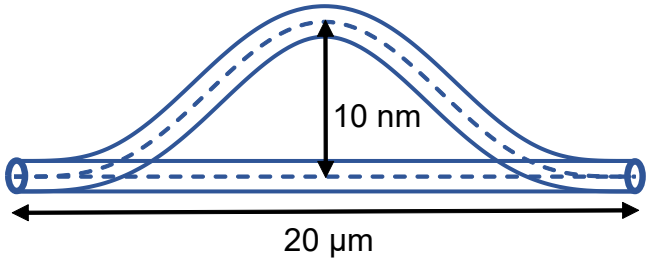

Figure 5.4: Initial condition imposed for the simulations of the tube dynamics.

the sets of boundary conditions in the tube extremes.

This example allows one to see how boundary conditions influence the tube dynamics and could potentially allow experimentalists to understand to which of the idealized sets of boundary conditions their specific experiment belongs.

Simulations of the tube dynamics are illustrated in Fig. 5.5 for the pinned-pinned, clamped-clamped and pinned-clamped cases. For each set of boundary conditions, the tube displacements at the middle of the tube ($z = 0.5$) are plotted as a function of time, when the tube is filled with a stagnant fluid (first column) and when the tube is filled with a fluid with a flow velocity $v = 0.5m/s$ (second column). The third column shows the frequency spectrum of both cases illustrating clearly that the fundamental frequency is smaller when the fluid is being transported with a finite velocity than when the fluid is stagnant within the tube. It also shows that the fundamental mode occurs at different frequency values for each set of boundary conditions.

The complete derivation of the solution of the tube dynamics [Eq. (4.11)] with initial and boundary conditions is given in Appendix A.8.

5.6 Experimental feasibility

We analyze the feasibility of a potential experiment according to the state of the art of experimental apparatus. Most of the experiments in the detection of motion and mechanical response of carbon nanotubes can be classified in two big groups: determination of the force exerted on a tube due to an imposed static deflection by means

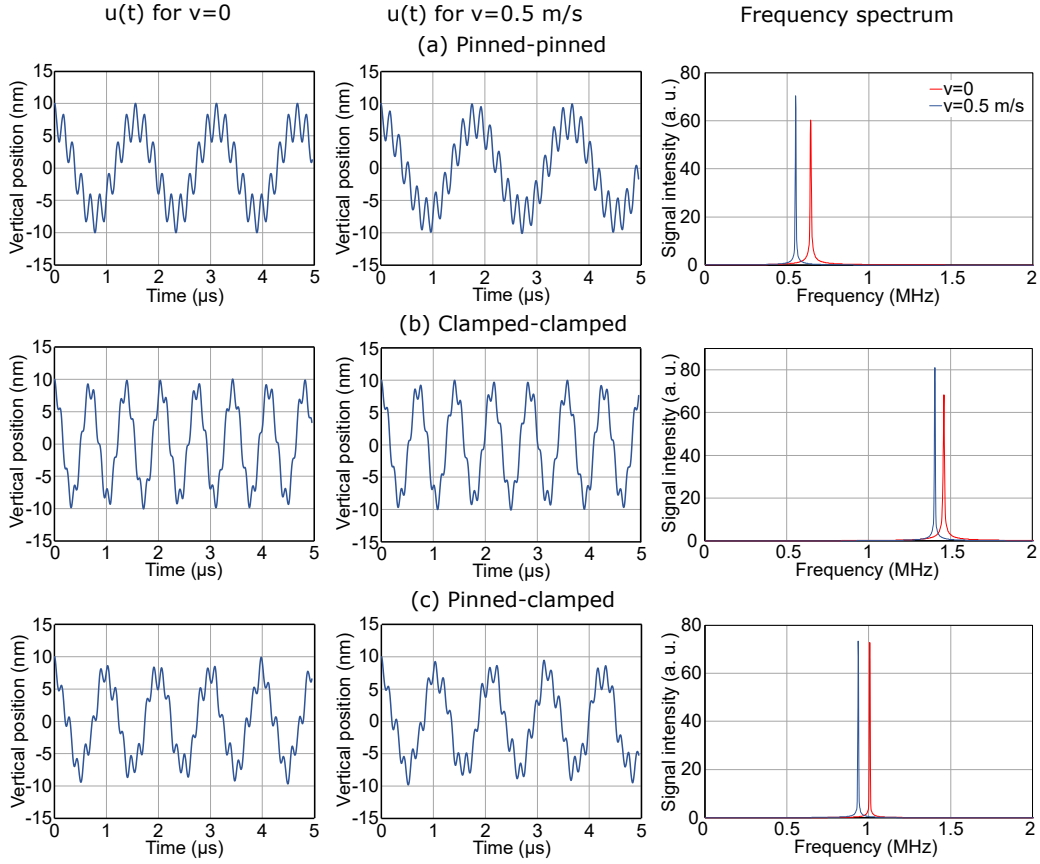

Figure 5.5: Simulation of the tube dynamics with different boundary conditions at their edges. For each set of boundary conditions, the tube displacements at the middle of the tube ($z = 0.5$) are plotted as a function of time; left column, when the tube is filled with a stagnant fluid; middle column, when the tube is filled with a fluid with flow velocity $v = 0.5m/s$. The right column shows the frequency spectrum of both cases illustrating clearly that the fundamental mode is smaller when the fluid is being transported with a finite velocity than when the fluid is stagnant within the tube. It also shows that the fundamental mode occurs at different values for each set of boundary conditions. Calculations were done for a nanotube with inner and outer tube radius of 8 and 15 nm, respectively.

of AFM, where the determination relies on a single measurement, and has a considerable amount of error [144, 145, 146, 147, 148]; and tests of the nanotubes proficiency as resonators in response to external steady oscillatory perturbations produced by piezoelectric actuators [149, 150, 151, 152, 153]. A different strategy is conceived here. If a certain amount of data, that account for the time evolution of the tube motion, is registered and subsequently treated by Fourier analysis, the uncertainty in the peaks of the frequency spectrum will depend on the apparatus resolution to measure distances and time, and importantly, on the sampling time [154, 155].

The minimal elements that an experiment should have in order to determine flow using our analytical framework, are three: 1) an external driving force allowing for fluid flow inside the nanotube, 2) a device allowing for an initial perturbation of the tube, and 3) a transducer device allowing for the detection and registration of the tube motion.

The incorporation of two closed reservoirs at the tube edges and the induction of a pressure difference by mechanical means, -a syringe or a piston- is not suitable at nanoscales, since the imperfections of the junctions between the reservoirs and tube extremes would cause water leaking. A better strategy could be to induce an electrophoretic flow by a voltage difference across the tube as done by Qin [78]. A steady flow would be obtained shortly after the tube is full of water.

An initial perturbation could be induced, for example, by pushing the tube with the tip of an AFM [144, 156], by direct mechanical coupling of a piezoelectric material pulsed by an AC electric source [149, 157, 158], or by indirect excitation of the nanotube by acoustic means [159, 160, 161, 162].

In general, four detection ways seem to be suitable for accurate measurements with a sub-nm resolution and within the range of a few nm in the vertical displacement of a nanotube: field-effect transistors [163, 164, 165, 166, 167], piezo-resistive effect [153, 149], capacitive response [152] and optical interferometry [168, 169].

The space of a nanodevice does not allow for an easy incorporation of multiple

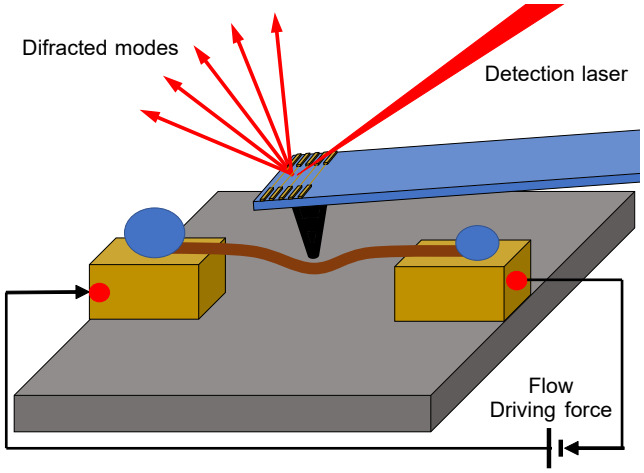

Figure 5.6: Example of a minimal experimental setting to indirectly determine flow velocities by means of recording the tube displacements in time. The setting includes an electrophoretic driving force for fluid flow, while the tube deformation and detection are both done by means of an AFM with interdigitated prints that allow for accurate detection via interferometry.

instruments or the aligning of a microdevice with external components and probes. The most suitable device would be the one that allows for the simplest setting that incorporates an actuator, a detector and a driving force for fluid flow.

A possible minimal setting, compatible with the simulation of the tube dynamics of the previous section, is illustrated in Fig. 5.6. This one would include an electrophoretic driving force for the fluid, while the tube deformation and the detection could be both done by means of an AFM with interdigitated prints, that allow for accurate detection via interferometry, as developed by Manalis [170, 171]. The arrangement of tube and AFM tip could be as the one in the work of Salvetat [144].

Frequently, the actuation or detection of the tube motion will involve external forces that should be incorporated into the model. Moreover, depending on the environmental conditions of the experiment, a damping force could affect the experimental results. However, all these external forces can be incorporated into equation (4.11) in a straightforward manner. The theoretical treatment provided in this work (and fully explained in Appendix A.7) can incorporate such external forces, allowing the obtention of analytical expressions for the specific experiment developed. However,

in general, these external forces exert only slight modifications to the flow/frequency relations shown in Fig. 5.3, because in most cases, the large Young Moduli of CNTs would cause the elastic force to be the dominant force of the system.

5.7 *Considerations on the uncertainty and sensibility of the method*

The flow/frequency relation in Eq. (5.16) -and the equivalent relations for other B.C.- associates dimensionless flow and dimensionless frequency. A suitable manner to use such relation is by performing two experiments, one at finite flow velocity and another one at zero flow and to record the fundamental frequency for both experiments.

The dimensional frequency obtained by a measurement at a given flow velocity v will be denoted by ω_v^{BC}, where BC reminds that the fundamental frequency depends on the specific set of boundary conditions. The frequency of a tube filled with a stagnant fluid, ω_0^{BC}, can be related to the characteristic frequency ω_c in Eq. (5.1) by the following relation:

$$\omega_0^{BC} = a\omega_c \ , \tag{5.22}$$

where the value of a depends on the boundary conditions. For a pinned-pinned tube, $a = 1$, for a clamped-clamped and a free-free tube, $a = 9/4$, for a pinned-clamped and a free-free tube, $a = 25/16$ and for a clamped-free tube, $a = 1/4$.

Therefore, the ratio of both dimensional measured frequencies ω_v^{BC} and ω_0^{BC} leads to the following result:

$$\begin{aligned} \frac{\omega_v^{BC}}{\omega_0^{BC}} &= \frac{1}{a}\frac{\omega_v^{BC}}{\omega_c} \\ &= \frac{1}{a}\omega \ , \end{aligned} \tag{5.23}$$

which allows one to compute the dimensionless frequency, ω, directly from two experiments, without the need to determine directly ω_c by means of the Young modulus of the tube.

Doing so would be useful for the reduction of uncertainty, because in this way the relative uncertainty of flow is computable directly from the dimensionless equation (5.16) or equivalent expressions for other boundary conditions[1]1]By using a single frequency measurement, it would be necessary to account for the uncertainty in the characteristic flow velocity shown in Eq. (5.1), which implies to account for the high uncertainty involved in the determination of the Young modulus. In turn, a two-frequencies measurement scheme has a much smaller flow magnitude uncertainty.. First, the dimensional uncertainty of both frequency measurements is incorporated in the uncertainty of the dimensionless frequency, ω, as:

$$\begin{aligned}\Delta\omega^2 &= \left(\frac{\partial\omega}{\partial\omega_v^{BC}}\right)^2\left(\Delta\omega_v^{BC}\right)^2+\left(\frac{\partial\omega}{\partial\omega_0^{BC}}\right)^2\left(\Delta\omega_0^{BC}\right)^2\\ &= \frac{a^2}{\left(\omega_v^{BC}\right)^2}\left(\Delta\omega_v^{BC}\right)^2+a^2\frac{\left(\omega_v^{BC}\right)^2}{\left(\omega_0^{BC}\right)^4}\left(\Delta\omega_0^{BC}\right)^2\end{aligned} \tag{5.24}$$

And then, the uncertainty in the dimensionless frequency, ω, is incorporated in the uncertainty of the dimensionless flow velocity, $v(\omega,\alpha)$, given by Eq. (5.16) -or equivalent expressions for the other boundary conditions- as

$$\Delta v=\sqrt{\left(\frac{\partial v}{\partial\omega}\right)^2(\Delta\omega)^2+\left(\frac{\partial v}{\partial\alpha}\right)^2(\Delta\alpha)^2}\ , \tag{5.25}$$

where the uncertainty $\Delta\alpha$ can be computed from the uncertainty in densities, outer and inner tube radii. Therefore, from Eqs. (5.24) and (5.25), it is possible to establish that uncertainty on flow depends essentially on the dimensional uncertainty of both frequency measurements, on the dimensional uncertainty of densities and radii and on the slope of the dimensionless flow/frequency function, $\partial v/\partial\omega$ and the slope of the dimensionless flow/thickness ratio function, $\partial v/\partial\alpha$.

Among all of the factors that affect the flow velocity uncertainty, the most important one is the slope of flow velocity/frequency function, because it depends drastically on the magnitude of the flow velocity itself, and it diverges for flow velocities close to

[1] [

zero. This result is presented in Fig. 5.7(a), where it is possible to see that for large tubes and intermediate flow velocities, the uncertainty reaches an asymptotic lower value, which is given by the uncertainty of the thickness ratio, α.

According to our analysis, we consider that our method could be implemented in typical carbon nanotubes between 10 and 100 μm in length, with initial amplitudes between 1 and 50 nm. Our calculations predict that a tube of these dimensions will have natural frequencies on the range of $kHz - MHz$. After a literature review on the spatial and time resolution of AFM, a resolution of 0.1 nm in the measurement of the vertical displacement of the tube [172, 173] and a time resolution of 0.05 μs would be possible [174, 175, 176]. For shorter tubes (between $1 - 10$ μm in length), the Experimental Setting in Fig. 5.6 would not be suitable, since would not be capable of detecting MHz-GHz frequencies.

Uncertainty in Fig. 5.7 would change slightly if different actuators or sensors are considered. However, the qualitative behavior would remain the same, since its origin is the slope of the flow/frequency relation.

Such calculations were done by considering a simple treatment for the uncertainty in frequency by using a discrete Fourier transform of a one-mode sinusoidal signal plus white noise [177, 155, 154]. For this, we have that

$$\Delta\omega_v^{BC} = \frac{\Delta u}{U_0 T}\sqrt{\frac{24}{N}} \ , \tag{5.26}$$

where N is the number of measurements in time, T is the total sampling time, U_0 is the amplitude of the sinusoidal mode, and Δu is the uncertainty in the tube vertical position in time domain.

Fig. 5.7(b) shows that the uncertainty in flow velocity is not significantly diminished by an increase on the amplitude of the initial condition, so an initial amplitude of about 5-10 nm can be enough to carry out the experiment. In contrast, uncertainty is strongly dependent of sampling time, because it affects directly the uncertainty in frequency determination.

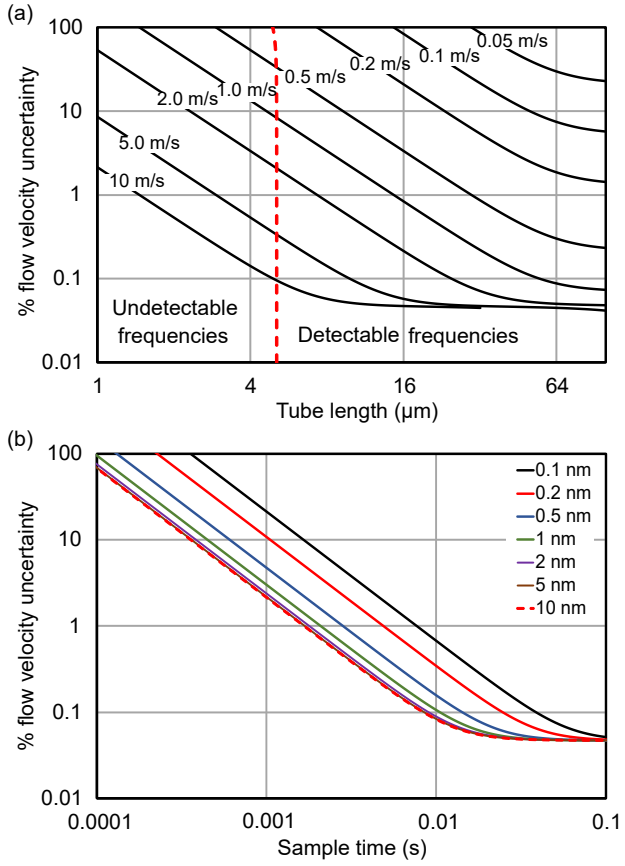

Figure 5.7: Effect of the main experimental parameters on the uncertainty in flow determination. (a) Expected uncertainty in the flow velocity as a function of the magnitude of the flow velocity for different tube lengths, with an initial amplitude of 5 nm. The time resolution of 0.05 μs determines an upper bound for the range of detectable frequencies. Such limit -given by the Nyquist frequency- is shown in the red dashed line. (b) Expected uncertainty in the flow velocity as a function of the sampling time for different amplitudes of the initial condition, with a tube length of 20 μm and a magnitude of flow velocity of 0.5 $\frac{m}{s}$. Calculations were done for a nanotube with pinned edges and the following physical parameters: inner and outer tube radius of 8 and 15 nm, respectively, water and carbon densities of 1000 and 2300 kg/m^3, respectively, uncertainty in radius of 0.1 nm, and uncertainty in densities of 0.1 kg/m^3.

Boundary condition	Range of frequency (MHz)	Range of flow velocity (m/s)
Pinned-pinned	0.58-0.9	0.3-40
Clamped-clamped	1.03-1.35	0.7-90
Pinned-clamped	0.64-0.9	0.3-60
Free-free	1.03-1.35	0.7-90
Pinned-free	0.64-0.9	0.5-60
Clamped-free	0.13-0.23	0.5-60

Table 5.2: Approximated range of suitability for a tube of 20 μm of length, subject to different boundary conditions. The range of flow magnitudes and frequencies is given in terms of the accurately-measurable flows and fundamental frequencies, i.e., the ones that reach an uncertainty of 5 % or lower in flow determination.

In general, flow determination is better for intermediate flow velocities, as the magnitude of the slope of the flow velocity/frequency function decreases with increasing flow magnitude. However, the range of such intermediate flow velocities, which are ideal for measurements, depends on the boundary conditions imposed on the specific experiment. This is illustrated in Table 5.2.

According to this, the best boundary condition will depend on the specific limitations of the actuators and sensors of a particular experimental setting. For the cases where the experimental time resolution is limited, the fundamental frequency of a clamped-free tube is the lowest and allows for an easier detection. Besides, if the driving pressure gradient is limited and only low flows could be generated, then pinned-pinned would be the preferred setting.

5.8 Final remarks

A theoretical framework to indirectly measure flow velocities within nanotubes has been developed. This one would give smaller uncertainties in flow velocities than conventional methodologies -that determine flow magnitude in systems of nanotubes

embedded in membranes-, because of the fact that it is limited by frequency measurements, and not by knowledge of the effective area to flow.

Our strategy does not assume a particular interaction between water and graphene, so it could be used regardless of the natural degree of hydrophobicity of the interaction, and it could also be used for functionalized nanotubes.

In our model, the average flow velocity, v, determines the bending frequency spectrum of the tube regardless of the presence or absence of slip in the system. Once v is experimentally determined, analytical expressions for steady state flow in the presence of slip, considering for example the Navier hypothesis for the slip velocity, could be used to determine slip lengths. These ones might differ from the ones currently reported in the literature.

However, such strategy can go further, by knowing not only the magnitude of the flow inside a nanotube but some characteristics of its radial profile. This might help to partially clarify the existing controversy concerning the real velocity profile inside carbon nanotubes, in order to quantify slip lengths [35, 36, 37, 38]. Also, it might shed light onto the discussion regarding the effects of shear thinning and viscoelasticity in mica channels [3, 178, 62].

Our work might constitute the basis to propose a wide range of experiments of flow across nanostructures in different experimental situations focusing on frequency measurements. It also constitutes a basic framework that could be extended to determine other structural and rheological fluid properties by means of indirect frequency measurements rather than by conventional methods.

6

Fluid dynamics influenced by simple tube motion

In Chapter 4, the physical interpretation of the modified Navier-Stokes equation was given in terms of the role of tube/fluid interactions that tend to cancel the forces that arise in a non-inertial frame of reference in order to allow the fluid to flow parallel to the walls.

In order to complete the physical picture of the fluid dynamics influenced by tube vibration, a deeper insight is needed. A comprehensive and quantitative study requires to impose a specific condition for the tube dynamics and, subsequently, analyse the phenomenology that arises under such condition.

To do so, the fluid dynamics is studied for a tube that moves in a single vibration mode. It is the simplest motion of tube dynamics and it gives a simple expression for the tube/fluid forces $\rho g(t)v$ and $\rho h(t)$. It constitutes the natural departing point to establish the consequences of tube/fluid coupling into the fluid dynamics.

As an example of the different phenomena that our methodology allows to unveil, we report a new phenomenon in the limit in which the tube modifies the dynamics of the fluid, *i.e.*, it gives a modified Navier-Stokes equation, accounting for the tube effect on the fluid motion. We predict an oscillatory velocity of the fluid, that persists at high frequencies, even for a fluid externally driven by a constant pressure drop.

6.1 Establishment of simple tube vibration

In contrast to the dynamics presented in Chapter 5, where the result can be compared immediately with previous results in the literature [108], this is the first time, to the best of our knowledge, that flow velocity is solved analytically in this type of system.

Since the tube dynamics is solved independently of the fluid motion, a particular solution for tube dynamics is obtained first. Then, the tube dynamics is incorporated into the fluid dynamics equation, via the functions $g(t)$ and $h(t)$. This implies that a specific form of $u(z,t)$, determines the features of fluid motion.

In general, $u(z,t)$ is obtained by solving Eq. (4.1) accounting for boundary and initial conditions, with solutions of the form:

$$u(z,t) = \sum_{m=1}^{\infty} C_m f_m(z) \cos(\omega_m t + \varphi_m) \ . \tag{6.1}$$

A set of boundary conditions is chosen among the five different combinations detailed in Chapter 3, which are a consequence of the experimental setting intended to model, related to the way in which the tube edges are fixed. The chosen set (pinned-pinned, clamped-clamped, etc.) determines the shape of the vibration modes, *i.e.*, the modulation function $f_m(z)$ and frequency spectrum ω_m. The initial condition accounts for the initial deformation exerted on the tube, in order to start its vibration. This one determines the number of modes excited at once, through the amplitude of each vibration mode, C_m, and its corresponding phase, φ_m. The frequency spectrum of each set of boundary conditions is summarized in Table 6.1. Analytical expressions for $f_m(z)$ are given in Appendix A.9.

The simplest way to induce tube vibrations consists of the excitation of a single mode. Regardless of the specific set of boundary conditions, the tube dynamics of a tube excited only in its *n-th* vibration mode, is given by

$$u(z,t) = U_0 f_n(z) \cos(\omega_n t) \ , \tag{6.2}$$

Boundary conditions	Frequency spectrum ω_n
Pinned-pinned	$n^2\omega_0$
Clamped-clamped	$\left(n+\frac{1}{2}\right)^2\omega_0$
Pinned-clamped	$\left(n+\frac{1}{4}\right)^2\omega_0$
Pinned-free	$\left(n+\frac{1}{4}\right)^2\omega_0$
Clamped-free	$\left(n-\frac{1}{2}\right)^2\omega_0$

Table 6.1: Frequency spectrum for each set of boundary conditions. Each frequency is expressed in terms of a reference frequency ω_0 defined as $\omega_0 = \frac{\pi^2}{L^2}\sqrt{\frac{EI}{\rho A_f + \rho_t A_t}}$.

where U_0 corresponds to the C_n coefficient, and the phase is set to $\varphi_n = 0$.

6.2 *Tube-induced forces for a one-mode vibration: local vs global behavior*

When the tube displacement in Eq. (6.2) is incorporated into Eqs. (3.41)-(3.42), expressions for the terms $g(t)$ and $h(t)$ are obtained:

$$g(t) = \frac{\omega_n A U_0^2}{L^2}\sin(2\omega_n t) \ , \tag{6.3}$$

$$h(t) = \frac{\omega_n^2 B U_0^2}{L}\cos(2\omega_n t) \ , \tag{6.4}$$

where A and B are geometrical factors, different for each set of boundary conditions at the tube extremes. Their analytical expressions are included in Appendix A.9.

Geometrical factors A and B convey information of the local behavior of tube motion, characteristic of the spatial modulation of each vibration mode. Particularly, it turns out that $B = 0$ for all sets of boundary conditions, except for the ones where one edge is free. In physical terms, it means that the effective pushing force is cancelled when integrated along the tube for tubes with fixed edges.

Such a trend can be understood by inspection of the integrand of $g(t)$ and $h(t)$ in Eqs. (3.41)-(3.42). Both integrands are of the form $g_L(z,t)$ and $h_L(z,t)$. They give the

local behavior of the system. It is necessary to recall that $g(t)$ and $h(t)$ incorporate the tube motion into Navier-Stokes equation. For compressible fluids, such local forces would cause axial profiles of the fluid velocity; however, for incompressible fluids subject to uniaxial flow, as the one considered in the present study, only the integral contributions of the tube-induced forces have an effect on the fluid. Thus, an insight into the local behavior of $g_L(z,t)$ and $h_L(z,t)$ is useful.

The most important difference between the local $g_L(z,t)$ and $h_L(z,t)$ can be understood in terms of cooperative and competing effects (see integrands in Eqs. (3.41)-(3.42)). Since the angular velocity, $\frac{\partial^2 u}{\partial z \partial t}$, and the tube slope, $\frac{\partial u}{\partial z}$, change sign at the same points in the tube for all sets of boundary conditions, with at least one fixed edge (see Figs. 6.1a-6.1f), the Coriolis term, $g_L(z,t)$, drives the fluid in the same direction at every region within the tube (see Figs. 6.1g-6.1i). Therefore, the local effect on the fluid is determined by two cooperating effects, which has the same sign all along the tube.

In contrast, the sign of the local force $h_L(z,t)$, is subject to competing effects, since the tube vertical acceleration, $\frac{\partial^2 u}{\partial t^2}$, only changes sign at the nodes of the tube displacement, which in general, are located at different points than the ones where the slope changes sign. For tubes with fixed edges, the spatial contributions to $h(t)$ are cancelled along the tube in between nodes; whereas the tubes with a free edge exhibit an additional contribution, where there is no node at the tube extreme. The region from the last node to the free edge, is called the free region (see Fig. 6.1f). The force at this region is responsible for the special features in tubes with one free edge.

6.3 Analytical solution of flow velocity

The expressions for $g(t)$ and $h(t)$ in Eqs. (6.3) and (6.4) are incorporated into the solution for $v(r,t)$ given in Eq. (4.24). An analytical solution for the one-mode vibration

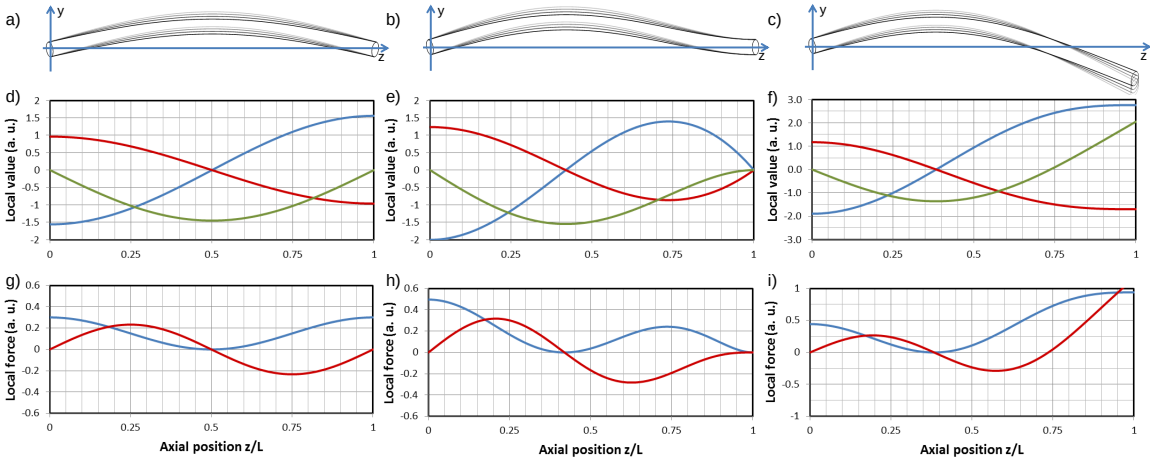

Figure 6.1: Local forces on the tube. First row shows three different sets of boundary conditions: pinned-pinned, pinned-clamped and pinned-free. Their vibration is represented with evanescent gray lines to emphasize the position of the tube nodes (regions with no displacement). The second row shows the value of the local angular velocity (blue line), tube slope (red line) and tube acceleration (green line). The third row shows the local value of $g_L(z,t)$ (blue line) and $h_L(z,t)$ (red line).

tube will be obtained afterwards. As Eq. (4.24) shows, it is necessary to compute the Fourier transform of both, $\frac{\partial p}{\partial z} e^{\int_{t_0}^{t} g(t)dt}$ and $\rho h(t) e^{\int_{t_0}^{t} g(t)dt}$, which is not possible by analytical means.[1] However, it is possible to approximate such computation by expressing $e^{\int_0^t g(t)dt}$ as

$$\begin{aligned} e^{\int_{t_0}^{t} g(t)dt} &= e^{\frac{AU_0^2}{2L^2}(1-\cos(2\omega_n t))} \\ &= e^{\frac{AU_0^2}{2L^2}} \sum_{m=0}^{\infty} \frac{1}{m!} \left(-\frac{AU_0^2}{2L^2} \cos(2\omega_n t) \right)^m . \end{aligned} \tag{6.5}$$

The series defined in Eq. (6.6) is absolutely convergent because each term's amplitude depends on successive powers of U_0^2/L^2, which is equal or lower than 10^{-4}, for the purpose of this work, within the small deformation limit. Also, such expansion is useful because the Fourier Transform of each term can be computed by analytical means.

After the computation of the integrals in Eq. (4.24) and an expansion to fourth order in the relative deformation ε, defined as $\varepsilon = U_0/L$, the following expression is

[1]The lower limit in such integrals is an arbitrary time t_0. For practical purposes, we perform computations considering $t_0 = 0$.

obtained for the radially-averaged flow velocity, $\langle v \rangle$, as

$$\langle v \rangle = K_0 + K_{2\omega}^c \cos(2\omega_n t) + K_{2\omega}^s \sin(2\omega_n t) \tag{6.6}$$

where K_0, $K_{2\omega}^c$ and $K_{2\omega}^s$ are given, respectively, by

$$K_0 = -\frac{\partial p}{\partial z}\frac{R^2}{8\mu} + \left(-\frac{\partial p}{\partial z}\frac{A^2\varepsilon^4 R^2}{64\mu} + \frac{\rho\omega_n^2 LAB\varepsilon^4 R^2}{32\mu}\right)\left(1 + \Re f_{bes}\left(\frac{2\rho\omega_n R^2}{\mu}\right)\right) , \tag{6.7}$$

$$K_{2\omega}^c = -\frac{\partial p}{\partial z}\frac{A\varepsilon^2 R^2}{16\mu} + \left(-\frac{\partial p}{\partial z}\frac{A\varepsilon^2 R^2}{16\mu} + \frac{\rho\omega_n^2 LB\varepsilon^2 R^2}{8\mu}\right)\Re f_{bes}\left(\frac{2\rho\omega_n R^2}{\mu}\right) , \tag{6.8}$$

$$K_{2\omega}^s = \left(-\frac{\partial p}{\partial z}\frac{A\varepsilon^2 R^2}{16\mu} + \frac{\rho\omega_n^2 LB\varepsilon^2 R^2}{8\mu}\right)\Im f_{bes}\left(\frac{2\rho\omega_n R^2}{\mu}\right) , \tag{6.9}$$

with f_{bes} given by

$$f_{bes}(x) = \frac{8}{ix}\left(1 - \frac{2J_1\sqrt{ix}}{\sqrt{ix}\,J_0\sqrt{ix}}\right) , \tag{6.10}$$

and $\Re f_{bes}$ and $\Im f_{bes}$ account for its real and imaginary parts, respectively.

6.4 Qualitative analysis of the results

Two main consequences arise from Eq. (6.6).

First, the Coriolis term, $g(t)$, proportional to $A\varepsilon^2$, is capable to induce a change in the net flow by itself or by its interaction with the tube effective pushing $h(t)$. This phenomenon can be appreciated by inspection of K_0 in Eq. (6.7), where the zero-frequency flow caused by the constant driving force, namely, $-\frac{\partial p}{\partial z}\frac{R^2}{8\mu}$, is modified by two terms that depend on the square amplitude of $g(t)$, namely, $A^2\varepsilon^4$; and the amplitude of $g(t)h(t)$, namely, $AB\varepsilon^4$. These terms have an overall dependence on ε^4. Thus, even for relative large values of the tube deformation (around $\varepsilon \approx 10^{-2}$), all the terms proportional to ε^4 cause a change in net flow which is eight-orders of magnitude lower than the flow exerted by the constant pressure gradient. In other words, a tube vibrating in a single mode is able to produce a net flow enhancement, however, such an enhancement is negligible for all practical purposes.

The second consequence is that the tube oscillation is capable to induce oscillations in the flow velocity. This can be appreciated by observing the oscillatory terms in

Eq. (6.6). It is interesting to note that the amplitude of the oscillatory component of flow, computed as $v_{osc} = \sqrt{(K_{2\omega,c})^2 + (K_{2\omega,s})^2}$, varies with ε^2, which leads to an amplitude of the oscillation small but non negligible. Therefore, the tube vibration provides a mechanism to induce oscillatory flow within elastic nanostructures.

In general, this type of system tends to couple all the characteristic times that are present in the driving force. For a given driving force with two characteristic frequencies, namely, ω_n and ω_m, the final response incorporates a term with a frequency $\omega_n + \omega_m$ and another with a frequency $\omega_n - \omega_m$.

Inspection of Eq. (6.6) allows one to understand that the oscillatory flow velocity developed within an oscillating tube, is caused by two contributions:

- The interaction between the constant pressure gradient and the Coriolis force, that corresponds to the terms proportional to $A\varepsilon^2$ in Eqs. (6.8)-(6.9).
- The pulsatile driving force exerted by the tube pushing, given by the term $-\rho h(t)$, that corresponds to the terms proportional to $B\varepsilon^2$ in Eqs. (6.8)-(6.9).

An interesting manner to study such oscillatory flow is by comparing it with the classical mechanism to generate pulsatile flow via an oscillatory pressure gradient of the form $\frac{\partial p}{\partial z} = \frac{\partial p_0}{\partial z}\cos(2\omega_n t)$. That is, a one-mode oscillatory pressure gradient of amplitude $-\frac{\partial p_0}{\partial z}$ and frequency $2\omega_n$. The flow velocity, v_{press}, is given by [179, 136]:

$$v_{press} = -\left|\frac{1}{2i\rho\omega_n}\left(1 - \frac{2J_1\sqrt{\frac{2i\rho\omega_n R^2}{\mu}}}{\sqrt{\frac{2i\rho\omega_n R^2}{\mu}}J_0\sqrt{\frac{2i\rho\omega_n R^2}{\mu}}}\right)\right|\frac{\partial p_0}{\partial z}\cos(2\omega_n t + \varphi), \tag{6.11}$$

where φ, is the phase between velocity and pressure gradient.

The first contribution to pulsatile flow in our model is given by the tube pushing, when no external pressure gradient is exerted on the fluid, that is, when $\frac{\partial p}{\partial z} = 0$ in Eq. (4.24). In this case, Eq. (6.6) leads to an expression of the form:

$$v_h = \left|\frac{1}{2i\rho\omega_n}\left(1 - \frac{2J_1\sqrt{\frac{2i\rho\omega_n R^2}{\mu}}}{\sqrt{\frac{2i\rho\omega_n R^2}{\mu}}J_0\sqrt{\frac{2i\rho\omega_n R^2}{\mu}}}\right)\right|\rho\omega_n^2 BL\varepsilon^2\cos(2\omega_n t + \varphi) \tag{6.12}$$

Comparison of Eqs. 6.11 and 6.12 allows one to think of a pulsatile flow caused by an oscillatory driving force, of frequency $2\omega_n$ and amplitude $\rho\omega_n^2 BL\varepsilon^2$, which, in turn, is the amplitude of $\rho h(t)$ in Eq. (6.4). In other words, the tube pushing force plays a similar role than an oscillatory pressure gradient, and leads to the classical response of a pulsatile newtonian fluid.

Moreover, we can compare the pulsatile pressure gradient scheme, with the second contribution to pulsatile flow in our model, when our system is studied in the absence of tube pushing, that is $h(t) = 0$ in Eq. (4.24).[1] In such case, the oscillatory flow velocity is given only by the interaction between the Coriolis force and the constant pressure gradient, as

$$v_g = -\frac{A\varepsilon^2 R^2}{16\mu}\frac{\partial p}{\partial z}\cos(2\omega_n t) - \frac{A\varepsilon^2}{2}\left|\frac{1}{2i\omega_n\rho}\left(1 - \frac{2J_1\sqrt{\frac{3i\rho\omega_n R^2}{\mu}}}{\sqrt{\frac{2i\rho\omega_n R^2}{\mu}}J_0\sqrt{\frac{2i\rho\omega_n R^2}{\mu}}}\right)\right|\frac{\partial p}{\partial z}\cos(2\omega_n t+\varphi)\,, \tag{6.13}$$

In contrast to the previous expressions for pulsatile flow, v_g exhibits an anomalous behavior. v_g can be understood as the sum of two components: the first one is always in phase with the Coriolis force and has an amplitude independent of the vibration frequency; the second one, is the typical response of a pulsatile flow with frequency 2ω and an oscillating driving force of amplitude $-\frac{\partial p}{\partial z}\frac{A\varepsilon^2}{2}$.

The peculiar behavior of v_g is more evident when compared with v_{press} in the zero-frequency and infinite-frequency limits. At low frequencies, the amplitude of flow velocity v_{press} is finite, and given by $-\frac{R^2}{8\mu}\frac{\partial p_0}{\partial z}$. In contrast, v_g leads to

$$\lim_{\omega_n\to 0} v_g = -\frac{\partial p}{\partial z}\frac{A\varepsilon^2 R^2}{16\mu} + \frac{\partial p}{\partial z}\frac{A\varepsilon^2}{2}\left(\frac{R^2}{8\mu}\right) = 0\,. \tag{6.14}$$

Eq. (6.14) shows that both terms cancel each other in the zero frequency limit.

On the other hand, in the infinite-frequency limit, the amplitude of flow velocity of v_{press} tends to zero. In contrast, the first term in v_g oscillates with constant amplitude,

[1] Such condition is achieved for tubes with both edges fixed, as previously stated in this Chapter.

whereas the second term vanishes, leading to the following result:

$$\lim_{\omega_n \to \infty} |v_g| \quad = -\frac{\partial p}{\partial z} \frac{A\varepsilon^2 R^2}{16\mu} \,. \tag{6.15}$$

Finally, it is possible to compare the pulsatile pressure scheme with ours, for the case of a tube subject to both, tube pushing and a constant pressure gradient. The cooperative role between the pressure-Coriolis and the tube pushing effects lead to very interesting results. This case will be studied in the following section.

6.5 Quantitative behavior of oscillatory flow velocity via dimensionless parameters

To achieve a simple and complete description of such conditions, it is useful to define three dimensionless parameters, that summarize the physics described in the previous analysis.

First the separation between low and high frequencies can be stated in terms of the ratio between the tube vibration frequency and the viscous frequency, $\omega_\mu = \frac{\mu}{\rho R^2}$, given by the Womersley number, Wo, as

$$\mathrm{Wo} \equiv \frac{\omega_n}{\omega_\mu} \tag{6.16}$$

Second, the relative dominance between pressure gradient and tube effective pushing is quantified by defining the dimensionless pressure gradient F, as

$$F \equiv -\frac{\frac{\partial p}{\partial z}}{\rho \omega^2 L} = -\frac{\partial p}{\partial z} \frac{1}{\rho L \mathrm{Wo}^2 \omega_\mu^2} \,. \tag{6.17}$$

Finally, flow velocity is reescaled in a way as to have the ratio of velocity and driving force, to coincide with the classical description of flow driven by a pulsatile pressure gradient in a rigid tube, when the Coriolis force is irrelevant. In other words, when the contribution given by Eq. (6.13) is negligible when compared to the one given by Eq. (6.12). Such a reescaled flow velocity, v^*, is defined as

$$v^* \equiv \frac{\langle v \rangle}{v_{charact}} = \frac{8}{L}\frac{\langle v \rangle}{\mathrm{Wo}^2 \omega_\mu} \tag{6.18}$$

In terms of Wo, F, and v^*, flow velocity in Eq. (6.6) is rewritten as

$$v^* = K_0^* + K_{2\omega,c}^* \cos(2\mathrm{Wo}\,\omega_\mu t) + K_{2\omega,s}^* \sin(2\mathrm{Wo}\,\omega_\mu t) \tag{6.19}$$

where K_0^*, $K_{2\omega,c}^*$ and $K_{2\omega,s}^*$, in Eqs.(6.7-6.9) are given, respectively, by

$$K_0^* = F + \left(\frac{FA^2\varepsilon^4}{8} + \frac{AB\varepsilon^4}{4}\right)\left(1 + \Re f_{bes}(2\mathrm{Wo})\right) , \tag{6.20}$$

$$K_{2\omega,c}^* = \frac{FA\varepsilon^2}{2} + \left(\frac{FA\varepsilon^2}{2} + B\varepsilon^2\right)\Re f_{bes}(2\mathrm{Wo}) , \tag{6.21}$$

$$K_{2\omega,s}^* = \left(\frac{FA\varepsilon^2}{2} + B\varepsilon^2\right)\Im f_{bes}(2\mathrm{Wo}) , \tag{6.22}$$

whereas the amplitude of the oscillatory component of flow velocity, is

$$v_{osc}^* = \sqrt{\left(K_{2\omega,c}^*\right)^2 + \left(K_{2\omega,s}^*\right)^2} . \tag{6.23}$$

v_{osc}^* is plotted, with continuos lines, as a function of the dimensionless frequency, Wo, for different values of the dimensionless driving force, F, in Fig. 6.2. It can be understood in terms of the relative contributions of the terms containing FA, and the terms containing B, to the oscillatory flow velocity, which are additive, in Eqs. (6.21 and 6.22). One contribution, given by $FA = 0$, corresponding to the pushing case of the previous section, (included as a monotonically decreasing dashed red line in Fig. 6.2); and another one, when $B = 0$, corresponding to the Coriolis regime (included as monotonically increasing dashed lines in Fig. 6.2), for a given A and various values of F.

At zero or low values of F (up to 10^{-1} in the picture) and low Wo (up to 1 in the picture), the effective pushing is orders of magnitude larger that the Coriolis force. Therefore, the amplitude of the velocity as a function of frequency exhibits the typical behavior of the one of an oscillating driving force acting on the confined fluid, namely, at low frequencies, there is a plateau in a log-log scale. For higher

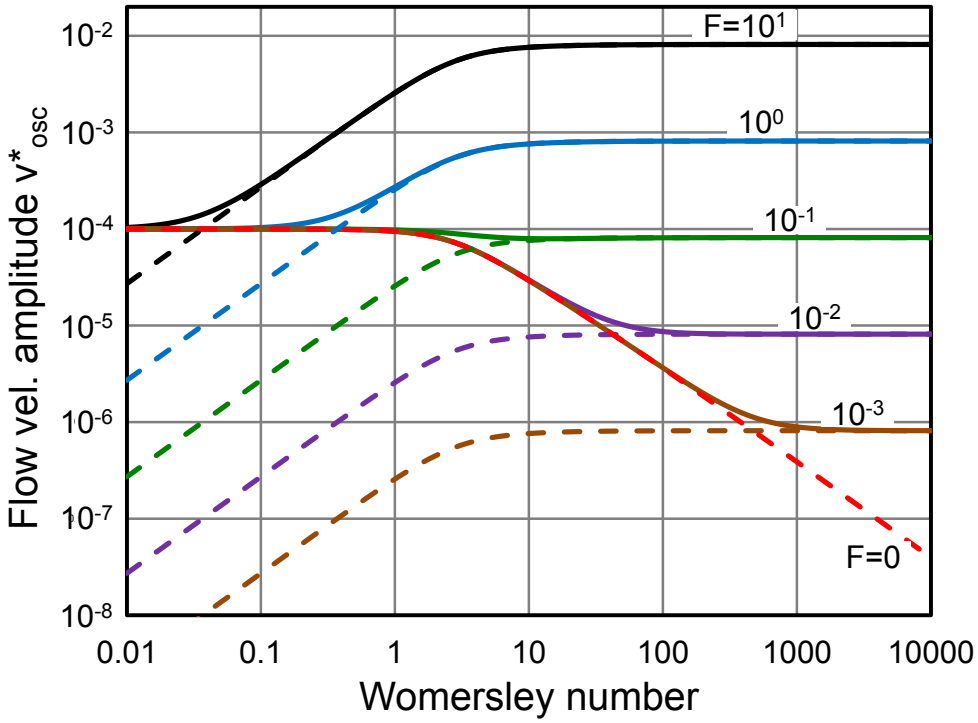

Figure 6.2: Effect of the magnitude of the pressure gradient and the frequency of tube oscillation in amplitude of the oscillatory flow induced within a pinned-free tube vibrating at its fundamental mode. Each continuous curve represents the amplitude/frequency relationship for different values of the dimensionless pressure gradient, F. Also, the individual contributions to the flow amplitude are shown, namely, the effective pushing contribution (red dashed line) and the Coriolis contributions (dashed lines in other colors).

values of Wo, (above 1 in the picture) the shorter the forcing period, the smaller the amplitude of fluid motion. That is, there is a frequency region where the classical monotonic decrease of flow amplitude can be appreciated for any value of F, on the range that is being discussed. On the other hand, from the different dashed lines with a monotonic increase with Wo, it is clear that the Coriolis force, increases with increasing value of Wo. This happens up to a critical value of Wo, different for each value of F, where the Coriolis force is of the same magnitude than the pushing force. This can be appreciated when the different Coriolis contributions, given by the monotonically increasing dashed lines, cross the monotonically decreasing dashed red line, that gives the pushing contribution to the velocity. After the crossing, for larger values of Wo, the dominant force of the system is the Coriolis force. This one causes the flow velocity to reach a constant amplitude.

In contrast, at high values of the dimensionless driving force F (for instance see $F = 10$ in the picture), such panorama changes. This is the case of having a much larger pressure gradient than the forcing caused by pushing, for any frequency. As can be appreciated in the figure, the crossover between the Coriolis force and the effective pushing (dashed red line) occurs at much lower values of Wo, in the region where the pushing force still has a low-frequency plateau, in a log-log scale. This leads to an atypical flow magnitude/frequency relationship, that, for low values of Wo, increases as a function of Wo. Such regime, characterized by a positive flow/frequency slope, ends up when the pulsation frequency reaches the viscous frequency, that is Wo=1, and the flow velocity amplitude reaches an asymptotic value, which in turn, is the same than the discussed for low-pressure gradients in Eq. (6.25).

The transition between the low and high driving forces regimes, occurs at

$$F_{transition} = \frac{2B}{A} \ . \tag{6.24}$$

For values of F smaller than $F_{transition}$, the high-frequency plateau is below the one of low frequency. For values of F larger than $F_{transition}$, the high-frequency plateau is

above the one of low frequency.

The asymptotic value of flow amplitude at large frequencies is given by

$$\lim_{\mathrm{Wo}\to\infty} v^*_{osc} = \frac{FA\varepsilon^2}{2} \ . \tag{6.25}$$

In terms of dimensional variables it gives an assymptotic value only dependent on the magnitude of the pressure gradient, showing clearly that a finite pressure gradient is needed in order for the Coriolis force to modify flow due to tube vibrations.

$$\lim_{\omega\to\infty} v_{osc} = -\frac{A\varepsilon^2 R^2}{16\mu}\frac{\partial p}{\partial z} \ . \tag{6.26}$$

This asymptotic behavior is determined by the amplitude of the first term in Eq. (6.13), when the inertial and viscous forces have produced the decaying regime, both, in the second term of Eq. (6.13), and on Eq. (6.12).

6.6 Final remarks

Results of our model imply that generating tube vibrations constitute a potential strategy to experimentally induce oscillatory flow within nanostructures. Specially, this could be exploited for high frequencies, where the conventional mechanisms to induce flow oscillation have been demonstrated to be very limited. Our strategy would allow one to overcome high-frequency limitations, because of the non-linear nature of the Coriolis force, which guarantees an asymptotic amplitude for oscillatory flow at high frequencies, as long as a Hagen-Pouiseuille profile is developed by a constant pressure gradient to which the Coriolis force is coupled.

It is worth noticing that this behavior could be sustained as long as the oscillatory tube deformation exists. So, one can say that in order to generate high frequency oscillatory flows experimentally, our methodology predicts that a hardly achievable effect, namely, producing oscillatory flow by means of pulsatile pressure gradients, has been replaced by the problem of sustaining tube vibrations [144, 163, 180]. Since for many carbon nanotubes, deformations require very little energy, in fact, as little as

room temperature thermal energies, as discussed previously, our results indicate that a hardly achievable effect by conventional means, has become an easily achievable effect.

It would be necessary to deepen on this study in order to have a comprehensive picture of the role of Coriolis force in flow within nanostructures, when the tube dynamics is subject to a more complex deformation than the one analyzed in this work. The coupling of the tube and pressure gradient could be exploited in the future as a strategy to control flow within nanostructures by different mechanisms involving the capabilities of modern devices to perform nanometric manipulation of tubes conveying flow.

7

Conclusions and perspectives

Nanoscopic systems offer a surprising world of possibilities. In this work, we have explored a specific set of nanostructures: nanotubes conveying flow, capable to sustain bending motion because of their elasticity.

The intricate nature of the coupling between tube and fluid motion has been studied from two completely different points of view:

On the one hand, it is possible to detect and determine properties of flow velocity by detection of anomalies on the tube vibration spectrum. In other words, since fluid flow affects tube motion, a change in tube vibration could be related to properties of flow velocity. On the other hand, it is possible to modify the flow velocity inside nanotubes by externally and periodically bending the tube.

Despite the fact that the high amplitude flow detected in CNT membranes cannot be explained in terms of tube vibrations, both approaches have given us new insights on the capabilities to detect and control flow at nanoscales.

From the point of view of the author, there are two main perspectives from the theoretical work developed in this thesis, from a conceptual point of view:

First, the design of better strategies for indirect detection of complex properties of fluids confined inside nanotubes. Just as certain details of flow velocity and radial profile can be determined in this framework, it could be possible to go further, in order to detect more fluid flow details and rheological properties, that have been predicted by theoretical means in the literature, but have not been measured experimentally

due to the limitations of direct flow measurements at nanoscales.

Finally, the design of better strategies to control flow across nanotubes, by taking advantage of its coupling with tube vibrations. In this work, the simplest type of tube vibration was studied. It would be natural to go further and explore more complex schemes to generate and control tube vibrations, with a consequent improvement in the capabilities to generate sophisticated fluid responses. Here, we have shown that a simple single-mode vibration was able to induce oscillatory flows that do not vanish at ultra-high frequencies. What could be obtained, when more vibration modes and characteristic times are involved, is not intuitive and not obvious but it might eventually lead to produce a tailored fluid dynamics by mechanical means.

In the future, the capabilities to control flow across nanostructures via tube vibrations could offer an alternative to the current paradigm of chemical functionalization to optimize the permeability of nanoscale-pore membranes. In other words, the mechanical manipulation of nanostructures could therefore constitute an alternative way, much simpler and, perhaps, more efficient, to optimize flow in nanoscopic pores, filters and sieves.

8

Abstract in Spanish

Dinámica de fluidos en nanotubos oscilantes: Un estudio de medios continuos.

Introducción

La dinámica de fluidos sujetos a confinamiento nanométrico, es un área de gran importancia para el desarrollo de la ciencia básica y aplicada. El mundo de la nanoescala ofrece una ventana para la observación de conceptos físicos y químicos que no pudieron ser probados experimentalmente por siglos. Ideas tales como el resbalamiento y la fricción en la interfase sólido/líquido, el rol de las interacciones intermoleculares en la respuesta reológica de los fluidos, la relación entre la rugosidad de un tubo y la estructura del fluido —en la proximidad de la pared— en la formación de la capa límite hidrodinámica, han sido corroboradas y observadas en años recientes, gracias a las nuevas metodologías para diseñar dispositivos micro y nanofluídicos, junto con el desarrollo de técnicas y estrategias para controlar y medir la velocidad de flujo en esas escalas.

El comportamiento físico y químico de algunos dispositivos nanofluídicos ha desafiado la concepción clásica de la interacción tubo/fluido, de manera que ha sido necesario revisar las suposiciones y consideraciones que sustentan nuestra comprensión de los líquidos y sólidos interactuando en situaciones fuera del equilibrio.

En algunos casos, los sistemas nanométricos de flujo exigen una descripción física más compleja que los sistemas macroscópicos, requieren una visión fisicoquímica que tome en cuenta la formación de agregados y estructuras moleculares complejas que no se encuentran en sistemas macroscópicos. La mayoría de los esfuerzos teóricos que se realizan para mejorar los modelos fisicoquímicos que describen sistemas nanoscópicos de flujo, han seguido este enfoque.

En algunos otros casos, las características del mundo nanoscópico permiten realizar suposiciones que resultan inadecuadas para el modelado teórico de sistemas macroscópicos. Sorprendentemente, algunas de estas consideraciones dan lugar a una simplificación de las ecuaciones que determinan la dinámica de sistemas nanofluídicos, en comparación con las ecuaciones que modelan sistemas macroscópicos análogos. Esto es posible porque el mundo nanoscópico ofrece una escala única en su tipo, donde convergen dos situaciones físicas singulares: la cantidad de moléculas es suficientemente grande para llevar a cabo una descripción del sistema en términos de propiedades y descriptores continuos; y el tamaño del confinamiento es suficientemente pequeño, de manera que no pueden desarrollarse algunos fenómenos que se manifiestan en sistemas de flujo macroscópicos sujetos a esfuerzos complejos, tales como flujo secundario y patrones tridimensionales de flujo. Tales fenómenos requieren un espacio mínimo para formarse y desarrollarse.

Los artefactos micro y nanofluídicos constituyen sustratos prometedores. La miniaturización de los procesos implica una reducción considerable de la cantidad de reactivos y residuos químicos involucrados. Al mismo tiempo, el control de fenómenos difusivos mejora significativamente en canales en la micro y nanoescala, debido a que efectos convectivos tales como la inestabilidad de flujo, la formación de vórtices y turbulencia, son prácticamente inexistentes en esta escala de confinamiento. Por lo tanto, es posible fabricar sistemas de flujo donde las condiciones del mezclado de fluidos y la estabilidad de interfaces fluido/fluido sean controladas perfectamente.

La mayoría de las aplicaciones actuales de los dispositivos nanofluídicos están inspi-

radas en la mimetización de canales biológicos [25], con nanoestructuras de tamaños y geometrías similares [26, 27, 28]. Como consecuencia, se ha ampliado el espectro de las nanoestructuras existentes para transportar fluido en su interior. Hoy en día, los sistemas nanofluídicos están hechos de una diversidad de materiales y arreglos de canales [29, 30, 31], cuyo tamaño va de unos pocos nanómetros hasta cientos de micras, tanto en longitud como en radio [32, 33, 34]. Sin embargo, entender la física subyacente en el flujo de fluidos a través de nanoestructuras sigue siendo un reto en cuanto a la predicción del orden de magnitud del flujo y su control.

Antecedentes

Los enfoques teóricos existentes para el estudio de sistemas nanotubo/fluido pueden clasificarse en tres grandes grupos: modelos atomísticos de dinámica molecular; modelos basados en la mecánica de medios continuos; y, finalmente, modelos híbridos de los dos anteriores.

Ambos tipos de enfoques, discreto o continuo, han resultado de utilidad bajo diferentes situaciones físicas.

Las simulaciones de dinámica molecular son particularmente útiles en el estudio de los nanotubos de radios más pequeños, donde se presentan fuertes fluctuaciones en la densidad de los fluidos y una descripción discreta es indispensable para entender regímenes de flujo tales como el flujo balístico en el que las moléculas de agua forman un arreglo unidimensional, o en el denominado flujo de Knudsen, en el que la dinámica del flujo se encuentra dominada por las colisiones e interacciones de moléculas aisladas de fluido con la pared [95, 35].

Las simulaciones de dinámica molecular han sido fundamentales para entender las fluctuaciones de la densidad del agua en la proximidad de las paredes de un tubo; asimismo, se ha demostrado que las moléculas de agua al interior de nanotubos de carbono muy pequeños, se relajan formando estructuras complejas que no tienen

equivalente en las fases macroscópicas conocidas. Estos resultados han permitido establecer un marco teórico de las interacciones tubo/fluido y su influencia en la desviación de las propiedades continuas en la nanoescala. Sin embargo, la simulación de tubos largos o de tiempos de simulación relativamente altos, no es posible en este tipo de simulaciones, debido a su alto costo computacional. Aunado a esto, los parámetros de los campos de fuerza utilizado en las simulaciones de dinámica molecular deben ajustarse de acuerdo con el arreglo experimental que se desea simular [98, 99, 100]. Estas limitaciones han sido un obstáculo para establecer tendencias generales en el comportamiento de fluidos nanoconfinados.

A diferencia de los modelos atomísticos, la mecánica de medios continuos ha resultado de utilidad para simular tubos relativamente grandes, en prácticamente cualquier escala temporal [2, 107, 108, 109, 110, 111]. Un modelo continuo ofrece una comprensión de la compleja interacción tubo/fluido, a través de una descripción promedio de la misma.

En la literatura, los estudios de medios continuos en nanoestructuras que transportan fluido, comenzó considerando tubos rígidos estáticos. En tales simulaciones, la interacción tubo/fluido se incorpora mediante el resbalamiento de fluido en la interface fluido/pared [2, 10]. Asimismo, los estudios en la dinámica de fluidos a través de tubos doblados han arrojado resultados analíticos en los que el fluido exhibe un flujo complejo que consiste de un flujo primario, paralelo al tubo, y un flujo secundario que forma un patrón helicoide tridimensional en las líneas de corriente [6]. A diferencia de los patrones obtenidos en otras geometrías, estas líneas de flujo no presentan una inestabilidad turbulenta [112]. Este resultado aparece solamente para tubos doblados con una curvatura local relativamente alta.

La incorporación de la vibración del tubo a la descripción de flujo nanoscópico, se ha llevado a cabo únicamente para flujos tipo tapón, sin tomar en consideración las peculiaridades de la respuesta del fluido a la fuerza motriz, ni información de la dinámica y perfiles espaciales del flujo; es decir, en esos modelos, la velocidad del

fluido es un parámetro constante dentro del modelo [107, 108, 109, 113, 114]. Un modelo continuo que incorpore tanto el efecto del fluido en la dinámica del tubo, como la descripción de la dinámica del fluido influida por las oscilaciones del tubo, se encuentra ausente en la literatura.

El interés por tomar en cuenta ambos niveles de descripción física del sistema de flujo, ha inspirado el desarrollo de modelos híbridos [7, 126, 127, 128]. Los primeros intentos de conjuntar la visión continua y atomística de estos sistemas, se desarrollaron con el propósito de simular sistemas electromecánicos micro y nanoscópicos, llamados MEMS y NEMS, que incorporan sistemas fluídicos complejos en los cuales canales macro, micro y nanoscópicos se embeben en redes y geometrías intrincadas.

Es conveniente recalcar que los problemas asociados a los modelos atomistas persisten en los modelos híbridos, en lo concerniente a la imposibilidad de establecer tendencias generales, dado que los resultados obtenidos son particulares del fluido, de las dimensiones y de la representación física de la interacción fluido/pared.

Modelando la interacción tubo/fluido en situaciones dinámicas

En este trabajo, se propone un marco teórico dentro de la mecánica de medios continuos, con el fin de estudiar fluidos confinados al interior de nanotubos oscilantes doblados. Para ello, se propone una consideración física fundamental: el fluido sólo puede moverse paralelamente al tubo.

Esta suposición se justifica debido a la imposibilidad de los fluidos de desarrollar un flujo secundario a escalas nanométricas. Esto resulta muy conveniente en un sentido matemático, porque permite un estudio analítico de este sistema dinámico, tanto en lo concerniente a la obtención de las ecuaciones que rigen su dinámica, como para su solución.

Nuestro tratamiento se basa en el Principio de Mínima Acción, el cual ha sido utilizado de manera exitosa para establecer la dinámica de Navier Stokes cuando un

fluido está sujeto a un amplio rango de fuerzas y restricciones físicas [115, 122, 116, 117, 118, 119, 123, 120]. Tal metodología resulta especialmente útil cuando existen restricciones impuestas en el sistema físico, ya que es posible incorporar tales consideraciones en la ecuación de movimiento resultante, de una manera clara, intuitiva y consistente [124, 121, 115]. El principio de mínima acción para un sistema abierto a temperatura constante, está dado por

$$\delta S + \delta W + \delta C = 0 \ , \tag{8.1}$$

donde S es la acción del Sistema, dada a partir del lagrangiano, $L = T - V$.

Se modela un sistema tubo/fluido a través de dos variables dinámicas: el desplazamiento vertical del tubo, u, y la velocidad del fluido, v. Para hacerlo, se modela al tubo como una cilindro hueco elástico de Euler-Bernoulli, sujeto a deformaciones pequeñas, en ausencia de tensión axial. Asimismo, se considera que el radio del tubo es mucho más pequeño que su longitud y que el radio de curvatura que alcanza el tubo en su punto de máxima deflexión. El interior del tubo se encuentra lleno de un fluido newtoniano incompresible. El sistema se mantiene en condiciones isotérmicas.

La acción, S, se expresa en términos del lagrangiano del sistema tubo/fluido, L, como sigue:

$$L = T_t + T_f - V_t - V_f - V_{t/f} \ , \tag{8.2}$$

donde T_t, T_f , V_t y V_f denotan la energía cinética y potencial del tubo y fluido, respectivamente; $V_{t/f}$ es la energía potencial de interacción entre el tubo y el fluido.

La energía potencial del tubo está dado por la energía elástica, como

$$V_t = \int_V \frac{1}{2} EI \left(\frac{\partial^2 u}{\partial z^2} \right)^2 dV \ . \tag{8.3}$$

La energía potencial del fluido refleja la interacción que existe entre las partículas de fluido. En el marco de medios continuos, esta energía responde a cambios en la densidad del fluido, ρ, así como a la deformación $\frac{\partial \vec{r}_{fluid}}{\partial r}$. Por esta razón, la energía

potencial de fluidos incompresibles que no presentan propiedades elásticas se considera constante.

La presión y la viscosidad del fluido son considerados mediante el término W en la ecuación (8.1). Las fuerzas viscosas fueron excluidas del término de energía potencial, porque son disipativas. En estos términos, el trabajo W se expresa como

$$\delta W = \int_t \int_S (-p + \tau_{rz}) \delta z_{fluid} \, dS \, dt \ . \tag{8.4}$$

La primera restricción considerada en el sistema permite incorporar el acoplamiento entre la dinámica del tubo y del fluido. Mientras el tubo oscila, su dirección también cambia con el tiempo. Nuestra suposición establece que la velocidad relativa entre el fluido y el tubo es siempre paralela a la dirección del tubo. Matemáticamente, esto se expresa como

$$\vec{v}_{fluid} = \vec{v}_{tube} + v(r,t)\vec{q}_{tan} \ , \tag{8.5}$$

en donde $\vec{q}_{tan}$ es un vector unitario que apunta en la dirección del tubo.

La ecuación (8.5) es suficiente para tomar en cuenta la interacción tubo/fluido; por ello, la energía potencial de interacción entre el tubo y el fluido se considera nula, es decir, $V_{tube/fluid} = 0$. La segunda restricción es la conservación de masa del fluido, dada por

$$\int_V \frac{\partial z_{fluid}}{\partial z} dV = 0 \ . \tag{8.6}$$

Al incorporar todos los términos de las ecuaciones (8.3), (8.4), (8.5) y (8.6) en el Principio de Hamilton (Ec. (8.1)), se obtienen dos ecuaciones de movimiento, que acoplan el desplazamiento del tubo, $u(z;t)$ y la velocidad del fluido $v(r;t)$, como se expresa a continuación:

$$EI\frac{\partial^4 u}{\partial z^4} + \rho A_f \langle v^2 \rangle \frac{\partial^2 u}{\partial z^2} + 2\rho A_f \langle v \rangle \frac{\partial^2 u}{\partial z \partial t} + \rho A_f \frac{\partial u}{\partial z}\frac{\partial \langle v \rangle}{\partial t} + \left(\rho A_f + \rho_t A_t\right)\frac{\partial^2 u}{\partial t^2} = 0 \ , \tag{8.7}$$

$$\rho \frac{\partial v}{\partial t} + \rho g(t) v + \rho h(t) + \frac{\partial p}{\partial z} - \mu \left(\frac{\partial^2 v}{\partial r^2} + \frac{1}{r}\frac{\partial v}{\partial r} \right) = 0 \ . \tag{8.8}$$

Resulta de utilidad darle un nombre a los términos involucrados en la Ecuación (8.8). El término $\rho g(t) v$ es la fuerza de Coriolis; el término $\rho h(t)$, que denominamos

la fuerza efectiva de empuje del tubo, es la suma de dos contribuciones: la fuerza centrífuga, dada por $\frac{\partial^u}{\partial z \partial t}\frac{\partial u}{\partial t}$, y la fuerza de empuje que ejerce el tubo sobre el fluido, dada por $\frac{\partial^u}{\partial t^2}\frac{\partial u}{\partial z}$. De manera análoga, en la ecuación (8.7), el término $\rho A_f v^2 \frac{\partial^2 u}{\partial z^2}$ se llama fuerza centrífuga; el término $2\rho A_f v \frac{\partial^2 u}{\partial z \partial t}$ es la fuerza de Coriolis; y el término $\rho A_f \frac{\partial v}{\partial t}\frac{\partial u}{\partial z}$ es la fuerza de empuje del fluido en el tubo.

A fin de tener un marco teórico completo para estudiar la dinámica acoplada del tubo y fluido, es necesario incorporar condiciones de frontera, tanto en la interfase fluido/pared como en los extremos del tubo. En este trabajo, se desea establecer los cambios que suceden en la dinámica del fluido como consecuencia de las vibraciones del tubo y que no involucren el resbalamiento del fluido en la pared. Por esta razón, se considera una condición de no resbalamiento en la interfase fluido/pared.

Por otro lado, las condiciones de frontera en los extremos del tubo reflejan el arreglo experimental que se utiliza en el sistema de estudio, pues reflejan la manera en que se fijan los extremos del tubo. Típicamente, un extremo puede estar clavado, anclado o libre. Todos esos casos son explorados en este trabajo.

Generalidades sobre la interacción tubo/fluido en situaciones dinámicas

A fin de extraer resultados relevantes de las ecuaciones de movimiento obtenidas, es necesario definir una estrategia para su solución. El procedimiento típico para abordar sistemas complejos no lineales de ecuaciones integro-diferenciales, consiste en la integración numérica de las ecuaciones a través de diversos métodos numéricos.

Por otro lado, las soluciones analíticas son útiles para el análisis posterior. En primer lugar, el tratamiento analítico permite identificar y entender el rol de cada parámetro físico y fuerza en la solución final para la dinámica del tubo y fluido. Además, el cálculo de casos límite y de resultados asintóticos es relativamente sencillo, de modo que el modelo teórico desarrollado puede ser puesto a prueba y com-

parado con resultados previos existentes en la literatura. Sin embargo, la obtención de soluciones analíticas usualmente conlleva aproximaciones y simplificaciones que la hacen diferir de la solución exacta.

En este trabajo, se desarrolla un tratamiento teórico para derivar expresiones analíticas de la solución del sistema de ecuaciones acopladas (3.36) y (3.37). En primer lugar, el sistema de ecuaciones se expresa en términos de parámetros adimensionales, que permiten comparar la influencia de una de las variables respecto a la otra de una manera sistemática. Tales parámetros resultan la amplitud del desplazamiento del tubo, respecto a su longitud, dado por U_0/L, y la velocidad del fluido respecto a la velocidad de propagación de ondas elásticas en el tubo, dado por v/v_{prop}.

El sistema completamente desacoplado asociado a las ecuaciones (3.36) y (3.37) está dado por

$$EI\frac{\partial^4 u}{\partial z^4} + \left(\rho A_f + \rho_t A_t\right)\frac{\partial^2 u}{\partial t^2} = 0 \ , \tag{8.9}$$

$$\rho\frac{\partial v}{\partial t} + \frac{\partial p}{\partial z} - \mu\left(\frac{\partial^2 v}{\partial r^2} + \frac{1}{r}\frac{\partial v}{\partial r}\right) = 0 \ . \tag{8.10}$$

La ecuación (8.9) corresponde al modelo de Euler-Bernoulli de un cilindro elástico hueco, lleno de un fluido estancado. La ecuación (8.10) es la ecuación de Navier-Stokes para un flujo uniaxial que se desarrolla al interior de un cilindro estático. Al comparar las ecuaciones (8.7) y (8.8) con las ecuaciones (8.9) y (8.10), es posible pensar en las ecuaciones desacopladas como un caso particular de las ecuaciones acopladas. Es decir, la ecuación (8.9) puede verse como un caso particular de la ecuación (8.7) en el que la velocidad del fluido es nula ($v(r;t) = 0$). Del mismo modo, la ecuación (8.10) es un caso particular de la ecuación (8.8) en el cual la amplitud de movimiento del tubo es nula ($u(z;t) = 0$). Por tanto, la ecuación (8.7) es la ecuación de Euler-Bernoulli modificada por efecto del tubo, mientras que la ecuación (8.8) es la ecuación de Navier-Stokes, modificada por la vibración del tubo.

Dinámica del tubo bajo la influencia del flujo de fluido

Cuando la amplitud del movimiento del tubo es muy pequeña (del orden de 10^{-4} o menor), es posible considerar que el fluido se mueve de manera independiente del tubo. De este modo, se puede modelar al sistema con las ecuaciones (8.7) y (8.10), para centrar nuestra atención en la influencia del fluido en la dinámica del tubo.

La consecuencia más importante de tal influencia, radica en que el flujo del fluido es capaz de modificar la frecuencia con la que el tubo oscila. Tal relación entre frecuencia y magnitud del flujo, puede ser aprovechada para determinar la velocidad del fluido, si se determina el espectro de vibración de un tubo. Nuestro tratamiento propone registrar el desplazamiento del nanotubo como función del tiempo (por ejemplo, mediante mediciones de microscopía de fuerza atómica); luego, usar esta información para determinar las frecuencias características del movimiento del tubo mediante el análisis de Fourier; y, finalmente, determinar la magnitud de la velocidad de fluido al interior del nanotubo, a través de la relación analítica entre la frecuencia y la velocidad de flujo, desarrollada en este trabajo.

La estrategia desarrollada puede utilizarse sin importar el grado de hidrofobicidad de la interacción fluido/pared; es decir, que sin importar la presencia de resbalamiento del fluido en la pared, este tratamiento permite determinar la magnitud de la velocidad y permite, además, estimar la longitud de resbalamiento. Esto puede resultar de utilidad para contribuir a esclarecer el debate concerniente a la longitud de resbalamiento en estos sistemas, pues los resultados en la literatura no presentan un acuerdo común. Esta estrategia puede llevarse más allá, para conocer otros detalles estructurales del fluido, reflejados en el perfil radial de la velocidad de flujo.

En suma, esta propuesta podría dar un marco conceptual para proponer un amplio rango de experimentos de flujo al interior de nanoestructuras en diferentes situaciones experimentales, centrados en la medición del espectro de frecuencias de vibración del tubo. Tales mediciones indirectas, podrían arrojar información estructural y reológica

difícil de determinar por métodos convencionales de medición directa de velocidades de flujo.

Dinámica del fluido bajo la influencia de la vibración del tubo

Cuando la velocidad del fluido es muy pequeña en comparación con la velocidad de propagación de las ondas elásticas en el tubo, es posible considerar que el tubo se mueve de manera independiente del fluido. De este modo, se puede modelar al sistema con las ecuaciones (8.9) y (8.8), para centrar nuestra atención en la influencia de la vibración del tubo en la dinámica del fluido.

En contraste con el resultado presentado en la sección previa, que puede ser comparado inmediatamente con trabajos previos en la literatura [108], esta es la primera vez, hasta donde sabemos, que la velocidad de flujo es determinada analíticamente en este tipo de sistema.

Primero, se resuelve la dinámica del tubo para condiciones particulares. A continuación, se incorpora a través de las funciones auxiliares $g(t)$ y $h(t)$, en la solución del fluido, que está dada por

$$\begin{aligned} v(r,t) &= \frac{e^{-\int_{t_0}^{t} g(t')dt'}}{2\pi} \\ &\times \int_{-\infty}^{\infty} \frac{1}{i\rho\lambda} \left(1 - \frac{J_0\sqrt{\frac{i\rho\lambda r^2}{\mu}}}{J_0\sqrt{\frac{i\rho\lambda R^2}{\mu}}}\right) \int_{-\infty}^{\infty} \left(\frac{\partial p}{\partial z} + \rho\, h(t')\right) e^{\int_{t_0}^{t'} g(t'')dt''} e^{-i\lambda t'} dt' e^{i\lambda t} d\lambda \end{aligned} \tag{8.11}$$

Esto implica que la forma específica de $u(z,t)$ estudiada, determina los fenómenos observados en el movimiento del fluido. A fin de establecer un punto de partida en este estudio, se propone el movimiento del tubo más simple posible, que corresponde a un tubo excitado en uno solo de sus modos de vibración.

La principal consecuencia del estudio de la influencia de la vibración del tubo en la dinámica de un fluido sujeto a un gradiente de presión constante, consiste en la

generación de un flujo de fluido oscilatorio de una frecuencia igual al doble de la del tubo. Este resultado constituye una estrategia para generar flujos oscilatorios al interior de nanotubos, mediante la vibración del tubo. Esto podría ser especialmente útil a altas frecuencias, debido a que los medios convencionales para inducir flujo oscilante presentan muchas limitaciones para generar flujos de amplitud significativa a alta frecuencia. Esto se debe a la baja permeabilidad de un nanotubo estático ante gradientes de presión pulsados. En contraste, nuestra estrategia permite superar esas limitaciones, debido a la naturaleza no lineal de la fuerza de Coriolis y a su dependencia con la frecuencia, lo cual ocasiona que el flujo oscilatorio a frecuencias altas alcance un valor asintótico, que además es proporcional a la magnitud del gradiente de presión constante utilizado.

Con el fin de aprovechar de manera óptima este acoplamiento entre tubo y fluido, es necesario profundizar este estudio en el futuro, y explorar el efecto que tiene un tubo que vibra con múltiples modos excitados. El acoplamiento entre el tubo y el gradiente de presión podría ser utilizado en el futuro, como una estrategia para controlar flujo al interior de nanoestructuras empleando diferentes tipos de actuadores involucrados en los dispositivos modernos para la manipulación mecánica a nivel nanométrico [144, 163, 180].

Conclusiones y perspectivas

Los sistemas nanoscópicos ofrecen un espectro de posibilidades sorprendente. En este trabajo, hemos explorado un tipo específico de nanoestructuras: nanotubos que transportan fluido, capaces de sostener vibración en respuesta a una deflección, debido a sus propiedades elásticas.

El acoplamiento entre el movimiento de tubo y fluido ha sido estudiado en este trabajo, desde dos enfoques complementarios. Por un lado, es posible detectar y determinar propiedades de la velocidad del fluido al interior del nanotubo, al detectar

anormalidades en el espectro de vibración del tubo. Por otro lado, es posible modificar el flujo producido al interior de un nanotubo, por medio de una perturbación oscilante que doble periódicamente al tubo.

Desde el punto de vista del autor, existen dos perspectivas principales que se desprenden de este trabajo. Primero, el diseño de mejores estrategias para la detección indirecta de propiedades complejas que surgen en fluidos confinados al interior de nanotubos. De la misma manera que algunos detalles de la velocidad de flujo y del perfil radial de velocidades fueron determinados en el marco de este trabajo, se podría ir más allá, con miras a la detección de propiedades reológicas de los fluidos, las cuales han sido predichas en trabajos teóricos en la literatura, pero que no han sido encontradas experimentalmente debido a las limitaciones en las mediciones directas de flujo en sistemas nanométricos.

Finalmente, el diseño de mejores estrategias para controlar el flujo a través de nanotubos, al aprovechar el acoplamiento del flujo con las vibraciones del tubo. En este trabajo, se estudió el tipo más simple de vibración. El siguiente paso sería explorar esquemas más complejos para generar y controlar la vibración de un nanotubo, con una inminente mejora en la capacidad de generar una respuesta compleja en el fluido. En este trabajo se mostró que un tubo que vibra en una sola frecuencia es capaz de inducir flujos oscilatorios que no disminuyen a ultra alta frecuencia. Lo que podría obtenerse al involucrar más modos de vibración y tiempos característicos merece una exploración profunda, ya que podría conducir al diseño de flujos nanométricos a la medida, para una aplicación ambiental, industrial o médica, mediante manipulación mecánica de los nanotubos.

En el futuro, la capacidad de controlar el flujo al interior de nanoestructuras mediante vibración podría ofrecer una alternativa al paradigma actual de la optimización de la permeabilidad de membranas de nanotubos mediante la funcionalización química de los poros. En otras palabras, la manipulación mecánica de nanoestructures podría constituir una alternativa más simple y, tal vez, más eficiente de optimizar el flujo en

sistemas nanométricos de filtración y purificación.

Appendices

A.1 Debye model for an oscillating deflected tube at thermal equilibrium

Previous work on literature has demonstrated the effect of temperature on the description of tube oscillatory motion.

In order to understand such effects, an analysis of the studied system within statistical mechanics is done by considering an ensemble of vibrating nanotubes as an ideal gas of non-interacting fonons.

The classical comprehension of this physical model of a tube oscillating in thermal equilibrium consist in considering the vibrations in our tube as a ensemble of harmonic oscillators, whose energy is quantized for each vibration mode. Quantized energy for the $j\text{-}th$ mode, denoted as E_j, is given by

$$E_j = n_j \hbar \omega_j \ , \tag{A.1}$$

where n_j is the total number of excited $j\text{-}th$ mode fonons.

Therefore, the state of the system of fonons is described by the occupation vector n_j. The total energy of the set of a micro-state of fonons with a determined occupation vector, is expressed as

$$E_{\{n_j\}} = \sum_{j=1}^{\infty} n_j \hbar \omega_j \ . \tag{A.2}$$

Thus, a statistical analysis of such a system requires to consider a canonical ensemble of fonons at a constant temperature, volume and number of fonons. Each subsystem has a fluctuating energy, which is actually given by the fluctuations in the occupation vector n_j.

Canonical partition function of such a system is given as

$$Z(T,V) = \sum_{n_j} e^{-\frac{E_{\{n_j\}}}{kT}} = \prod_{j=1}^{\infty} (1 - e^{-\frac{\hbar\omega_j}{kT}})^{-1} \ . \tag{A.3}$$

From Eq. (A.3), it is possible to get the average occupation number of each vibration mode, denoted by $\langle n_j \rangle$ as follows:

$$\langle n_j \rangle = -kT \frac{\partial ln Z}{\partial(\hbar\omega_j)} = \frac{1}{e^{\frac{\hbar\omega_j}{kT}}} \ , \tag{A.4}$$

and the average energy, as

$$\langle E \rangle = -\frac{\partial ln Z}{\partial(\frac{1}{kT})} = \sum_{j=1}^{\infty} \frac{\hbar\omega_j}{e^{\frac{\hbar\omega_j}{kT}} - 1} = \sum_{j=1}^{\infty} \hbar\omega_j \langle n_j \rangle \ . \tag{A.5}$$

From this point, it is possible to determine the value of all the thermodynamic properties of this model of a vibrating carbon nanotube. However, a very important property required to understand the nature and amplitude of oscillations in thermal equilibrium, is the average probability amplitude of a tube oscillating in a single mode, which is given by by $\langle P_j(y) \rangle$, i.e., the statistical thermodynamic average of the probability to find the nanotube oscillating between the position y and $y + dy$ when it is vibrating in its j-th mode.

The classical expression for $P_j(y)$ for a single harmonic oscillator, is derived as follows. We start from the equation of motion of an oscillator, given by

$$y = u_j \cos(\omega_j t) \ , \tag{A.6}$$

where u_j is the oscillation amplitude and depends on the oscillator energy. Then, differentiation of Eq. (A.6) leads to

$$dy = -u_j \omega_j \sin(\omega t) dt \tag{A.7}$$

and afterwards, dt is computed as follows:

$$dt = -\frac{dy}{\omega\sqrt{u_j^2 - y^2}}; -u_j \leq y \leq u_n \ . \tag{A.8}$$

Finally, the last consideration required to obtain $P_j(y)$ is to consider that probability of a particle to be in a portion of space is proportional to the time spent within that region, and thus, P(y)dy is proportional to the magnitude of dt. Therefore, $P_j(y)$ is obtained simply given by normalization of dt in Eq. (A.8), as

$$P_j(y) = \begin{cases} \frac{1}{\pi}\sqrt{u_j^2 - y^2}, & \text{if } |y| \leq u_j \\ 0, & \text{if } |y| \geq u_j \end{cases} \tag{A.9}$$

Now, it is possible to compute the average probability $\langle P_j(y)\rangle$ as follows:

$$\langle P_i(y)\rangle = \frac{1}{Z}\sum_{n_j} P_i(y) e^{-\frac{E_{\{n_j\}}}{kT}} = \prod_{j=1}^{\infty}(1 - e^{-\frac{\hbar\omega_j}{kT}}) \sum_{n_j} P_i(y) e^{-\frac{E_{\{n_j\}}}{kT}} \ . \tag{A.10}$$

This set of sums is simplified as summands sweep over one single mode, thus it is possible to distinguish this sum respect to the others and separate them, as follows:

$$\langle P_i(y)\rangle = \frac{1}{Z}\sum_{n_1=1}^{\infty}\sum_{n_2=1}^{\infty}...\sum_{n_i=1}^{\infty} P_i(y) e^{-\frac{E_{\{n_j\},j\neq i}}{kT}} e^{-\frac{E_i}{kT}} = \frac{1}{Z}\sum_{\{n_j\},j\neq i} e^{-\frac{E_{\{n_j\},j\neq i}}{kT}} \sum_{n_i=1}^{\infty} P_i(y) e^{-\frac{E_i}{kT}} \ . \tag{A.11}$$

Analogous to the deduction of partition function, sum over all modes and occupations except for the i-th, is given as the product of geometric series for each mode, as follows:

$$\langle P_i(y)\rangle = \frac{1}{Z}\prod_{j=1,j\neq i}^{\infty}(1 - e^{-\frac{\hbar\omega_j}{kT}})^{-1} \sum_{n_i=1}^{\infty} P_i(y) e^{-\frac{E_i}{kT}} \ , \tag{A.12}$$

and Z can be expressed in terms of products, as

$$\langle P_i(y)\rangle = \prod_{r=1}^{\infty}(1 - e^{-\frac{\hbar\omega_r}{kT}}) \prod_{j=1,j\neq i}^{\infty}(1 - e^{-\frac{\hbar\omega_j}{kT}})^{-1} \sum_{n_i=1}^{\infty} P_i(y) e^{-\frac{E_i}{kT}} \ . \tag{A.13}$$

Factors inside the product over j cancel all the factors inside product over r but the *i-th* factor. Thus, products are simplified to

$$\langle P_i(y)\rangle = (1 - e^{-\frac{\hbar\omega_i}{kT}}) \sum_{n_i=1}^{\infty} P_i(y) e^{-\frac{E_i}{kT}} \ . \tag{A.14}$$

In order to solve the sum over all the possible occupation numbers of the *i-th* mode, the continuum limit is taken, so sum is approximated by an integral, by the following procedure.

First, Eq. (A.10) is given in terms of the occupation number (as n_i is the explicit variable of sum) as it has been established that

$$E_i = n_i \hbar \omega_i \tag{A.15}$$

and

$$P_i(y) = \frac{1}{\pi\sqrt{u_i^2 - y^2}} \ . \tag{A.16}$$

Amplitude u_i is related to the total energy of every vibration mode. If we consider a pinned-pinned tube as an example of such dependence, within slow deformation approximation, the tube motion is given by

$$w_i(z,t) = u_i \cos(\omega_i t) \sin(\frac{i\pi z}{L}) \tag{A.17}$$

and total energy of such a tube is given by

$$E_i = \int_{z=0}^{z=L} \left(\frac{1}{2} EI \left(\frac{\partial^2 w_i}{\partial z} \right)^2 + \frac{1}{2} \left(\rho A_f + \rho_t A_t \right) \left(\frac{\partial w_i}{\partial t} \right)^2 \right) dz \ . \tag{A.18}$$

Total energy is conserved at all times. However, in order to evaluate integral in Eq. (A.18), a specific time t_r is chosen, in which tube is completely flat, given by

$$t_r = \frac{\pi}{2\omega_i} \tag{A.19}$$

such as, at time $t = t_r$, derivatives are simplified as follows:

$$w_i(z,t_r) = 0 \ , \tag{A.20}$$

$$\frac{\partial w_i}{\partial t}(z,t_r) = -u_i \omega_i \sin(\frac{i\pi z}{L}) \ , \tag{A.21}$$

$$\frac{\partial w_i}{\partial z}(z,t_r) = 0 \ , \tag{A.22}$$

and total energy in Eq. (A.18) is thus simplified to

$$E_i = \int_{z=0}^{z=L} \Big(\frac{1}{2} \big(\rho_f A_f + \rho_t A_t \big) \big(\frac{\partial w_i}{\partial t} \big)^2 + \frac{1}{2} \rho_f A_f v^2 \Big) dz \ . \tag{A.23}$$

Computation of E_i leads the following result:

$$E_i = \frac{u_i^2 i^4 \pi^4 EI}{4L^3} \ . \tag{A.24}$$

Eq. (A.24) can be expressed as the energy of a harmonic oscillator with an effective spring constant given by c_i, as shown below:

$$E_i(y) = \frac{1}{2} c_i u_i^2 \ , \tag{A.25}$$

where c_i is given by

$$c_i = \frac{EI\, i^4 \pi^4}{2L^3} \ . \tag{A.26}$$

Eqs. (A.15), (A.16) and (A.25) are substituted into Eq. (A.10) to express the average probability in terms of the occupation number as follows:

$$\langle P_i(y) \rangle = (1 - e^{-\frac{\hbar\omega_i}{kT}}) \sum_{n_i=1}^{\infty} \frac{1}{\pi \sqrt{\frac{2n_i\hbar\omega_i}{c_i} - y^2}} (y) e^{-\frac{n_i\hbar\omega_i}{kT}} \ . \tag{A.27}$$

Now, each factor is multiplied by the following unitary number:

$$\Delta n_i \equiv (n_i + 1) - n_i = 1 \ . \tag{A.28}$$

Therefore, sum in A.10 is given by

$$\langle P_i(y) \rangle = (1 - e^{-\frac{\hbar\omega_i}{kT}}) \sum_{n_i=1}^{\infty} \frac{1}{\pi \sqrt{\frac{2n_i\hbar\omega_i}{c_i} - y^2}} (y) e^{-\frac{n_i\hbar\omega_i}{kT}} \Delta n_i \ . \tag{A.29}$$

In the continuum limit, sum is expressed as an integral and Δn_i tends to dn_i, leading to

$$\langle P_i(y) \rangle = (1 - e^{-\frac{\hbar\omega_i}{kT}}) \int_{n_i=1}^{\infty} \frac{1}{\pi \sqrt{\frac{2n_i\hbar\omega_i}{c_i} - y^2}} (y) e^{-\frac{n_i\hbar\omega_i}{kT}} dn_i \ . \tag{A.30}$$

Afterwards, the integral in Eq. (A.30) is expressed in terms of energy, by the following change of variable:

$$E_i(n_i) = n_i \hbar\omega_i \ , \tag{A.31}$$

$$dE_i(n_i) = \hbar\omega_i \, dn_i \ , \tag{A.32}$$

in order to get the following integral in terms of the energy and the constrain between y and the energy of system as shown below:

$$\langle P_i(y) \rangle = \int_{E_i=\frac{y^2 c_i}{2}}^{E_i=\infty} \frac{\left(1 - e^{-\frac{\hbar\omega_i}{kT}}\right) e^{-\frac{E_i}{kT}}}{\pi\hbar\omega_i \sqrt{\frac{2E_i}{c_i} - y^2}} dE_i \ . \tag{A.33}$$

The following change of variable is done on energy:

$$x \equiv \sqrt{\frac{2E_i}{c_i} - y^2} \ , \tag{A.34}$$

which leads to the following expression for E_i and dE_i:

$$E_i = \frac{c_i}{2}\left(x^2 + y^2\right) \ , \tag{A.35}$$

$$dE_i = c_i x dx \ . \tag{A.36}$$

Substituting E_i and dE_i in Eq. (A.33), gives the following expression:

$$\langle P_i(y)\rangle = \frac{c_i}{\pi\hbar\omega_i}\left(1 - e^{-\frac{\hbar\omega_i}{kT}}\right)e^{-\frac{c_i y^2}{2kT}} \int_{x=0}^{x=\infty} e^{-\frac{c_i x^2}{2kT}} dx = \frac{1}{\hbar\omega_i}\sqrt{\frac{c_i kT}{2\pi}}\left(1 - e^{-\frac{\hbar\omega_i}{kT}}\right)e^{-\frac{c_i y^2}{2kT}} \ . \tag{A.37}$$

Eq. (A.10) states that probability density of finding a tube within y and $y + dy$ has a Gaussian form whose variance is given by

$$\sigma_j = \frac{kT}{c_j} \tag{A.38}$$

A nanotube in thermal equilibrium is oscillating in all the possible vibration modes and, as fonons are independent, their probabilities add decoherently. Therefore, the average probability of motion in all the vibration modes is equal to the probability density of the sum of the random variable for each vibration mode, that is,

$$\begin{aligned} \langle P_{global}(y)\rangle \ &= \ P\left(y = \sum_{j=1}^{\infty} y_j\right) = \lim_{N\to\infty} \int_{y_1=-\infty}^{y_1=\infty} \int_{y_2=-\infty}^{y_2=\infty} \\ &\ldots \int_{y_{N-1}=-\infty}^{y_{N-1}=\infty} P_1(y_1)P_2(y_2 - y_1)\ldots P_{N-1}(y_{N-1} - y_{N-2})P_N(y - y_{N-1}) \ . \end{aligned} \tag{A.39}$$

When this is applied to our single-mode probability density functions, the following global probability density is found:

$$\langle P_{global}(y)\rangle = \frac{e^{-\frac{y^2}{2kT\sum_{j=1}^{\infty}\frac{1}{c_j}}}}{\sqrt{2\pi kT\sum_{j=1}^{\infty}\frac{1}{c_j}}} \prod_{j=1}^{\infty} \frac{kT}{\hbar\omega_j}\left(1 - e^{-\frac{\hbar\omega_j}{kT}}\right) \ . \tag{A.40}$$

The most important feature arising is that variance of the global density is equal to the sum of the variance of each single-mode probability density, as stated below:

$$\sigma^2_{global} = \sum_{j=1}^{\infty} \sigma_j^2 \ . \tag{A.41}$$

Eqs. (A.40) provides a manner to determine the elastic properties of nanotubes from direct observation of the tube vibration via TEM, as has benn effectively proofed in literature [93].

A.2 Derivation of coupled equations of motion

The Hamilton's Principle for an open system at constant temperature, is rewritten as follows:

$$\delta S + \delta W + \delta C = 0 \ . \tag{A.42}$$

The application of the variation of each term is given in the following section.

Variation of the kinetic energy of the fluid

It is given by

$$\delta \int_t T_f dt = \delta \int_t \int_V \frac{1}{2} \rho \left| \vec{v}_{fluid} \right|^2 dV \, dt \ . \tag{A.43}$$

In Cartesian coordinates, fluid velocity vector $\vec{v}_{fluid}$ is given as follows:

$$\vec{v}_{fluid} = \left(0, \frac{\partial u}{\partial t} + v \frac{\frac{\partial u}{\partial z}}{\sqrt{1 + \left(\frac{\partial u}{\partial z}\right)^2}}, v \frac{1}{\sqrt{1 + \left(\frac{\partial u}{\partial z}\right)^2}} \right) \ . \tag{A.44}$$

In the small deformation limit, it is possible to expand the term $\frac{1}{\sqrt{1+\left(\frac{\partial u}{\partial z}\right)^2}}$, as follows:

$$\frac{1}{\sqrt{1 + \left(\frac{\partial u}{\partial z}\right)^2}} = 1 - \frac{1}{2} \left(\frac{\partial u}{\partial z} \right)^2 + \frac{3}{8} \left(\frac{\partial u}{\partial z} \right)^4 + ... \approx 1 \tag{A.45}$$

and, subsequently, fluid velocity vector is simplified to

$$\vec{v}_{fluid} \approx \left(0, \frac{\partial u}{\partial t} + v \frac{\partial u}{\partial z}, v \right) \tag{A.46}$$

and, accordingly, the magnitude of $\vec{v}_{fluid}$ is given by

$$\left| \vec{v}_{fluid} \right|^2 = v^2 + \left(\frac{\partial u}{\partial t} \right)^2 + 2v \frac{\partial u}{\partial t} \frac{\partial u}{\partial z} + v^2 \left(\frac{\partial u}{\partial z} \right)^2 \ . \tag{A.47}$$

Afterwards, $|\vec{v}_{fluid}|$ from Eq. (A.47) is incorporated into the Kinetic Energy in Eq. (A.44). The variation of the kinetic energy of the fluid leads to the following expression:

$$\begin{aligned} \delta \int_t T_f dt = \int_t \int_V & \left(-\rho \frac{\partial^2 u}{\partial t^2} - \rho v^2 \frac{\partial^2 u}{\partial z^2} - 2\rho v \frac{\partial^2 u}{\partial t \partial z} - \rho \frac{\partial v}{\partial t} \frac{\partial u}{\partial z} - \rho \frac{\partial v}{\partial z} \frac{\partial u}{\partial t} \right) \delta u \\ + & \left(-\rho \frac{\partial v}{\partial t} \left(1 + \left(\frac{\partial u}{\partial z} \right)^2 \right) - 2\rho v \frac{\partial u}{\partial z} \frac{\partial^2 u}{\partial z \partial t} - \rho \left(\frac{\partial^2 u}{\partial t^2} \frac{\partial u}{\partial z} + \frac{\partial u}{\partial t} \frac{\partial^2 u}{\partial z \partial t} \right) \right) \delta z_{fluid} \, dV \, dt \ . \end{aligned} \tag{A.48}$$

Variation of the kinetic energy of the tube

It is given by

$$\delta \int_t T_t dt = \delta \int_t \int_{V_1} \frac{1}{2} \rho \left| \vec{v}_{tube} \right|^2 dV \, dt \ . \tag{A.49}$$

In Cartesian coordinates,

$$\vec{v}_{tube} = \left(0, \frac{\partial u}{\partial t} + v \frac{\frac{\partial u}{\partial z}}{\sqrt{1 + \left(\frac{\partial u}{\partial z}\right)^2}}, v \frac{1}{\sqrt{1 + \left(\frac{\partial u}{\partial z}\right)^2}} \right) \tag{A.50}$$

and the magnitude of tube velocity vector is given by

$$\left| \vec{v}_{tube} \right|^2 = \left(\frac{\partial u}{\partial t} \right)^2 \ . \tag{A.51}$$

Subsequently, substituting the magnitude of tube velocity from Eq. (A.51) into the kinetic energy of tube in Eq. (A.50). The computation of the variation leads to the following expression:

$$\delta \int_t T_t dt = \int_t \int_{V_1} \left(-\rho_t \frac{\partial^2 u}{\partial t^2} \right) \delta u \, dV \, dt \ . \tag{A.52}$$

Variation of the potential energy of the tube

It is given by the following expression:

$$\delta \int_t V_1 dt = \delta \int_t \int_{V_1} \frac{1}{2} E y^2 \left(\frac{\partial^2 u}{\partial z^2} \right)^2 dV \, dt \ , \tag{A.53}$$

and its variation is computed as follows:

$$\delta \int_t V_1 dt = \delta \int_t \int_{V_1} E y^2 \frac{\partial^4 u}{\partial z^4} \delta u \, dV \, dt \ . \tag{A.54}$$

Variation of the external work

It is given as the expression previously stated in Chapter 3, as

$$\delta W_{ext} = \int_t \int_{S_2} \vec{F}_{ext} \cdot \delta \vec{r} \, dS \, dt = \int_t \int_{S_2} (-p + \tau_z) \delta z_{fluid} \, dS \, dt \ . \tag{A.55}$$

Variation of the constrains

The conservation of fluid mass has been incorporated as a restriction in the following form:

$$\delta C = \delta \int_t \int_{V_2} \Lambda \nabla \cdot \vec{r}_{fluid} dV \, dt \ . \tag{A.56}$$

From the properties of the differential operators, it is obtained that

$$\nabla \cdot \Lambda \vec{r}_{fluid} = \vec{r}_{fluid} \cdot \nabla \Lambda + \Lambda \nabla \cdot \vec{r}_{fluid} \tag{A.57}$$

and, by a rearrangement, the following expression is obtained:

$$\Lambda \nabla \cdot \vec{r}_{fluid} = \nabla \cdot \Lambda \vec{r}_{fluid} - \vec{r}_{fluid} \cdot \nabla \Lambda \ . \tag{A.58}$$

Substituting Eq. (A.58) into Eq. (A.56), leads to

$$\int_{V_2} \Lambda \nabla \cdot \vec{r}_{fluid} dV = \int_{V_2} \nabla \cdot \Lambda \vec{r}_{fluid} dV - \int_V \vec{r}_{fluid} \cdot \nabla \Lambda dV \ . \tag{A.59}$$

By the divergence theorem, the following expression is obtained:

$$\int_{V_2} \nabla \cdot \Lambda \vec{r}_{fluid} \, dV = \int_{S_2} \Lambda \vec{r}_{fluid} \cdot \vec{n} \, dS \ , \tag{A.60}$$

which is incorporated in the constrain, as follows:

$$\int_{V_2} \Lambda \nabla \cdot \vec{r}_{fluid} dV = \int_{S_2} \Lambda \vec{r}_{fluid} \cdot \vec{n} \, dS - \int_{V_2} \vec{r}_{fluid} \cdot \nabla \Lambda dV \ . \tag{A.61}$$

By considering that the fluid motion only occurs along the axial direction of the tube as stated in the main body, is given as below:

$$\vec{r}_{fluid} = \vec{r}_{tube} + z_{fluid} \vec{q}_{tan} \ , \tag{A.62}$$

which corresponds to the statement in the body of the article, as

$$\vec{v}_{fluid} = \vec{v}_{tube} + v \vec{q}_{tan} \ . \tag{A.63}$$

Within the limit of small deformation, the differential operators are simplified to the following expressions:

$$\nabla \cdot \vec{r}_{fluid} = \frac{\partial z_{fluid}}{\partial z} \ , \tag{A.64}$$

$$\vec{r}_{fluid} \cdot \vec{n} = z_{fluid} \ , \tag{A.65}$$

$$\vec{r}_{fluid} \cdot \nabla\Lambda = z_{fluid} \frac{\partial \Lambda}{\partial z} \ . \tag{A.66}$$

Afterwards, the considerations in Eqs. (A.61), (A.64) and (A.65) are incorporated in the constrain in Eq. (A.56), and the variation is computed, leading to the following result:

$$\delta C = \int_t \int_{S_2} \Lambda \delta z_{fluid} \, dS \, dt - \int_t \int_{V_2} \frac{\partial \Lambda}{\partial z} \delta z_{fluid} \, dV \, dt \ . \tag{A.67}$$

Finally, the expressions in Eqs. (A.49), (A.52), (A.54), (A.55) and (A.67) are incorporated in the Hamilton's principle stated in Eq. (A.42), the following expression is obtained:

$$\begin{aligned}
&\int_t \int_V \left(-(\rho + \rho_t) \frac{\partial^2 u}{\partial t^2} - \rho v^2 \frac{\partial^2 u}{\partial z^2} - 2\rho v \frac{\partial^2 u}{\partial t \partial z} - \rho \frac{\partial v}{\partial t} \frac{\partial u}{\partial z} - \rho \frac{\partial v}{\partial z} \frac{\partial u}{\partial t} - E y^2 \frac{\partial^4 u}{\partial z^4} \right) \delta u \, dV \, dt \\
&+ \int_t \int_V \left(-\rho \frac{\partial v}{\partial t} - 2\rho v \frac{\partial u}{\partial z} \frac{\partial^2 u}{\partial z \partial t} - \rho \left(\frac{\partial^2 u}{\partial t^2} \frac{\partial u}{\partial z} + \frac{\partial u}{\partial t} \frac{\partial^2 u}{\partial z \partial t} \right) - \frac{\partial \Lambda}{\partial z} \right) \delta z_{fluid} \, dV \, dt \\
&+ \int_t \int_S \left(-p + \tau_z + \Lambda \right) \delta z_{fluid} \, dS \, dt = 0 \ ,
\end{aligned} \tag{A.68}$$

where the sub-indexes in volume regions V_1, V_2 and the surfaces S_1, S_2 where omitted for the sake of simplicity in the expression; however, each term in the integrals should be performed on its corresponding region. Equation (A.68) leads to one equation of motion for the variation of each of the field variables (which are u and z_{fluid}).

For the variation of tube displacement, δu, it is obtained the following expression:

$$\int_V \left(-\rho \frac{\partial^2 u}{\partial t^2} - \rho v^2 \frac{\partial^2 u}{\partial z^2} - 2\rho v \frac{\partial^2 u}{\partial t \partial z} - \rho \frac{\partial v}{\partial t} \frac{\partial u}{\partial z} - \rho \frac{\partial v}{\partial z} \frac{\partial u}{\partial t} - \rho_t \frac{\partial^2 u}{\partial t^2} - E y^2 \frac{\partial^4 u}{\partial z^4} \right) dV = 0 \ . \tag{A.69}$$

For the variation of of fluid displacement δz_{fluid}, it is obtained the following expression:

$$\begin{aligned}
&\int_V \left(-\rho \frac{\partial v}{\partial t} \left(1 + \left(\frac{\partial u}{\partial z} \right)^2 \right) - 2\rho v \frac{\partial u}{\partial z} \frac{\partial^2 u}{\partial z \partial t} - \rho \left(\frac{\partial^2 u}{\partial t^2} \frac{\partial u}{\partial z} + \frac{\partial u}{\partial t} \frac{\partial^2 u}{\partial z \partial t} \right) - \frac{\partial \Lambda}{\partial z} \right) dV \\
&+ \int_S \left(-p + \tau_z + \Lambda \right) dS = 0 \ .
\end{aligned} \tag{A.70}$$

Integrals in Eq. A.70 are applied on different integration regions: first one is a volumetric integral, whereas the second one is a surface integral. Therefore, each integral vanishes independently, leading to the following expression for the volume integral:

$$\int_V \left(-\rho \frac{\partial v}{\partial t} \left(1 + \left(\frac{\partial u}{\partial z} \right)^2 \right) - 2\rho v \frac{\partial u}{\partial z} \frac{\partial^2 u}{\partial z \partial t} - \rho \left(\frac{\partial^2 u}{\partial t^2} \frac{\partial u}{\partial z} + \frac{\partial u}{\partial t} \frac{\partial^2 u}{\partial z \partial t} \right) - \frac{\partial \Lambda}{\partial z} \right) dV = 0 \ , \tag{A.71}$$

and this is the expression given for the surface integral:

$$\int_{S_2} (-p + \tau_{rz} + \Lambda) \, dS = 0 \ . \tag{A.72}$$

From Eq. (A.72), it is possible to obtain the value of the Lagrangian multiplier Λ, as

$$\Lambda = p - \tau_{rz} \ . \tag{A.73}$$

Therefore, the physical meaning of the Lagrangian multiplier Λ is the net stress applied along the plane in which fluid flow occurs. Incorporating Λ from Eq. (A.73) into Eq. (A.71), the following expression is obtained:

$$\int_V \left(-\rho \frac{\partial v}{\partial t} - 2\rho v \frac{\partial u}{\partial z} \frac{\partial^2 u}{\partial z \partial t} - \rho \left(\frac{\partial^2 u}{\partial t^2} \frac{\partial u}{\partial z} + \frac{\partial u}{\partial t} \frac{\partial^2 u}{\partial z \partial t} \right) - \frac{\partial p}{\partial z} + \frac{\partial \tau_z}{\partial z} \right) dV = 0 \ . \tag{A.74}$$

A.3 Solution of flow velocity influenced by tube vibration

For the case of small flow velocity respect to the velocity of propagation of elastic waves along the tube, the equations of motion are rewritten below:

$$EI\frac{\partial^4 u}{\partial z^4} + \left(\rho A_f + \rho_t A_t\right)\frac{\partial^2 u}{\partial t^2} = 0 \tag{A.75}$$

$$\rho\frac{\partial v}{\partial t} + \rho g(t)v + \rho h(t) + \frac{\partial p}{\partial z} - \mu\left(\frac{\partial^2 v}{\partial r^2} + \frac{1}{r}\frac{\partial v}{\partial r}\right) = 0 \tag{A.76}$$

where E corresponds to Young modulus of the tube, I is the second moment of inertia, which for a cylindrical shell is given by

$$I = \frac{\pi}{4}\left(R_o^4 - R^4\right) \tag{A.77}$$

where R_o and R are the outer and inner radius, respectively.

Eq. (A.75) is solved when initial and boundary conditions are given, and leads to a solution of the form

$$u(z,t) = \sum_{n=1}^{N} A_n \sin(k_n z - \omega_n t) \ , \tag{A.78}$$

where A_n is the amplitude of each plane wave, k_n is the spatial modulation and ω_n is the corresponding frequency, which is obtained by the dispersion relation associated to Eq. (A.75), as

$$\omega(k) = \pm k^2\sqrt{\frac{EI}{\rho A_f + \rho_t A_t}} \ . \tag{A.79}$$

Then, the solution $u(z,t)$ is incorporated in $g(t)$ and $h(t)$. In the following treatment, the solution of Eq. (A.76) for flow velocity is provided for arbitrary functions $g(t)$ and $h(t)$.

Eq. (A.76) is a linear non-homogeneous partial differential equation with time-dependent coefficients -particularly, $g(t)$-. The non-homogeneous term is only dependent on time as well -$h(t)$-. Therefore, it is possible to write the general solution of such differential equation in the following form:

$$v(r,t) = v_{homo}(r,t) + v_{part}(t) \tag{A.80}$$

where $v_{homo}(r,t)$ is the solution of the associated homogeneous differential equation, whereas $v_{part}(t)$ is a particular solution of the inhomogeneous term. Equation for $v_{homo}(r,t)$ is

$$\frac{\partial v_{homo}}{\partial t} + g(t)v_{homo} - \frac{\mu}{\rho}\left(\frac{\partial^2 v_{homo}}{\partial r^2} + \frac{1}{r}\frac{\partial v_{homo}}{\partial r}\right) = 0 \ . \tag{A.81}$$

By performing separation of variables, $v_{homog}(r,t) = R(r)T(t)$ and substituting in Eq. (A.81), we have

$$\frac{1}{T}\frac{\partial T}{\partial t} + g(t) = \frac{1}{R}\frac{\mu}{\rho}\left(\frac{\partial^2 R}{\partial r^2} + \frac{1}{r}\frac{\partial R}{\partial r}\right) = -i\lambda \tag{A.82}$$

where $-i\lambda$ is the constant of separation, it has been expressed in such a way in order to simplify further treatment. In all the integrals involved, we will omit the primed indexes for integration over time, for the sake of simplicity during the derivation. Separation of variables allows one to solve two independent ordinary differential equations from Eq. (A.82). First, the equation for $T(t)$ results:

$$\frac{dT}{dt} + \left(i\lambda + g(t)\right)T = 0 \ , \tag{A.83}$$

whose solution is given by

$$T = T_0 e^{-i\lambda t} e^{-\int_{t_0}^{t} g(t)dt} \ . \tag{A.84}$$

The equation for $R(r)$ is given as

$$r^2\frac{d^2R}{dr^2} + r\frac{dR}{dr} + \frac{i\lambda\rho}{\mu}r^2R = 0 \tag{A.85}$$

with the following solution:

$$R(r) = R_1 J_0\left(\sqrt{\frac{i\lambda\rho}{\mu}}r\right) + R_2 Y_0\left(-\sqrt{\frac{i\lambda\rho}{\mu}}r\right) \ . \tag{A.86}$$

Incorporating expressions from Eqs. (A.84) and (A.86) in v_{homo} and after renaming the constant coefficients, the solution of Eq. (A.81) is given by

$$v_{homo}(r,t) = \left[C_1 J_0\left(\sqrt{\frac{\lambda\rho}{\mu}}r\right) + C_2 Y_0\left(-\sqrt{\frac{\lambda\rho}{\mu}}r\right)\right] e^{-i\lambda t} e^{-\int_0^t g(t)dt} \ . \tag{A.87}$$

Afterwards, differential equation for $v_{part}(t)$ is

$$\frac{dv_{part}}{dt} + g(t)v_{part} + \frac{1}{\rho}\frac{\partial p}{\partial z} + h(t) = 0 \ . \tag{A.88}$$

Eq. A.88 is a first-order ordinary differential equation; hence, it is possible to rewrite Eq. A.88 as a differential form, as follows:

$$M(v_{part}, t)dv_{part} + N(v_{part}, t)dt = 0 \ , \tag{A.89}$$

with

$$M(v_{part}, t) = 1 \ , \tag{A.90}$$

and

$$N(v_{part}, t) = g(t)v_{part} + \frac{1}{\rho}\frac{\partial p}{\partial z} + h(t) \ . \tag{A.91}$$

An exact differential form for the function $F(v_{part}, t)$ is given by

$$dF = \frac{\partial F}{\partial v_{part}}dv_{part} + \frac{\partial F}{\partial t}dt \tag{A.92}$$

with equal cross derivatives, as stated below:

$$\frac{\partial M}{\partial v_{part}} = \frac{\partial N}{\partial t} \ . \tag{A.93}$$

However, Eq. (A.90) is not an exact differential form, because the cross derivatives are unequal, as

$$\frac{\partial M}{\partial t} = 0 \ , \tag{A.94}$$

and

$$\frac{\partial N}{\partial v_{part}} = g(t) \ . \tag{A.95}$$

An integrand factor $\mu(t)$ is incorporated in differential form (A.90), to obtain the following exact differential form:

$$dF = \mu(t)\left[M(v, t)dv + N(v, t)dt\right] = 0 \ , \tag{A.96}$$

where $\mu(t)$ is given by

$$\begin{aligned}\mu(t) &= \exp\left(\int \frac{\frac{\partial N}{\partial v_{part}} - \frac{\partial M}{\partial t}}{M} dt\right) \\ &= \exp\left(\int g(t)dt\right) \ . \end{aligned} \tag{A.97}$$

The solution of the differential form is given by

$$F(v,t) = constant \ , \tag{A.98}$$

where the partial derivatives of $F(v,t)$ correspond to

$$\frac{\partial F}{\partial v_{part}} = e^{\int g(t)dt} \tag{A.99}$$

and

$$\frac{\partial F}{\partial t} = e^{\int g(t)dt}\left(g(t)v_{part} + \frac{1}{\rho}\frac{\partial p}{\partial z} + h(t)\right) \ . \tag{A.100}$$

By partial integration of Eqs. (A.99) and (A.100), the solution of Eq. (A.88) is shown below:

$$F = v_{part}(t)e^{\int g(t)dt} + \int e^{\int g(t)dt}\left(\frac{1}{\rho}\frac{\partial p}{\partial z} + h(t)\right)dt = C_0 \ . \tag{A.101}$$

A rearrangement of terms allows one to obtain the following explicit expression for v_{part}, as

$$v_{part}(t) = e^{-\int g(t)dt}\left(C_0 - \int e^{\int g(t)dt}\left(\frac{1}{\rho}\frac{\partial p}{\partial z} + h(t)\right)dt\right) \ . \tag{A.102}$$

The expressions for v_{homog} in Eq. (A.87) and v_{part} in Eq. (A.102) are incorporated in Eq. (A.76), leading to

$$\begin{aligned} v(r,t) = e^{-\int_{t_0}^{t} g(t)dt}\Bigg(& C_0 + e^{-i\lambda t}C_1 J_0\left(\sqrt{\frac{i\lambda\rho}{\mu}}r\right) + e^{-i\lambda t}C_2 Y_0\left(-\sqrt{\frac{i\lambda\rho}{\mu}}r\right) \\ & - \int_{t_0}^{t} e^{\int_0^t g(t)dt}\left(\frac{1}{\rho}\frac{\partial p}{\partial z} + h(t)\right)dt\Bigg) \ . \end{aligned} \tag{A.103}$$

where t_0 is an arbitrary lower time for integration. For practical purposes, we will compute such integrals by considering $t_0 = 0$.

Equation (A.103) is not general in the sense that considers that a single value of λ has been provided. However, some boundary conditions require several values of the eigenvalue. Thus, a general solution of Eq. (A.76) can be expressed as a linear combination of expressions like the one in Eq. (A.103). Moreover, the eigenvalue λ can spread any real value, i. e., $\lambda\epsilon(-\infty,\infty)$, so the linear combination is generalized to an integral, as follows:

$$v(r,t) = e^{-\int_{t_0}^{t} g(t)dt}\left(\int_{-\infty}^{\infty} e^{-i\lambda t}\left(C_1(\lambda)J_0\left(\sqrt{\frac{i\lambda\rho}{\mu}}r\right) + C_2(\lambda)Y_0\left(-\sqrt{\frac{i\lambda\rho}{\mu}}r\right)\right) d\lambda \right.$$
$$\left. - \int e^{\int_{t_0}^{t} g(t)dt}\left(\frac{1}{\rho}\frac{\partial p}{\partial z} + h(t)\right) dt \right) . \tag{A.104}$$

where the term C_0 has been omitted since it is incorporated in $C_1(\lambda)$ as

$$C_1(\lambda)e^{-i\lambda t}J_0\left(\sqrt{\frac{i\lambda\rho}{\mu}}r\right)\Bigg|_{\lambda=0} = C_0 \ . \tag{A.105}$$

Eq. (A.104) is capable to account for any boundary condition. Particularly, it is desired to study the classical conditions of Hagen-Poiseuille flow, i. e., finite flow in the center of the tube, given by;

$$v(r,t)\Big|_{r=0} = \text{finite} \ . \tag{A.106}$$

and the no-slip condition at the tube walls, which is given by

$$v(r,t)\Big|_{r=R} = 0 \ . \tag{A.107}$$

Incorporation of finite flow stated in Eq. (A.106) leads to the following result:

$$C_2 = 0 \ , \tag{A.108}$$

since the Neumann function diverges at $r = 0$. Besides, the no-slip condition stated in Eq. (A.107) is substituted into Eq. (A.104), and leads to the following:

$$e^{-\int_{t_0}^{t} g(t)dt}\left(\int_{-\infty}^{\infty} e^{-i\lambda t}C_1(\lambda)J_0\left(\sqrt{\frac{i\lambda\rho}{\mu}}R\right) d\lambda - \int_{0}^{t} e^{\int_{t_0}^{t} g(t)dt}\left(\frac{1}{\rho}\frac{\partial p}{\partial z} + h(t)\right) dt \right) = 0 \tag{A.109}$$

In order to solve Eq. (A.109) for the coefficients $C_1(\lambda)$, it is necessary to rewrite the time-dependent integral in terms of the Fourier identity, as follows:

$$\begin{aligned}
&\int_{t_0}^{t} e^{\int_{t_0}^{t} g(t)dt}\left(\frac{1}{\rho}\frac{\partial p}{\partial z}+h(t)\right)dt \\
&=\frac{1}{2\pi}\int_{-\infty}^{\infty}\int_{-\infty}^{\infty}\left(\int_{0}^{t} e^{\int_{t_0}^{t} g(t)dt}\left(\frac{1}{\rho}\frac{\partial p}{\partial z}+h(t)\right)dt\right)\ e^{i\lambda t}dt\ e^{-i\lambda t}d\lambda \\
&=-\frac{1}{2\pi}\int_{-\infty}^{\infty}\frac{1}{i\lambda}\int_{-\infty}^{\infty} e^{\int_{t_0}^{t} g(t)dt}\left(\frac{1}{\rho}\frac{\partial p}{\partial z}+h(t)\right)\ e^{i\lambda t}dt\ e^{-i\lambda t}d\lambda
\end{aligned} \tag{A.110}$$

Substituting Eq. (A.110) into the no-slip condition in Eq. A.107, it is obtained the following expression:

$$\begin{aligned}
&\int_{-\infty}^{\infty} e^{-i\lambda t}C_1(\lambda)J_0\left(\sqrt{\frac{i\lambda\rho}{\mu}}R\right)d\lambda \\
&+\frac{1}{2\pi}\int_{-\infty}^{\infty}\frac{1}{i\lambda}\int_{-\infty}^{\infty} e^{\int_{t_0}^{t} g(t)dt}\left(\frac{1}{\rho}\frac{\partial p}{\partial z}+h(t)\right)\ e^{i\lambda t}dt\ e^{-i\lambda t}d\lambda=0
\end{aligned} \tag{A.111}$$

Integral on λ can be reagruped in Eq. A.111, leading to the following:

$$\int_{-\infty}^{\infty}\left(C_1(\lambda)J_0\left(\sqrt{\frac{i\lambda\rho}{\mu}}R\right)+\frac{1}{2\pi i\lambda}\int_{-\infty}^{\infty} e^{\int_{t_0}^{t} g(t)dt}\left(\frac{1}{\rho}\frac{\partial p}{\partial z}+h(t)\right)\ e^{i\lambda t}dt\ \right)e^{-i\lambda t}d\lambda=0 \tag{A.112}$$

The integrand on Eq. (A.112) must vanish, leading to the following expression for $C_1(\lambda)$:

$$C_1(\lambda)=-\frac{1}{2\pi i\lambda J_0\left(\sqrt{\frac{i\lambda\rho}{\mu}}R\right)}\int_{-\infty}^{\infty} e^{\int_{t_0}^{t} g(t)dt}\left(\frac{1}{\rho}\frac{\partial p}{\partial z}+h(t)\right)\ e^{i\lambda t}dt \tag{A.113}$$

Finally, incorporating $C_1(\lambda)$ in Eq. (A.113) and $C_2(\lambda)$ in Eq. (A.108) in the general solution (A.104), the following result is obtained for the no-slip flow velocity:

$$\begin{aligned}
v(r,t) \;=\; & \frac{e^{-\int_{t_0}^{t} g(t)dt}}{2\pi}\int_{-\infty}^{\infty}\frac{1}{i\rho\lambda}\left(1-\frac{J_0\left(\sqrt{\frac{i\lambda\rho}{\mu}}r\right)}{J_0\left(\sqrt{\frac{i\lambda\rho}{\mu}}R\right)}\right) \\
& \int_{-\infty}^{\infty} e^{\int_{t_0}^{t} g(t)dt}\left(\frac{\partial p}{\partial z}+\rho\, h(t)\right)\ e^{i\lambda t}dt\, e^{-i\lambda t}d\lambda
\end{aligned} \tag{A.114}$$

A.4 General notions of the dispersion relation of tubes conveying flow

Derivation of the range of each dispersive regime

From the dimensionless dispersion relation, given by

$$\omega = \alpha\beta kv \pm \sqrt{k^4 - k^2v^2\left(1-\alpha^2\beta^2\right)}\ , \tag{A.115}$$

which, for simplicity, will be rewritten in terms of each branch of the squared-root, as

$$\omega^+ = \alpha\beta kv + \sqrt{k^4 - k^2v^2\left(1-\alpha^2\beta^2\right)}\ , \tag{A.116}$$

$$\omega^- = \alpha\beta kv - \sqrt{k^4 - k^2v^2\left(1-\alpha^2\beta^2\right)}\ . \tag{A.117}$$

We desire to determine the range of values of k and v which lead to each dispersive regime of the three ones described in the main paper. Every regime developed in the dispersion relation is described in terms of the behavior of its frequency. Hence, the first step is to express each regime in a mathematical expression for ω, as follows.

The two-ways regime is accomplished by the following condition:

$$\Re(\omega^+) > 0, \quad \Re(\omega^-) < 0 \quad \text{and} \quad \Im(\omega^\pm) = 0\ . \tag{A.118}$$

Last condition in Eq. (A.118) is accomplished if the argument of square root in Eqs. (A.116) and (A.117) has a positive value, *i.* e.,

$$k^4 - k^2v^2\left(1-\alpha^2\beta^2\right) \geq 0\ . \tag{A.119}$$

As a wavenumber k is defined to be a positive real number, inequality (A.119) is simplified to

$$k \geq v\sqrt{1-\alpha^2\beta^2}\ . \tag{A.120}$$

Besides, the first condition in Eq. (A.118) is given by the following inequality:

$$\alpha\beta kv + \sqrt{k^4 - k^2v^2\left(1-\alpha^2\beta^2\right)} \geq 0\ . \tag{A.121}$$

The first term in the left-hand side of inequality (A.121) is positive because α, β, k and v are all positive quantities. The second term is positive because of the constrain given in the first condition, established in Ineq. (A.120). Therefore, expression (A.120) accomplishes the first and third conditions in Eq. (A.118). The only condition remaining is the second one in Eq. (A.118), which is expressed as

$$\alpha\beta kv - \sqrt{k^4 - k^2v^2\left(1-\alpha^2\beta^2\right)} \leq 0 \ , \tag{A.122}$$

and it is rearranged to give

$$\alpha\beta kv \leq \sqrt{k^4 - k^2v^2\left(1-\alpha^2\beta^2\right)} \ . \tag{A.123}$$

At both sides of Ineq. (A.123), the condition

$$\alpha^2\beta^2k^2v^2 \leq k^4 - k^2v^2\left(1-\alpha^2\beta^2\right) \tag{A.124}$$

should be satisfied. An algebraic manipulation of Ineq. (A.124) leads to the following result:

$$0 \leq k^4 - k^2v^2 \ . \tag{A.125}$$

As wavenumber and flow velocity are positively defined, Ineq. (A.125) leads to

$$k \geq v \ . \tag{A.126}$$

Thus, conditions for the two way regime are obtained if expressions (A.120) and (A.126) are both accomplished. However, as $0 < \alpha < 1$ and $0 < \beta < 1$, it leads to $v^2 > v^2\left(1-\alpha^2\beta^2\right)$. The consequence of this is that condition A.126 encloses condition A.120. Therefore, the only condition required to allow for the two-ways regime, is

$$k \geq v \ . \tag{A.127}$$

The one-way regime is accomplished by the following condition:

$$\Re(\omega^+) > 0, \quad \Re(\omega^-) > 0 \quad \text{and} \quad \Im(\omega^\pm) = 0 \ . \tag{A.128}$$

The first and third conditions in Eq. (A.128) are exactly the same than the ones in the two-ways regime, leading to Eq. (A.120). The second condition in (A.128) leads to the following expression:

$$\alpha\beta kv - \sqrt{k^4 - k^2v^2\left(1-\alpha^2\beta^2\right)} \geq 0 \ , \tag{A.129}$$

and, by the same manipulation than the one performed for the two-ways regime, we obtain

$$k \leq v \ . \tag{A.130}$$

Both conditions, (A.120) and (A.130), must be accomplished in the one-way regime, leading to a single condition for the arising of the one-way regime, as stated below:

$$v\sqrt{1-\alpha^2\beta^2} \leq k \leq v \ . \tag{A.131}$$

The no-transmission regime is accomplished by the following condition:

$$\Im(\omega^{\pm}) \neq 0 \ , \tag{A.132}$$

which leads to

$$k^4 - k^2v^2\left(1-\alpha^2\beta^2\right) < 0 \ . \tag{A.133}$$

Considering a positive value of the wavenumber, expression (A.133) is simplified to

$$k < v\sqrt{1-\alpha^2\beta^2} \ . \tag{A.134}$$

Dispersion relation in Infinite tube simulation

The target is to solve the following dimensionless equation:

$$\frac{\partial^4 u}{\partial z^4} + v^2\frac{\partial^2 u}{\partial z^2} + 2\alpha\beta v\frac{\partial^2 u}{\partial z \partial t} + \frac{\partial^2 u}{\partial t^2} = 0 \ , \tag{A.135}$$

subject to the imposition of an initial perturbation, given by a harmonic spatial wave with wavenumber k_0. Such physical condition is shown below:

$$u(z, t=0) = A_0 \sin(k_0 z) \tag{A.136}$$

and

$$\frac{\partial u}{\partial t}(z, t = 0) = 0 \ . \tag{A.137}$$

We perform the Fourier transform in space of Eq. (A.135), in order to obtain the following result:

$$k^4\hat{u}(k,t) - \pi^2 v^2 k^2 \hat{u}(k,t) - 2i\pi^3\alpha\beta v k\frac{d\hat{u}(k,t)}{dt} + \pi^4\frac{d^2\hat{u}(k,t)}{dt^2} = 0 \ . \tag{A.138}$$

Eq. (A.138) is a linear ordinary differential equation for $\hat{u}(t)$, whose general solution is given by

$$\hat{u}(t) = C_1 e^{it\omega^+(k)} + C_2 e^{it\omega^-(k)} \ . \tag{A.139}$$

We then perform the Fourier transform in space of the initial condition of tube, given in Eqs. (A.136) and (A.137), as follows:

$$\hat{u}(k, t = 0) = \frac{A_0}{2i}\left(\delta(k - k_0) - \delta(k + k_0)\right) \tag{A.140}$$

and

$$\frac{d\hat{u}}{dt}(k, t = 0) = 0 \ . \tag{A.141}$$

The particular solution of Eq. (A.138) with initial conditions (A.140) and (A.141) is given below:

$$\begin{aligned} u(z,t) \ = \ & \frac{\omega^-(k_0)}{\omega^+(k_0) - \omega^-(k_0)}\sin(k_0 z - \omega^+(k_0)t) \\ & -\frac{\omega^+(k_0)}{\omega^+(k_0) - \omega^-(k_0)}\sin(k_0 z - \omega^-(k_0)t) \end{aligned} \tag{A.142}$$

A.5 Expression of the determinant associated to each set of boundary conditions

For each set of boundary conditions considered in this work, the expression for the determinant is shown below. It is important to recall that k_1, k_2, k_3 and k_4 are functions of ω, α and β as stated in Eq. (5.7).

- Pinned-pinned

$$D_{PP} = \begin{vmatrix} 1 & 1 & 1 & 1 \\ -k_1^2 & -k_2^2 & -k_3^2 & -k_4^2 \\ e^{ik_1} & e^{ik_2} & e^{ik_3} & e^{ik_4} \\ -k_1^2 e^{ik_1} & -k_2^2 e^{ik_2} & -k_3^2 e^{ik_3} & -k_4^2 e^{ik_4} \end{vmatrix} \tag{A.143}$$

- Clamped-clamped

$$D_{CC} = \begin{vmatrix} 1 & 1 & 1 & 1 \\ ik_1 & ik_2 & ik_3 & ik_4 \\ e^{ik_1} & e^{ik_2} & e^{ik_3} & e^{ik_4} \\ ik_1 e^{ik_1} & ik_2 e^{ik_2} & ik_3 e^{ik_3} & ik_4 e^{ik_4} \end{vmatrix} \tag{A.144}$$

- Pinned-clamped

$$D_{PC} = \begin{vmatrix} 1 & 1 & 1 & 1 \\ ik_1 & ik_2 & ik_3 & ik_4 \\ e^{ik_1} & e^{ik_2} & e^{ik_3} & e^{ik_4} \\ -k_1^2 e^{ik_1} & -k_2^2 e^{ik_2} & -k_3^2 e^{ik_3} & -k_4^2 e^{ik_4} \end{vmatrix} \tag{A.145}$$

- Pinned-free

$$D_{FP} = \begin{vmatrix} 1 & 1 & 1 & 1 \\ -k_1^2 & -k_2^2 & -k_3^2 & -k_4^2 \\ -k_1^2 e^{ik_1} & -k_2^2 e^{ik_2} & -k_3^2 e^{ik_3} & -k_4^2 e^{ik_4} \\ -ik_1^3 e^{ik_1} & -ik_2^3 e^{ik_2} & -ik_3^3 e^{ik_3} & -ik_4^3 e^{ik_4} \end{vmatrix} \tag{A.146}$$

- Clamped-free

$$D_{FC} = \begin{vmatrix} 1 & 1 & 1 & 1 \\ ik_1 & ik_2 & ik_3 & ik_4 \\ -k_1^2 e^{ik_1} & -k_2^2 e^{ik_2} & -k_3^2 e^{ik_3} & -k_4^2 e^{ik_4} \\ -ik_1^3 e^{ik_1} & -ik_2^3 e^{ik_2} & -ik_3^3 e^{ik_3} & -ik_4^3 e^{ik_4} \end{vmatrix} \tag{A.147}$$

A.6 Flow/frequency relation for each set of boundary conditions

The flow frequency relations of the fundamental mode for the different sets of boundary conditions are given in Fig. A.1.

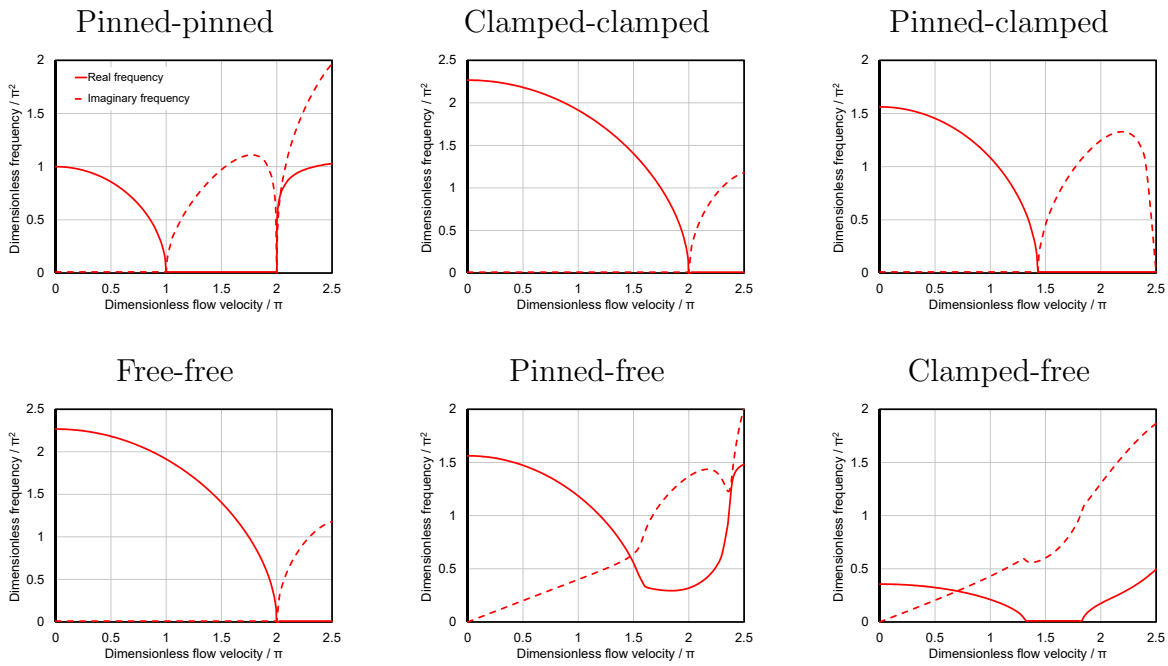

Figure A.1: Effect of flow in the fundamental frequency of the tube oscillations for the different sets of boundary conditions described in this work. Solid lines correspond to the real part of the frequency and dashed lines to its imaginary part. A typical value of the thickness ratio $\alpha = 0.6$ is used in the calculations.

A.7 Analytical expressions for flow as a function of frequency

The expressions of the determinants for the different sets of boundary conditions, as given in Eqs. (A.229)-(A.233) should satisfy

$$D(v,\alpha,\beta,\omega) = 0 \ . \tag{A.148}$$

The second-order Taylor expansion of $D(v,\alpha,\beta,\omega)$ around $v=0$ is given by

$$D(v,\alpha,\beta,\omega)) \approx D\Big|_{v=0} + \frac{\partial D}{\partial v}\Big|_{v=0} v + \frac{1}{2}\frac{\partial^2 D}{\partial v^2}\Big|_{v=0} v^2 \ . \tag{A.149}$$

An explicit expression for v is given by solving the second-order algebraic equation, as

$$v = \frac{-\frac{\partial D}{\partial v}\big|_{v=0} \pm \sqrt{\left(\frac{\partial D}{\partial v}\big|_{v=0}\right)^2 - 2\frac{\partial^2 D}{\partial v^2}\big|_{v=0} D\big|_{v=0}}}{\frac{\partial^2 D}{\partial v^2}\big|_{v=0}} \ . \tag{A.150}$$

Expressions for the first and second derivatives of the determinant respect to flow evaluated at zero flow are required.

The first derivative of a 4×4 determinant is given by

$$\frac{\partial D}{\partial v} = \frac{\partial}{\partial v}\begin{vmatrix} d_{11} & d_{21} & d_{31} & d_{41} \\ d_{12} & d_{22} & d_{32} & d_{42} \\ d_{13} & d_{23} & d_{33} & d_{43} \\ d_{14} & d_{24} & d_{34} & d_{44} \end{vmatrix} = \begin{vmatrix} \frac{\partial d_{11}}{\partial v} & d_{21} & d_{31} & d_{41} \\ \frac{\partial d_{12}}{\partial v} & d_{22} & d_{32} & d_{42} \\ \frac{\partial d_{13}}{\partial v} & d_{23} & d_{33} & d_{43} \\ \frac{\partial d_{14}}{\partial v} & d_{24} & d_{34} & d_{44} \end{vmatrix} + \begin{vmatrix} d_{11} & \frac{\partial d_{21}}{\partial v} & d_{31} & d_{41} \\ d_{12} & \frac{\partial d_{22}}{\partial v} & d_{32} & d_{42} \\ d_{13} & \frac{\partial d_{23}}{\partial v} & d_{33} & d_{43} \\ d_{14} & \frac{\partial d_{24}}{\partial v} & d_{34} & d_{44} \end{vmatrix}$$
$$+ \begin{vmatrix} d_{11} & d_{21} & \frac{\partial d_{31}}{\partial v} & d_{41} \\ d_{12} & d_{22} & \frac{\partial d_{32}}{\partial v} & d_{42} \\ d_{13} & d_{23} & \frac{\partial d_{33}}{\partial v} & d_{43} \\ d_{14} & d_{24} & \frac{\partial d_{34}}{\partial v} & d_{44} \end{vmatrix} + \begin{vmatrix} d_{11} & d_{21} & d_{31} & \frac{\partial d_{41}}{\partial v} \\ d_{12} & d_{22} & d_{32} & \frac{\partial d_{42}}{\partial v} \\ d_{13} & d_{23} & d_{33} & \frac{\partial d_{43}}{\partial v} \\ d_{14} & d_{24} & d_{34} & \frac{\partial d_{44}}{\partial v} \end{vmatrix}$$

and, subsequently, the second derivative of a determinant is the sum of 16 determinants. This result is applied for all the sets of boundary conditions. The following step is to evaluate such derivatives for a stagnant fluid, $v=0$. However, it is easier

to do the derivative in the 4×4 matrices and afterwards evaluate the determinant of such expressions. This strategy is useful as the analytical expressions of the determinants before evaluation are enormous. The terms involved in these calculations are:

$$k_1\Big|_{v=0} = i\sqrt{\omega}, \quad k_2\Big|_{v=0} = ik_1\Big|_{v=0}, \quad k_3\Big|_{v=0} = -ik_1\Big|_{v=0}, \quad k_4\Big|_{v=0} = -k_1\Big|_{v=0} \tag{A.151}$$

$$\frac{\partial k_2}{\partial v}\Big|_{v=0} = -\frac{\partial k_1}{\partial v}\Big|_{v=0}, \qquad \frac{\partial k_3}{\partial v}\Big|_{v=0} = -\frac{\partial k_1}{\partial v}\Big|_{v=0}, \quad \frac{\partial k_4}{\partial v}\Big|_{v=0} = \frac{\partial k_1}{\partial v}\Big|_{v=0},$$
$$\text{where} \quad \frac{\partial k_1}{\partial v}\Big|_{v=0} = \frac{\alpha}{2}, \tag{A.152}$$

$$\frac{\partial^2 k_2}{\partial v^2}\Big|_{v=0} = -i\frac{\partial^2 k_1}{\partial v^2}\Big|_{v=0}, \qquad \frac{\partial^2 k_3}{\partial v^2}\Big|_{v=0} = i\frac{\partial^2 k_1}{\partial v^2}\Big|_{v=0}, \quad \frac{\partial^2 k_4}{\partial v^2}\Big|_{v=0} = -\frac{\partial^2 k_1}{\partial v^2}\Big|_{v=0},$$
$$\text{where} \quad \frac{\partial^2 k_1}{\partial v^2}\Big|_{v=0} = \frac{(\alpha^2-2)i}{4\sqrt{\omega}}, \tag{A.153}$$

By expressing the Taylor expansion in terms of Eqs. (A.151)-(A.153), it is possible to compute the determinant and its first and second derivatives in order to incorporate them into the Taylor Expansion in Eq. (A.150), and finally, to solve such equation for v, leading to the following expressions:

- Pinned-pinned

$$v_{P-P}(\omega, \alpha) = \sqrt{\frac{A_{PP}}{B_{PP}}} \tag{A.154}$$

where A_{PP} and B_{PP} are given by

$$A_{PP} = 8\omega \sin(\sqrt{\omega}) \sinh(\sqrt{\omega}) \tag{A.155}$$

$$B_{PP} = 4\alpha^2 - \cosh(\sqrt{\omega}) G_{PP} - \sqrt{\omega} \sinh(\sqrt{\omega}) H_{PP} \tag{A.156}$$

and G_{PP} and H_{PP} are given by

$$G_{PP} = 4\alpha^2 \cos(\sqrt{\omega}) + (\alpha^2 - 2)\sqrt{\omega} \sin(\sqrt{\omega}) \tag{A.157}$$

$$H_{PP} = (2 - \alpha^2) \cos(\sqrt{\omega}) \tag{A.158}$$

- Clamped-clamped

$$v_{C-C}(\omega,\alpha) = \sqrt{\frac{A_{CC}}{B_{CC}}} \tag{A.159}$$

where A_{CC} and B_{CC} are given by

$$A_{CC} = 8\omega\left(\cos(\sqrt{\omega})\cosh(\sqrt{\omega}) - 1\right) \tag{A.160}$$

$$\begin{aligned} B_{CC} &= +\sinh(\sqrt{\omega})\left(\sqrt{\omega}(2-\alpha^2)\cos(\sqrt{\omega}) + 2(3\alpha^2-2)\sin(\sqrt{\omega})\right) \\ &\quad -4\alpha^2\omega + (2-\alpha^2)\sqrt{\omega}\cosh(\sqrt{\omega})\sin(\sqrt{\omega}) \end{aligned} \tag{A.161}$$

- Pinned-clamped

$$v_{PC}(\omega,\alpha) = \sqrt{\frac{A_{PC}}{B_{PC}}} \tag{A.162}$$

where A_{PC} and B_{PC} are given by

$$A_{PC} = (4+4i)\omega\left(\sin((1+i)\sqrt{\omega}) - \sinh((1+i)\sqrt{\omega})\right) \tag{A.163}$$

$$\begin{aligned} B_{PC} &= \cosh(\sqrt{\omega})\left(2\sqrt{\omega}(\alpha^2-2)\cos(\sqrt{\omega}) + (2-5\alpha^2)\sin(\sqrt{\omega})\right) \\ &\quad +8\alpha^2\sqrt{\omega} + (2-5\alpha^2)\cos(\sqrt{\omega})\sinh(\sqrt{\omega}) \end{aligned} \tag{A.164}$$

- Pinned-free

$$v_{PF}(\omega,\alpha) = \frac{8i\alpha\sqrt{\omega}\sin(\sqrt{\omega})\sinh(\sqrt{\omega}) - \sqrt{-4(1+i)\omega A_{PF}}}{B_{PF}} \tag{A.165}$$

where A_{PF} and B_{PF} are given by

$$A_{PF} = 8(1-i)\alpha^2 sin^2(\sqrt{\omega})sinh^2(\sqrt{\omega}) + G_{PF}H_{PF} \tag{A.166}$$

$$\begin{aligned} B_{PF} &= \cosh(\sqrt{\omega})\left(2(\alpha^2-2)\sqrt{\omega}\cos(\sqrt{\omega}) + (2+3\alpha^2)\sin(\sqrt{\omega})\right) \\ &\quad -8\alpha^2\sqrt{\omega} + (2+3\alpha^2)\cos(\sqrt{\omega})\sinh(\sqrt{\omega}) \end{aligned} \tag{A.167}$$

where G_{PF} and H_{PF} are given by

$$G_{PF} = \sin((1+i)\sqrt{\omega}) - \sinh((1+i)\sqrt{\omega}) \tag{A.168}$$

$$\begin{aligned} H_{PF} &= -\cosh(\sqrt{\omega})\left(2(\alpha^2-2)\sqrt{\omega}\cos(\sqrt{\omega}) + (2+3\alpha^2)\sin(\sqrt{\omega})\right) \\ &\quad 8\alpha^2\sqrt{\omega} - (2+3\alpha^2)\cos(\sqrt{\omega})\sinh(\sqrt{\omega}) \end{aligned} \tag{A.169}$$

- Clamped-free

$$v_{CF}(\omega,\alpha) = \frac{2\alpha\sqrt{\omega}(1-i)\left(\sin((1+i)\sqrt{\omega}) - \sinh((1+i)\sqrt{\omega})\right) - \sqrt{-8\omega A_{CF}}}{B_{CF}} \tag{A.170}$$

where A_{CF} and B_{CF} are given by

$$\begin{aligned} A_{CF} &= i\alpha^2\left(\sin((1+i)\sqrt{\omega}) - \sinh((1+i)\sqrt{\omega})\right)^2 \\ &\quad -(\cos(\sqrt{\omega})\cosh(\sqrt{\omega}) + 1)G_{CF} \end{aligned} \tag{A.171}$$

$$\begin{aligned} B_{CF} &= \left((2-\alpha^2)\sqrt{\omega}\cos(\sqrt{\omega}) - 2(\alpha^2+2)\sin(\sqrt{\omega})\right)\sinh(\sqrt{\omega}) \\ &\quad +4\alpha^2\omega + (2-\alpha^2)\sqrt{\omega}\cosh(\sqrt{\omega})\sin(\sqrt{\omega}) \end{aligned} \tag{A.172}$$

where G_{CF} is given by

$$\begin{aligned} G_{CF} &= -\left((\alpha^2-2)\sqrt{\omega}\cos(\sqrt{\omega}) + 2(2+\alpha^2)\sin(\sqrt{\omega})\right)\sinh(\sqrt{\omega}) \\ &\quad +4\alpha^2\omega + (2-\alpha^2)\sqrt{\omega}\cosh(\sqrt{\omega})\sin(\sqrt{\omega}) \end{aligned} \tag{A.173}$$

These expressions are given for a second-order expansion around zero flow and, therefore, are accurate for low flow velocities. In order to numerically determine the range of accuracy of the approximations, it is necessary to compare the exact numerical solution of the flow/frequency relation for each set of boundary conditions, with the analytical approximated results.

To obtain flow-frequency relations for low and medium flows, higher-order Taylor expansions are necessary. High order derivatives of k_1, k_2, k_3, k_4 are given by

$$\left.\frac{\partial^3 k_1}{\partial v^3}\right|_{v=0} = 0, \quad \left.\frac{\partial^3 k_2}{\partial v^3}\right|_{v=0} = 0, \quad \left.\frac{\partial^3 k_3}{\partial v^3}\right|_{v=0} = 0, \quad \left.\frac{\partial^3 k_4}{\partial v^3}\right|_{v=0} = 0 \tag{A.174}$$

$$\left.\frac{\partial^4 k_2}{\partial v^4}\right|_{v=0} = i\left.\frac{\partial^4 k_1}{\partial v^4}\right|_{v=0}, \quad \left.\frac{\partial^4 k_3}{\partial v^4}\right|_{v=0} = -i\left.\frac{\partial^4 k_1}{\partial v^4}\right|_{v=0}, \quad \left.\frac{\partial^4 k_4}{\partial v^4}\right|_{v=0} = -\left.\frac{\partial^4 k_1}{\partial v^4}\right|_{v=0},$$
$$\text{where} \quad \left.\frac{\partial^4 k_1}{\partial v^4}\right|_{v=0} = \frac{3i(7\alpha^4 - 12\alpha^2 + 4)}{16\omega^{\frac{3}{2}}}, \tag{A.175}$$

$$\left.\frac{\partial^5 k_2}{\partial v^5}\right|_{v=0} = -\left.\frac{\partial^5 k_1}{\partial v^5}\right|_{v=0}, \quad \left.\frac{\partial^5 k_3}{\partial v^5}\right|_{v=0} = -\left.\frac{\partial^5 k_1}{\partial v^5}\right|_{v=0}, \quad \left.\frac{\partial^5 k_4}{\partial v^5}\right|_{v=0} = \left.\frac{\partial^5 k_1}{\partial v^5}\right|_{v=0},$$
$$\text{where} \quad \left.\frac{\partial^5 k_1}{\partial v^5}\right|_{v=0} = -\frac{15\alpha(\alpha^2 - 1)^2}{2\omega^2}, \tag{A.176}$$

$$\left.\frac{\partial^6 k_2}{\partial v^6}\right|_{v=0} = -i\left.\frac{\partial^6 k_1}{\partial v^6}\right|_{v=0}, \quad \left.\frac{\partial^6 k_3}{\partial v^6}\right|_{v=0} = i\left.\frac{\partial^6 k_1}{\partial v^6}\right|_{v=0}, \quad \left.\frac{\partial^6 k_4}{\partial v^6}\right|_{v=0} = -\left.\frac{\partial^6 k_1}{\partial v^6}\right|_{v=0},$$
$$\text{where} \quad \left.\frac{\partial^6 k_1}{\partial v^6}\right|_{v=0} = -\frac{45i(39\alpha^6 - 90\alpha^4 + 60\alpha^2 - 8)}{64\omega^{\frac{5}{2}}}, \tag{A.177}$$

$$\left.\frac{\partial^7 k_1}{\partial v^7}\right|_{v=0} = 0, \quad \left.\frac{\partial^7 k_2}{\partial v^7}\right|_{v=0} = 0, \quad \left.\frac{\partial^7 k_3}{\partial v^7}\right|_{v=0} = 0, \quad \left.\frac{\partial^7 k_4}{\partial v^7}\right|_{v=0} = 0 \tag{A.178}$$

$$\left.\frac{\partial^8 k_2}{\partial v^8}\right|_{v=0} = i\left.\frac{\partial^8 k_1}{\partial v^8}\right|_{v=0}, \quad \left.\frac{\partial^8 k_3}{\partial v^8}\right|_{v=0} = -i\left.\frac{\partial^8 k_1}{\partial v^8}\right|_{v=0}, \left.\frac{\partial^8 k_4}{\partial v^8}\right|_{v=0} = -\left.\frac{\partial^8 k_1}{\partial v^8}\right|_{v=0},$$
$$\text{where} \quad \left.\frac{\partial^8 k_1}{\partial v^8}\right|_{v=0} = -\frac{1575i(209\alpha^8 - 616\alpha^6 + 616\alpha^4 - 224\alpha^2 + 16)}{256\omega^{\frac{7}{2}}}, \tag{A.179}$$

Expressions in Eqs. (A.174)-(A.179) are incorporated into the derivatives of the determinants of Eqs. (A.229)-(A.233), in order to obtain the Taylor coefficients of the expansion and, subsequently, solve such truncated polynomials for the flow velocity.

As mentioned in Chapter 5, odd-order derivatives of the determinants are zero for the pinned-pinned, clamped-clamped and pinned-clamped cases. As a consequence, it is possible to obtain algebraic equations for the square of the flow magnitude, v^2, up to the 4^{th} truncation order. The solution for the flow velocity for each truncation order -where the notation $A_n = \frac{1}{n!}\frac{\partial^n D}{\partial v^n}$ is used- is given by

- First-order truncation

$$v^2 = -\frac{A_0}{A_2} \tag{A.180}$$

- Second-order truncation

$$v^2 = \frac{-A_2 + \sqrt{A_2^2 - 4A_0A_4}}{2A_4} \tag{A.181}$$

- Third-order truncation

$$v^2 = -\frac{A_4}{3A_6} + \frac{(1 - i\sqrt{3})(3A_2A_6 - A_4^2)}{3(2^{\frac{2}{3}})A_6Q^{\frac{1}{3}}} - \frac{1 + i\sqrt{3}}{6(2^{\frac{1}{3}})A_6}Q^{\frac{1}{3}} \tag{A.182}$$

with

$$\begin{aligned} Q = \quad & -2A_4^3 + 9A_2A_4A_6 - 27A_0A_6^2 \\ & + \sqrt{4\left(3A_2A_6 - A_4^2\right)^3 + \left(-2A_4^3 + 9A_2A_4A_6 - 27A_0A_6^2\right)^2} \end{aligned} \tag{A.183}$$

- Fourth-order truncation

$$\begin{aligned} v^2 = \quad & -\frac{A_6}{4A_8} + \frac{1}{2}\sqrt{\frac{A_6^2}{4A_8^2} - \frac{2A_4}{3A_8} + R} \\ & -\frac{1}{2}\sqrt{\frac{A_6^2}{2A_8^2} - \frac{4A_4}{3A_8} - R + \frac{-\frac{A_6^3}{A_8^3} + \frac{4A_4A_6}{A_8^2} - \frac{8A_2}{A_8}}{4\sqrt{\frac{A_6^2}{4A_8^2} - \frac{2A_4}{3A_8} + R}}} \end{aligned} \tag{A.184}$$

where

$$R = \frac{2^{\frac{1}{3}}(A_4^2 - 3A_2A_6 + 12A_0A_8)}{3A_8S^{\frac{1}{3}}} + \frac{S^{\frac{1}{3}}}{3(2^{\frac{1}{3}})A_8} \tag{A.185}$$

$$S = 2A_4^3 - 9A_2A_4A_6 + 27A_0A_6^2 + 27A_2^2A_8 - 72A_0A_4A_8 + T \tag{A.186}$$

and T is given by

$$\begin{aligned} T^2 = \quad & \left(2A_4^3 - 9A_2A_4A_6 + 27A_0A_6^2 + 27A_2^2A_8 - 72A_0A_4A_8\right)^2 \\ & -4\left(A_4^2 - 3A_2A_6 + 12A_0A_8\right)^3 \end{aligned} \tag{A.187}$$

For pinned-free and clamped-free cases, all derivatives are non-zero and therefore, it is only possible to obtain analytical solutions for v (not for v^2) up to 4th truncation

Table A.1: Example of the computation of more than one solution for v^2 for the algebraic equation obtained with the 8th truncation order for a pinned-pinned tube. The physical solution is printed in bold characters

Frequency	First solution	Second solution	Third Solution	Fourth solution
0.8573	-6.8265	**0.25002**	2.0434-0.9894i	2.0434+0.9894i
3.8829	-31.8472	**0.24999**	4.5815-2.5189i	4.5815+2.5189i
8.8889	-66.6262	**0.24999**	6.8837-3.8981i	6.8837+3.8981i
15.8918	-108.7703	**0.24999**	9.2119-5.2630i	9.2119+5.2630i

order, leading to completely analogous expressions to Eqs. (A.180)-(A.184), when replacing the left hand side (v^2) in Eqs. (A.180)-(A.184) by v and doing the following replacements in the right side of the equations: $A_2 \rightarrow A_1$, $A_4 \rightarrow A_2$, $A_6 \rightarrow A_3$ and $A_8 \rightarrow A_4$.

A comparison of the error for each truncation level is shown in Fig. A.2. The purpose of this one is to choose the most suitable expression according to the range of flows and accuracy required in a specific experiment. In general, for low flow magnitude measurements (about $v < 0.1$), a first or second order-truncated expression might be enough, but for intermediate flows ($0.1 < v < 0.6$) a higher order truncation might be required.

As stated in Chapter 5, the analytical expressions only depend on the boundary conditions and not on the number of the vibration mode. The fact that all the different frequencies ω_n lead to the same flow is illustrated in Fig. A.3.

For higher truncation orders, the solution of the algebraic equations lead to more than one solution for v (or v^2). However, the choice of the correct solution is not a problem, since the non-physical solutions lead to complex or non-plausible values. See for example Table A.1.

A.8 Mathematical details of the tube dynamics simulation with initial and boundary conditions at the extremes

In order to simulate the tube dynamics, it is necessary to provide the following information:

- The flow velocity, v.
- The inner and outer tube radii, in order to compute the thickness ratio, α.
- The flow radial profile, in order to compute the fluid structure factor, β.
- The boundary conditions at the tube edges.
- The vertical displacement and velocity of the tube at a given time (i.e., an initial condition).

When the boundary conditions at the tube edges are known, it is possible to incorporate them in the general solution (Eq. (5.6) in Chapter 5). From this, an algebraic system of 4 equations for the coefficients C_1, C_2, C_3, C_4 is obtained. This strategy, in principle, would allow one to obtain the values of all the coefficients. However, the system of equations produced by the boundary conditions is homogeneous and, therefore, it leads to the trivial solution $C_1 = C_2 = C_3 = C_4 = 0$. In order to obtain a non-trivial solution, it is necessary that the determinant of the matrix of coefficients of the system vanishes (Eq. (A.229) in Chapter 5). This in turn causes one of the 4 equations for the coefficients, to be a linear combination of the other three, which leaves one of the coefficients as a free parameter, for instance C_1, and the others coefficients as functions of this one.

When the fluid velocity and thickness ratio are known, it is possible to incorporate them into Eq. (5.6) in Chapter 5. Such equation turns out to be an algebraic equation for the frequency, ω. Moreover, the solution of Eq. (5.6) leads to an infinite set of

discretized values of ω, denoted by ω_n, where n is an integer number. Because of the complexity of this equation, the solution, in general, is given via numerical methods to solve algebraic equations. For the purpose of this work, the Newton-Raphson method was used within Wolfram Mathematica utilities.

Each one of the discretized frequencies, ω_n, is related to a given vibration mode. Therefore, when all the vibration modes are known, it is possible to express any solution of the tube dynamics as a linear combination of all the vibration modes. The coefficients of such combination are given by the initial conditions of the tube. This constitutes the general outline of the simulation of the tube dynamics.

A possible solution, considering C_1 as a the free parameter, is given below for the different sets of boundary conditions. It is necessary to recall that k_1, k_2, k_3 and k_4 are given by the Eqs. (5.8) and ((5.9)) in Chapter 5, and depend on ω_n.

- Pinned-pinned

$$C_2 = -C_1 \frac{\left(e^{ik_3} - e^{ik_4}\right)\left(k_1^2 - k_4^2\right) - \left(e^{ik_1} - e^{ik_4}\right)\left(k_3^2 - k_4^2\right)}{\left(e^{ik_3} - e^{ik_4}\right)\left(k_2^2 - k_4^2\right) - \left(e^{ik_2} - e^{ik_4}\right)\left(k_3^2 - k_4^2\right)} \tag{A.188}$$

$$C_3 = C_1 \frac{e^{ik_4}\left(k_2^2 - k_1^2\right) + e^{ik_2}\left(k_1^2 - k_4^2\right) + e^{ik_1}\left(k_4^2 - k_2^2\right)}{e^{ik_4}\left(k_3^2 - k_2^2\right) + e^{ik_3}\left(k_2^2 - k_4^2\right) + e^{ik_2}\left(k_4^2 - k_3^2\right)} \tag{A.189}$$

$$C_4 = C_1 \frac{e^{ik_3}\left(k_2^2 - k_1^2\right) + e^{ik_2}\left(k_1^2 - k_3^2\right) + e^{ik_1}\left(k_3^2 - k_2^2\right)}{e^{ik_4}\left(k_2^2 - k_3^2\right) + e^{ik_2}\left(k_3^2 - k_4^2\right) + e^{ik_3}\left(k_4^2 - k_2^2\right)} \tag{A.190}$$

- Clamped-clamped

$$C_2 = C_1 \frac{e^{ik_4}\left(k_3 - k_1\right) + e^{ik_3}\left(k_1 - k_4\right) + e^{ik_1}\left(k_4 - k_3\right)}{e^{ik_4}\left(k_2 - k_3\right) + e^{ik_2}\left(k_3 - k_4\right) + e^{ik_3}\left(k_4 - k_2\right)} \tag{A.191}$$

$$C_3 = C_1 \frac{e^{ik_4}\left(k_2 - k_1\right) + e^{ik_2}\left(k_1 - k_4\right) + e^{ik_1}\left(k_4 - k_2\right)}{e^{ik_4}\left(k_3 - k_2\right) + e^{ik_3}\left(k_2 - k_4\right) + e^{ik_2}\left(k_4 - k_3\right)} \tag{A.192}$$

$$C_4 = C_1 \frac{e^{ik_3}\left(k_2 - k_1\right) + e^{ik_2}\left(k_1 - k_3\right) + e^{ik_1}\left(k_3 - k_2\right)}{e^{ik_4}\left(k_2 - k_3\right) + e^{ik_2}\left(k_3 - k_4\right) + e^{ik_3}\left(k_4 - k_2\right)} \tag{A.193}$$

- Pinned-clamped

$$C_2 = -C_1 \frac{\left(e^{ik_3} - e^{ik_4}\right)\left(k_1^2 - k_4^2\right) - \left(e^{ik_1} - e^{ik_4}\right)\left(k_3^2 - k_4^2\right)}{\left(e^{ik_3} - e^{ik_4}\right)\left(k_2^2 - k_4^2\right) - \left(e^{ik_2} - e^{ik_4}\right)\left(k_3^2 - k_4^2\right)} \tag{A.194}$$

$$C_3 = C_1 \frac{e^{ik_4}\left(k_2^2 - k_1^2\right) + e^{ik_2}\left(k_1^2 - k_4^2\right) + e^{ik_1}\left(k_4^2 - k_2^2\right)}{e^{ik_4}\left(k_3^2 - k_2^2\right) + e^{ik_3}\left(k_2^2 - k_4^2\right) + e^{ik_2}\left(k_4^2 - k_3^2\right)} \tag{A.195}$$

$$C_4 = C_1 \frac{e^{ik_3}\left(k_2^2 - k_1^2\right) + e^{ik_2}\left(k_1^2 - k_3^2\right) + e^{ik_1}\left(k_3^2 - k_2^2\right)}{e^{ik_4}\left(k_2^2 - k_3^2\right) + e^{ik_2}\left(k_3^2 - k_4^2\right) + e^{ik_3}\left(k_4^2 - k_2^2\right)} \tag{A.196}$$

- Pinned-free

$$C_2 = C_1 \frac{e^{ik_4}k_4^2\left(k_1^2 - k_3^2\right) + e^{ik_3}k_3^2\left(k_4^2 - k_1^2\right) + e^{ik_1}k_1^2\left(k_3^2 - k_4^2\right)}{e^{ik_4}k_4^2\left(k_3^2 - k_2^2\right) + e^{ik_3}k_3^2\left(k_2^2 - k_4^2\right) + e^{ik_2}k_2^2\left(k_4^2 - k_3^2\right)} \tag{A.197}$$

$$C_3 = C_1 \frac{e^{ik_4}k_4^2\left(k_1^2 - k_2^2\right) + e^{ik_2}k_2^2\left(k_4^2 - k_1^2\right) + e^{ik_1}k_1^2\left(k_2^2 - k_4^2\right)}{e^{ik_4}k_4^2\left(k_2^2 - k_3^2\right) + e^{ik_3}k_3^2\left(k_4^2 - k_2^2\right) + e^{ik_2}k_2^2\left(k_3^2 - k_4^2\right)} \tag{A.198}$$

$$C_4 = C_1 \frac{e^{ik_3}k_3^2\left(k_1^2 - k_2^2\right) + e^{ik_2}k_2^2\left(k_3^2 - k_1^2\right) + e^{ik_1}k_1^2\left(k_2^2 - k_3^2\right)}{e^{ik_4}k_4^2\left(k_3^2 - k_2^2\right) + e^{ik_3}k_3^2\left(k_2^2 - k_3^2\right) + e^{ik_2}k_2^2\left(k_4^2 - k_3^2\right)} \tag{A.199}$$

- Clamped-free

$$C_2 = C_1 \frac{e^{ik_3}k_3^2\left(k_1 - k_4\right) + e^{ik_1}k_1^2\left(k_4 - k_3\right) + e^{ik_4}k_4^2\left(k_3 - k_1\right)}{e^{ik_3}k_3^2\left(k_4 - k_2\right) + e^{ik_2}k_2^2\left(k_3 - k_4\right) + e^{ik_4}k_4^2\left(k_2 - k_3\right)} \tag{A.200}$$

$$C_3 = C_1 \frac{e^{ik_2}k_2^2\left(k_1 - k_4\right) + e^{ik_1}k_1^2\left(k_4 - k_2\right) + e^{ik_4}k_4^2\left(k_2 - k_1\right)}{e^{ik_3}k_3^2\left(k_2 - k_4\right) + e^{ik_2}k_2^2\left(k_4 - k_3\right) + e^{ik_4}k_4^2\left(k_3 - k_2\right)} \tag{A.201}$$

$$C_4 = C_1 \frac{e^{ik_2}k_2^2\left(k_1 - k_3\right) + e^{ik_1}k_1^2\left(k_3 - k_2\right) + e^{ik_3}k_3^2\left(k_2 - k_1\right)}{e^{ik_3}k_3^2\left(k_4 - k_2\right) + e^{ik_2}k_2^2\left(k_3 - k_4\right) + e^{ik_4}k_4^2\left(k_2 - k_3\right)} \tag{A.202}$$

The expressions for the coefficients C_1, C_2, C_3 and C_4 from Eqs. (A.188)-(A.202) are incorporated into the general solution (Eq. (5.6) in Chapter 5), to give each of the vibration modes as follows:

$$\phi_n \equiv \hat{u}_n(z, \omega_n) = C_1 e^{ik_1(\omega_n)z} + C_2(\omega_n)e^{ik_2(\omega_n)z} + C_3(\omega_n)e^{ik_3(\omega_n)z} + C_4(\omega_n)e^{ik_4(\omega_n)z} \tag{A.203}$$

these ones are denoted by ϕ_n, and are normalized for the sake of simplicity in the rest of analytical and numerical treatment -this is possible by an adequate choice of the value of C_1-. Each ϕ_n is associated with an ω_n and, in general, are complex functions in the frequency domain.

For didactic purposes, it is worth pointing out that for simple models of elastic materials, such as an elastic string, each normal mode is given by simple expressions

like $\sin(n\pi z)$ or $\cos(n\pi z)$. However, the vibration modes for a tube conveying fluid, ϕ_n, are not expressed in such simple terms because of the symmetry breaking produced by the flow direction of the fluid inside the elastic tube.

Eq. (A.203) is only valid for the discretized values of ω_n. In order to do the inverse Fourier transform, it is necessary to extend $\hat{u}_n$ to a continuous domain in ω. This leads to the following expression:

$$\hat{u}_n(z,\omega) = \phi_n(z,\omega)\delta(\omega - \omega_n) \ , \tag{A.204}$$

which in time domain is:

$$u_n(z,t) = \phi_n(z,\omega_n)e^{-i\omega_n t} \ . \tag{A.205}$$

A general solution in time domain is a linear combination of all the normal modes satisfying the given set of boundary conditions,

$$u(z,t) = \sum_{n=-\infty}^{\infty} A_n\phi_n(z,\omega_n)e^{-i\omega_n t} \ . \tag{A.206}$$

Since the equation of the tube motion is a second order differential equation in time, two conditions in time are required. In most of experimental situations, it is possible to establish these conditions as the initial position and velocity of the tube. These conditions are expressed as:

$$u\Big|_{t=0} = g(z) \tag{A.207}$$

$$\frac{\partial u}{\partial t}\Big|_{t=0} = h(z) \tag{A.208}$$

where $g(z)$ corresponds to the position profile and $h(z)$ to the velocity profile of the tube at $t = 0$.

Substituting (A.207) and (A.208) into Eq. (A.206), gives the following expressions for $g(z)$ and $h(z)$ in terms of the normal modes:

$$g(z) = \sum_{n=-\infty}^{\infty} A_n\phi_n(z,\omega_n) \tag{A.209}$$

$$h(z) = -i \sum_{n=-\infty}^{\infty} \omega_n A_n \phi_n(z, \omega_n) \,. \tag{A.210}$$

The coefficients A_n should be found in order to satisfy (A.209) and (A.210). However, this is not a straightforward procedure, because this set of functions is complete but not orthogonal.

In order to overcome this difficulty and obtain the target values A_n, it is necessary to express the functions $g(z)$, $h(z)$ and ϕ_n in terms of an orthogonal set of functions. The choice made in our treatment is the set $\{\sin(n\pi z)\}$, where n is a positive integer number. By considering this, Eqs. (A.209) and (A.210) are rewritten as:

$$\sum_{m=1}^{\infty} g_m \sin(m\pi z) = \sum_{n=-\infty}^{\infty} A_n \sum_{m=1}^{\infty} \alpha_{n,m} \sin(m\pi z) \tag{A.211}$$

$$\sum_{m=1}^{\infty} h_m \sin(m\pi z) = -i \sum_{n=-\infty}^{\infty} \omega_n A_n \sum_{m=1}^{\infty} \alpha_{n,m} \sin(m\pi z) \tag{A.212}$$

where the coefficients of each Fourier series are given by

$$g_m = 2 \int_{z=0}^{z=1} g(z) \sin(m\pi z)\, dz \tag{A.213}$$

$$h_m = 2 \int_{z=0}^{z=1} h(z) \sin(m\pi z)\, dz \tag{A.214}$$

$$\alpha_{n,m} = 2 \int_{z=0}^{z=1} \phi_n(z, \omega_n) \sin(m\pi z)\, dz \tag{A.215}$$

The coefficients g_m, h_m and $\alpha_{n,m}$ can be computed from the initial condition and the normal vibration modes ϕ_n. Therefore, the only unknown quantities in equations (A.211) and (A.212) are the coefficients A_n. These ones are compute by the following procedure. First, Eqs. (A.211) and (A.212) are rearranged in the following form:

$$\sum_{m=1}^{\infty} \left(g_m - \sum_{n=-\infty}^{\infty} A_n \alpha_{n,m} \right) \sin(m\pi z) = 0 \tag{A.216}$$

$$\sum_{m=1}^{\infty} \left(h_m + i \sum_{n=-\infty}^{\infty} \omega_n A_n \alpha_{n,m} \right) \sin(m\pi z) = 0 \tag{A.217}$$

Each coefficient of the Fourier series in Eqs. (A.216) and (A.217) must vanish, leading to the following system of algebraic equations for A_n:

$$g_m = \sum_{n=-\infty}^{\infty} A_n \alpha_{n,m}, \;\; m = 1, 2, 3, ... \tag{A.218}$$

$$h_m = -i \sum_{n=-\infty}^{\infty} \omega_n A_n \alpha_{n,m}, \;\; m = 1, 2, 3, ... \tag{A.219}$$

For a numerical simulation, it is necessary to truncate the series in Eqs. (A.218) and (A.219) up to an N_{max} term, leading to the following expression:

$$g_m = \sum_{n=-N_{max}}^{N_{max}} A_n \alpha_{n,m}, \;\; \text{for } m = 1, 2, ..., N_{max} \tag{A.220}$$

$$h_m = -i \sum_{n=-N_{max}}^{N_{max}} \omega_n A_n \alpha_{n,m}, \;\; \text{for } m = 1, 2, ..., N_{max} \tag{A.221}$$

Such truncation implies that the infinite set of linear algebraic equations has been truncated to a linear algebraic system with $2N_{max}$ algebraic equations. In order to obtain a consistent system of equations with a unique solution, it is necessary to also truncate the values of m up to N_{max}. By solving the $2N_{max} \times 2N_{max}$ system of linear algebraic equations, the coefficients A_n are obtained and are incorporated into the particular solution given in Eq. (A.206), which in turn contains all the information to simulate the tube dynamics.

A.9 Details of the solution of fluid dynamics influenced by a tube moving in a single vibration mode

Eq. (A.114) allows one to solve fluid dynamics if the condition of tube motion is previously given and computed in $g(t)$ and $h(t)$, as defined in the body of article. Tube dynamics, as stated in Eq. (3.36) is solved along with boundary conditions, which are shown below.

A specific experimental setting of the tube would determine the way in which edges are fixed in an experiment [181]. Experimental literature on elastic nano-tubes shows three common geometrical conditions for the tube edges [93]:

- Pinned edge. It means that the displacement of the tube edge is zero, and that there is no curvature at that point. Physically, this implies that no elastic strain is imposed at the tube edge. Mathematically, for a tube edge located at $z = z_0$, this is written as:

$$u\Big|_{z=z_0} = 0 \qquad \text{and} \qquad \frac{\partial^2 u}{\partial z^2}\Big|_{z=z_0} = 0 \tag{A.222}$$

- Clamped edge. It means that the displacement of the tube edge is zero, and that the tube at that point is constrained to be horizontal. Mathematically, for a tube edge located at $z = z_0$, this is written as:

$$u\Big|_{z=z_0} = 0 \qquad \text{and} \qquad \frac{\partial u}{\partial z}\Big|_{z=z_0} = 0 \tag{A.223}$$

- Free edge. It means that the displacement of the tube edge is not fixed, the only constrain is that there is no curvature at that point and on its neighborhood. Mathematically, for a tube edge located at $z = z_0$, this is written in the following way:

$$\frac{\partial^2 u}{\partial z^2}\Big|_{z=z_0} = 0 \qquad \text{and} \qquad \frac{\partial^3 u}{\partial z^3}\Big|_{z=z_0} = 0 \tag{A.224}$$

For a finite-size tube, which has two edges, any combination of these three possibilities should be, in principle, experimentally possible. This gives 6 sets of boundary conditions that discretize differently the dispersion relation, namely, pinned-pinned, clamped-clamped, pinned-clamped, pinned-free and clamped-free. Each of these sets imply four conditions on u and/or its spatial derivatives and leads to different vibration modes.

Fourier transform of Eq. (3.36) leads to

$$EI\frac{d^4\hat{u}}{dz^4} - (\rho A_f + \rho_t A_t)\omega^2\hat{u} = 0 \tag{A.225}$$

where $\hat{u}(z,\omega)$ denotes the Fourier transform of $u(z,t)$.

The general solution of Eq. A.225 is given by

$$\hat{u}(z,\omega) = C_1 e^{ikz} + C_2 e^{-ikz} + C_3 e^{kz} + C_4 e^{-kz} \tag{A.226}$$

where k is given by

$$k = \left(\frac{(\rho A_f + \rho_t A_t)\omega^2}{EI}\right)^{\frac{1}{4}} \quad . \tag{A.227}$$

In order to know the particular solution of Eq. (A.225) for each set of boundary conditions, Eqs. (A.222)-(A.224) are incorporated in the general solution in Eq. (A.226), leading to a 4×4 system of algebraic homogeneous equations for C_1, C_2, C_3 and C_4. An homogeneous system leads to non-trivial solutions only if the determinant of its coefficients vanishes, as stated below:

$$D_{BC} = 0 \tag{A.228}$$

where the suffix BC accounts for each set of boundary conditions. For such case, the expression of the determinant is given below:

- Pinned-pinned

$$D_{PP} = \begin{vmatrix} 1 & 1 & 1 & 1 \\ -k^2 & -k^2 & k^2 & k^2 \\ e^{ikL} & e^{-ikL} & e^{kL} & e^{-kL} \\ -k^2 e^{ikL} & -k^2 e^{-ikL} & k^2 e^{kL} & k^2 e^{-kL} \end{vmatrix} = 16ik^4 \sin(kL)\sinh(kL) \tag{A.229}$$

- Clamped-clamped

$$D_{CC} = \begin{vmatrix} 1 & 1 & 1 & 1 \\ ik & -ik & k & -k \\ e^{ikL} & e^{-ikL} & e^{kL} & e^{-kL} \\ ike^{ikL} & -ike^{-ikL} & ke^{kL} & -ke^{-kL} \end{vmatrix} = 8ik^2(\cos(kL)\cosh(kL) - 1) \tag{A.230}$$

- Pinned-clamped

$$\begin{aligned} D_{PC} &= \begin{vmatrix} 1 & 1 & 1 & 1 \\ ik & -ik & k & -k \\ e^{ikL} & e^{-ikL} & e^{kL} & e^{-kL} \\ -k^2 e^{ikL} & -k^2 e^{-ikL} & k^2 e^{kL} & k^2 e^{-kL} \end{vmatrix} \\ &= 8ik^3(\cosh(kL)\sin(kL) - \cos(kL)\sinh(kL)) \end{aligned} \tag{A.231}$$

- Pinned-free

$$\begin{aligned} D_{PF} &= \begin{vmatrix} 1 & 1 & 1 & 1 \\ -k^2 & -k^2 & k^2 & k^2 \\ -k^2 e^{ikL} & -k^2 e^{-ikL} & k^2 e^{kL} & k^2 e^{-kL} \\ -ik^3 e^{ikL} & ik^3 e^{-ikL} & k^3 e^{kL} & -k^3 e^{-kL} \end{vmatrix} \\ &= -8ik^7(\cosh(kL)\sin(kL) - \cos(kL)\sinh(kL)) \end{aligned} \tag{A.232}$$

- Clamped-free

$$D_{FC} = \begin{vmatrix} 1 & 1 & 1 & 1 \\ ik & -ik & k & -k \\ -k^2 e^{ikL} & -k^2 e^{-ikL} & k^2 e^{kL} & k^2 e^{-kL} \\ -ik^3 e^{ikL} & ik^3 e^{-ikL} & k^3 e^{kL} & -k^3 e^{-kL} \end{vmatrix} = -8ik^6(\cos(kL)\cosh(kL)+1) \tag{A.233}$$

The condition for non-trivial solutions, as stated in Eqs. (A.229)-(A.233), is only accomplished for certain values of k, leading to discretized values k_n, which are summarized in Table (A.2).

Table A.2: Discretization of $k = k_n$ induced by the different sets of boundary conditions. Values shown for k_n are asymptotic approximated solutions for Eqs. A.229-A.233.

Set of boundary conditions	k_n
Pinned-pinned	$\frac{n\pi}{L}$
Clamped-clamped	$\left(n+\frac{1}{2}\right)\frac{\pi}{L}$
Free-free	$\left(n+\frac{1}{2}\right)\frac{\pi}{L}$
Pinned-clamped	$\left(n+\frac{1}{4}\right)\frac{\pi}{L}$
Pinned-free	$\left(n+\frac{1}{4}\right)\frac{\pi}{L}$
Clamped-free	$\left(n-\frac{1}{2}\right)\frac{\pi}{L}$

The discretization of $k = k_n$ implies also the discretization of the frequency $\omega = \omega_n$, since k and ω are related by Eq. (A.227).

After discretization of k_n and ω_n, each 4×4 system of equations is simplified to a 4×3 system of equations in which one of the variables is left as a degree of freedom.

Such treatment leads to a non-trivial solution of the following form:

$$\hat{u}_n(z,\omega) = f_n(z)\left(C_{1,n}\delta(\omega-\omega_n) + D_{1,n}\delta(\omega+\omega_n)\right) \tag{A.234}$$

where $f(z)$ is a spatial function obtained for each set of B.C. By performing the inverse Fourier transform of Eq. (A.234), the following expression is obtained for $u_n(z,t)$, as

follows:

$$u_n(z,t) = U_0 f_n(z) \sin(\omega_n t + \varphi) \tag{A.235}$$

The explicit expression for $f_n(z)$ for the different sets of boundary conditions is provided below:

- Pinned-pinned

$$f_n(z) = \sin(k_n z) \tag{A.236}$$

- Clamped-clamped

$$f_n(z) = \sin(k_n z) - \sinh(k_n z) + \frac{(-1)^n - \sinh(k_n L)}{\cosh(k_n L)} \left(\cos(k_n z) - \cosh(k_n z)\right) \tag{A.237}$$

- Pinned-clamped

$$f_n(z) = \sin(k_n z) - \frac{(-1)^n}{\sqrt{2}} \frac{\sinh(k_n z)}{\sinh(k_n L)} \tag{A.238}$$

- Pinned-free

$$f_n(z) = \sin(k_n z) + \frac{(-1)^n}{\sqrt{2}} \frac{\sinh(k_n z)}{\sinh(k_n L)} \tag{A.239}$$

- Clamped-free

$$f_n(z) = \sin(k_n z) - \sinh(k_n z) + \frac{(-1)^n - \sinh(k_n L)}{\cosh(k_n L)} \left(\cos(k_n z) - \cosh(k_n z)\right) \tag{A.240}$$

The solution $u_n(z,t)$ from Eq. (A.235) is incorporated into the Coriolis and pulling forces denoted by $g(t)$ and $h(t)$. The phase $\phi = 0$ is considered for simplicity, leading to the following result:

$$g(t) = \frac{U_0^2 A \omega}{L^2} \sin(2\omega t) \tag{A.241}$$

$$h(t) = \frac{U_0^2 B \omega^2}{L} \cos(2\omega t) \tag{A.242}$$

where A and B are factors that depend on the specific boundary conditions, as shown below:

- Pinned-pinned

$$A = \frac{n^2\pi^2}{2} \tag{A.243}$$

$$B = 0 \tag{A.244}$$

- Clamped-clamped

$$A = \frac{2\beta_n\pi\left(4(-1)^n\cosh(\beta_n\pi) + 2\beta_n\pi(\cosh(2\beta_n\pi)+1) - 4\sinh(2\beta_n\pi)\right)}{8(\cosh(\beta_n\pi))^2} \tag{A.245}$$

$$B = 0 \tag{A.246}$$

- Pinned-clamped

$$A = \frac{\pi\beta_n(2 + (4\beta_n\pi - 2)\cosh(2\pi\beta_n) - 2\sinh(2\pi\beta_n))}{16(\sinh(\beta_n\pi))^2} \tag{A.247}$$

$$B = 0 \tag{A.248}$$

- Pinned-free

$$A = \frac{\pi\beta_n((6 + 4\pi\beta_n)\cosh(2\pi\beta_n) + 6(\sinh(2\pi\beta_n) - 1))}{16(\sinh(\pi\beta_n))^2} \tag{A.249}$$

$$B = 1 \tag{A.250}$$

- Clamped-free

$$\begin{aligned} A \;=\; & -\frac{2\pi\beta_n(\sinh(\pi\beta_n) - 3(-1)^n)}{4\cosh(\pi\beta_n)} - \frac{\pi\beta_n(-1)^n(1+i)\cosh((2in - \beta_n)\pi)}{4\cosh^2(\pi\beta_n)} \\ & + \frac{\pi\beta_n(1-i)(-1)^n\cosh(\pi\beta_n(1+2i))}{4\cosh^2(\pi\beta_n)} - \frac{2\pi^2\beta_n^2}{4\cosh^2(\pi\beta_n)} \\ & + \frac{\pi\beta_n(\beta_n\pi\cosh(2\pi\beta_n) + 5\sinh(2\pi\beta_n))}{4\cosh^2(\pi\beta_n)} \end{aligned} \tag{A.251}$$

$$B = 2 \tag{A.252}$$

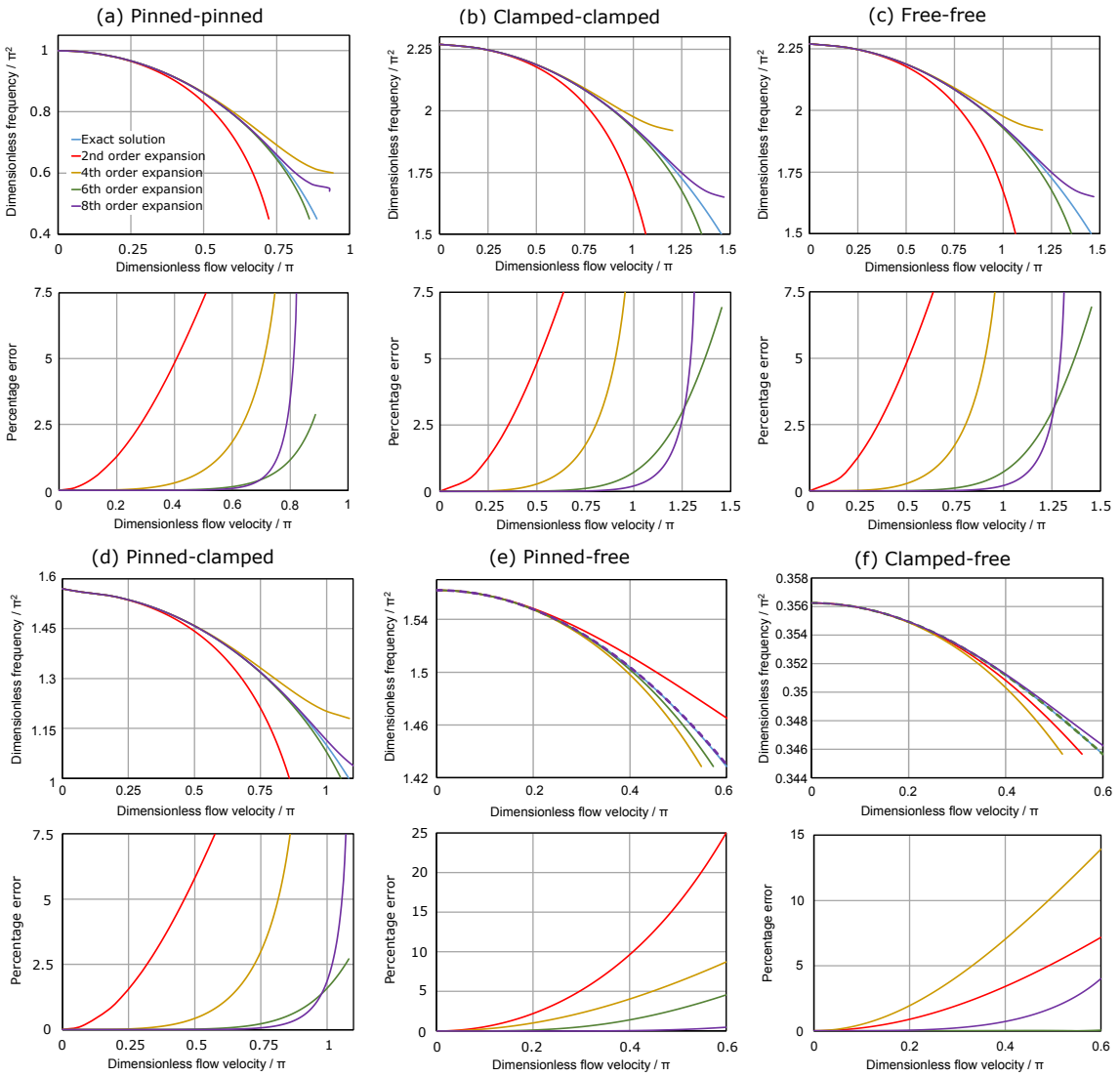

Figure A.2: Comparison between approximated analytical expressions and the exact numerical relation for flow and frequency. As expected, incorporation of more terms in the Taylor expansion leads to an increase in the accuracy and flow range of applicability of the analytical expressions. However, in the pinned-free and clamped-free cases, there is an alternating degree of precision with the order of truncation of the Taylor expansion. This is not an issue for the purpose of this treatment, since all the analytical expressions approximate very well the exact results obtained by numerical means. A typical value of the thickness ratio $\alpha = 0.6$ is used in the calculations.

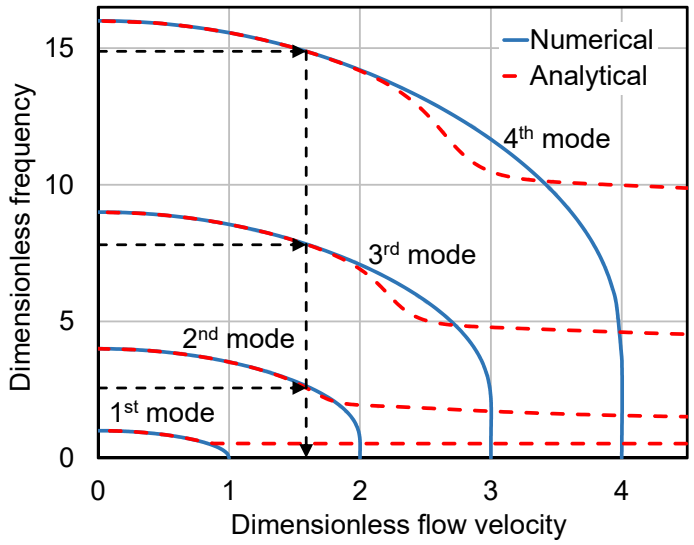

Figure A.3: Comparison between the analytical expression of the 8th truncation order and the exact numerical relation for flow and frequency. Two messages are to be taken from this figure. First, a single analytical expression is capable to approximate for the flow/frequency relation for each of the vibration modes. Second, the range in which the analytical solution is valid is wider for high-order vibration modes.

Bibliography

[1] M. L. Kovarik and S. C. Jacobson. Nanofluidics in lab-on-a-chip devices. *Analytical Chemistry*, 81(17):7133–7140, 2009. PMID: 19663470.

[2] M. Whitby and N. Quirke. Fluid flow in carbon nanotubes and nanopipes. *Nature nanotechnology*, 2(2):87, 2007.

[3] K. Kapoor and S. Patil. Viscoelasticity and shear thinning of nanoconfined water. *Phys. Rev. E*, 89:013004, Jan 2014.

[4] J. A. Thomas and A. J. H. McGaughey. Density, distribution, and orientation of water molecules inside and outside carbon nanotubes. *The Journal of Chemical Physics*, 128(8):084715, 2008.

[5] Y. Maniwa, H. Kataura, M. Abe, A. Udaka, S. Suzuki, Y. Achiba, H. Kira, K. Matsuda, H. Kadowaki, and Y. Okabe. Ordered water inside carbon nanotubes: formation of pentagonal to octagonal ice-nanotubes. *Chemical Physics Letters*, 401(4):534 – 538, 2005.

[6] S. A. Berger, L. Talbot, and L. S. Yao. Flow in curved pipes. *Annual review of fluid mechanics*, 15(1):461–512, 1983.

[7] K. M. Mohamed and A. A. Mohamad. A review of the development of hybrid atomistic–continuum methods for dense fluids. *Microfluidics and Nanofluidics*, 8(3):283–302, 2010.

[8] S. T. O'Connell and P. A. Thompson. Molecular dynamics–continuum hybrid computations: A tool for studying complex fluid flows. *Phys. Rev. E*, 52:R5792–R5795, Dec 1995.

[9] E. G. Flekkøy, G. Wagner, and J. Feder. Hybrid model for combined particle and continuum dynamics. *Europhysics Letters (EPL)*, 52(3):271–276, nov 2000.

[10] M. Majumder, N. Chopra, R. Andrews, and B. J. Hinds. Nanoscale hydrodynamics: enhanced flow in carbon nanotubes. *Nature*, 438(7064):44, 2005.

[11] J. P. Lu. Elastic properties of carbon nanotubes and nanoropes. *Phys. Rev. Lett.*, 79:1297–1300, Aug 1997.

[12] J. P. Watt, G. F. Davies, and R. J. O'Connell. The elastic properties of composite materials. *Reviews of Geophysics*, 14(4):541–563, 1976.

[13] E. Hernández, C. Goze, P. Bernier, and A. Rubio. Elastic properties of c and $B_xC_yN_z$ composite nanotubes. *Phys. Rev. Lett.*, 80:4502–4505, May 1998.

[14] H. G. Park and Y. Jung. Carbon nanofluidics of rapid water transport for energy applications. *Chem. Soc. Rev.*, 43:565–576, 2014.

[15] H. M. Cassard and H. G. Park. How to select the optimal membrane distillation system for industrial applications. *Journal of Membrane Science*, 565:402 – 410, 2018.

[16] H. G. Park, J. Chung, C. P. Grigoropoulos, R. Greif, M. Havstad, and J. D. Morse. Transport in a microfluidic catalytic reactor. Technical report, Lawrence Livermore National Lab., Livermore, CA (US), 2003.

[17] D. A. Stirling. Nanotechnology applications. In *The Nanotechnology Revolution*, pages 281–434. Pan Stanford, 2018.

[18] R. Zhiani, I. Razavipanah, and S. Emrani. Functionalized single-walled carbon nanotube for ketamine sensing: Dft and md studies. *Structural Chemistry*, 29(6):1807–1815, 2018.

[19] E. Díaz-Cervantes, J. Robles, and F. Aguilera-Granja. Understanding the structure, electronic properties, solubility in water, and protein interactions of three novel nano-devices against ovarian cancer: a computational study. *Journal of Nanoparticle Research*, 20(10):266, 2018.

[20] K. Sears, L. Dumée, J. Schütz, M. She, C. Huynh, S. Hawkins, M. Duke, and S. Gray. Recent developments in carbon nanotube membranes for water purification and gas separation. *Materials*, 3(1):127–149, 2010.

[21] J. Davey and A.I. Schäfer. Ultrafiltration to supply drinking water in international development: a review of opportunities. In *Appropriate technologies for environmental protection in the developing world*, pages 151–168. Springer, 2009.

[22] W.H. Chu, R. Chin, T. Huen, and M. Ferrari. Silicon membrane nanofilters from sacrificial oxide removal. *Journal of Microelectromechanical Systems*, 8(1):34–42, 1999.

[23] S. Joseph and N.R. Aluru. Why are carbon nanotubes fast transporters of water? *Nano letters*, 8(2):452–458, 2008.

[24] R. Das, M. E. Ali, S. B. A. Hamid, S. Ramakrishna, and Z. Z. Chowdhury. Carbon nanotube membranes for water purification: a bright future in water desalination. *Desalination*, 336:97–109, 2014.

[25] K. Murata, K. Mitsuoka, T. Hirai, T. Walz, P. Agre, J. B. Heymann, A. Engel, and Y. Fujiyoshi. Structural determinants of water permeation through aquaporin-1. *Nature*, 407(6804):599, 2000.

[26] X. Hou, W. Guo, and L. Jiang. Biomimetic smart nanopores and nanochannels. *Chemical Society Reviews*, 40(5):2385–2401, 2011.

[27] R. J. Walczak, A. Boiarski, M. Cohen, T. West, K. Melnik, J. Shapiro, S. Sharma, and M. Ferrari. Long-term biocompatibility of nanogate drug delivery implant. *Nanobiotechnology*, 1(1):35–42, 2005.

[28] H. Fang, R. Wan, X. Gong, H. Lu, and S. Li. Dynamics of single-file water chains inside nanoscale channels: physics, biological significance and applications. *Journal of Physics D: Applied Physics*, 41(10):103002, 2008.

[29] S. Kim, F. Fornasiero, H. G. Park, J. B. In, E. Meshot, G. Giraldo, M. Stadermann, M. Fireman, J. Shan, C. P. Grigoropoulos, and O. Bakajin. Fabrication of flexible, aligned carbon nanotube/polymer composite membranes by in-situ polymerization. *Journal of Membrane Science*, 460:91 – 98, 2014.

[30] J. Buchheim, R. M. Wyss, C. M. Kim, M. Deng, and H. G. Park. Novel graphene membranes-theory and application. In *Emerging Membrane Technology for Sustainable Water Treatment*, pages 371–388. Elsevier, 2016.

[31] Q. Xie, M. A. Alibakhshi, S. Jiao, Z. Xu, M. Hempel, J. Kong, H. G. Park, and C. Duan. Fast water transport in graphene nanofluidic channels. *Nature Nanotechnology*, 13(3):238, 2018.

[32] F. Martin, R. Walczak, A. Boiarski, M. Cohen, T. West, C. Cosentino, and M. Ferrari. Tailoring width of microfabricated nanochannels to solute size can be used to control diffusion kinetics. *Journal of Controlled Release*, 102(1):123–133, 2005.

[33] S. K. Youn, N. Yazdani, J. Patscheider, and H. G. Park. Facile diameter control of vertically aligned, narrow single-walled carbon nanotubes. *RSC Adv.*, 3:1434–1441, 2013.

[34] R. M. Wyss, J. E. Klare, H. G. Park, A. Noy, O. Bakajin, and V. Lulevich. Water-assisted growth of uniform 100 mm diameter swcnt arrays. *ACS Applied Materials & Interfaces*, 6(23):21019–21025, 2014. PMID: 25408997.

[35] J. K. Holt, H. G. Park, Y. Wang, M. Stadermann, A. B. Artyukhin, C. P. Grigoropoulos, A. Noy, and O. Bakajin. Fast mass transport through sub-2-nanometer carbon nanotubes. *Science*, 312(5776):1034–1037, 2006.

[36] M. Whitby, L. Cagnon, M. Thanou, and N. Quirke. Enhanced fluid flow through nanoscale carbon pipes. *Nano letters*, 8(9):2632–2637, 2008.

[37] S. K. Kannam, B. D. Todd, J. S. Hansen, and P. J. Daivis. How fast does water flow in carbon nanotubes? *The Journal of chemical physics*, 138(9):094701, 2013.

[38] K. Ritos, D. Mattia, F. Calabrò, and J. M. Reese. Flow enhancement in nanotubes of different materials and lengths. *The Journal of chemical physics*, 140(1):014702, 2014.

[39] G. Hu and D. Li. Multiscale phenomena in microfluidics and nanofluidics. *Chemical Engineering Science*, 62(13):3443 – 3454, 2007. Frontier of Chemical Engineering - Multi-scale Bridge between Reductionism and Holism.

[40] B. J. Kirby. *Micro-and nanoscale fluid mechanics: transport in microfluidic devices*. Cambridge university press, 2010.

[41] A. Noy, H. G. Park, F. Fornasiero, J. K. Holt, C. P. Grigoropoulos, and O. Bakajin. Nanofluidics in carbon nanotubes. *Nano Today*, 2(6):22 – 29, 2007.

[42] S. Kim, L. Chen, J. K. Johnson, and E. Marand. Polysulfone and functionalized carbon nanotube mixed matrix membranes for gas separation: theory and experiment. *Journal of Membrane Science*, 294(1-2):147–158, 2007.

[43] S. Qiu, L. Wu, X. Pan, L. Zhang, H. Chen, and C. Gao. Preparation and properties of functionalized carbon nanotube/psf blend ultrafiltration membranes. *Journal of Membrane Science*, 342(1-2):165–172, 2009.

[44] M. Majumder, N. Chopra, and B. J. Hinds. Effect of tip functionalization on transport through vertically oriented carbon nanotube membranes. *Journal of the American Chemical Society*, 127(25):9062–9070, 2005.

[45] W. F. Chan, H. y. Chen, A. Surapathi, M. G. Taylor, X. Shao, E. Marand, and J. K. Johnson. Zwitterion functionalized carbon nanotube/polyamide nanocomposite membranes for water desalination. *Acs Nano*, 7(6):5308–5319, 2013.

[46] X. Wei and T. Luo. Effects of electrostatic interaction and chirality on the friction coefficient of water flow inside single-walled carbon nanotubes and boron nitride nanotubes. *The Journal of Physical Chemistry C*, 122(9):5131–5140, 2018.

[47] J. Feng, S. Xiong, Z. Wang, Z. Cui, S. P. Sun, and Y. Wang. Atomic layer deposition of metal oxides on carbon nanotube fabrics for robust, hydrophilic ultrafiltration membranes. *Journal of Membrane Science*, 550:246–253, 2018.

[48] G. Hummer, J. C Rasaiah, and J. P. Noworyta. Water conduction through the hydrophobic channel of a carbon nanotube. *Nature*, 414(6860):188, 2001.

[49] D. J. Bonthuis, K. F. Rinne, K. Falk, C. N. Kaplan, D. Horinek, A. N. Berker, L. Bocquet, and R. R. Netz. Theory and simulations of water flow through carbon nanotubes: prospects and pitfalls. *Journal of Physics: Condensed Matter*, 23(18):184110, 2011.

[50] H. Hu, L. Bao, N. V. Priezjev, and K. Luo. Identifying two regimes of slip of simple fluids over smooth surfaces with weak and strong wall-fluid interaction energies. *The Journal of Chemical Physics*, 146(3):034701, 2017.

[51] M. Shaat. Viscosity of water interfaces with hydrophobic nanopores: Application to water flow in carbon nanotubes. *Langmuir*, 33(44):12814–12819, 2017. PMID: 29035046.

[52] S. A. Miller, V. Y. Young, and C. R. Martin. Electroosmotic flow in template-prepared carbon nanotube membranes. *Journal of the American Chemical Society*, 123(49):12335–12342, 2001.

[53] T. Kyotani, L. F. Tsai, and A. Tomita. Preparation of ultrafine carbon tubes in nanochannels of an anodic aluminum oxide film. *Chemistry of Materials*, 8(8):2109–2113, 1996.

[54] D. Mattia, M. P. Rossi, B. M. Kim, G. Korneva, H. H. Bau, and Y. Gogotsi. Effect of graphitization on the wettability and electrical conductivity of cvd-carbon nanotubes and films. *The Journal of Physical Chemistry B*, 110(20):9850–9855, 2006.

[55] D. Mattia, H. H. Bau, and Y. Gogotsi. Wetting of cvd carbon films by polar and nonpolar liquids and implications for carbon nanopipes. *Langmuir*, 22(4):1789–1794, 2006.

[56] M. P. Rossi, H. Ye, Y. Gogotsi, S. Babu, P. Ndungu, and J. C. Bradley. Environmental scanning electron microscopy study of water in carbon nanopipes. *Nano Letters*, 4(5):989–993, 2004.

[57] W. Cao, L. Huang, M. Ma, L. Lu, and X. Lu. Water in narrow carbon nanotubes: Roughness promoted diffusion transition. *The Journal of Physical Chemistry C*, 122(33):19124–19132, 2018.

[58] A. Kalra, S. Garde, and G. Hummer. Osmotic water transport through carbon nanotube membranes. *Proceedings of the National Academy of Sciences*, 100(18):10175–10180, 2003.

[59] Y. Yang, X. Li, J. Jiang, H. Du, L. Zhao, and Y. Zhao. Control performance and biomembrane disturbance of carbon nanotube artificial water channels by nitrogen-doping. *ACS Nano*, 4(10):5755–5762, 2010.

[60] D. Li, Y. Wang, Y. Pan, and X. Zhao. Measurements of slip length for flows over graphite surface with gas domains. *Applied Physics Letters*, 109(15):151602, 2016.

[61] K. Wu, Z. Chen, J. Li, X. Li, J. Xu, and X. Dong. Wettability effect on nanoconfined water flow. *Proceedings of the National Academy of Sciences*, 114(13):3358–3363, 2017.

[62] M. Kageshima. Layer-resolved relaxation dynamics of confined water analyzed through subnanometer shear measurement. *EPL (Europhysics Letters)*, 107(6):66001, sep 2014.

[63] B. Kim, S. Kwon, M. Lee, Q. Kim, S. An, and W. Jhe. Probing nonlinear rheology layer-by-layer in interfacial hydration water. *Proceedings of the National Academy of Sciences*, 112(51):15619–15623, 2015.

[64] A. Dequidt, J. Devmy, and P. Malfreyt. Confined kcl solution between two mica surfaces: Equilibrium and frictional properties. *The Journal of Physical Chemistry C*, 119(38):22080–22085, 2015.

[65] V. Y. Rudyak and A. A. Belkin. Fluid viscosity under confined conditions. *Doklady Physics*, 59(12):604–606, Dec 2014.

[66] M. C. Gordillo and J. Mart. Hydrogen bonding in supercritical water confined in carbon nanotubes. *Chemical Physics Letters*, 341(3):250 – 254, 2001.

[67] T. D. Li and E. Riedo. Nonlinear viscoelastic dynamics of nanoconfined wetting liquids. *Phys. Rev. Lett.*, 100:106102, Mar 2008.

[68] Y. Grosu, A. Giacomello, S. Meloni, L. Gonzlez-Fernndez, M. Chorazewski, M. Geppert-Rybczynska, A. Faik, J. M. Nedelec, and J. P. Grolier. Viscosity at the nanoscale: Confined liquid dynamics and thermal effects in self-recovering nanobumpers. *The Journal of Physical Chemistry C*, 122(26):14248–14256, 2018.

[69] E. C. Yusko, J. M. Johnson, S. Majd, P. Prangkio, R. C. Rollings, J. Li, J. Yang, and M. Mayer. Controlling protein translocation through nanopores with bio-inspired fluid walls. *Nature Nanotechnology*, 6(4):253, 2011.

[70] B. Yameen, M. Ali, R. Neumann, W. Ensinger, W. Knoll, and O. Azzaroni. Synthetic proton-gated ion channels via single solid-state nanochannels modified with responsive polymer brushes. *Nano Letters*, 9(7):2788–2793, 2009.

[71] C. Dekker. Solid-state nanopores. *Nature Nanotechnology*, 2(4):209, 2007.

[72] A. J. Storm, J. H. Chen, X. S. Ling, H. W. Zandbergen, and C. Dekker. Fabrication of solid-state nanopores with single-nanometre precision. *Nature Materials*, 2(8):537, 2003.

[73] X. Li, C. A. Fustin, N. Lefèvre, J. F. Gohy, S. De Feyter, J. De Baerdemaeker, W. Egger, and I. F. J. Vankelecom. Ordered nanoporous membranes based on diblock copolymers with high chemical stability and tunable separation properties. *Journal of Materials Chemistry*, 20(21):4333–4339, 2010.

[74] M. R. Rahman. *Silica and Clay Dispersed Polymer Nanocomposites: Preparation, Properties and Applications*. Woodhead Publishing Series in Composites Science and Engineering. Elsevier Science, 2018.

[75] P. H. C. Camargo, K. G. Satyanarayana, and F. Wypych. Nanocomposites: synthesis, structure, properties and new application opportunities. *Materials Research*, 12:1 – 39, 03 2009.

[76] G. Kortaberria and A. Tercjak. *Block Copolymer Nanocomposites*. Pan Stanford, 2016.

[77] S. Y. Yang, J. A. Yang, E. S. Kim, G. Jeon, E. J. Oh, K. Y. Choi, S. K. Hahn, and J. K. Kim. Single-file diffusion of protein drugs through cylindrical nanochannels. *ACS Nano*, 4(7):3817–3822, 2010.

[78] X. Qin, Q. Yuan, Y. Zhao, S. Xie, and Z. Liu. Measurement of the rate of water translocation through carbon nanotubes. *Nano Letters*, 11(5):2173–2177, 2011.

[79] R. De La Rica and H. Matsui. Applications of peptide and protein-based materials in bionanotechnology. *Chemical Society Reviews*, 39(9):3499–3509, 2010.

[80] A. Alcaraz, P. Ramírez, E. García-Giménez, M. L. Lopez, A. Andrio, and V. M. Aguilella. A ph-tunable nanofluidic diode: electrochemical rectification in a reconstituted single ion channel. *The Journal of Physical Chemistry B*, 110(42):21205–21209, 2006.

[81] Y. Jung, H. Bayley, and L. Movileanu. Temperature-responsive protein pores. *Journal of the American Chemical Society*, 128(47):15332–15340, 2006.

[82] R. S. Ruoff, D. Qian, and W. K. Liu. Mechanical properties of carbon nanotubes: theoretical predictions and experimental measurements. *Comptes Rendus Physique*, 4(9):993–1008, 2003.

[83] R. S. Ruoff, D. Qian, and W. K. Liu. Mechanical properties of carbon nanotubes: theoretical predictions and experimental measurements. *Comptes Rendus Physique*, 4(9):993 – 1008, 2003. Dossier: Carbon nanotubes: state of the art and applications.

[84] B. Ji and H. Gao. Mechanical properties of nanostructure of biological materials. *Journal of the Mechanics and Physics of Solids*, 52(9):1963–1990, 2004.

[85] J. G. Guo and Y. P. Zhao. The size-dependent bending elastic properties of nanobeams with surface effects. *Nanotechnology*, 18(29):295701, 2007.

[86] X. Q. Feng, R. Xia, X. Li, and B. Li. Surface effects on the elastic modulus of nanoporous materials. *Applied Physics Letters*, 94(1):011916, 2009.

[87] X. Zhao, Y. Ando, L. C. Qin, H. Kataura, Y. Maniwa, and R. Saito. Radial breathing modes of multiwalled carbon nanotubes. *Chemical Physics Letters*, 361(1-2):169–174, 2002.

[88] M. Machón, S. Reich, H. Telg, J. Maultzsch, P. Ordejón, and C. Thomsen. Strength of radial breathing mode in single-walled carbon nanotubes. *Physical Review B*, 71(3):035416, 2005.

[89] P. T. Araujo, I. O. Maciel, P. B. C. Pesce, M. A. Pimenta, S. K. Doorn, H. Qian, A. Hartschuh, M. Steiner, L. Grigorian, K. Hata, et al. Nature of the constant factor in the relation between radial breathing mode frequency and tube diameter for single-wall carbon nanotubes. *Physical Review B*, 77(24):241403, 2008.

[90] J. P. Salvetat, J. M. Bonard, N. H. Thomson, A. J. Kulik, L. Forro, W. Benoit, and L. Zuppiroli. Mechanical properties of carbon nanotubes. *Applied Physics A*, 69(3):255–260, 1999.

[91] O. Lourie and H. D. Wagner. Evaluation of young's modulus of carbon nanotubes by micro-raman spectroscopy. *Journal of Materials Research*, 13(9):2418–2422, 1998.

[92] P. Poncharal, Z. L. Wang, D. Ugarte, and W. A. De Heer. Electrostatic deflections and electromechanical resonances of carbon nanotubes. *science*, 283(5407):1513–1516, 1999.

[93] A. Krishnan, E. Dujardin, T. W. Ebbesen, P. N. Yianilos, and M. M. J. Treacy. Youngs modulus of single-walled nanotubes. *Physical Review B*, 58(20):14013, 1998.

[94] R. F. Gibson, E. O. Ayorinde, and Y. F. Wen. Vibrations of carbon nanotubes and their composites: a review. *Composites Science and Technology*, 67(1):1–28, 2007.

[95] J. A. Thomas and A. J. H. McGaughey. Water flow in carbon nanotubes: transition to subcontinuum transport. *Physical Review Letters*, 102(18):184502, 2009.

[96] E. M. Kotsalis, J. H. Walther, and P. Koumoutsakos. Multiphase water flow inside carbon nanotubes. *International Journal of Multiphase Flow*, 30(7):995 – 1010, 2004. A Collection of Papers in Honor of Professor G. Yadigaroglu on the Occasion of his 65th Birthday.

[97] T. Werder, J. H. Walther, R. L. Jaffe, T. Halicioglu, F. Noca, and P. Koumoutsakos. Molecular dynamics simulation of contact angles of water droplets in carbon nanotubes. *Nano Letters*, 1(12):697–702, 2001.

[98] T. Werder, J. H. Walther, R. L. Jaffe, T. Halicioglu, and P. Koumoutsakos. On the water- carbon interaction for use in molecular dynamics simulations of graphite and carbon nanotubes. *The Journal of Physical Chemistry B*, 107(6):1345–1352, 2003.

[99] Y. Nakamura and T. Ohno. Structure of water confined inside carbon nanotubes and water models. *Materials Chemistry and Physics*, 132(2-3):682–687, 2012.

[100] A. Alexiadis and S. Kassinos. Molecular simulation of water in carbon nanotubes. *Chemical Reviews*, 108(12):5014–5034, 2008.

[101] R. J. Mashl, S. Joseph, N. R. Aluru, and E. Jakobsson. Anomalously immobilized water: a new water phase induced by confinement in nanotubes. *Nano Letters*, 3(5):589–592, 2003.

[102] K. Koga, G. Gao, H. Tanaka, and X. C. Zeng. Formation of ordered ice nanotubes inside carbon nanotubes. *Nature*, 412:802–805, 2001.

[103] L. L. Huang, L. Z. Zhang, Q. Shao, J. Wang, L. H. Lu, X. H. Lu, S. Y. Jiang, and W. F. Shen. Molecular dynamics simulation study of the structural characteristics of water molecules confined in functionalized carbon nanotubes. *The Journal of Physical Chemistry B*, 110(51):25761–25768, 2006. PMID: 17181218.

[104] J. Shiomi, T. Kimura, and S. Maruyama. Molecular dynamics of ice-nanotube formation inside carbon nanotubes. *The Journal of Physical Chemistry C*, 111(33):12188–12193, 2007.

[105] A. Striolo. The mechanism of water diffusion in narrow carbon nanotubes. *Nano Letters*, 6(4):633–639, 2006. PMID: 16608257.

[106] X. Gao, T. Zhao, and Z. Li. Fluid breakup in carbon nanotubes: An explanation of ultrafast ion transport. *Physics of Fluids*, 29(9):092003, 2017.

[107] J. Yoon, C. Q. Ru, and A. Mioduchowski. Vibration and instability of carbon nanotubes conveying fluid. *Composites Science and Technology*, 65(9):1326–1336, 2005.

[108] L. Wang and Q. Ni. On vibration and instability of carbon nanotubes conveying fluid. *Computational Materials Science*, 43(2):399–402, 2008.

[109] Y. Zhen and B. Fang. Thermal–mechanical and nonlocal elastic vibration of single-walled carbon nanotubes conveying fluid. *Computational Materials Science*, 49(2):276–282, 2010.

[110] M. Gărăjeu, H. Gouin, and G. Saccomandi. Scaling navier-stokes equation in nanotubes. *Physics of Fluids*, 25(8):082003, 2013.

[111] S. Kelly, M. T. Balhoff, and C. Torres-Verdín. Quantification of bulk solution limits for liquid and interfacial transport in nanoconfinements. *Langmuir*, 31(7):2167–2179, 2015.

[112] H. K. Moffatt and A. Tsinober. Helicity in laminar and turbulent flow. *Annual Review of Fluid Mechanics*, 24(1):281–312, 1992.

[113] L. Wang. A modified nonlocal beam model for vibration and stability of nanotubes conveying fluid. *Physica E: Low-dimensional Systems and Nanostructures*, 44(1):25 – 28, 2011.

[114] H. Liu, Y. Liu, J. Dai, and Q. Cheng. An improved model of carbon nanotube conveying flow by considering comprehensive effects of knudsen number. *Microfluidics and Nanofluidics*, 22(6):66, 2018.

[115] A. Bedford. *Hamilton's principle in continuum mechanics*, volume 139. Pitman advanced publishing program Boston/London/Melbourne, 1985.

[116] R. Salmon. Practical use of hamilton's principle. *Journal of Fluid Mechanics*, 132:431–444, 1983.

[117] S. Sieniutycz and R. S. Berry. Conservation laws from hamiltons principle for nonlocal thermodynamic equilibrium fluids with heat flow. *Physical Review A*, 40(1):348, 1989.

[118] D. Djukic and B. Vujanovic. On a new variational principle of hamiltonian type for classical field theory. *ZAMM-Journal of Applied Mathematics and Mechanics/Zeitschrift für Angewandte Mathematik und Mechanik*, 51(8):611–616, 1971.

[119] G. J. Lebon and J. H. Lambermont. Generalization of hamilton's principle to continuous dissipative systems. *The Journal of Chemical Physics*, 59(6):2929–2936, 1973.

[120] H. Benaroya and T. Wei. Hamilton's principle for external viscous fluid–structure interaction. *Journal of Sound and Vibration*, 238(1):113–145, 2000.

[121] A. Bedford and D. S. Drumheller. Theories of immiscible and structured mixtures. *International Journal of Engineering Science*, 21(8):863–960, 1983.

[122] T. G. Shepherd. Symmetries, conservation laws, and hamiltonian structure in geophysical fluid dynamics. In *Advances in Geophysics*, volume 32, pages 287–338. Elsevier, 1990.

[123] C. M. Leech. Hamilton's principle applied to fluid mechanics. *The Quarterly Journal of Mechanics and Applied Mathematics*, 30(1):107–130, 1977.

[124] V. M. Teshukov and S. L. Gavrilyuk. Kinetic model for the motion of compressible bubbles in a perfect fluid. *European Journal of Mechanics-B/Fluids*, 21(4):469–491, 2002.

[125] Q. Sun, J. X. Zhou, and L. Zhang. An adaptive beam model and dynamic characteristics of magnetorheological materials. *Journal of Sound and Vibration*, 261(3):465–481, 2003.

[126] A. Alexiadis, D. A. Lockerby, M. K. Borg, and J. M. Reese. A laplacian-based algorithm for non-isothermal atomistic-continuum hybrid simulation of micro and nano-flows. *Computer Methods in Applied Mechanics and Engineering*, 264:81–94, 2013.

[127] K. Ritos, M. K. Borg, D. A. Lockerby, D. R. Emerson, and J. M. Reese. Hybrid molecular-continuum simulations of water flow through carbon nanotube membranes of realistic thickness. *Microfluidics and Nanofluidics*, 19(5):997–1010, 2015.

[128] T. Werder, J. H. Walther, and P. Koumoutsakos. Hybrid atomistic–continuum method for the simulation of dense fluid flows. *Journal of Computational Physics*, 205(1):373–390, 2005.

[129] N. G. Hadjiconstantinou and A. T. Patera. Heterogeneous atomistic-continuum representations for dense fluid systems. *International Journal of Modern Physics C*, 08(04):967–976, 1997.

[130] J. Li, D. Liao, and S. Yip. Coupling continuum to molecular-dynamics simulation: Reflecting particle method and the field estimator. *Phys. Rev. E*, 57:7259–7267, Jun 1998.

[131] J. Li, D. Liao, and S. Yip. Nearly exact solution for coupled continuum/md fluid simulation. *Journal of Computer-Aided Materials Design*, 6(2-3):95–102, 1999.

[132] S. S. Chen. Flow-induced vibration of circular cylindrical structures. Technical report, Argonne National Lab.(ANL), Argonne, IL (United States), 1985.

[133] O. A. Bauchau and J. I. Craig. Euler-bernoulli beam theory. In *Structural analysis*, pages 173–221. Springer, 2009.

[134] L. D. Landau, E. M. Lifshitz, A. M. Kosevich, J. B. Sykes, L. P. Pitaevskii, and W. H. Reid. *Theory of Elasticity*. Course of theoretical physics. Elsevier Science, 1986.

[135] L. D. Landau and E. M. Lifshitz. *Fluid Mechanics*. Number v. 6 in Course of theoretical physics. Elsevier Science, 1987.

[136] R. Collepardo-Guevara and E. Corvera Poiré. Controlling viscoelastic flow by tuning frequency during occlusions. *Physical Review E*, 76(2):026301, 2007.

[137] S. Nakao. Determination of pore size and pore size distribution: 3. filtration membranes. *Journal of Membrane Science*, 96(1):131 – 165, 1994.

[138] H. G. L. Coster, K. J. Kim, K. Dahlan, J. R. Smith, and C. J. D. Fell. Characterisation of ultrafiltration membranes by impedance spectroscopy. i. determination of the separate electrical parameters and porosity of the skin and sublayers. *Journal of Membrane Science*, 66(1):19 – 26, 1992.

[139] N. C. Nguyen and J. Peraire. Hybridizable discontinuous galerkin methods for partial differential equations in continuum mechanics. *Journal of Computational Physics*, 231(18):5955 – 5988, 2012.

[140] O. C. Zienkiewicz and R. L. Taylor. *The finite element method for solid and structural mechanics*. Elsevier, 2005.

[141] Y. Yan, X. Q. He, L. X. Zhang, and Q. Wang. Flow-induced instability of double-walled carbon nanotubes based on an elastic shell model. *Journal of Applied Physics*, 102(4):044307, 2007.

[142] Y. Yan, X. Q. He, L. X. Zhang, and C. M. Wang. Dynamic behavior of triple-walled carbon nanotubes conveying fluid. *Journal of Sound and Vibration*, 319(3):1003 – 1018, 2009.

[143] L. Wang, Q. Ni, and M. Li. Buckling instability of double-wall carbon nanotubes conveying fluid. *Computational Materials Science*, 44(2):821 – 825, 2008.

[144] J. P. Salvetat, G. A. D. Briggs, J. M. Bonard, R. R. Bacsa, A. J. Kulik, T. Stöckli, N. A. Burnham, and L. Forró. Elastic and shear moduli of single-walled carbon nanotube ropes. *Phys. Rev. Lett.*, 82:944–947, Feb 1999.

[145] M. F. Yu, O. Lourie, M. J. Dyer, K. Moloni, T. F. Kelly, and R. S. Ruoff. Strength and breaking mechanism of multiwalled carbon nanotubes under tensile load. *Science*, 287(5453):637–640, 2000.

[146] M. F. Yu, B. S. Files, S. Arepalli, and R. S. Ruoff. Tensile loading of ropes of single wall carbon nanotubes and their mechanical properties. *Phys. Rev. Lett.*, 84:5552–5555, Jun 2000.

[147] B. Bhushan. *Nanotribology and Nanomechanics I: Measurement Techniques and Nanomechanics*, volume 1. Springer Science & Business Media, 2011.

[148] H. J. Butt, B. Cappella, and M. Kappl. Force measurements with the atomic force microscope: Technique, interpretation and applications. *Surface Science Reports*, 59(1):1 – 152, 2005.

[149] K. L. Ekinci, Y. T. Yang, X. M. H. Huang, and M. L. Roukes. Balanced electronic detection of displacement in nanoelectromechanical systems. *Applied Physics Letters*, 81(12):2253–2255, 2002.

[150] J. Cao, Q. Wang, and H. Dai. Electromechanical properties of metallic, quasimetallic, and semiconducting carbon nanotubes under stretching. *Phys. Rev. Lett.*, 90:157601, Apr 2003.

[151] B. Mahar, C. Laslau, R. Yip, and Y. Sun. Development of carbon nanotube-based sensorsa review. *IEEE Sensors Journal*, 7(2):266–284, Feb 2007.

[152] M. Li, H. Tang, and M. Roukes. Ultra-sensitive nems-based cantilevers for sensing, scanned probe and very high-frequency applications. *Nature Nanotechnology*, 2:114–120, 2007.

[153] R. He, X. L. Feng, M. L. Roukes, and P. Yang. Self-transducing silicon nanowire electromechanical systems at room temperature. *Nano Letters*, 8(6):1756–1761, 2008. PMID: 18481896.

[154] M. H. Montgomery and D. Odonoghue. A derivation of the errors for least squares fitting to time series data. *Delta Scuti Star Newsletter*, 13:28, 1999.

[155] G. Betta, C. Liguori, and A. Pietrosanto. Propagation of uncertainty in a discrete fourier transform algorithm. *Measurement*, 27(4):231 – 239, 2000.

[156] H. W. C. Postma, A. Sellmeijer, and C. Dekker. Manipulation and imaging of individual single-walled carbon nanotubes with an atomic force microscope. *Advanced Materials*, 12(17):1299–1302, 2000.

[157] A. Nordenfelt. Selective Self-Excitation of Higher Vibrational Modes of Graphene Nano-Ribbons and Carbon Nanotubes Through Magnetomotive Instability. *Journal of Computational and Nonlinear Dynamics*, 8(1), 06 2012. 011011.

[158] A. Nordenfelt, Y. A. Tarakanov, L. Y. Gorelik, R. I. Shekhter, and M. Jonson. Magnetomotive instability and generation of mechanical vibrations in suspended semiconducting carbon nanotubes. *New Journal of Physics*, 12(12):123013, dec 2010.

[159] M. Ayub, A. C. Zander, C. Q. Howard, B. S. Cazzolato, V. N. Shanov, N. T. Alvarez, and D. M. Huang. Acoustic absorption behaviour of carbon nanotube arrays. In *Inter-noise and Noise-Con congress and conference proceedings*, volume 249, pages 929–938. Institute of Noise Control Engineering, 2014.

[160] M. Ayub, A. Zander, C. Howard, B. S. Cazzolato, D. Huang, N. T. Alvarez, and V. N. Shanov. Acoustic absorption behaviour of a tall carbon nanotube forest. *Proceedings of Acoustics*, 2016.

[161] M. Ayub, A. C. Zander, C. Q. Howard, B. S. Cazzolato, D. M. Huang, V. N. Shanov, and N. T. Alvarez. Normal incidence acoustic absorption characteristics of a carbon nanotube forest. *Applied Acoustics*, 127:223 – 239, 2017.

[162] M. Ayub, A. C. Zander, D. M. Huang, C. Q. Howard, and B. S. Cazzolato. Molecular dynamics simulations of acoustic absorption by a carbon nanotube. *Physics of Fluids*, 30(6):066101, 2018.

[163] A. Bachtold, P. Hadley, T. Nakanishi, and C. Dekker. Logic circuits with carbon nanotube transistors. *Science*, 294(5545):1317–1320, 2001.

[164] D. M. Sun, C. Liu, W. C. Ren, and H. M. Cheng. A review of carbon nanotube- and graphene-based flexible thin-film transistors. *Small*, 9(8):1188–1205, 2013.

[165] J. Svensson, Y. Tarakanov, D. S. Lee, J. M. Kinaret, Y. W. Park, and E. E. B. Campbell. A carbon nanotube gated carbon nanotube transistor with 5 ps gate delay. *Nanotechnology*, 19(32):325201, jul 2008.

[166] J. Svensson, N. Lindahl, H. Yun, M. Seo, D. Midtvedt, Y. Tarakanov, N. Lindvall, O. Nerushev, J. Kinaret, S. W. Lee, and E. E. B. Campbell. Carbon nanotube field effect transistors with suspended graphene gates. *Nano Letters*, 11(9):3569–3575, 2011. PMID: 21848317.

[167] Y. A. Tarakanov and J. M. Kinaret. A carbon nanotube field effect transistor with a suspended nanotube gate. *Nano Letters*, 7(8):2291–2294, 2007. PMID: 17604404.

[168] D. Ramos, E. Gil-Santos, O. Malvar, J. M. Llorens, V. Pini, A. San Paulo, M. Calleja, and J. Tamayo. Silicon nanowires: where mechanics and optics meet at the nanoscale. *Scientific reports*, 3:3445, 2013.

[169] M. R. Foreman, J. D. Swaim, and F. Vollmer. Whispering gallery mode sensors. *Adv. Opt. Photon.*, 7(2):168–240, Jun 2015.

[170] S. R. Manalis, S. C. Minne, A. Atalar, and C. F. Quate. Interdigital cantilevers for atomic force microscopy. *Applied Physics Letters*, 69(25):3944–3946, 1996.

[171] C. A. Savran, A. W. Sparks, J. Sihler, J. Li, W. C. Wu, D. E. Berlin, T. P. Burg, J. Fritz, M. A. Schmidt, and S. R. Manalis. Fabrication and characterization of a micromechanical sensor for differential detection of nanoscale motions. *Journal of Microelectromechanical Systems*, 11(6):703–708, Dec 2002.

[172] D. Müller and Y. Dufrêne. Atomic force microscopy as a multifunctional molecular toolbox in nanobiotechnology. *Nature Nanotechnology*, 3:261–269, 2008.

[173] P. Hinterdorfer and Y. Dufrêne. Detection and localization of single molecular recognition events using atomic force microscopy. *Nature Methods*, 3:347–355, 2006.

[174] M. Stark, R. W. Stark, W. M. Heckl, and R. Guckenberger. Inverting dynamic force microscopy: From signals to time-resolved interaction forces. *Proceedings of the National Academy of Sciences*, 99(13):8473–8478, 2002.

[175] O. Sahin, S. Magonov, C. Su, C. Quate, and O. Solgaard. An atomic force microscope tip designed to measure time-varying nanomechanical forces. *Nature Nanotechnology*, 2:507–514, 2007.

[176] A. D. L. Humphris, M. J. Miles, and J. K. Hobbs. A mechanical microscope: High-speed atomic force microscopy. *Applied Physics Letters*, 86(3):034106, 2005.

[177] T. Kallinger, P. Reegen, and W. W. Weiss. A heuristic derivation of the uncertainty for frequency determination in time series data. *Astronomy & Astrophysics*, 481(2):571–574, 2008.

[178] S. Carpentier, M. S. Rodrigues, M. V. Vitorino, L. Costa, E. C., and J. Chevrier. Out of equilibrium anomalous elastic response of a water nano-meniscus. *Applied Physics Letters*, 107(20):204101, 2015.

[179] J. A. Del Rio, M. López De Haro, and S. Whitaker. Enhancement in the dynamic response of a viscoelastic fluid flowing in a tube. *Physical Review E*, 58(5):6323, 1998.

[180] F. Valmorra, G. Scalari, C. Maissen, W. Fu, C. Schnenberger, J. W. Choi, H. G. Park, M. Beck, and J. Faist. Low-bias active control of terahertz waves by coupling large-area cvd graphene to a terahertz metamaterial. *Nano Letters*, 13(7):3193–3198, 2013. PMID: 23802181.

[181] B. Arash and Q. Wang. A review on the application of nonlocal elastic models in modeling of carbon nanotubes and graphenes. *Computational Materials Science*, 51(1):303 – 313, 2012.

An analytical framework to determine flow velocities within nanotubes from their vibration frequencies

U. Torres-Herrera[1] and E. Corvera Poiré[1,2]
[1]*Departamento de Física y Química Teórica, Facultad de Química, Universidad Nacional Autónoma de México, Mexico City 04510, Mexico*
[2]*Universitat de Barcelona Institute of Complex Systems (UBICS), Universitat de Barcelona, Barcelona 08028, Spain*

(Received 4 August 2018; accepted 13 November 2018; published online 5 December 2018)

We develop a theoretical framework to determine fluid velocities within nanotubes. We demonstrate that the fluid/tube dynamic coupling could be exploited to determine flow velocities based on knowledge of the bending frequency spectrum of a single nanotube. We develop an analytical methodology that allows one to associate any of the frequencies in the spectrum with a single value of the fluid velocity. We discuss the feasibility of experiments by state-of-the-art atomic force microscopy and perform numerical simulations to determine uncertainties in fluid velocities. These are below 5% for common nanotube sizes, which are considerably smaller than the ones reported in the literature for conventional methods. *Published by AIP Publishing.* https://doi.org/10.1063/1.5050998

I. INTRODUCTION

Understanding water flow within nanostructures is promising for the design of ultrafast water filters and nanoscale fluid components within microdevices. Most of the experimental work regarding water flow in nanostructures is focused on carbon nanotubes embedded like pores within polymer membranes, subject to a pressure difference across them.[1] It has been found that flow velocities are several orders of magnitude higher than the ones predicted by the classical Poiseuille flow of Continuum Mechanics (CM), with no-slip boundary conditions in rigid tubes. Currently, the best explanation for this flow enhancement is given in terms of the frictionless transport due to the repulsive interactions between a nonpolar wall and water that cause huge slip lengths.[2–7] This has been corroborated via Molecular Dynamics (MD) simulations, in which it is demonstrated that small changes in the repulsion term of a force field—used to model the water/graphene interaction—have a strong effect on flow, and leads to flow enhancement inside nanotubes.[8–10] Such flow enhancement is more pronounced in tubes of very small radii.[11–14] The formation of different ordered structures of water molecules is also predicted.[15–19] The relation between some of these water structures and transport properties has allowed to understand, for instance, the mechanism of enhanced ion transport in carbon nanotubes.[20]

Despite all of the experimental advances and theoretical efforts toward the comprehension of enhanced water flow within nanostructures, there are current limitations, both, experimental and theoretical ones, regarding the precision with which flow is determined. Moreover, flow enhancement differs by orders of magnitude among the different experimental studies in the literature.[21–24] The main experimental difficulties in the determination of flow are related to the uncertainty in the cross-sectional area available for flow in carbon nanotube membranes. These lead to uncertainties of over 50% in flow measurements.[2–4] Techniques used to determine porosity in materials, such as the BET isotherm and impedance spectroscopy,[25,26] lead to huge errors in pore density and cross-sectional areas that in turn affect the precision in the determination of flow velocity. Moreover, at nanoscales, it is not clear that the pore surface, which is determined by nitrogen adsorption, is the same as the effective cross-sectional area available for water flow. This is because repulsion might lead to empty spaces between the tube and the fluid that diminish the effective area for flow. Alternative ways to measure flow velocities within nanotubes seem to be necessary. On the theoretical side, most of the efforts toward the understanding of enhanced flow in nanotubes are performed using MD simulations.[8,19,27] The enormous computational cost that such simulations demand limits the system sizes to a few thousand atoms. Typical sizes of tubes studied by MD lie between 1 and 10 nm in diameter and 10-100 nm in length, while typical sizes of real nanotubes are in the range of up to tenths of nanometers in radius and hundreds of microns in length. In turn, simulation times are limited to a few nanoseconds. This implies that MD simulations allow for a systematic theoretical study of the transient oscillatory tube dynamics but cannot reach the appearance of steady deflective vibrations observed in experiments,[28] and it is currently an insufficient tool for understanding the effect of fluid motion in the mechanical stability or instability of nanotubes.

In turn, CM to study flow within nanotubes is especially useful to study system sizes above several nanometers in radius[29–32] and it is appropriate to study any time scale of the vibration dynamics. Typical sizes of nanotubes lie on the boundary of the capabilities of MD and CM approaches. Both methodologies provide complementary and necessary information to understand these systems. Theoretical efforts to study flow in carbon nanotubes using CM have considered slip but have neglected the oscillatory dynamics of the tube and its coupling to the fluid.[1–6] Such coupling is necessary since

there are important elastic responses of the nanotubes when subject to different types of deformations.[33,34] Other CM models that do consider the coupling between tube motion and the fluid velocity have not addressed the problem of flow determination, not to mention the explanation of flow enhancement. Such models include the study of non-viscous flow within an oscillating elastic single-walled carbon nanotube,[35] models that incorporate their concentric multi-layered structure, and models that consider the elastic and viscous forces acting on the tube.[36–38] More sophisticated models consider the effect of a non-local tube elasticity.[39,40] All of these models are focused on the effect that a given flow velocity has on the natural oscillation frequencies of the tube, subject to particular boundary conditions at its edges. They propose equations that are solved numerically for the specific boundary conditions studied. The potential of such approaches to propose alternative ways to determine the magnitude of flow velocity has been overlooked.

In this work, we develop a theoretical framework to demonstrate that a CM approach, taking into account the coupling between the fluid and the tube dynamics, could be exploited to determine flow velocities based on knowledge of the vibration frequency spectrum of a single nanotube. This methodology could be applied to different sets of boundary conditions at the nanotube edges. We obtain analytical expressions for the fluid velocity as a function of the natural frequencies of the nanotube deflection, which allow for an easy error propagation analysis of the uncertainties involved in each of the system parameters. Our expressions allow us to establish the framework for indirect determination of flow, via experimental measurements of the nanotube oscillatory bending motion. Our analysis indicates that the experimental uncertainties in the flow magnitude could be dramatically reduced in wide ranges of tube sizes and flow velocities, by using the proposed methodology. Our approach proposes to record the nanotube displacement as a function of time (for example, by AFM measurements), to use this information to determine the relevant frequencies associated with the tube dynamics via Fourier Analysis, and finally, to determine the magnitude of flow velocity inside a nanostructure, through the analytical relations between frequency and flow velocity obtained in this work.

This paper is structured as follows: first, a physical model is presented that incorporates the interaction between an elastic tube and the fluid transported inside it. From this, we obtain relations between flow velocity and the natural vibration frequencies of the nanotube. These would allow for the determination of the flow velocity, if the frequency spectrum of a nanotube were known in two situations: with the fluid flowing within the nanotube with an unknown velocity—to be determined—and also with a stagnant fluid inside it. The experimental feasibility is discussed based on the state-of-the-art capabilities of atomic force microscopy (AFM). Finally, we perform numerical simulations for different sets of boundary conditions, which might approximate different experimental settings, and determine flow uncertainties that depend on sampling times, as well as on the spatial and time resolution of the apparatus. These uncertainties allow one to know under which circumstances the proposed framework to measure flow velocities would lead to accurate results.

II. MODEL

We consider a nanotube as an elastic cylindrical hollow, conveying flow, subject to small deformations. The equation of motion for the tube displacement, $u(z,\ t)$, contains the fluid velocity along the tube, v, as a parameter,[35,41] and is written as

$$EI\frac{\partial^4 u}{\partial z^4} + (\rho_f A_f v^2 - T)\frac{\partial^2 u}{\partial z^2} + 2\rho_f A_f v\frac{\partial^2 u}{\partial t \partial z} + (\rho_t A_t + \rho_f A_f)\frac{\partial^2 u}{\partial t^2} = 0. \quad (1)$$

In this equation, ρ_f is the density of the fluid, ρ_t is the density of the tube, A_t and A_f are the tube and fluid cross-sectional areas, respectively; T is the tension along the tube, E is the Young Modulus of the tube, I is the second moment of inertia of the cylindrical tube, z is a spatial coordinate that coincides with an undeformed tube, and t is time. The model tube and the definition of the vertical displacement, u, are illustrated in Fig. 1. For nanotubes in typical experimental conditions, there is normally no tension,[42,43] so we consider $T = 0$. Equation (1) is nothing but Newton's second law for the forces acting on the tube per unit length. The term $(\rho_t A_t + \rho_f A_f)\frac{\partial^2 u}{\partial t^2}$ is the mass times the acceleration; $-EI\frac{\partial^4 u}{\partial z^4}$ is the elastic force; $-\rho_f A_f v^2\frac{\partial^2 u}{\partial z^2}$ is the centrifugal force; and $-2\rho_f A_f v\frac{\partial^2 u}{\partial z \partial t}$ is the Coriolis force. Consideration of small deformations is necessary in order to have a linear equation that allows for analytical solutions, which in turn allow for an analytical error propagation analysis.

It is important to remark that in this model, the average flow velocity, v, appearing in Eq. (1), could come from different velocity profiles and flows with different slip velocities. It is only the average flow velocity that matters as far as the tube dynamics is concerned.

A visual inspection of Eq. (1) allows one to find, from the first and fourth terms, a characteristic frequency of the system, ω_c, in the absence of flow, when $v = 0$. That is, a frequency characteristic of a tube of length L with a stagnant fluid inside it,

$$\omega_c = \frac{1}{L^2}\sqrt{\frac{EI}{\rho_t A_t + \rho_f A_f}}. \quad (2)$$

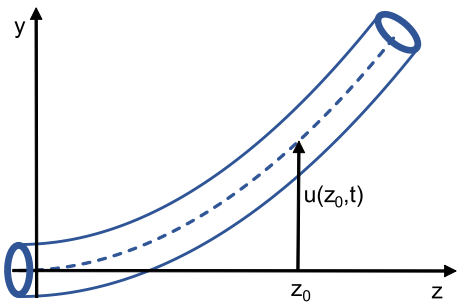

FIG. 1. Representation of a nanotube portion. Its dynamics is described by an equation for the tube displacement, $u(z,\ t)$, illustrated in the figure, where z is the coordinate along the undeformed nanotube, t is time, and y is the coordinate in which the tube displacement occurs.

It also allows us to find, from the first and second terms, a characteristic flow velocity for a steady tube in the absence of vibrations, v_c, when the partial derivatives in time of the tube displacement are zero,

$$v_c = \frac{1}{L}\sqrt{\frac{EI}{\rho_f A_f}}. \tag{3}$$

These characteristic quantities allow us to rewrite Eq. (1) in terms of the dimensionless variables, $\tilde{z} = \frac{z}{L}$, $\tilde{t} = \omega_c t$, and $\tilde{v} = \frac{v}{v_c}$ as

$$\frac{\partial^4 u}{\partial \tilde{z}^4} + \tilde{v}^2\frac{\partial^2 u}{\partial \tilde{z}^2} + 2\alpha\tilde{v}\frac{\partial^2 u}{\partial \tilde{z}\partial \tilde{t}} + \frac{\partial^2 u}{\partial \tilde{t}^2} = 0, \tag{4}$$

where the quantity α, which we name the *thickness ratio*, has been defined as

$$\alpha^2 \equiv \frac{1}{1+\frac{\rho_t A_t}{\rho_f A_f}}. \tag{5}$$

Such a thickness ratio, α, might take values between 0 and 1. It decreases when the tube thickness increases because of the ratio of cross-sectional areas, of tube and fluid, in the denominator of Eq. (5). In order to have a simple notation, we will omit tildes from this point, but z, t, and v refer to non-dimensional variables.

The dimensionless equation for the tube displacement [Eq. (4)] is a differential equation in space and time, which depends explicitly on only two physical parameters, namely:

- The dimensionless flow velocity, v, that has been normalized with the flow in a steady tube.
- The thickness ratio, α, which depends only on the ratio of tube and fluid densities, and the ratio of tube and fluid cross-sectional areas.

III. BOUNDARY CONDITIONS

In an infinite tube, in principle, a wave of any wavelength can be transmitted. However, when the finite size of a system is considered, the dispersion relation has to satisfy certain conditions, according to the way in which the tube edges are fixed. This results in the discretization of the allowed frequencies and wavelengths.

A specific experimental setting of the tube would determine the way in which edges are fixed.[39] The experimental literature on elastic nanotubes shows three common geometrical conditions for the tube edges:[28]

- Pinned edge. It means that the displacement of the tube edge is zero and that there is no curvature at that point. Physically, this implies that no elastic strain is imposed at the tube edge. Mathematically, for a tube edge located at $z = z_0$, this is written as

$$u\Big|_{z=z_0} = 0 \quad \text{and} \quad \frac{\partial^2 u}{\partial z^2}\Big|_{z=z_0} = 0. \tag{6}$$

- Clamped edge. It means that the displacement of the tube edge is zero and that the tube at that point is constrained to be horizontal. Mathematically, for a tube edge located at $z = z_0$, this is written as

$$u\Big|_{z=z_0} = 0 \quad \text{and} \quad \frac{\partial u}{\partial z}\Big|_{z=z_0} = 0. \tag{7}$$

- Free edge. It means that the displacement of the tube edge is not fixed, and the only constrain is that there is no curvature at that point and on its neighborhood. Mathematically, for a tube edge located at $z = z_0$, this is written in the following way:

$$\frac{\partial^2 u}{\partial z^2}\Big|_{z=z_0} = 0 \quad \text{and} \quad \frac{\partial^3 u}{\partial z^3}\Big|_{z=z_0} = 0. \tag{8}$$

For a finite-size tube, which has two edges, any combination of these three possibilities should be, in principle, experimentally possible. This gives 6 sets of boundary conditions that discretize differently the dispersion relation, namely, pinned-pinned (P-P), clamped-clamped (C-C), free-free (F-F), pinned-clamped (P-C), pinned-free (P-F), and clamped-free (C-F). Each of these sets implies four conditions on u and/or its spatial derivatives.

IV. RELATION BETWEEN FLOW MAGNITUDE AND TUBE FREQUENCY

The Fourier Transform in time of Eq. (4) leads to

$$\frac{d^4\hat{u}}{dz^4} + v^2\frac{d^2\hat{u}}{dz^2} - 2i\omega\alpha v\frac{d\hat{u}}{dz} - \omega^2\hat{u} = 0, \tag{9}$$

where $\hat{u}(z,\omega)$ denotes the displacement in frequency domain. As this is a linear fourth-order differential equation for $\hat{u}(z,\omega)$ with constant coefficients, the solution of Eq. (9) is the superposition of four terms, resulting in a general form given by

$$\hat{u}(z,\omega) = C_1 e^{ik_1 z} + C_2 e^{ik_2 z} + C_3 e^{ik_3 z} + C_4 e^{ik_4 z}, \tag{10}$$

where k_1, k_2, k_3, and k_4 are wavenumbers and are functions of v, ω and α. For a given tube and fluid, the latter is a constant. The wavenumbers are given as follows:

$$k_1 = -a-b; \quad k_2 = -a+b; \quad k_3 = a-b; \quad k_4 = a+b, \tag{11}$$

where a and b are given by

$$a = \frac{1}{2}\sqrt{\frac{2v^2}{3} + \frac{2^{\frac{1}{3}}(v^4-12\omega^2)}{3q^{\frac{1}{3}}} + \frac{q^{\frac{1}{3}}}{3(2)^{\frac{1}{3}}}}, \tag{12}$$

$$b^2 = \frac{v^2}{3} - \frac{2^{\frac{1}{3}}(v^4-12\omega^2)}{12q^{\frac{1}{3}}} - \frac{q^{\frac{1}{3}}}{12(2)^{\frac{1}{3}}} - \frac{v\alpha\omega}{\sqrt{\frac{2v^2}{3} + \frac{2^{\frac{1}{3}}(v^4-12\omega^2)}{3q^{\frac{1}{3}}} + \frac{q^{\frac{1}{3}}}{3(2)^{\frac{1}{3}}}}} \tag{13}$$

and q is given by

$$q = -2v^6 - 72v^2\omega^2 + 108v^2\alpha^2\omega^2 + \sqrt{s}, \tag{14}$$

where s is

$$s = \left(2v^6 + 72v^2\omega^2 - 108v^2\alpha^2\omega^2\right)^2 - 4\left(v^4 - 12\omega^2\right)^3. \tag{15}$$

When a set of boundary conditions at the tube edges is chosen, one obtains a linear homogeneous 4×4 system of

algebraic equations for the coefficients C_n. Such a system allows for a non-trivial solution, only if the determinant, D, vanishes. This discretizes the allowed values of the wavenumbers and therefore the allowed values of the frequency, ω, giving rise to the different vibration frequency modes of the tube, ω_n. Moreover, such determinant is different for each set of boundary conditions. As an example, for a pinned-pinned tube, the determinant, D_{PP}, is given by

$$D_{PP}(v,\omega) = \begin{vmatrix} 1 & 1 & 1 & 1 \\ -k_1^2 & -k_2^2 & -k_3^2 & -k_4^2 \\ e^{ik_1} & e^{ik_2} & e^{ik_3} & e^{ik_4} \\ -k_1^2 e^{ik_1} & -k_2^2 e^{ik_2} & -k_3^2 e^{ik_3} & -k_4^2 e^{ik_4} \end{vmatrix}. \tag{16}$$

Explicit expressions for the determinants for the other sets of boundary conditions are given in Sec. A of the supplementary material.

As stated above, the condition for non-trivial solutions of the tube dynamics is achieved when

$$D(v,\omega_n) = 0. \tag{17}$$

From Eq. (17), it is possible to know the relation between the frequency of a tube oscillating in any of its vibration modes, ω_n, and the flow velocity, v, inside it.

From this point, we use two different approaches in order to obtain the flow/frequency relations from Eq. (17): an analytical approach, which will be discussed in Sec. V, and a numerical approach, which we implement in order to determine the range of validity of our analytical solutions. The latter consists of the numerical obtention of the frequency of every vibration mode, ω_n, given a known value of the flow velocity. This treatment is useful when the tube starts in an initial deformed condition with a known flow velocity induced inside it and allows for a determination of the tube dynamics. The frequency of each mode is obtained with any degree of precision, so it can be considered as the exact solution of $\omega_n(v)$. We solved Eq. (17) by a Newton-Raphson method using Wolfram Mathematica 11. The effect of a specific set of boundary conditions in the fundamental frequency vs. flow diagram is illustrated in Fig. 2 for the pinned-pinned and clamped-clamped cases. The qualitative behavior of the curves in Fig. 2 has been studied in the literature,[44,45] by the numerical solution of Eq. (1), with the purpose of identifying the flow conditions that induce unstable tube motion. For the lowest flow velocities, a purely real frequency is obtained, which leads to stable oscillatory motion of the tube. On the other hand, when the frequency is purely imaginary, the dynamics leads to buckling, or when it is complex, with non-zero real and imaginary parts, it leads to fluttering.[35–38]

In Fig. 2, a decrease in the fundamental mode, ω_1, with increasing flow velocity in the stable motion zone can be observed; this implies that the larger the flow velocity is, the smaller the fundamental frequency is; when flow increases above a certain threshold that depends on the set of boundary conditions, an unstable behavior emerges—indicated by a non-zero imaginary part of the frequency. For the other sets of boundary conditions, equivalent figures are included in Sec. B of the supplementary material.

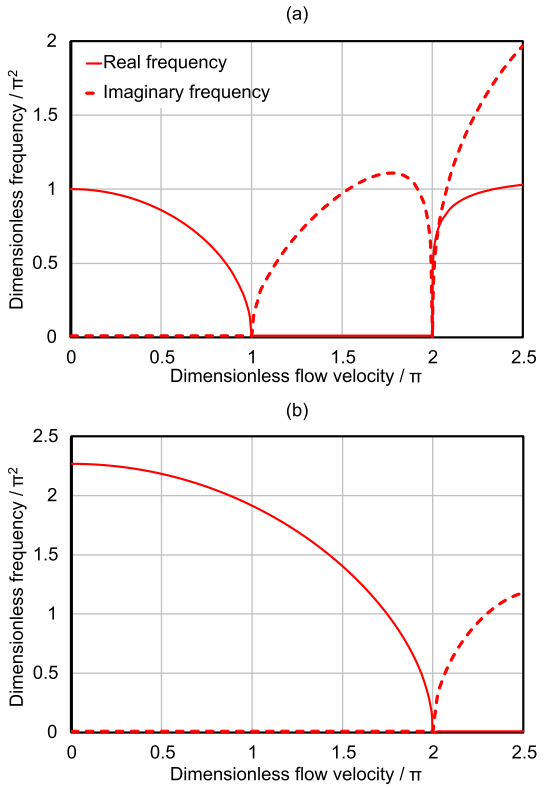

FIG. 2. Effect of flow in the fundamental frequency mode of the tube oscillations, for two sets of boundary conditions. Solid lines correspond to the real part of the frequency and dashed lines to its imaginary part. A typical value of the thickness ratio $\alpha = 0.6$ is used in the calculations. (a) Pinned-pinned. (b) Clamped-clamped.

V. ANALYTICAL APPROACH

An alternative approach to solve Eq. (17) that is key to the proposed framework for flow determination consists of obtaining analytical expressions for the flow velocity as a function of the tube oscillation modes, $v(\omega_n)$. The purpose of this is to determine the flow magnitude inside a tube when the frequency spectrum of tube bending motion is known. Such strategy is based on the assumption that experimentally attainable flows are small in comparison to the critical flow velocity of the first mode, given by the characteristic flow velocity in Eq. (3). This assumption is supported by the typical flow velocities measured within carbon nanotubes.[1] With this consideration, it is possible to perform a Taylor expansion, around small flow velocities, of the determinant, D, in Eq. (17), as follows:

$$D(v,\omega) = D\Big|_{v=0} + \sum_{n=1}^{\infty} \frac{\partial^n D}{\partial v^n}\Big|_{v=0} \frac{v^n}{n!}. \tag{18}$$

It turns out that, for several sets of boundary conditions (P-P, C-C, F-F, and P-C), the odd derivatives of the determinant vanish. For these cases, a truncation to order m in Eq. (18) leads to an algebraic equation of order $\frac{m}{2}$ for $v^2(\omega)$. Since analytic solutions of polynomial equations are known up to quartic order, we have obtained analytic approximations of Eq. (18) for v^2, for truncation orders $m = 2, 4, 6$, and 8. As an example, a second-order truncation of the determinant in Eq. (18) for the pinned-pinned case is

$$v_{P-P}(\omega,\alpha)=\sqrt{\frac{A_{PP}}{B_{PP}}}, \tag{19}$$

where A_{PP} and B_{PP} are given by

$$A_{PP}=8\omega\sin(\sqrt{\omega})\sinh(\sqrt{\omega}), \tag{20}$$

$$B_{PP}=4\alpha^2-\cosh(\sqrt{\omega})G_{PP}-\sqrt{\omega}\sinh(\sqrt{\omega})H_{PP} \tag{21}$$

and G_{PP} and H_{PP} are given by

$$G_{PP}=4\alpha^2\cos(\sqrt{\omega})+(\alpha^2-2)\sqrt{\omega}\sin(\sqrt{\omega}), \tag{22}$$

$$H_{PP}=(2-\alpha^2)\cos(\sqrt{\omega}). \tag{23}$$

A comparison of the analytical expression in Eq. (19) (and equivalent expressions to higher truncation orders) with the exact numerical solutions is shown in Fig. 3(a), in order to exhibit the range of velocities in which each of the approximations is adequate. Figure 3(b) shows the percentage error between the different analytical approximations and the exact numerical solution. We can observe that there is a wide range of flow velocities in which the analytical approximations differ no more than few percentage points from the exact solution. For excited modes (not shown in Fig. 3), the analytical approximations are valid for wider velocity ranges than the fundamental mode.

For the two sets of boundary conditions for which odd derivatives of the determinant do not vanish (P-F and C-F), algebraic equations for v (and not for v^2) can be obtained up to quartic order. Analytic expressions for higher truncation orders (needed for higher flow velocities) and for the other sets of boundary conditions, as well as figures comparing analytical expressions of the fundamental mode with numerical solutions, are included in Sec. C of the supplementary material.

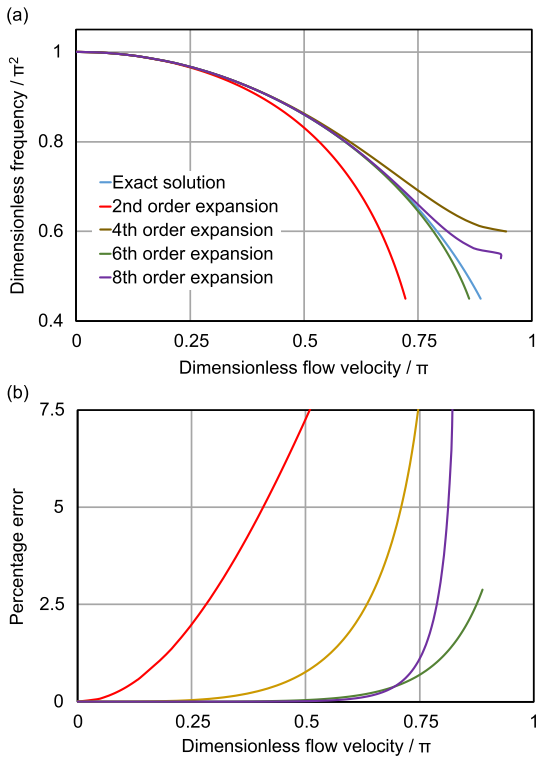

FIG. 3. (a) Comparison between the approximated analytical expressions and the exact numerical solution for the flow velocity as a function of the fundamental frequency for the pinned-pinned case. As expected, incorporation of more terms in the Taylor expansion for v^2 leads to an increase in accuracy and the range of applicability of the analytical expressions for higher flows. (b) Percentage error in the velocity as a function of the flow velocity. A typical value of the thickness ratio $\alpha=0.6$ is used in the calculations.

Contrary to exact solutions that are multivalued, our analytical solutions for the first degree of truncation give expressions for $v(\omega_n)$ such that for each value of ω only one value of the velocity could be obtained. Moreover, the expression for the velocity is exactly the same for each of the tube vibration modes in the spectrum. Therefore, if the frequency spectrum of the tube dynamics were available, any of the frequencies composing it could be in principle used in Eq. (19), and the same flow velocity would be obtained. This together with the knowledge of the range of flow velocities in which the approximation is valid (for example, from Fig. 3) gives an important advantage of our analytical approach over numerical schemes.[44,45] This fact could be useful in real experiments, where different sources of uncertainty may induce noise and spurious peaks in the frequency spectra because every physical peak must be related to the same flow velocity. For higher truncation orders of the determinant in Eq. (18), the analytical solution will give several values for the flow velocity; however, careful analysis would allow to distinguish which is the physical solution because this should give a real value for the velocity (see, for example, Table I in Sec. C of the supplementary material). The physical solution will also comply with the fact that any of the frequencies in the spectrum will be associated with a single value of the fluid velocity (see, for example, Fig. 3 in Sec. C of the supplementary material for the fourth truncation order for v^2).

VI. SIMULATION OF THE TUBE DYNAMICS

An illustrative example of our proposal consists of the theoretical solution of a tube with an initial condition that imitates a possible deformation induced by AFM; this is given by

$$u(z,t=0)=256\left(z^4-4z^5+6z^6-4z^7+z^8\right)$$

and

$$\dot{u}(z,t=0)=0. \tag{24}$$

Geometrical details of the tube used in this example and its initial condition are illustrated in Fig. 4. A polynomial function was chosen in order to satisfy any of the sets of boundary conditions in the tube extremes.

This example allows one to see how boundary conditions influence the tube dynamics and could potentially allow experimentalists to understand that to which of the idealized sets of boundary conditions their specific experiment belongs.

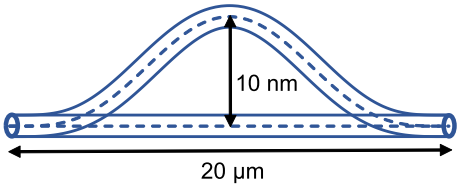

FIG. 4. Initial condition imposed for the simulations of the tube dynamics.

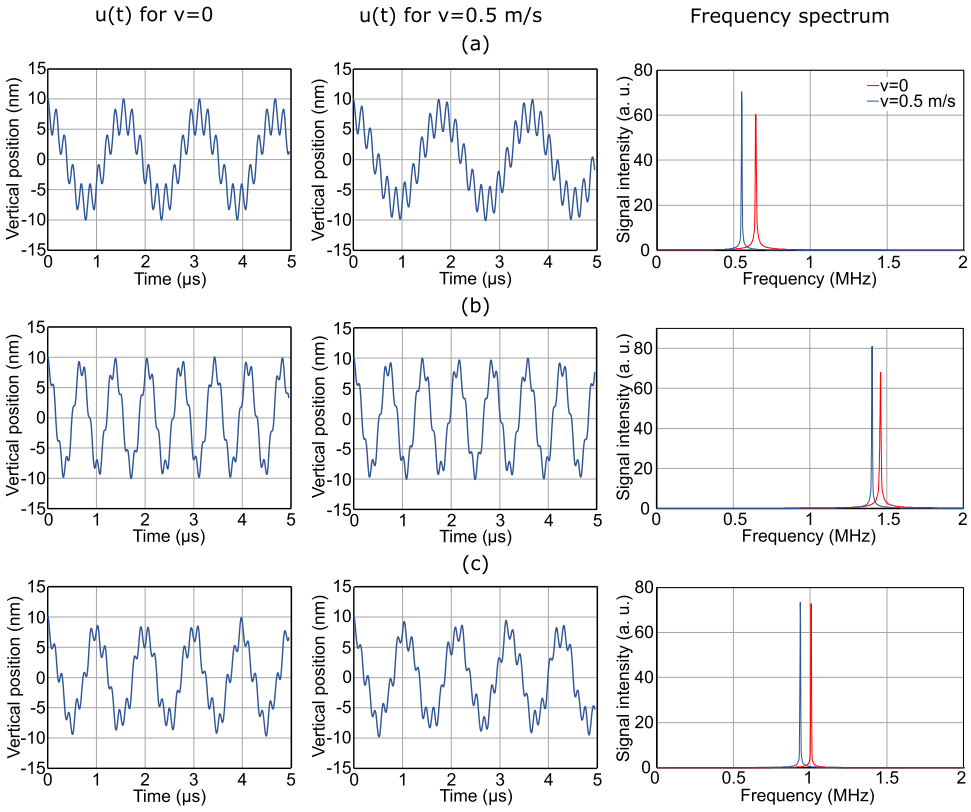

FIG. 5. Simulation of the tube dynamics with different boundary conditions at their edges. For each set of boundary conditions, the tube displacements at the middle of the tube (z = 0.5) are plotted as a function of time; left column, when the tube is filled with a stagnant fluid; middle column, when the tube is filled with a fluid with flow velocity v = 0.5 m/s. The right column shows the frequency spectrum of both cases illustrating clearly that the fundamental mode is smaller when the fluid is being transported with a finite velocity than when the fluid is stagnant within the tube. It also shows that the fundamental mode occurs at different values for each set of boundary conditions. Calculations were performed for a nanotube with inner and outer tube radii of 8 and 15 nm, respectively. (a) Pinned-pinned. (b) Clamped-clamped. (c) Pinned-clamped.

Simulations of the tube dynamics are illustrated in Fig. 5 for the pinned-pinned, clamped-clamped, and pinned-clamped cases. For each set of boundary conditions, the tube displacements at the middle of the tube ($z = 0.5$) are plotted as a function of time, when the tube is filled with a stagnant fluid (first column) and when the tube is filled with a fluid with a flow velocity $v = 0.5$ m/s (second column). The third column shows the frequency spectrum of both cases illustrating clearly that the fundamental frequency is smaller when the fluid is being transported with a finite velocity than when the fluid is stagnant within the tube. It also shows that the fundamental mode occurs at different frequency values for each set of boundary conditions.

The complete derivation of the solution of the tube dynamics [Eq. (1)] with initial and boundary conditions is given in Sec. D of the supplementary material.

VII. EXPERIMENTAL FEASIBILITY

We analyze the feasibility of a potential experiment according to the state of the art of the experimental apparatus. Most of the experiments in the detection of motion and mechanical response of carbon nanotubes can be classified into two big groups: determination of the force exerted on a tube due to an imposed static deflection by means of AFM, where the determination relies on a single measurement and has a considerable amount of error,[46–50] and tests of the nanotubes' proficiency as resonators in response to external steady oscillatory perturbations produced by piezoelectric actuators.[42,43,51–53] A different strategy is conceived here. If a certain amount of data, which account for the time evolution of the tube motion, are registered and subsequently treated by Fourier analysis, the uncertainty in the peaks of the frequency spectrum will depend on the apparatus resolution to measure distances and time and, importantly, on the sampling time.[54,55]

The minimal elements that an experiment should have in order to determine flow using our analytical framework are three: (1) an external driving force allowing for fluid flow inside the nanotube, (2) a device allowing for an initial perturbation of the tube, and (3) a transducer device allowing for the detection and registration of the tube motion.

The incorporation of two closed reservoirs at the tube edges and the induction of a pressure difference by mechanical means—a syringe or a piston—are not suitable at nanoscales since the imperfections of the junctions between the reservoirs and tube extremes would cause water leaking. A better strategy could be to induce an electrophoretic flow by a voltage difference across the tube as performed by Qin.[13] A steady flow would be obtained shortly after the tube is full of water.

An initial perturbation could be induced, for example, by pushing the tube with the tip of an AFM,[48,56] by direct mechanical coupling of a piezoelectric material pulsed by an AC electric source,[53,57,58] or by indirect excitation of the nanotube by acoustic means.[59–62]

In general, four detection ways seem to be suitable for accurate measurements with a sub-nm resolution and within the range of a few nm in the vertical displacement of a nanotube: field-effect transistors,[63–67] piezo-resistive effect,[51,53] capacitive response,[52] and optical interferometry.[68,69]

The space of a nanodevice does not allow for an easy incorporation of multiple instruments or the aligning of a microdevice with external components and probes. The most

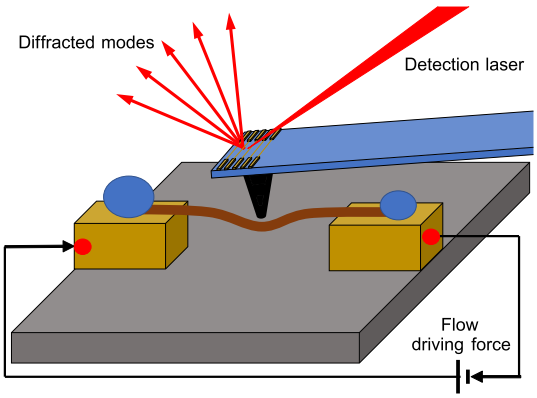

FIG. 6. An example of a minimal experimental setting to indirectly determine flow velocities by means of recording the tube displacements in time. The setting includes an electrophoretic driving force for fluid flow, while the tube deformation and detection are both performed by means of an AFM with interdigitated prints that allow for accurate detection via interferometry.

suitable device would be the one that allows for the simplest setting that incorporates an actuator, a detector, and a driving force for fluid flow.

A possible minimal setting, compatible with the simulation of the tube dynamics of Sec. VI, is illustrated in Fig. 6. This would include an electrophoretic driving force for the fluid, while the tube deformation and the detection could be both performed by means of an AFM with interdigitated prints, which allow for accurate detection via interferometry, as developed by Manalis.[70,71] The arrangement of the tube and AFM tip could be as the one in the work of Salvetat.[48]

Frequently, the actuation or detection of the tube motion will involve external forces that should be incorporated into the model. Moreover, depending on the environmental conditions of the experiment, a damping force could affect the experimental results. However, all these external forces can be incorporated into Eq. (1) in a straightforward manner. The theoretical treatment provided in this work (and fully explained in Sec. C of the supplementary material) can incorporate such external forces, allowing the obtention of analytical expressions for the specific experiment developed. However, in general, these external forces exert only slight modifications to the flow/frequency relations shown in Fig. 3 because in most cases, the large Young Moduli of CNTs would cause the elastic force to be the dominant force of the system.

VIII. CONSIDERATIONS ON THE UNCERTAINTY AND SENSIBILITY OF THE METHOD

The flow/frequency relation in Eq. (19) and the equivalent relations for other B.C. relate dimensionless flow and dimensionless frequency. A suitable manner to use such a relation is by performing two experiments, one at finite flow velocity and the other at zero flow, and to record the fundamental frequency for both experiments.

The dimensional frequency obtained by a measurement at a given flow velocity v will be denoted by ω_v^{BC}, where BC reminds that the fundamental frequency depends on the specific set of boundary conditions. The frequency of a tube filled with a stagnant fluid, ω_0^{BC}, can be related to the characteristic frequency ω_c in Eq. (2) by the following relation:

$$\omega_0^{BC} = a\omega_c, \tag{25}$$

where the value of a depends on the boundary conditions. For a pinned-pinned tube, $a = 1$; for a clamped-clamped and a free-free tube, $a = 9/4$; for a pinned-clamped and a free-free tube, $a = 25/16$; and for a clamped-free tube, $a = 1/4$.

Therefore, the ratio of both dimensional measured frequencies ω_v^{BC} and ω_0^{BC} leads to the following result:

$$\frac{\omega_v^{BC}}{\omega_0^{BC}} = \frac{1}{a}\frac{\omega_v^{BC}}{\omega_c} = \frac{1}{a}\omega, \tag{26}$$

which allows one to compute the dimensionless frequency, ω, directly from the two experiments, without the need to determine directly ω_c by means of the Young modulus of the tube.

Doing so would be useful for the reduction of uncertainty because in this way the relative uncertainty of flow is computable directly from the dimensionless equation (19) or equivalent expressions for other boundary conditions.[78] First, the dimensional uncertainty of both frequency measurements is incorporated in the uncertainty of the dimensionless frequency, ω, as

$$\begin{aligned}\Delta\omega^2 &= \left(\frac{\partial\omega}{\partial\omega_v^{BC}}\right)^2\left(\Delta\omega_v^{BC}\right)^2 + \left(\frac{\partial\omega}{\partial\omega_0^{BC}}\right)^2\left(\Delta\omega_0^{BC}\right)^2 \\ &= \frac{a^2}{\left(\omega_v^{BC}\right)^2}\left(\Delta\omega_v^{BC}\right)^2 + a^2\frac{\left(\omega_v^{BC}\right)^2}{\left(\omega_0^{BC}\right)^4}\left(\Delta\omega_0^{BC}\right)^2.\end{aligned} \tag{27}$$

And then, the uncertainty in the dimensionless frequency, ω, is incorporated in the uncertainty of the dimensionless flow velocity, $v(\omega, \alpha)$, given by Eq. (19)—or equivalent expressions for the other boundary conditions—as

$$\Delta v = \sqrt{\left(\frac{\partial v}{\partial\omega}\right)^2(\Delta\omega)^2 + \left(\frac{\partial v}{\partial\alpha}\right)^2(\Delta\alpha)^2}, \tag{28}$$

where the uncertainty $\Delta\alpha$ can be computed from the uncertainty in densities and outer and inner tube radii. Therefore, from Eqs. (27) and (28), it is possible to establish that uncertainty on flow depends essentially on the dimensional uncertainty of both frequency measurements, on the dimensional uncertainty of densities and radii, and on the slope of the dimensionless flow/frequency function, $\partial v/\partial\omega$, and the slope of the dimensionless flow/thickness ratio function, $\partial v/\partial\alpha$.

Among all the factors that affect the flow velocity uncertainty, the most important one is the slope of flow velocity/frequency function because it depends drastically on the magnitude of the flow velocity itself and it diverges for flow velocities close to zero. This result is presented in Fig. 7(a), where it is possible to see that for large tubes and intermediate flow velocities, the uncertainty reaches an asymptotic lower value, which is given by the uncertainty of the thickness ratio, α.

According to our analysis, we consider that our method could be implemented in typical carbon nanotubes between 10 and 100 μm in length, with initial amplitudes between 1 and 50 nm. Our calculations predict that a tube of these dimensions will have natural frequencies on the range of kHz–MHz.

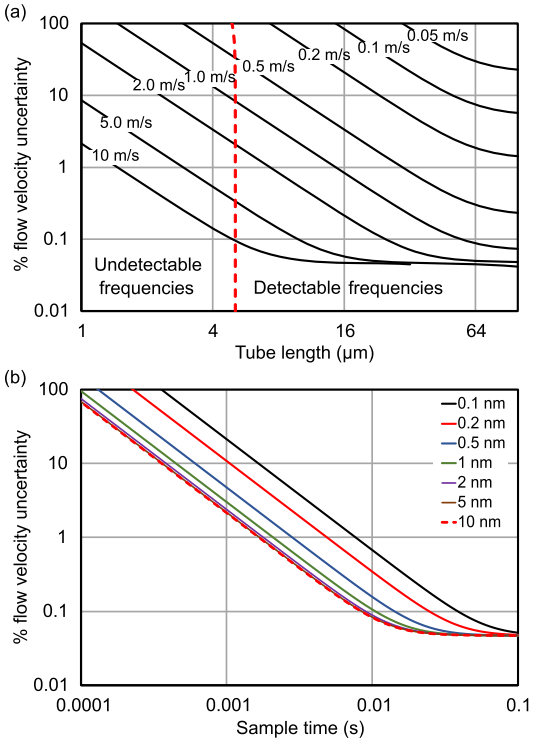

FIG. 7. Effect of the main experimental parameters on the uncertainty in flow determination. (a) Expected uncertainty in the flow velocity as a function of the magnitude of the flow velocity for different tube lengths, with an initial amplitude of 5 nm. The time resolution of 0.05 μs determines an upper bound for the range of detectable frequencies. Such a limit—given by the Nyquist frequency—is shown in the red dashed line. (b) Expected uncertainty in the flow velocity as a function of the sampling time for different amplitudes of the initial condition, with a tube length of 20 μm and a magnitude of flow velocity of 0.5 m/s. Calculations were performed for a nanotube with pinned edges and the following physical parameters: inner and outer tube radii of 8 and 15 nm, respectively; water and carbon densities of 1000 and 2300 kg/m^3, respectively; uncertainty in radius of 0.1 nm; and uncertainty in densities of 0.1 kg/m^3.

After a literature review on the spatial and time resolution of AFM, a resolution of 0.1 nm in the measurement of the vertical displacement of the tube[72,73] and a time resolution of 0.05 μs would be possible.[74–76] For shorter tubes (between 1 and 10 μm in length), the experimental setting in Fig. 6 would not be suitable since it is incapable of detecting MHz-GHz frequencies.

Uncertainty in Fig. 7 would change slightly if different actuators or sensors are considered. However, the qualitative behavior would remain the same since its origin is the slope of the flow/frequency relation.

Such calculations were performed by considering a simple treatment for the uncertainty in frequency by using a discrete Fourier transform of a one-mode sinusoidal signal plus white noise.[54,55,77] For this, we have that

$$\Delta\omega_v^{BC} = \frac{\Delta u}{aT}\sqrt{\frac{24}{N}}, \tag{29}$$

where N is the number of measurements in time, T is the total sampling time, a is the amplitude of the sinusoidal mode, and Δu is the uncertainty in the tube vertical position in time domain.

Figure 7(b) shows that the uncertainty in flow velocity is not significantly diminished by an increase in the amplitude of the initial condition, so an initial amplitude of about 5-10 nm can be enough to carry out the experiment. By contrast, uncertainty is strongly dependent on sampling time because it affects directly the uncertainty in frequency determination.

TABLE I. Approximated range of suitability for a tube of 20 μm of length, subject to different boundary conditions. The range of flow magnitudes and frequencies is given in terms of the accurately measurable flows and fundamental frequencies, i.e., the ones that reach an uncertainty of 5% or lower in flow determination.

Boundary condition	Range of frequency (MHz)	Range of flow velocity (m/s)
Pinned-pinned	0.58-0.9	0.3-40
Clamped-clamped	1.03-1.35	0.7-90
Pinned-clamped	0.64-0.9	0.3-60
Free-free	1.03-1.35	0.7-90
Pinned-free	0.64-0.9	0.5-60
Clamped-free	0.13-0.23	0.5-60

In general, flow determination is better for intermediate flow velocities, as the magnitude of the slope of the flow velocity/frequency function decreases with increasing flow magnitude. However, the range of such intermediate flow velocities, which are ideal for measurements, depends on the boundary conditions imposed on the specific experiment. This is illustrated in Table I.

According to this, the best boundary condition will depend on the specific limitations of the actuators and sensors of a particular experimental setting. For the cases where the experimental time resolution is limited, the fundamental frequency of a clamped-free tube is the lowest and allows for an easier detection. Besides, if the driving pressure gradient is limited and only low flows could be generated, then pinned-pinned would be the preferred setting.

IX. CONCLUSIONS

A theoretical framework to indirectly measure flow velocities within nanotubes has been developed. This would give smaller uncertainties in flow velocities than conventional methodologies—which determine the flow magnitude in systems of nanotubes embedded in membranes—because of the fact that it is limited by frequency measurements and not by knowledge of the effective area to flow.

Our strategy does not assume a particular interaction between water and graphene, so it could be used regardless of the natural degree of hydrophobicity of the interaction, and it could also be used for functionalized nanotubes.

In our model, the average flow velocity, v, determines the bending frequency spectrum of the tube regardless of the presence or absence of slip in the system. Once v is experimentally determined, analytical expressions for steady state flow in the presence of slip, considering, for example, the Navier hypothesis for the slip velocity, could be used to determine slip lengths. These might differ from those currently reported in the literature.

Our work might constitute the basis to propose a wide range of experiments of flow across nanostructures in different experimental situations focusing on frequency measurements.

It also constitutes a basic framework that could be extended to determine other structural and rheological fluid properties by means of indirect frequency measurements rather than by conventional methods.

SUPPLEMENTARY MATERIAL

Further details are provided in supplementary material, organized in four sections, as follows:

- Section A. Expressions of the determinant for the different sets of boundary conditions.
- Section B. Flow/frequency relation for the different sets of boundary conditions.
- Section C. Derivation of the analytical expressions for flow as a function of frequency.
- Section D. Simulation of the tube dynamics.

ACKNOWLEDGMENTS

The authors thank Peter Grutter for discussions regarding the experimental feasibility of the proposal. U.T. acknowledges financial support from CONACyT (Mexico) through Fellowship No. 589015. E.C.P. acknowledges financial support from CONACyT (Mexico) through Project No. 219584 and the Faculty of Chemistry at UNAM through PAIP Project No. 5000-9011.

[1]M. Whitby and N. Quirke, "Fluid flow in carbon nanotubes and nanopipes," Nat. Nanotechnol. **2**, 87–94 (2007).
[2]M. Majumder, N. Chopra, and B. J. Hinds, "Nanoscale hydrodynamics: Enhanced flow in carbon nanotubes," Nature **438**, 44 (2005).
[3]S. Joseph and N. R. Aluru, "Why are carbon nanotubes fast transporters of water?," Nano Lett. **8**, 452–458 (2008).
[4]G. Hummer, J. C. Rasaiah, and J. P. Noworyta, "Water conduction through the hydrophobic channel of a carbon nanotube," Nature **414**, 188–190 (2001).
[5]D. J. Bonthuis, K. F. Rinne, K. Falk, C. N. Kaplan, D. Korinek, A. N. Berker, L. Bocquet, and R. R. Netz, "Theory and simulations of water flow through carbon nanotubes: Prospects and pitfalls," J. Phys.: Condens. Matter **23**, 184110 (2011).
[6]M. Gărăjeu, H. Gouin, and G. Saccomandi, "Scaling Navier-Stokes equation in nanotubes," Phys. Fluids **25**, 082003 (2013).
[7]S. Kelly, M. T. Balhoff, and C. Torres-Verdin, "Quantification of bulk solution limits for liquid and interfacial transport in nanoconfinements," Langmuir **31**, 2167–2179 (2015).
[8]T. Werder, J. H. Walter, R. L. Jaffe, T. Halicioglu, and P. Koumoutsakos, "On the watercarbon interaction for use in molecular dynamics simulations of graphite and carbon nanotubes," J. Phys. Chem. B **107**, 1345–1352 (2003).
[9]Y. Nakamura and T. Ohno, "Structure of water confined inside carbon nanotubes and water models," Mater. Chem. Phys. **132**, 682–687 (2012).
[10]A. Alexiadis and S. Kassinos, "Molecular simulation of water in carbon nanotubes," Chem. Rev. **108**, 5014–5034 (2008).
[11]A. Barati Farimani and N. R. Aluru, "Spatial diffusion of water in carbon nanotubes: From Fickian to ballistic motion," J. Phys. Chem. B **115**, 12145–12149 (2011).
[12]R. J. Mashl, S. Joseph, N. R. Aluru, and E. Jakobsson, "Anomalously immobilized water: A new water phase induced by confinement in nanotubes," Nano Lett. **3**, 589–592 (2003).
[13]X. Qin, Q. Yuan, Y. Zhao, S. Xie, and Z. Liu, "Measurement of the rate of water translocation through carbon nanotubes," Nano Lett. **11**, 2173–2177 (2011).
[14]L. L. Huang, L. Z. Zhang, Q. Shao, J. Wang, L. H. Lu, X. H. Lu, and W. F. Shen, "Molecular dynamics simulation study of the structural characteristics of water molecules confined in functionalized carbon nanotubes," J. Phys. Chem. B **110**, 25761–25768 (2006).
[15]J. A. Thomas and A. J. H. McGaughey, "Density, distribution, and orientation of water molecules inside and outside carbon nanotubes," J. Chem. Phys. **128**, 084715 (2008).
[16]J. Shiomi, T. Kimura, and S. Maruyama, "Nanoscale hydrodynamics: Enhanced flow in carbon nanotubes," J. Phys. Chem. C **111**, 12188–12193 (2007).
[17]E. M. Kotsalis, J. H. Walther, and P. Koumoutsakos, "Multiphase water flow inside carbon nanotubes," Int. J. Multiphase Flow **30**, 995–1010 (2004).
[18]M. C. Gordillo and J. Martí, "Hydrogen bonding in supercritical water confined in carbon nanotubes," Chem. Phys. Lett. **341**, 250–254 (2001).
[19]K. Koga, G. T. Gao, H. Tanaka, and X. C. Zeng, "Formation of ordered ice nanotubes inside carbon nanotubes," Nature **412**, 802–805 (2001).
[20]X. Gao, T. Zhao, and Z. Li, "Fluid breakup in carbon nanotubes: An explanation of ultrafast ion transport," Phys. Fluids **29**, 092003 (2017).
[21]J. K. Holt, H. G. Park, Y. Wang, M. Stadermann, A. B. Artyukhin, C. P. Grigoropoulos, A. Noy, and O. Bakajin, "Fast mass transport through sub-2-nanometer carbon nanotubes," Science **312**, 1034–1037 (2006).
[22]M. Whitby, L. Cagnon, M. Thanou, and N. Quirke, "Enhanced fluid flow through nanoscale carbon pipes," Nano Lett. **8**, 2632–2637 (2008).
[23]S. K. Kannam, B. D. Todd, J. S. Hansen, and P. J. Daivis, "How fast does water flow in carbon nanotubes?," J. Chem. Phys. **138**, 094701 (2013).
[24]K. Ritos, D. Mattia, F. Calabrò, and J. M. Reese, "Flow enhancement in nanotubes of different materials and lengths," J. Chem. Phys. **140**, 014702 (2014).
[25]S. I. Nakao, "Determination of pore size and pore size distribution: 3. Filtration membranes," J. Membr. Sci. **96**, 131–165 (1994).
[26]H. G. L. Coster, K. J. Kim, K. Dahlan, J. R. Smith, and C. J. D. Fell, "Characterisation of ultrafiltration membranes by impedance spectroscopy. I. Determination of the separate electrical parameters and porosity of the skin and sublayers," J. Membr. Sci. **66**, 19–26 (1992).
[27]T. Werder, J. H. Walther, R. L. Jaffe, T. Halicioglu, F. Noca, and P. Koumoutsakos, "Molecular dynamics simulation of contact angles of water droplets in carbon nanotubes," Nano Lett. **1**, 697–702 (2001).
[28]A. Krishnan, E. Dujardin, T. W. Ebbesen, P. N. Yianilos, and M. M. J. Treacy, "Young's modulus of single-walled nanotubes," Phys. Rev. B **58**, 14013 (1998).
[29]H. Gouin, "Statics and dynamics of fluids in nanotubes," Note Mat. **32**, 105–124 (2012).
[30]B. J. Kirby, *Micro- and Nanoscale Fluid Mechanics: Transport in Microfluidic Devices* (Cambridge University Press, Cambridge, 2010).
[31]K. M. Mohamed and A. A. Mohamad, "A review of the development of hybrid atomistic-continuum methods for dense fluids," Microfluid. Nanofluid. **8**, 283–302 (2010).
[32]G. Hu and D. Li, "Multiscale phenomena in microfluidics and nanofluidics," Chem. Eng. Sci. **62**, 3443–3454 (2007).
[33]R. S. Ruoff, D. Quian, and W. K. Liu, "Mechanical properties of carbon nanotubes: Theoretical predictions and experimental measurements," C. R. Phys. **4**, 993–1008 (2003).
[34]J. P. Lu, "Elastic properties of carbon nanotubes and nanoropes," Phys. Rev. Lett. **79**, 1297 (1997).
[35]L. Wang and Q. Ni, "On vibration and instability of carbon nanotubes conveying fluid," Comput. Mater. Sci. **43**, 399–402 (2008).
[36]Y. Yan, X. Q. He, L. X. Zhang, and C. M. Wang, "Dynamic behavior of triple-walled carbon nanotubes conveying fluid," J. Sound Vib. **319**, 1003–1018 (2009).
[37]L. Wang, Q. Ni, and M. Li, "Buckling instability of double-wall carbon nanotubes conveying fluid," Comput. Mater. Sci. **44**, 821–825 (2008).
[38]Y. Yan, X. Q. He, L. X. Zhang, and Q. Wang, "Flow-induced instability of double-walled carbon nanotubes based on an elastic shell model," J. Appl. Phys. **102**, 044307 (2007).
[39]B. Arash and Q. Wang, "A review on the application of nonlocal elastic models in modeling of carbon nanotubes and graphenes," Comput. Mater. Sci. **51**, 303–313 (2012).
[40]L. Wang, "A modified nonlocal beam model for vibration and stability of nanotubes conveying fluid," Physica E **44**, 25–28 (2011).
[41]S. S. Chen, *Flow-Induced Vibration of Circular Cylindrical Structures* (Argonne National Laboratory, Argonne, 1985).
[42]J. Cao, Q. Wang, and H. Dai, "Electromechanical properties of metallic, quasimetallic, and semiconducting carbon nanotubes under stretching," Phys. Rev. Lett. **90**, 157601 (2003).
[43]B. Mahar, C. Laslau, R. Yip, and Y. Sun, "Development of carbon nanotube-based sensors—A review," IEEE Sens. J. **7**, 266–284 (2007).

[44]N. C. Nguyen and J. Peraire, "Hybridizable discontinuous Galerkin methods for partial differential equations in continuum mechanics," J. Comput. Phys. **231**, 5955–5988 (2012).
[45]O. C. Zienkiewicz and R. L. Taylor, *The Finite Element Method for Solid and Structural Mechanics* (Elsevier, Oxford, 2005).
[46]M. F. Yu, O. Lourie, M. J. Dyer, K. Moloni, T. F. Kelly, and R. S. Ruoff, "Strength and breaking mechanism of multiwalled carbon nanotubes under tensile load," Science **287**, 637–640 (2000).
[47]M. F. Yu, B. S. Files, S. Arepalli, and R. S. Ruoff, "Tensile loading of ropes of single wall carbon nanotubes and their mechanical properties," Phys. Rev. Lett. **84**, 5552 (2000).
[48]J. P. Salvetat, G. A. D. Briggs, J. M. Bonard, R. R. Bacsa, A. J. Kulik, T. Stöckli, N. A. Burnham, and L. Forró, "Elastic and shear moduli of single-walled carbon nanotube ropes," Phys. Rev. Lett. **82**, 944 (1999).
[49]B. Bhushan, *Nanotribology and Nanomechanics* (Springer, Cham, 2017).
[50]H. J. Butt, B. Capella, and M. Kappl, "Force measurements with the atomic force microscope: Technique, interpretation and applications," Surf. Sci. Rep. **59**, 1–152 (2005).
[51]R. He, X. L. Feng, M. L. Roukes, and P. Yang, "Self-transducing silicon nanowire electromechanical systems at room temperature," Nano Lett. **8**, 1756–1761 (2008).
[52]M. Li, H. X. Tang, and M. L. Roukes, "Ultra-sensitive NEMS-based cantilevers for sensing, scanned probe and very high-frequency applications," Nat. Nanotechnol. **2**, 114 (2007).
[53]K. L. Ekinci, Y. T. Yang, X. M. H. Huang, and M. L. Roukes, "Balanced electronic detection of displacement in nanoelectromechanical systems," Appl. Phys. Lett. **81**, 2253–2255 (2002).
[54]G. Betta, C. Liguori, and A. Pietrosanto, "Propagation of uncertainty in a discrete Fourier transform algorithm," Measurement **27**, 231–239 (2000).
[55]M. H. Montgomery and D. Odonoghue, "A derivation of the errors for least squares fitting to time series data," Delta Scuti Star Newsl. **13**, 28 (1999).
[56]H. W. Postma, A. Sellmeijer, and C. Dekker, "Manipulation and imaging of individual single-walled carbon nanotubes with an atomic force microscope," Adv. Mater. **12**, 1299–1302 (2000).
[57]A. Nordenfelt, "Selective self-excitation of higher vibrational modes of graphene nano-ribbons and carbon nanotubes through magnetomotive instability," J. Comput. Nonlinear Dyn. **8**, 011011 (2013).
[58]A. Nordenfelt, Y. A. Tarakanov, L. Y. Gorelik, R. I. Shekhter, and M. Jonson, "Magnetomotive instability and generation of mechanical vibrations in suspended semiconducting carbon nanotubes," New J. Phys. **12**, 123013 (2010).
[59]M. Ayub, A. C. Zander, C. Q. Howard, B. S. Cazzolato, V. N. Shanov, N. T. Alvarez, and D. M. Huang, "Acoustic absorption behavior of carbon nanotube arrays," in *43rd International Congress on Noise Control Engineering (Inter Noise 2014)* (The Australian Acoustic Society, Melbourne, Australia, 2014), Vol. 249, pp. 929–938.
[60]M. Ayub, A. C. Zander, C. Q. Howard, B. S. Cazzolato, D. M. Huang, N. T. Alvarez, and V. N. Shanov, "Acoustic absorption behaviour of a tall carbon nanotube forest," in *Proceedings of Acoustics 2016* (The Australian Acoustical Society, Brisbane, Australia, 2016), pp. 1–10.
[61]M. Ayub, A. Zander, C. Howard, B. Cazzolato, D. Huang, V. Shanov, and N. Alvarez, "Normal incidence acoustic absorption characteristics of a carbon nanotube forest," Appl. Acoust. **127**, 223–229 (2017).
[62]M. Ayub, A. C. Zander, D. M. Huang, C. Q. Howard, and B. S. Cazzolato, "Molecular dynamics simulations of acoustic absorption by a carbon nanotube," Phys. Fluids **30**, 066101 (2018).
[63]A. Bachtold, P. Hadley, T. Nakanishi, and C. Dekker, "Logic circuits with carbon nanotube transistors," Science **294**, 1317–1320 (2001).
[64]D. M. Sun, C. Liu, W. C. Ren, and H. M. Cheng, "A review of carbon nanotube- and graphene-based flexible thin-film transistors," Small **9**, 1188–1205 (2013).
[65]J. Svenson, Y. Tarakanov, D. Lee, J. M. Kinaret, Y. Park, and E. E. Campbell, "A carbon nanotube gated carbon nanotube transistor with 5 ps gate delay," Nanotechnology **19**, 325201 (2008).
[66]J. Svensson, N. Lindahl, H. Yun, M. Seo, D. Midvedt, Y. Tarakanov, N. Lindvall, O. Nerushev, J. Kinaret, S. Lee, and E. E. Campbell, "Carbon nanotube field effect transistors with suspended graphene gates," Nano Lett. **11**, 3569–3575 (2011).
[67]Y. A. Tarakanov and J. M. Kinaret, "A carbon nanotube field effect transistor with a suspended nanotube gate," Nano Lett. **7**, 2291–2294 (2007).
[68]D. Ramos, E. Gil-Santos, O. Malvar, J. M. Llorens, V. Pini, A. San Paulo, and J. Tamayo, "Silicon nanowires: Where mechanics and optics meet at the nanoscale," Sci. Rep. **3**, 3445 (2013).
[69]M. R. Foreman, J. D. Swaim, and F. Volmer, "Whispering gallery mode sensors," Adv. Opt. Photonics **7**, 168–240 (2015).
[70]S. R. Manalis, S. C. Minne, A. Atalar, and C. F. Quate, "Nanoscale hydrodynamics: Enhanced flow in carbon nanotubes," Appl. Phys. Lett. **69**, 3944–3946 (1996).
[71]C. A. Savran, A. W. Sparks, J. Sihler, J. Li, W. C. Wu, D. E. Berlin, T. P. Burg, J. Fritz, M. A. Schmid, and S. R. Manalis, "Fabrication and characterization of a micromechanical sensor for differential detection of nanoscale motions," J. Microelectromech. Syst. **11**, 703–708 (2002).
[72]D. J. Müller and Y. F. Dufrene, "Atomic force microscopy as a multifunctional molecular toolbox in nanobiotechnology," Nat. Nanotechnol. **3**, 261–269 (2008).
[73]P. Hinterdorfer and Y. F. Dufrêne, "Detection and localization of single molecular recognition events using atomic force microscopy," Nat. Methods **3**, 347–355 (2006).
[74]M. Stark, R. W. Stark, W. M. Heckl, and R. Guckenberger "Inverting dynamic force microscopy: From signals to time-resolved interaction forces," Proc. Natl. Acad. Sci. U. S. A. **99**, 8473–8478 (2002).
[75]O. Sahin, S. Magonov, C. Su, C. F. Quate, and O. Solgaard, "An atomic force microscope tip designed to measure time-varying nanomechanical forces," Nat. Nanotechnol. **2**, 507–514 (2007).
[76]A. D. L. Humphris, M. J. Miles, and J. K. Hobbs, "A mechanical microscope: High-speed atomic force microscopy," Appl. Phys. Lett. **86**, 034106 (2005).
[77]T. Kallinger, P. Reegen, and W. W. Weiss, "A heuristic derivation of the uncertainty for frequency determination in time series data," Astron. Astrophys. **481**, 571–574 (2008).
[78]By using a single frequency measurement, it would be necessary to account for the uncertainty in the characteristic flow velocity shown in Eq. (2), which implies to account for the high uncertainty involved in the determination of the Young modulus. In turn, a two-frequency measurement scheme has a much smaller flow magnitude uncertainty.

An analytical framework to determine flow velocities within nanotubes from their vibration frequencies -Supplementary material-

U. Torres-Herrera and E. Corvera Poiré

A. EXPRESSIONS OF THE DETERMINANT FOR THE DIFFERENT SETS OF BOUNDARY CONDITIONS

For each set of boundary conditions considered in this work, the expression for the determinant is shown below. It is important to recall that k_1, k_2, k_3 and k_4 are functions of ω and α as stated in Eq.(10) of the main article.

- Pinned-pinned

$$D_{PP} = \begin{vmatrix} 1 & 1 & 1 & 1 \\ -k_1^2 & -k_2^2 & -k_3^2 & -k_4^2 \\ e^{ik_1} & e^{ik_2} & e^{ik_3} & e^{ik_4} \\ -k_1^2 e^{ik_1} & -k_2^2 e^{ik_2} & -k_3^2 e^{ik_3} & -k_4^2 e^{ik_4} \end{vmatrix} \tag{A.1}$$

- Clamped-clamped

$$D_{CC} = \begin{vmatrix} 1 & 1 & 1 & 1 \\ ik_1 & ik_2 & ik_3 & ik_4 \\ e^{ik_1} & e^{ik_2} & e^{ik_3} & e^{ik_4} \\ ik_1 e^{ik_1} & ik_2 e^{ik_2} & ik_3 e^{ik_3} & ik_4 e^{ik_4} \end{vmatrix} \tag{A.2}$$

- Free-free

$$D_{FF} = \begin{vmatrix} -k_1^2 & -k_2^2 & -k_3^2 & -k_4^2 \\ -ik_1^3 & -ik_2^3 & -ik_3^3 & -ik_4^3 \\ -k_1^2 e^{ik_1} & -k_2^2 e^{ik_2} & -k_3^2 e^{ik_3} & -k_4^2 e^{ik_4} \\ -ik_1^3 e^{ik_1} & -ik_2^3 e^{ik_2} & -ik_3^3 e^{ik_3} & -ik_4^3 e^{ik_4} \end{vmatrix} \tag{A.3}$$

- Pinned-clamped

$$D_{PC} = \begin{vmatrix} 1 & 1 & 1 & 1 \\ ik_1 & ik_2 & ik_3 & ik_4 \\ e^{ik_1} & e^{ik_2} & e^{ik_3} & e^{ik_4} \\ -k_1^2 e^{ik_1} & -k_2^2 e^{ik_2} & -k_3^2 e^{ik_3} & -k_4^2 e^{ik_4} \end{vmatrix} \tag{A.4}$$

- Pinned-free

$$D_{FP} = \begin{vmatrix} 1 & 1 & 1 & 1 \\ -k_1^2 & -k_2^2 & -k_3^2 & -k_4^2 \\ -k_1^2 e^{ik_1} & -k_2^2 e^{ik_2} & -k_3^2 e^{ik_3} & -k_4^2 e^{ik_4} \\ -ik_1^3 e^{ik_1} & -ik_2^3 e^{ik_2} & -ik_3^3 e^{ik_3} & -ik_4^3 e^{ik_4} \end{vmatrix} \tag{A.5}$$

- Clamped-free

$$D_{FC} = \begin{vmatrix} 1 & 1 & 1 & 1 \\ ik_1 & ik_2 & ik_3 & ik_4 \\ -k_1^2 e^{ik_1} & -k_2^2 e^{ik_2} & -k_3^2 e^{ik_3} & -k_4^2 e^{ik_4} \\ -ik_1^3 e^{ik_1} & -ik_2^3 e^{ik_2} & -ik_3^3 e^{ik_3} & -ik_4^3 e^{ik_4} \end{vmatrix} \tag{A.6}$$

B. FLOW/FREQUENCY RELATION FOR THE DIFFERENT SETS OF BOUNDARY CONDITIONS

The flow frequency relations of the fundamental mode for the different sets of boundary conditions are given in Fig. 1.

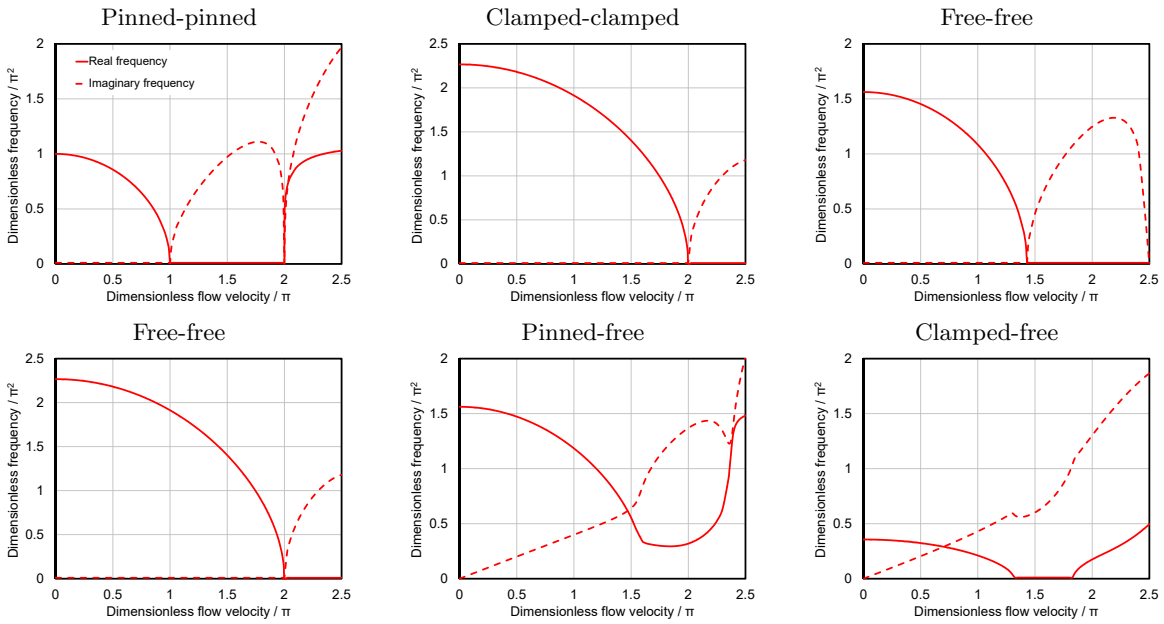

FIG. 1. Effect of flow in the fundamental frequency of the tube oscillations for the different sets of boundary conditions described in this work. Solid lines correspond to the real part of the frequency and dashed lines to its imaginary part. A typical value of the thickness ratio $\alpha = 0.6$ is used in the calculations.

C. DERIVATION OF THE ANALYTICAL EXPRESSIONS FOR FLOW AS A FUNCTION OF FREQUENCY

The expressions of the determinants for the different sets of boundary conditions, as given in Eqs. (A.1)-(A.6) should satisfy:

$$D(v, \alpha, \omega) = 0 \ . \tag{C.1}$$

The second-order Taylor expansion of $D(v, \alpha, \omega)$ around $v = 0$ is given by:

$$D(v, \alpha, \omega)) \approx D\Big|_{v=0} + \frac{\partial D}{\partial v}\Big|_{v=0} v + \frac{1}{2}\frac{\partial^2 D}{\partial v^2}\Big|_{v=0} v^2 \ . \tag{C.2}$$

An explicit expression for v is given by solving the second-order algebraic equation, as:

$$v = \frac{-\frac{\partial D}{\partial v}\big|_{v=0} \pm \sqrt{\left(\frac{\partial D}{\partial v}\big|_{v=0}\right)^2 - 2\frac{\partial^2 D}{\partial v^2}\big|_{v=0} D\big|_{v=0}}}{\frac{\partial^2 D}{\partial v^2}\big|_{v=0}} \ . \tag{C.3}$$

Expressions for the first and second derivatives of the determinant respect to flow evaluated at zero flow are required.

The first derivative of a 4×4 determinant is given by:

$$\frac{\partial D}{\partial v} = \frac{\partial}{\partial v}\begin{vmatrix} d_{11} & d_{21} & d_{31} & d_{41} \\ d_{12} & d_{22} & d_{32} & d_{42} \\ d_{13} & d_{23} & d_{33} & d_{43} \\ d_{14} & d_{24} & d_{34} & d_{44} \end{vmatrix} = \begin{vmatrix} \frac{\partial d_{11}}{\partial v} & d_{21} & d_{31} & d_{41} \\ \frac{\partial d_{12}}{\partial v} & d_{22} & d_{32} & d_{42} \\ \frac{\partial d_{13}}{\partial v} & d_{23} & d_{33} & d_{43} \\ \frac{\partial d_{14}}{\partial v} & d_{24} & d_{34} & d_{44} \end{vmatrix} + \begin{vmatrix} d_{11} & \frac{\partial d_{21}}{\partial v} & d_{31} & d_{41} \\ d_{12} & \frac{\partial d_{22}}{\partial v} & d_{32} & d_{42} \\ d_{13} & \frac{\partial d_{23}}{\partial v} & d_{33} & d_{43} \\ d_{14} & \frac{\partial d_{24}}{\partial v} & d_{34} & d_{44} \end{vmatrix}$$
$$+ \begin{vmatrix} d_{11} & d_{21} & \frac{\partial d_{31}}{\partial v} & d_{41} \\ d_{12} & d_{22} & \frac{\partial d_{32}}{\partial v} & d_{42} \\ d_{13} & d_{23} & \frac{\partial d_{33}}{\partial v} & d_{43} \\ d_{14} & d_{24} & \frac{\partial d_{34}}{\partial v} & d_{44} \end{vmatrix} + \begin{vmatrix} d_{11} & d_{21} & d_{31} & \frac{\partial d_{41}}{\partial v} \\ d_{12} & d_{22} & d_{32} & \frac{\partial d_{42}}{\partial v} \\ d_{13} & d_{23} & d_{33} & \frac{\partial d_{43}}{\partial v} \\ d_{14} & d_{24} & d_{34} & \frac{\partial d_{44}}{\partial v} \end{vmatrix}$$

and, subsequently, the second derivative of a determinant is the sum of 16 determinants. This result is applied for all the sets of boundary conditions. The following step is to evaluate such derivatives for a stagnant fluid, $v = 0$. However, it is easier to do the derivative in the 4×4 matrices and afterwards evaluate the determinant of such expressions. This strategy is useful as the analytical expressions of the determinants before evaluation are enormous. The terms involved in these calculations are:

$$k_1\Big|_{v=0} = i\sqrt{\omega}, \quad k_2\Big|_{v=0} = ik_1\Big|_{v=0}, \quad k_3\Big|_{v=0} = -ik_1\Big|_{v=0}, \quad k_4\Big|_{v=0} = -k_1\Big|_{v=0} \tag{C.5}$$

$$\frac{\partial k_2}{\partial v}\Big|_{v=0} = -\frac{\partial k_1}{\partial v}\Big|_{v=0}, \quad \frac{\partial k_3}{\partial v}\Big|_{v=0} = -\frac{\partial k_1}{\partial v}\Big|_{v=0}, \quad \frac{\partial k_4}{\partial v}\Big|_{v=0} = \frac{\partial k_1}{\partial v}\Big|_{v=0},$$
$$\text{where} \quad \frac{\partial k_1}{\partial v}\Big|_{v=0} = \frac{\alpha}{2}, \tag{C.6}$$

$$\frac{\partial^2 k_2}{\partial v^2}\Big|_{v=0} = -i\frac{\partial^2 k_1}{\partial v^2}\Big|_{v=0}, \quad \frac{\partial^2 k_3}{\partial v^2}\Big|_{v=0} = i\frac{\partial^2 k_1}{\partial v^2}\Big|_{v=0}, \quad \frac{\partial^2 k_4}{\partial v^2}\Big|_{v=0} = -\frac{\partial^2 k_1}{\partial v^2}\Big|_{v=0},$$
$$\text{where} \quad \frac{\partial^2 k_1}{\partial v^2}\Big|_{v=0} = \frac{(\alpha^2 - 2)i}{4\sqrt{\omega}}, \tag{C.7}$$

By expressing the Taylor expansion in terms of Eqs. (C.5)-(C.7), it is possible to compute the determinant and its first and second derivatives in order to incorporate them into the Taylor Expansion in Eq. (C.3), and finally, to solve such equation for v, leading to the following expressions:

- Pinned-pinned

$$v_{P-P}(\omega, \alpha) = \sqrt{\frac{A_{PP}}{B_{PP}}} \tag{C.8}$$

where A_{PP} and B_{PP} are given by

$$A_{PP} = 8\omega \sin(\sqrt{\omega}) \sinh(\sqrt{\omega}) \tag{C.9}$$

$$B_{PP} = 4\alpha^2 - \cosh(\sqrt{\omega}) G_{PP} - \sqrt{\omega} \sinh(\sqrt{\omega}) H_{PP} \tag{C.10}$$

and G_{PP} and H_{PP} are given by

$$G_{PP} = 4\alpha^2 \cos(\sqrt{\omega}) + (\alpha^2 - 2)\sqrt{\omega} \sin(\sqrt{\omega}) \tag{C.11}$$

$$H_{PP} = (2 - \alpha^2) \cos(\sqrt{\omega}) \tag{C.12}$$

- Clamped-clamped

$$v_{C-C}(\omega,\alpha)=\sqrt{\frac{A_{CC}}{B_{CC}}} \tag{C.13}$$

where A_{CC} and B_{CC} are given by

$$A_{CC}=8\omega\left(\cos(\sqrt{\omega})\cosh(\sqrt{\omega})-1\right) \tag{C.14}$$

$$\begin{aligned}B_{CC}=&-4\alpha^2\omega+(2-\alpha^2)\sqrt{\omega}\cosh(\sqrt{\omega})\sin(\sqrt{\omega})\\&+\sinh(\sqrt{\omega})\left(\sqrt{\omega}(2-\alpha^2)\cos(\sqrt{\omega})+2(3\alpha^2-2)\sin(\sqrt{\omega})\right)\end{aligned} \tag{C.15}$$

- Free-free

$$v_{FF}(\omega,\alpha)=\sqrt{\frac{A_{FF}}{B_{FF}}} \tag{C.16}$$

where A_{FF} and B_{FF} are given by

$$A_{FF}=8\omega\left(\cos(\sqrt{\omega})\cosh(\sqrt{\omega})-1\right) \tag{C.17}$$

$$\begin{aligned}B_{FF}=&-4\alpha^2\omega+(2-\alpha^2)\sqrt{\omega}\cosh(\sqrt{\omega})\sin(\sqrt{\omega})\\&+\sinh(\sqrt{\omega})\left(\sqrt{\omega}(2-\alpha^2)\cos(\sqrt{\omega})+2(3\alpha^2-2)\sin(\sqrt{\omega})\right)\end{aligned} \tag{C.18}$$

- Pinned-clamped

$$v_{PC}(\omega,\alpha)=\sqrt{\frac{A_{PC}}{B_{PC}}} \tag{C.19}$$

where A_{PC} and B_{PC} are given by

$$A_{PC}=(4+4i)\omega\left(\sin((1+i)\sqrt{\omega})-\sinh((1+i)\sqrt{\omega})\right) \tag{C.20}$$

$$\begin{aligned}B_{PC}=&8\alpha^2\sqrt{\omega}+(2-5\alpha^2)\cos(\sqrt{\omega})\sinh(\sqrt{\omega})\\&+\cosh(\sqrt{\omega})\left(2\sqrt{\omega}(\alpha^2-2)\cos(\sqrt{\omega})+(2-5\alpha^2)\sin(\sqrt{\omega})\right)\end{aligned} \tag{C.21}$$

- Pinned-free

$$v_{PF}(\omega,\alpha)=\frac{8i\alpha\sqrt{\omega}\sin(\sqrt{\omega})\sinh(\sqrt{\omega})-\sqrt{-4(1+i)\omega A_{PF}}}{B_{PF}} \tag{C.22}$$

where A_{PF} and B_{PF} are given by

$$A_{PF}=8(1-i)\alpha^2 sin^2(\sqrt{\omega})sinh^2(\sqrt{\omega})+G_{PF}H_{PF} \tag{C.23}$$

$$\begin{aligned}B_{PF}=&-8\alpha^2\sqrt{\omega}+(2+3\alpha^2)\cos(\sqrt{\omega})\sinh(\sqrt{\omega})\\&+\cosh(\sqrt{\omega})\left(2(\alpha^2-2)\sqrt{\omega}\cos(\sqrt{\omega})+(2+3\alpha^2)\sin(\sqrt{\omega})\right)\end{aligned} \tag{C.24}$$

where G_{PF} and H_{PF} are given by

$$G_{PF}=\sin((1+i)\sqrt{\omega})-\sinh((1+i)\sqrt{\omega}) \tag{C.25}$$

$$\begin{aligned}H_{PF}=&8\alpha^2\sqrt{\omega}-(2+3\alpha^2)\cos(\sqrt{\omega})\sinh(\sqrt{\omega})\\&-\cosh(\sqrt{\omega})\left(2(\alpha^2-2)\sqrt{\omega}\cos(\sqrt{\omega})+(2+3\alpha^2)\sin(\sqrt{\omega})\right)\end{aligned} \tag{C.26}$$

- Clamped-free

$$v_{CF}(\omega,\alpha)=\frac{2\alpha\sqrt{\omega}(1-i)\left(\sin((1+i)\sqrt{\omega})-\sinh((1+i)\sqrt{\omega})\right)-\sqrt{-8\omega A_{CF}}}{B_{CF}} \tag{C.27}$$

where A_{CF} and B_{CF} are given by

$$\begin{aligned}A_{CF}=&i\alpha^2\left(\sin((1+i)\sqrt{\omega})-\sinh((1+i)\sqrt{\omega})\right)^2\\&-(\cos(\sqrt{\omega})\cosh(\sqrt{\omega})+1)G_{CF}\end{aligned} \tag{C.28}$$

$$\begin{aligned}B_{CF}=&4\alpha^2\omega+(2-\alpha^2)\sqrt{\omega}\cosh(\sqrt{\omega})\sin(\sqrt{\omega})\\&+\left((2-\alpha^2)\sqrt{\omega}\cos(\sqrt{\omega})-2(\alpha^2+2)\sin(\sqrt{\omega})\right)\sinh(\sqrt{\omega})\end{aligned} \tag{C.29}$$

where G_{CF} is given by

$$\begin{aligned}G_{CF}=&4\alpha^2\omega+(2-\alpha^2)\sqrt{\omega}\cosh(\sqrt{\omega})\sin(\sqrt{\omega})\\&-\left((\alpha^2-2)\sqrt{\omega}\cos(\sqrt{\omega})+2(2+\alpha^2)\sin(\sqrt{\omega})\right)\sinh(\sqrt{\omega})\end{aligned} \tag{C.30}$$

These expressions are given for a second-order expansion around zero flow and, therefore, are accurate for low flow velocities. In order to numerically determine the range of accuracy of the approximations, it is necessary to compare the exact numerical solution of the flow-frequency relation for each set of boundary conditions, with the analytical approximated results.

To obtain flow-frequency relations for low and medium flows, higher-order Taylor expansions are necessary. High order derivatives of k_1, k_2, k_3, k_4 are given by

$$\left.\frac{\partial^3 k_1}{\partial v^3}\right|_{v=0}=0,\quad \left.\frac{\partial^3 k_2}{\partial v^3}\right|_{v=0}=0,\quad \left.\frac{\partial^3 k_3}{\partial v^3}\right|_{v=0}=0,\quad \left.\frac{\partial^3 k_4}{\partial v^3}\right|_{v=0}=0 \tag{C.31}$$

$$\begin{aligned}&\left.\frac{\partial^4 k_2}{\partial v^4}\right|_{v=0}=i\left.\frac{\partial^4 k_1}{\partial v^4}\right|_{v=0},\quad \left.\frac{\partial^4 k_3}{\partial v^4}\right|_{v=0}=-i\left.\frac{\partial^4 k_1}{\partial v^4}\right|_{v=0},\quad \left.\frac{\partial^4 k_4}{\partial v^4}\right|_{v=0}=-\left.\frac{\partial^4 k_1}{\partial v^4}\right|_{v=0},\\&\text{where}\quad \left.\frac{\partial^4 k_1}{\partial v^4}\right|_{v=0}=\frac{3i(7\alpha^4-12\alpha^2+4)}{16\omega^{\frac{3}{2}}},\end{aligned} \tag{C.32}$$

$$\begin{aligned}&\left.\frac{\partial^5 k_2}{\partial v^5}\right|_{v=0}=-\left.\frac{\partial^5 k_1}{\partial v^5}\right|_{v=0},\quad \left.\frac{\partial^5 k_3}{\partial v^5}\right|_{v=0}=-\left.\frac{\partial^5 k_1}{\partial v^5}\right|_{v=0},\quad \left.\frac{\partial^5 k_4}{\partial v^5}\right|_{v=0}=\left.\frac{\partial^5 k_1}{\partial v^5}\right|_{v=0},\\&\text{where}\quad \left.\frac{\partial^5 k_1}{\partial v^5}\right|_{v=0}=-\frac{15\alpha(\alpha^2-1)^2}{2\omega^2},\end{aligned} \tag{C.33}$$

$$\begin{aligned}&\left.\frac{\partial^6 k_2}{\partial v^6}\right|_{v=0}=-i\left.\frac{\partial^6 k_1}{\partial v^6}\right|_{v=0},\quad \left.\frac{\partial^6 k_3}{\partial v^6}\right|_{v=0}=i\left.\frac{\partial^6 k_1}{\partial v^6}\right|_{v=0},\quad \left.\frac{\partial^6 k_4}{\partial v^6}\right|_{v=0}=-\left.\frac{\partial^6 k_1}{\partial v^6}\right|_{v=0},\\&\text{where}\quad \left.\frac{\partial^6 k_1}{\partial v^6}\right|_{v=0}=-\frac{45i(39\alpha^6-90\alpha^4+60\alpha^2-8)}{64\omega^{\frac{5}{2}}},\end{aligned} \tag{C.34}$$

$$\left.\frac{\partial^7 k_1}{\partial v^7}\right|_{v=0}=0,\quad \left.\frac{\partial^7 k_2}{\partial v^7}\right|_{v=0}=0,\quad \left.\frac{\partial^7 k_3}{\partial v^7}\right|_{v=0}=0,\quad \left.\frac{\partial^7 k_4}{\partial v^7}\right|_{v=0}=0 \tag{C.35}$$

$$\begin{aligned}&\left.\frac{\partial^8 k_2}{\partial v^8}\right|_{v=0}=i\left.\frac{\partial^8 k_1}{\partial v^8}\right|_{v=0},\quad \left.\frac{\partial^8 k_3}{\partial v^8}\right|_{v=0}=-i\left.\frac{\partial^8 k_1}{\partial v^8}\right|_{v=0},\left.\frac{\partial^8 k_4}{\partial v^8}\right|_{v=0}=-\left.\frac{\partial^8 k_1}{\partial v^8}\right|_{v=0},\\&\text{where}\quad \left.\frac{\partial^8 k_1}{\partial v^8}\right|_{v=0}=-\frac{1575i(209\alpha^8-616\alpha^6+616\alpha^4-224\alpha^2+16)}{256\omega^{\frac{7}{2}}},\end{aligned} \tag{C.36}$$

Expressions in Eqs. (C.31)-(C.36) are incorporated into the derivatives of the determinants of Eqs. (A.1)-(A.6), in order to obtain the Taylor coefficients of the expansion and, subsequently, solve such truncated polynomials for the flow velocity.

As mentioned in the main manuscript, odd-order derivatives of the determinants are zero for the pinned-pinned, clamped-clamped, pinned-clamped and free-free cases. As a consequence, it is possible to obtain algebraic equations for the square of the flow magnitude, v^2, up to the 4^{th} truncation order. The solution for the flow velocity for each truncation order -where the notation $A_n = \frac{1}{n!}\frac{\partial^n D}{\partial v^n}$ is used- is given by

- First-order truncation

$$v^2 = -\frac{A_0}{A_2} \tag{C.37}$$

- Second-order truncation

$$v^2 = \frac{-A_2 + \sqrt{A_2^2 - 4A_0A_4}}{2A_4} \tag{C.38}$$

- Third-order truncation

$$v^2 = -\frac{A_4}{3A_6} + \frac{(1-i\sqrt{3})(3A_2A_6 - A_4^2)}{3(2^{\frac{2}{3}})A_6Q^{\frac{1}{3}}} - \frac{1+i\sqrt{3}}{6(2^{\frac{1}{3}})A_6}Q^{\frac{1}{3}} \tag{C.39}$$

with

$$\begin{aligned} Q =& -2A_4^3 + 9A_2A_4A_6 - 27A_0A_6^2 \\ &+\sqrt{4\left(3A_2A_6 - A_4^2\right)^3 + \left(-2A_4^3 + 9A_2A_4A_6 - 27A_0A_6^2\right)^2} \end{aligned} \tag{C.40}$$

- Fourth-order truncation

$$\begin{aligned} v^2 =& -\frac{A_6}{4A_8} + \frac{1}{2}\sqrt{\frac{A_6^2}{4A_8^2} - \frac{2A_4}{3A_8} + R} \\ &-\frac{1}{2}\sqrt{\frac{A_6^2}{2A_8^2} - \frac{4A_4}{3A_8} - R + \frac{-\frac{A_6^3}{A_8^3} + \frac{4A_4A_6}{A_8^2} - \frac{8A_2}{A_8}}{4\sqrt{\frac{A_6^2}{4A_8^2} - \frac{2A_4}{3A_8} + R}}} \end{aligned} \tag{C.41}$$

where

$$R = \frac{2^{\frac{1}{3}}(A_4^2 - 3A_2A_6 + 12A_0A_8)}{3A_8S^{\frac{1}{3}}} + \frac{S^{\frac{1}{3}}}{3(2^{\frac{1}{3}})A_8} \tag{C.42}$$

$$S = 2A_4^3 - 9A_2A_4A_6 + 27A_0A_6^2 + 27A_2^2A_8 - 72A_0A_4A_8 + T \tag{C.43}$$

and T is given by

$$\begin{aligned} T^2 =& \left(2A_4^3 - 9A_2A_4A_6 + 27A_0A_6^2 + 27A_2^2A_8 - 72A_0A_4A_8\right)^2 \\ &-4\left(A_4^2 - 3A_2A_6 + 12A_0A_8\right)^3 \end{aligned} \tag{C.44}$$

TABLE I. Example of the computation of more than one solution for v^2 for the algebraic equation obtained with the 8th truncation order for a pinned-pinned tube. The physical solution is printed in bold characters

Frequency	First solution	Second solution	Third Solution	Fourth solution
0.8573	-6.8265	**0.25002**	2.0434-0.9894i	2.0434+0.9894i
3.8829	-31.8472	**0.24999**	4.5815-2.5189i	4.5815+2.5189i
8.8889	-66.6262	**0.24999**	6.8837-3.8981i	6.8837+3.8981i
15.8918	-108.7703	**0.24999**	9.2119-5.2630i	9.2119+5.2630i

For pinned-free and clamped-free cases, all derivatives are non-zero and therefore, it is only possible to obtain analytical solutions for v (not for v^2) up to 4th truncation order, leading to completely analogous expressions to Eqs. (C.37)-(C.41), when replacing the left hand side (v^2) in Eqs. (C.37)-(C.41) by v and doing the following replacements in the right side of the equations: $A_2 \to A_1$, $A_4 \to A_2$, $A_6 \to A_3$ and $A_8 \to A_4$.

A comparison of the error for each truncation level is shown in Fig. 2. The purpose of this one is to choose the most suitable expression according to the range of flows and accuracy required in a specific experiment. In general, for low flow magnitude measurements (about $v < 0.1$), a first or second order-truncated expression might be enough, but for intermediate flows ($0.1 < v < 0.6$) a higher order truncation might be required.

As stated in the main article, the analytical expressions only depend on the boundary conditions and not on the number of the vibration mode. The fact that all the different frequencies ω_n lead to the same flow is illustrated in Fig. 3.

For higher truncation orders, the solution of the algebraic equations lead to more than one solution for v (or v^2). However, the choice of the correct solution is not a problem, since the non-physical solutions lead to complex or non-plausible values. See for example Table I.

D. SIMULATION OF THE TUBE DYNAMICS

In order to simulate the tube dynamics, it is necessary to provide the following information:

- The flow velocity, v.
- The inner and outer tube radii, in order to compute the thickness ratio, α.
- The boundary conditions at the tube edges.
- The vertical displacement and velocity of the tube at a given time (i.e., an initial condition).

When the boundary conditions at the tube edges are known, it is possible to incorporate them in the general solution (Eq. (10) of the main article). From this, an algebraic system of 4 equations for the coefficients C_1, C_2, C_3, C_4 is obtained. This strategy, in principle, would allow one to obtain the values of all the coefficients. However, the system of equations produced by the boundary conditions is homogeneous and, therefore, it leads to the trivial solution $C_1 = C_2 = C_3 = C_4 = 0$. In order to obtain a non-trivial solution, it is necessary that the determinant of the matrix of coefficients of the system vanishes (Eq. (17) of the main article). This in turn causes one of the 4 equations for the coefficients, to be a linear combination of the other three, which leaves one of the coefficients as a free parameter, for instance C_1, and the others coefficients as functions of this one.

When the fluid velocity and thickness ratio are known, it is possible to incorporate them into Eq. (17) of the main article. Such equation turns out to be an algebraic equation for the frequency, ω. Moreover, the solution of Eq. (17) leads to an infinite set of discretized values of ω, denoted by ω_n, where n is an integer number. Because of the complexity of this equation, the solution, in general, is given via numerical methods to solve algebraic equations. For the purpose of this work, the Newton-Raphson method was used within Wolfram Mathematica utilities.

Each one of the discretized frequencies, ω_n, is related to a given vibration mode. Therefore, when all the vibration modes are known, it is possible to express any solution of the tube dynamics as a linear

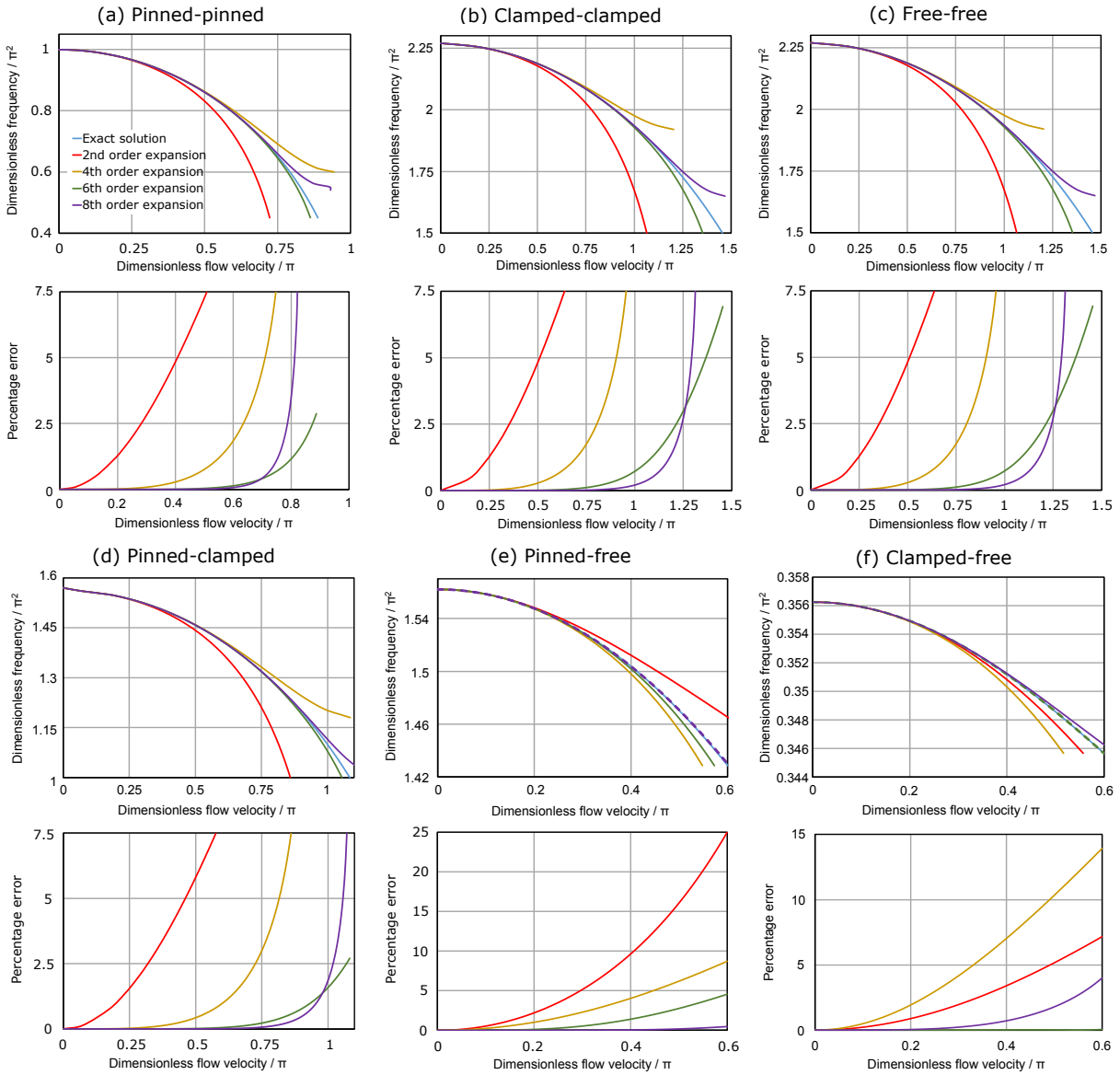

FIG. 2. Comparison between approximated analytical expressions and the exact numerical relation for flow and frequency. As expected, incorporation of more terms in the Taylor expansion leads to an increase in the accuracy and flow range of applicability of the analytical expressions. However, in the pinned-free and clamped-free cases, there is an alternating degree of precision with the order of truncation of the Taylor expansion. This is not an issue for the purpose of this treatment, since all the analytical expressions approximate very well the exact results obtained by numerical means. A typical value of the thickness ratio $\alpha = 0.6$ is used in the calculations.

combination of all the vibration modes. The coefficients of such combination are given by the initial conditions of the tube. This constitutes the general outline of the simulation of the tube dynamics.

A possible solution, considering C_1 as a the free parameter, is given below for the different sets of boundary conditions. It is necessary to recall that k_1, k_2, k_3 and k_4 are given by the Eq. (11) of the main article, and depend on ω_n.

- Pinned-pinned

$$C_2 = -C_1 \frac{\left(e^{ik_3} - e^{ik_4}\right)\left(k_1^2 - k_4^2\right) - \left(e^{ik_1} - e^{ik_4}\right)\left(k_3^2 - k_4^2\right)}{\left(e^{ik_3} - e^{ik_4}\right)\left(k_2^2 - k_4^2\right) - \left(e^{ik_2} - e^{ik_4}\right)\left(k_3^2 - k_4^2\right)} \tag{D.1}$$

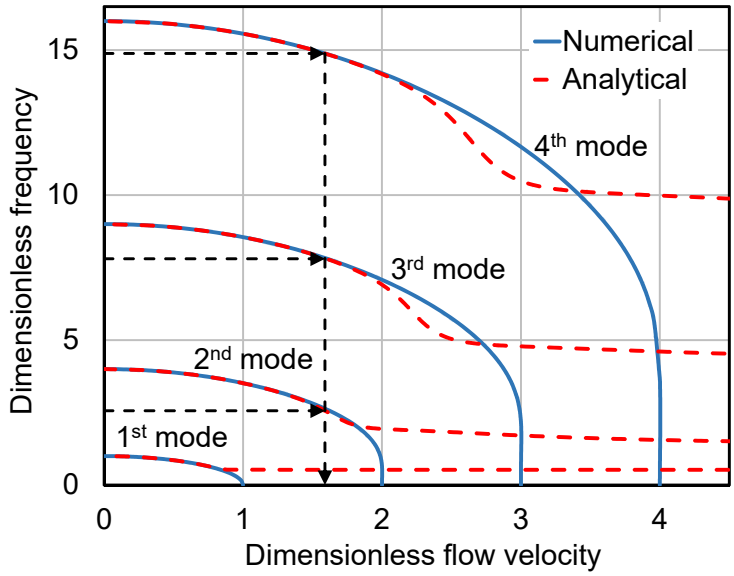

FIG. 3. Comparison between the analytical expression of the 8th truncation order and the exact numerical relation for flow and frequency. Two messages are to be taken from this figure. First, a single analytical expression is capable to approximate for the flow/frequency relation for each of the vibration modes. Second, the range in which the analytical solution is valid is wider for high-order vibration modes.

$$C_3 = C_1 \frac{e^{ik_4}\left(k_2^2 - k_1^2\right) + e^{ik_2}\left(k_1^2 - k_4^2\right) + e^{ik_1}\left(k_4^2 - k_2^2\right)}{e^{ik_4}\left(k_3^2 - k_2^2\right) + e^{ik_3}\left(k_2^2 - k_4^2\right) + e^{ik_2}\left(k_4^2 - k_3^2\right)} \tag{D.2}$$

$$C_4 = C_1 \frac{e^{ik_3}\left(k_2^2 - k_1^2\right) + e^{ik_2}\left(k_1^2 - k_3^2\right) + e^{ik_1}\left(k_3^2 - k_2^2\right)}{e^{ik_4}\left(k_2^2 - k_3^2\right) + e^{ik_2}\left(k_3^2 - k_4^2\right) + e^{ik_3}\left(k_4^2 - k_2^2\right)} \tag{D.3}$$

- Clamped-clamped

$$C_2 = C_1 \frac{e^{ik_4}\left(k_3 - k_1\right) + e^{ik_3}\left(k_1 - k_4\right) + e^{ik_1}\left(k_4 - k_3\right)}{e^{ik_4}\left(k_2 - k_3\right) + e^{ik_2}\left(k_3 - k_4\right) + e^{ik_3}\left(k_4 - k_2\right)} \tag{D.4}$$

$$C_3 = C_1 \frac{e^{ik_4}\left(k_2 - k_1\right) + e^{ik_2}\left(k_1 - k_4\right) + e^{ik_1}\left(k_4 - k_2\right)}{e^{ik_4}\left(k_3 - k_2\right) + e^{ik_3}\left(k_2 - k_4\right) + e^{ik_2}\left(k_4 - k_3\right)} \tag{D.5}$$

$$C_4 = C_1 \frac{e^{ik_3}\left(k_2 - k_1\right) + e^{ik_2}\left(k_1 - k_3\right) + e^{ik_1}\left(k_3 - k_2\right)}{e^{ik_4}\left(k_2 - k_3\right) + e^{ik_2}\left(k_3 - k_4\right) + e^{ik_3}\left(k_4 - k_2\right)} \tag{D.6}$$

- Pinned-clamped

$$C_2 = -C_1 \frac{\left(e^{ik_3} - e^{ik_4}\right)\left(k_1^2 - k_4^2\right) - \left(e^{ik_1} - e^{ik_4}\right)\left(k_3^2 - k_4^2\right)}{\left(e^{ik_3} - e^{ik_4}\right)\left(k_2^2 - k_4^2\right) - \left(e^{ik_2} - e^{ik_4}\right)\left(k_3^2 - k_4^2\right)} \tag{D.7}$$

$$C_3 = C_1 \frac{e^{ik_4}\left(k_2^2 - k_1^2\right) + e^{ik_2}\left(k_1^2 - k_4^2\right) + e^{ik_1}\left(k_4^2 - k_2^2\right)}{e^{ik_4}\left(k_3^2 - k_2^2\right) + e^{ik_3}\left(k_2^2 - k_4^2\right) + e^{ik_2}\left(k_4^2 - k_3^2\right)} \tag{D.8}$$

$$C_4 = C_1 \frac{e^{ik_3}\left(k_2^2 - k_1^2\right) + e^{ik_2}\left(k_1^2 - k_3^2\right) + e^{ik_1}\left(k_3^2 - k_2^2\right)}{e^{ik_4}\left(k_2^2 - k_3^2\right) + e^{ik_2}\left(k_3^2 - k_4^2\right) + e^{ik_3}\left(k_4^2 - k_2^2\right)} \tag{D.9}$$

- Free-free

$$C_2 = C_1 \frac{k_1^2}{k_2^2} \frac{e^{ik_4}\left(k_3 - k_1\right) + e^{ik_3}\left(k_1 - k_4\right) + e^{ik_1}\left(k_4 - k_3\right)}{e^{ik_4}\left(k_2 - k_3\right) + e^{ik_2}\left(k_3 - k_4\right) + e^{ik_3}\left(k_4 - k_2\right)} \tag{D.10}$$

$$C_3 = C_1 \frac{k_1^2}{k_3^2} \frac{e^{ik_4}\left(k_2 - k_1\right) + e^{ik_2}\left(k_1 - k_4\right) + e^{ik_1}\left(k_4 - k_2\right)}{e^{ik_4}\left(k_3 - k_2\right) + e^{ik_3}\left(k_2 - k_4\right) + e^{ik_2}\left(k_4 - k_3\right)} \tag{D.11}$$

$$C_4 = C_1 \frac{k_1^2}{k_4^2} \frac{e^{ik_3}\left(k_2 - k_1\right) + e^{ik_2}\left(k_1 - k_3\right) + e^{ik_1}\left(k_3 - k_2\right)}{e^{ik_4}\left(k_2 - k_3\right) + e^{ik_2}\left(k_3 - k_4\right) + e^{ik_3}\left(k_4 - k_2\right)} \tag{D.12}$$

- Pinned-free

$$C_2 = C_1 \frac{e^{ik_4}k_4^2\left(k_1^2 - k_3^2\right) + e^{ik_3}k_3^2\left(k_4^2 - k_1^2\right) + e^{ik_1}k_1^2\left(k_3^2 - k_4^2\right)}{e^{ik_4}k_4^2\left(k_3^2 - k_2^2\right) + e^{ik_3}k_3^2\left(k_2^2 - k_4^2\right) + e^{ik_2}k_2^2\left(k_4^2 - k_3^2\right)} \tag{D.13}$$

$$C_3 = C_1 \frac{e^{ik_4}k_4^2\left(k_1^2 - k_2^2\right) + e^{ik_2}k_2^2\left(k_4^2 - k_1^2\right) + e^{ik_1}k_1^2\left(k_2^2 - k_4^2\right)}{e^{ik_4}k_4^2\left(k_2^2 - k_3^2\right) + e^{ik_3}k_3^2\left(k_4^2 - k_2^2\right) + e^{ik_2}k_2^2\left(k_3^2 - k_4^2\right)} \tag{D.14}$$

$$C_4 = C_1 \frac{e^{ik_3}k_3^2\left(k_1^2 - k_2^2\right) + e^{ik_2}k_2^2\left(k_3^2 - k_1^2\right) + e^{ik_1}k_1^2\left(k_2^2 - k_3^2\right)}{e^{ik_4}k_4^2\left(k_3^2 - k_2^2\right) + e^{ik_3}k_3^2\left(k_2^2 - k_3^2\right) + e^{ik_2}k_2^2\left(k_4^2 - k_3^2\right)} \tag{D.15}$$

- Clamped-free

$$C_2 = C_1 \frac{e^{ik_3}k_3^2\left(k_1 - k_4\right) + e^{ik_1}k_1^2\left(k_4 - k_3\right) + e^{ik_4}k_4^2\left(k_3 - k_1\right)}{e^{ik_3}k_3^2\left(k_4 - k_2\right) + e^{ik_2}k_2^2\left(k_3 - k_4\right) + e^{ik_4}k_4^2\left(k_2 - k_3\right)} \tag{D.16}$$

$$C_3 = C_1 \frac{e^{ik_2}k_2^2\left(k_1 - k_4\right) + e^{ik_1}k_1^2\left(k_4 - k_2\right) + e^{ik_4}k_4^2\left(k_2 - k_1\right)}{e^{ik_3}k_3^2\left(k_2 - k_4\right) + e^{ik_2}k_2^2\left(k_4 - k_3\right) + e^{ik_4}k_4^2\left(k_3 - k_2\right)} \tag{D.17}$$

$$C_4 = C_1 \frac{e^{ik_2}k_2^2\left(k_1 - k_3\right) + e^{ik_1}k_1^2\left(k_3 - k_2\right) + e^{ik_3}k_3^2\left(k_2 - k_1\right)}{e^{ik_3}k_3^2\left(k_4 - k_2\right) + e^{ik_2}k_2^2\left(k_3 - k_4\right) + e^{ik_4}k_4^2\left(k_2 - k_3\right)} \tag{D.18}$$

The expressions for the coefficients C_1, C_2, C_3 and C_4 from Eqs. (D.1)-(D.18) are incorporated into the general solution (Eq. (10) of the main article), to give each of the vibration modes as follows:

$$\phi_n \equiv \hat{u}_n(z, \omega_n) = C_1 e^{ik_1(\omega_n)z} + C_2(\omega_n)e^{ik_2(\omega_n)z} + C_3(\omega_n)e^{ik_3(\omega_n)z} + C_4(\omega_n)e^{ik_4(\omega_n)z} \tag{D.19}$$

these ones are denoted by ϕ_n, and are normalized for the sake of simplicity in the rest of analytical and numerical treatment -this is possible by an adequate choice of the value of C_1-. Each ϕ_n is associated with an ω_n and, in general, are complex functions in the frequency domain.

For didactic purposes, it is worth pointing out that for simple models of elastic materials, such as an elastic string, each normal mode is given by simple expressions like $\sin(n\pi z)$ or $\cos(n\pi z)$. However, the vibration modes for a tube conveying fluid, ϕ_n, are not expressed in such simple terms because of the symmetry breaking produced by the flow direction of the fluid inside the elastic tube.

Eq. (D.19) is only valid for the discretized values of ω_n. In order to do the inverse Fourier transform, it is necessary to extend $\hat{u}_n$ to a continuous domain in ω. This leads to the following expression:

$$\hat{u}_n(z,\omega) = \phi_n(z,\omega)\delta(\omega - \omega_n) \ , \tag{D.20}$$

which in time domain is:

$$u_n(z,t) = \phi_n(z,\omega_n)e^{-i\omega_n t} \ . \tag{D.21}$$

A general solution in time domain is a linear combination of all the normal modes satisfying the given set of boundary conditions,

$$u(z,t) = \sum_{n=-\infty}^{\infty} A_n \phi_n(z,\omega_n)e^{-i\omega_n t} \ . \tag{D.22}$$

Since the equation of the tube motion is a second order differential equation in time, two conditions in time are required. In most of experimental situations, it is possible to establish these conditions as the initial position and velocity of the tube. These conditions are expressed as:

$$u\Big|_{t=0} = g(z) \tag{D.23}$$

$$\frac{\partial u}{\partial t}\Big|_{t=0} = h(z) \tag{D.24}$$

where $g(z)$ corresponds to the position profile and $h(z)$ to the velocity profile of the tube at $t = 0$.

Substituting (D.23) and (D.24) into Eq. (D.22), gives the following expressions for $g(z)$ and $h(z)$ in terms of the normal modes:

$$g(z) = \sum_{n=-\infty}^{\infty} A_n \phi_n(z,\omega_n) \tag{D.25}$$

$$h(z) = -i \sum_{n=-\infty}^{\infty} \omega_n A_n \phi_n(z,\omega_n) \, . \tag{D.26}$$

The coefficients A_n should be found in order to satisfy (D.25) and (D.26). However, this is not a straightforward procedure, because this set of functions is complete but not orthogonal.

In order to overcome this difficulty and obtain the target values A_n, it is necessary to express the functions $g(z)$, $h(z)$ and ϕ_n in terms of an orthogonal set of functions. The choice made in our treatment is the set $\{\sin(n\pi z)\}$, where n is a positive integer number. By considering this, Eqs. (D.25) and (D.26) are rewritten as:

$$\sum_{m=1}^{\infty} g_m \sin(m\pi z) = \sum_{n=-\infty}^{\infty} A_n \sum_{m=1}^{\infty} \alpha_{n,m} \sin(m\pi z) \tag{D.27}$$

$$\sum_{m=1}^{\infty} h_m \sin(m\pi z) = -i \sum_{n=-\infty}^{\infty} \omega_n A_n \sum_{m=1}^{\infty} \alpha_{n,m} \sin(m\pi z) \tag{D.28}$$

where the coefficients of each Fourier series are given by

$$g_m = 2\int_{z=0}^{z=1} g(z)\sin(m\pi z)\,dz \tag{D.29}$$

$$h_m = 2\int_{z=0}^{z=1} h(z)\sin(m\pi z)\,dz \tag{D.30}$$

$$\alpha_{n,m} = 2\int_{z=0}^{z=1} \phi_n(z,\omega_n)\sin(m\pi z)\,dz \tag{D.31}$$

The coefficients g_m, h_m and $\alpha_{n,m}$ can be computed from the initial condition and the normal vibration modes ϕ_n. Therefore, the only unknown quantities in equations (D.27) and (D.28) are the coefficients A_n. These ones are compute by the following procedure. First, Eqs. (D.27) and (D.28) are rearranged in the following form:

$$\sum_{m=1}^{\infty}\left(g_m - \sum_{n=-\infty}^{\infty} A_n\alpha_{n,m}\right)\sin(m\pi z) = 0 \tag{D.32}$$

$$\sum_{m=1}^{\infty}\left(h_m + i\sum_{n=-\infty}^{\infty} \omega_n A_n\alpha_{n,m}\right)\sin(m\pi z) = 0 \tag{D.33}$$

Each coefficient of the Fourier series in Eqs. (D.32) and (D.33) must vanish, leading to the following system of algebraic equations for A_n:

$$g_m = \sum_{n=-\infty}^{\infty} A_n\alpha_{n,m},\ \ m = 1,2,3,... \tag{D.34}$$

$$h_m = -i\sum_{n=-\infty}^{\infty} \omega_n A_n\alpha_{n,m},\ \ m = 1,2,3,... \tag{D.35}$$

For a numerical simulation, it is necessary to truncate the series in Eqs. (D.34) and (D.35) up to an N_{max} term, leading to the following expression:

$$g_m = \sum_{n=-N_{max}}^{N_{max}} A_n\alpha_{n,m},\ \ \text{for } m = 1,2,...,N_{max} \tag{D.36}$$

$$h_m = -i\sum_{n=-N_{max}}^{N_{max}} \omega_n A_n\alpha_{n,m},\ \ \text{for } m = 1,2,...,N_{max} \tag{D.37}$$

Such truncation implies that the infinite set of linear algebraic equations has been truncated to a linear algebraic system with $2N_{max}$ algebraic equations. In order to obtain a consistent system of equations with a unique solution, it is necessary to also truncate the values of m up to N_{max}. By solving the $2N_{max}\times 2N_{max}$ system of linear algebraic equations, the coefficients A_n are obtained and are incorporated into the particular solution given in Eq. (D.22), which in turn contains all the information to simulate the tube dynamics.